Experimental study of fluid inclusion re-equilibration in quartz

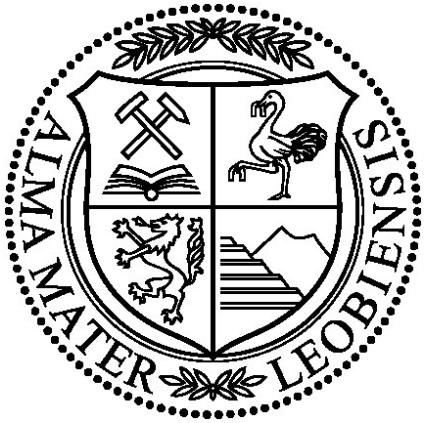

Dissertation

BSc Gerald Doppler, MSc
Ingenieurbüro für Technische Geologie

Montanuniversität Leoben

Department Angewandte Geowissenschaften und Geophysik

Lehrstuhl für Rohstoffmineralogie

Betreuer/Supervisor

Ao.Univ.-Prof. Dr. Ronald J. Bakker

Gutachter/Referees

Ao.Univ.-Prof. Dr. Ronald J. Bakker

Ao.Univ.-Prof. Dr.phil. Walter Prochaska

Juli/July 2014

Affidavit

I declare in lieu of oath, that I wrote this thesis and performed the associated research myself, using only the literature cited in this volume.

GERALD DOPPLER

"Alles, was gegen die Natur ist, hat auf die Dauer keinen Bestand."

Charles Darwin *1809 – †1882

Abstract

This PhD thesis is structured with six chapters that describe the experimental study on re-equilibration of synthetic fluid inclusions. Three chapters represent autonomous scientific units, which have been published in international scientific journals (one is in review). Another chapter explains the design of the used experimental setup of the hydrothermal laboratory. This thesis is complemented by an overall introduction chapter and by a general conclusion chapter.

In literature, some examples have been published about evidence of post-entrapment changes of fluid inclusions. Nevertheless fluid inclusion studies in general are still considered and interpreted with a closed-system behavior. Thus the present experimental work is designed to test potential post-entrapment behavior of fluid inclusions in quartz by systematically performed re-equilibration experiments. Different fluid species are used to determine the major factors of fluid inclusion modifications and their magnitude. Knowledge of diffusion rates of water-related chemical species and isotopes in quartz is important for interpreting fluid-rock interactions based on fluid inclusion research and reconstructing of the *P-T-t* history of earth's crustal rocks.

As a first approach pure H_2O and D_2O fluid was used to determine the re-equilibration potential of fluid inclusions; 1) distance to the quartz crystal surface, 2) the size of the inclusions, and 3) the time of re-equilibration experiments on the magnitude of fluid inclusion post-entrapment changes. This series of experiments was published in *Contributions to Mineralogy and Petrology 165:1259-1274 (2013)*.

Further investigations were based on the influence of the α-β quartz phase transition on the post-entrapment fluid inclusions changes was presented in a publication in *Lithos 198-199:14-23 (2014)*.

For getting insight in diffusion behavior of NaCl-H_2O fluid inclusions in quartz, adequate series of re-equilibration experiments have been performed and submitted to the scientific journal *Chemical Geology (2014) which is now under review*.

The newly acquired experimental data, obtained from this study, support the interpretation of natural fluid inclusions and the inclusions hosting rocks. It provides a framework of conditions which may result in post-entrapment modifications of fluid inclusions at constant *P–T*. More detailed starting information of each sub-project of this thesis precedes as sub-abstract of every chapter.

Zusammenfassung

Die vorliegende Doktorarbeit ist in sechs Abschnitte gegliedert, welche die durchgeführten Re-equilibrationsexperimente an synthetischen Flüssigkeitseinschlüssen behandeln. In drei Kapiteln sind jeweils eigenständige, wissenschaftliche Forschungsteilprojekte präsentiert, welche in internationalen wissenschaftlichen Journalen veröffentlicht wurden (eines davon ist momentan in Begutachtung). In einem eigenständigen, einführenden Kapitel werden Aufbau und Funktionsweise des Hydrothermallabors erläutert, welches für diese Arbeit verwendet wurde. Diese Doktorarbeit wird mit einer allgemeinen Einführung/Einleitung in das Forschungsgebiet sowie durch eine zusammenfassende, generelle Schlussfeststellung dieses Projektes abgerundet (abschließendes Kapitel).

In der Literatur findet man publizierte Beispiele, welche Anzeichen von Änderungen von Flüssigkeitseinschlüssen nach dem Zeitpunkt des Einschließens beschreiben. Trotzdem werden nach wie vor Flüssigkeitseinschlüsse im Allgemeinen als geschlossenes System betrachtet und interpretiert. Die gegenständliche experimentelle Arbeit zielt deshalb darauf ab, das Verhalten von Flüssigkeitseinschlüssen nach dem Zeitpunkt ihres Einschlusses mit Re-equilibrationsexperimente zu testen. Flüssigkeiten unterschiedlicher chemischer Zusammensetzung werden benützt, um die wesentlichen Faktoren der Änderungen der Einschlüsse zu bestimmen. Erfahrungen und Kenntnisse von Diffusionsraten von wasserähnlichen chemischen Spezies und Isotopen in Quarz sind für die Interpretation von Fluid-Gestein Wechselwirkung und für die Rekonstruktion der *P-T-t* Geschichte von Gesteinen der Erdkruste notwendig.

Als ersten Ansatz wurde reines H_2O und reines D_2O für die Experimente verwendet um den Einfluss von 1) Distanz zur Quarzkristalloberfläche, 2) Größe der Einschlüsse und 3) Re-equilibrationszeit auf die Stärke der Änderung von Flüssigkeitseinschlüssen festzustellen. Diese Experimentserie wurde im Journal *Contributions to Mineralogy and Petrology 165:1259-1274 (2013)* veröffentlicht.

Weitere Untersuchungen basierten auf der Änderung im Young's Modus des Flüssigkeitseinschlüsse beinhaltenden Quarzes. Der Einfluss des α-β Quarz Übergangs auf Änderungen der Flüssigkeitseinschlüsse wurde in Form einer Publikation im *Lithos 198-199:14-23 (2014)* veröffentlicht.

Um das Diffusionsverhalten von NaCl-H_2O beinhaltenden Flüssigkeitseinschlüssen im Quarz verstehen zu können wurde eine adäquate Serie an Re-equilibrationsexperimente durchgeführt, welche sich momentan in Begutachtung des wissenschaftlichen *Journals Chemical Geoloy (in preparation)* befinden.

Die neuesten experimentell erstellten Daten, welche dieser Doktorarbeit entstammen, unterstützen die Interpretation von natürlichen Flüssigkeitseinschlüssen und deren Trägergesteine enorm. Nähere abstrakte Informationen für jedes Teilprojekt dieser Arbeit gehen als Abstract jedem Kapitel voraus.

Acknowledgements / Danksagungen

Bevor die werte Leserin, der werte Leser mit der Lektüre meiner Doktorarbeit beginnt, möchte ich an dieser Stelle meine Dankbarkeit gegenüber einigen Personen zum Ausdruck bringen:

Das Fundament dieser Doktorarbeit stellt mein Betreuer Prof. Ronald J. Bakker dar. Die Grundidee der gegenständlichen Vorschungsarbeit stammt von ihm. Ich war von Anfang an begeistert unter seiner umseitigen Hilfe die Forschungsarbeit durchführen zu können. Für die vorhandene Unterstützung / Hilfestellung / Verbesserung während meiner Doktoratszeit möchte ich an dieser Stelle mein „Dankeschön" aussprechen.

Sämtlichen Mitarbeiterinnen und Mitarbeitern des Lehrstuhls für Rohstoffmineralogie, allen voran Frau Judith Bergthaler, gebührt ein ausdrücklich großes Dankeschön für sämtliche Unterstützung während meiner gesamten Zeit an diesem Institut. In diesem Atemzug gebührt mein ehrvolles Dankeschön dem unersetzlichen Herrn Helmut Mühlhans. Unserem lieben Herrn Prof. Oskar A.R. Thalhammer möchte ich danken für die immerwährende Unterstützung bei meinem Weg in die Wirtschaft und meiner persönlichen beruflichen Zukunft.

Besonderer Dank gilt meinem langjährigen Wegbegleiter Dr. Peter Kollegger, welcher seit dem Tag unserer Inskription in Erdwissenschaften, in Graz vor genau 10 Jahren, sowohl im studentisch-ausbildungstechnisch-beruflichen als auch im privaten Bereich stets eine verlässliche Stütze ist.

Für die stets vorhandene starke Schulter während persönlicher, Diss.-Ende-betreffender, Missstimmungen, bin ich überaus dankbar, dass Aleksandra M. Deręgowska mit ihrem clever-integer und vorausschauend, logisch-denkendem Geiste mir immer mit Rat zur Seite steht, vielen lieben Dank Olenia!

Last but not least gebührt mein größtes Dankeschön meiner Familie, welche mir die Voraussetzungen schaffte, das naturwissenschaftliche Studium der Erdwissenschaften / Geologie bis zur Erreichung des Doktorats durchzuführen und mich dabei ständig unterstützten.

Allen Freundinnen und Freunden, die hier nicht namentlich erwähnt sind, sei natürlich auch ein großes Dankeschön ausgesprochen.

Dem FWF – Fonds zur Förderung der wissenschaftlichen Forschung sei für die Finanzierung des Projekts (Nr. P 22446-N21) gedankt, aus welchem meine Dissertation entstammt.

I would like to thank the Austrian Research Fund (FWF) for financial support of the project (no. P 22446-N21), of which this dissertation is a part.

Contents

Scientific publications from this PhD project

A) Scientific papers

Contributions to Mineralogy and Petrology

Doppler G. and Bakker R.J. (2013) Fluid inclusion modification by H_2O and D_2O diffusion: the influence of inclusion depth, size, and shape in re-equilibration experiments. 165:1259–1274

Lithos

Doppler G. and Bakker R.J. (2014) The influence of the α–β phase transition of quartz on fluid inclusions during re-equilibration experiments. 198–199 (2014) 14–23

Contributions to Mineralogy and Petrology

Baumgartner M., Bakker R.J. and Doppler G. (2014) Re-equilibration of natural H_2O–CO_2–salt-rich fluid inclusions in quartz - Part 1: experiments in pure water at constant pressures and differential pressures at 600 °C

Chemical Geology

Doppler G. and Bakker R.J. (in preparation) Modification in fluid inclusion salinity during re-equilibration experiments at constant experimental *P-T*. Submitted for revision, August 2014

B) Conference transcript (Book)

Bakker R.J., Baumgartner M. and Doppler G. (2011) European Current Research on Fluid Inclusions, 21st Biennial Conference, Conference transcript

C) Abstracts (Oral presentation)

1) Doppler G., Baumgartner M. and Bakker R.J. (2011) Re-equilibration studies of synthetic fluid inclusions in quartz. European Current Research on Fluid Inclusions (ECROFI-XXI) Montanuniversität Leoben, Austria, 9–11 August, 2011. Abstracts, p. 74

2) Doppler G., Baumgartner M. and Bakker R.J. (2012) Experimental re-equilibration studies of H_2O-D_2O-NaCl through quartz. Pan-American Current Research on Fluid Inclusions (PACROFI-XI), University of Windsor, Ontario, Canada, June 18–20, 2012, Abstracts

3) Doppler G., Baumgartner M. and Bakker R.J. (2012) Fluid inclusion size, depth and shape: aspects of re-equilibration. Goldschmidt 2012 Montreal, Abstract Volume

4) Doppler G., Bakker R.J. and Baumgartner M. (2013) Relative NaCl-enrichment in re-equilibrated synthetic H_2O-NaCl bearing fluid inclusions in quartz. European Current Research on Fluid Inclusions (ECROFI-XXII) Kervansaray Hotel, Lara – Antalya / Turkey, 4-9 June 2013

D) Abstracts (Poster)

1) Doppler G., Baumgartner M. and Bakker R.J. (2011) Experimental technique for re-equilibration studies of water related species through quartz. European Current Research on Fluid Inclusions (ECROFI-XXI) Montanuniversität Leoben, Austria, 9–11 August, 2011. Abstracts, p. 72

2) Doppler G., Baumgartner M. and Bakker R.J. (2011) Do fluid inclusions preserve their initial composition? Experimental studies of H_2O diffusion through quartz. Goldschmidt Conference Prague, Goldschmidt Conference Abstracts

3) Doppler G., Baumgartner M. and Bakker R.J. (2011) Experimental diffusion studies on water-related species through quartz. Jahrestagung der Österreichischen Mineralogischen Gesellschaft (Salzburg, MinPet 2011)

4) Doppler G., Bakker R.J. and Baumgartner M. (2013) The effect of the α–β–quartz transition boundary in re-equilibration experiments. European Current Research on Fluid Inclusions (ECROFI-XXII) Kervansaray Hotel, Lara – Antalya / Turkey, 4-9 June 2013

5) Doppler G., Bakker R.J. and Baumgartner M. (2013) The role of water diffusion in quartz investigated by experimental fluid inclusion re-equilibration. 12th SGA Biennal Meeting 2013, August 11-15 2013, Uppsala, Sweden

6) Doppler G., Bakker R.J. and Baumgartner M. (2013) The effect of the α–β–quartz transition boundary in re-equilibration experiments. MinPet2013 conference, Technical University of Graz, 19-23 September 2013, MITT.ÖSTERR.MINER.GES. 159 (2013)

1. Overall introduction

The principal field of interest of this study is experimental work on fluid inclusions within nominally anhydrous quartz. A main focus within this largely extended field of investigation is to determine cause and effect of fluid inclusion re-equilibration. Investigations were done on synthetically trapped fluids of known composition and density in natural quartz crystals. The influence of various properties of fluid inclusions within the hosting quartz crystal and external conditions should give insight in the influence on diffusion of fluid components.

Knowledge of diffusion behavior of chemical components, such as H_2O, D_2O, H_2, O_2, NaCl, Na^+, and Cl^- in quartz is important for various reasons. Quartz is a common host mineral of fluid inclusions, which are commonly used for reconstruction and interpretation of geological processes within the earth's crust, i.e. *P-T-t* history of rocks. Most of the reconstruction assumptions are based on closed-system behavior of fluid inclusions. However there are indications for evidence of post-entrapment changes of fluid inclusions (publications from several authors). Thus systematically operated experimental work is needed for understanding and learning about all the potential factors which affect fluid inclusion properties.

During the present dissertation fluid inclusions were synthesized in quartz cracks, which have been induced by thermal shock. Fluid inclusions were entrapped by fracture healing of the cracked quartz under hydrothermal conditions. The laboratory setup described in detail in chapter 2 of this thesis. The initially synthesized fluid inclusions were qualitatively and quantitatively analyzed by using non-destructive methods, such as microscopy, microthermometry and Raman spectroscopy. Inclusion properties, such as position within the quartz sample, fluid density, fluid composition and inclusions size are the main properties of interest. Systematically designed re-equilibration experiments are performed complementarily after investigating the initial syntheses to obtain information about post-entrapment behavior of fluid inclusions.

The first approach of this complex study was published as a scientific paper in the journal *Contributions to Mineralogy and Petrology, 165:1259-1274* in 2013 and takes part of the present PhD thesis with the title "*Fluid inclusion modification by H_2O and D_2O diffusion: the influence of inclusion depth, size, and shape in re-equilibration experiments*" (chapter 3, page 24-44).

Based on the first approach, further investigations on diffusion behavior of fluid species through quartz have been carried out and were published in the scientific journal *Lithos, 198-199:14-23* in 2014 which is presented as chapter 4 in this thesis (page 45-61) with the title "*The influence of the α-β phase transition of quartz on fluid inclusions during re-equilibration experiments*".

Another approach of this study was to investigate how NaCl-H_2O solutions behave during re-equilibration experiments. It was tested by performing various experiments with different brine concentrations. The whole process with the related results of this major sub-project is presented in this thesis in chapter 5 (page 62-78) titled with "*Changes in fluid inclusion salinity during re-equilibration experiments*", which is now under review in the journal *Chemical Geology*.

2. Laboratory, hydrothermal high pressure – high temperature apparatus

2.1 Introduction

Fluid inclusions in the present PhD project are synthesized by fracture healing of cracked quartz crystals at elevated pressure and temperature conditions. A high pressure / high temperature apparatus is used to reach the required crystal forming conditions, which promote fracture healing to entrap fluids. The same temperature and pressure conditions were used for complementary re-equilibration experiments.

The hydrothermal laboratory at the University of Leoben, Chair of Resource Mineralogy, provides all requirements for both, synthesis and re-equilibration experiments. This apparatus allows simulating and reproducing natural processes at various fluid inclusion formation conditions.

2.2 Hydrothermal laboratory setup

The hydrothermal laboratory in Leoben includes 10 autoclaves which are specially designed to perform fluid inclusion synthesis and re-equilibration experiments (Fig. 1). The actual apparatus is a combination of a pressure unit and a temperature unit. The maximum pressure and temperature of the hydrothermal experimentation are 1 GPa and 700 °C.

Fig. 1 High pressure / high temperature hydrothermal laboratory device in Leoben

2.2.1 Pressure unit

2.2.1.1 Pumping system

The pressure unit (Fig. 2), which is connected to the autoclaves, is constructed in the form of a two-loop system. Pressures from 0.1 MPa (room-pressure – starting conditions) to 100 MPa are reached by a membrane compressor which is supported by compressed air to about 1 MPa (Fig. 3). This compressed low-pressure air (about 1 MPa) is provided by the in-house air supplying device. Higher pressures from 100 MPa up to 1 GPa can be reached by an air-driven liquid pump which supports the hydraulic intensifier (Fig. 2 and 3).

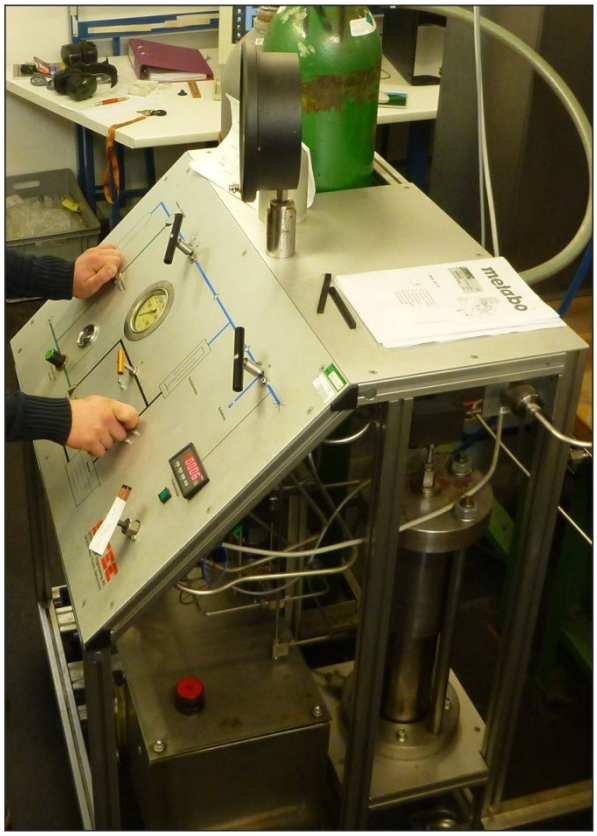

Fig. 2 Used pumping system and the pressure intensifier (bottom right). According to the manufacturer *SITEC* the experimental pressure can reach 150,000 PSI (1 GPa). The P_{max} of the membrane compressor is 100 MPa

2.2.1.2 Pressure-pipe system

The pressure medium within the pipes and the autoclaves is Argon (Fig. 3 and 4). For pressure supply ultra-high pressure tubes (UHP model 150-14XF6) are used (Fig. 5 and 7). The constructed valve-control system allows separate operation of each autoclave with individual pressures. The UHP valves are designed for pressures up to 1 GPa (Fig. 6). Both, tubes and valves are supplied by the manufacturer *HiP (http://www.highpressure.com/)*.

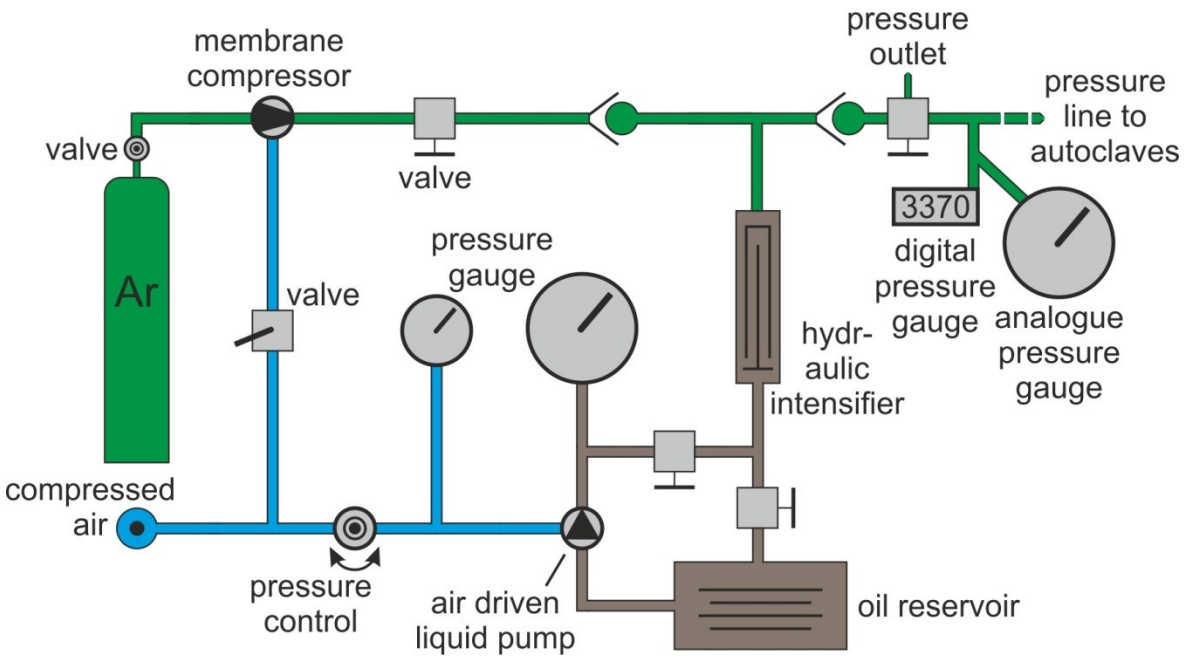

Fig. 3 The installation construction of the pressure-pump system

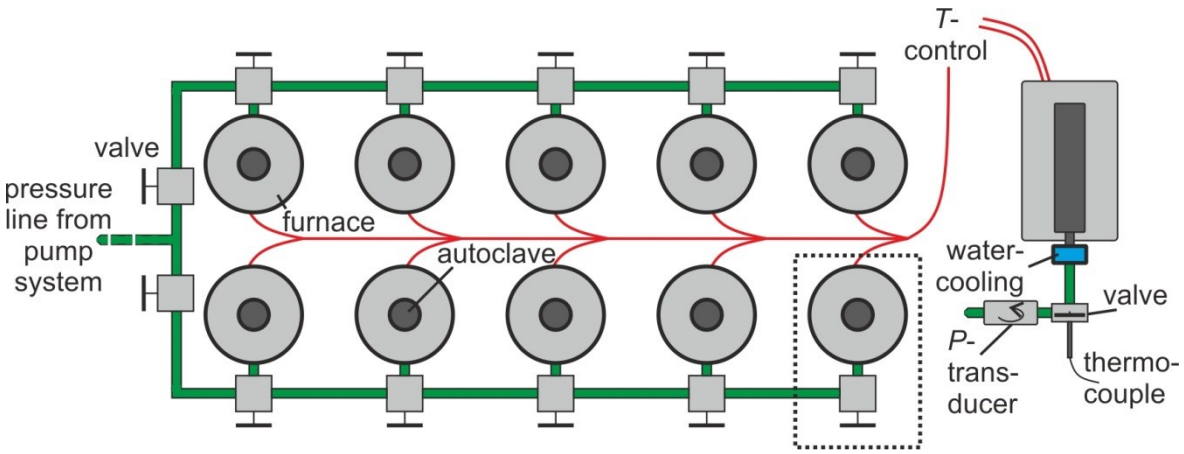

Fig. 4 The installation construction of the pressure-pipe system (green) and the temperature support cabling (red) in a floor plan view left, and a cross-section view of the furnace-autoclave combination

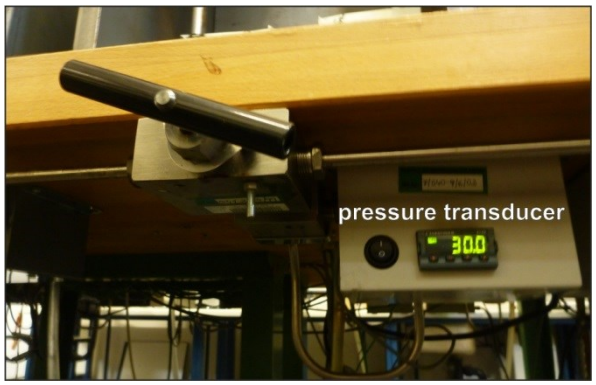

Fig. 5 (top left) UHP tube-system with a valve and the interposed pressure transducer

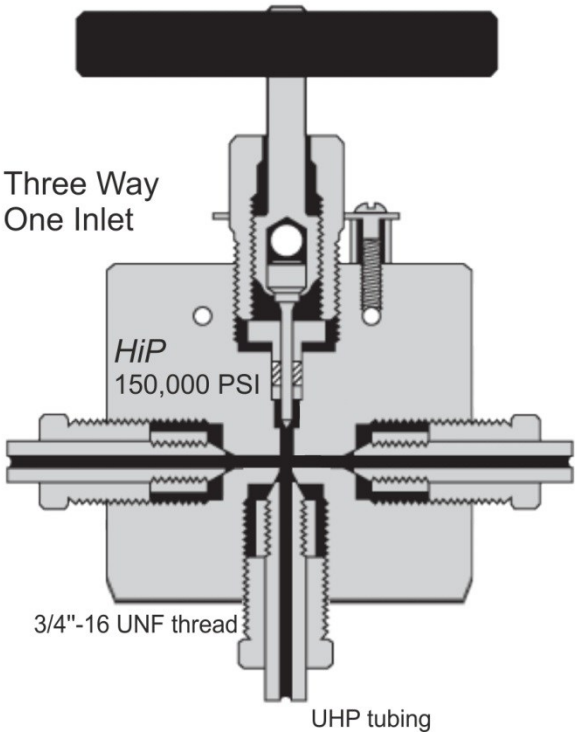

Fig. 6 (right) UHP valve which are used within the tubing construction. Model HiP (150-14XF6) 150,000 PSI (1 GPa)

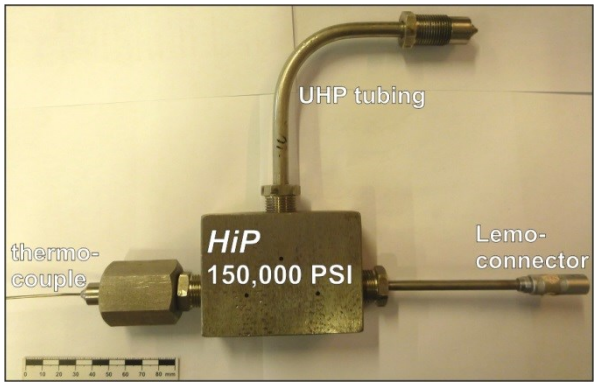

Fig. 7 (left) Combination of a tubing-component and the thermocouple. Tube-model HiP (150-14XF6) 150,000 PSI (1 GPa)

2.2.1.3 Pressure vessel

The cold seal pressure vessels (autoclaves; Fig. 8) consist of a Ni-Cr alloy (Nimonic IOS/René 41; see composition in Table 1) and are installed in a vertical position (Fig. 4 and 11a). Tensile tests showed a possible low plastic deformability of 1.5 % at room temperatures. For optimum strength the autoclaves were treated at 1080 °C for 30 minutes, and then air-cooled followed by the standard age of 760 °C for 16 hours before air-cooling. Heat treated material was tested again for tensile strength. The treated material showed increased plastic deformability of 7 %. The cone (Type Stora 67 1.2344; RC 50-52) is fixed to the autoclave with a closure nut (Fig. 9).

Table 1 Manufacturer's material analysis (mass-%$_{given}$) versus three self-performed analyses (mass-%$_{analized}$)

Element	mass-%$_{given}$	mass-%$_{anal.}$ (1)	mass-%$_{anal.}$ (2)	mass-%$_{anal.}$ (3)
Fe	3,02	3,08	2,77	3,09
Ti	3,10	2,65	2,66	2,94
S	0,0004	0,41	0,52	0,42
Co	11,02	11,32	11,73	11,7
Ni	51,25	52,74	51,57	51,47
Mo	9,92	9,00	8,4	8,51
Cr	19,76	17,77	19,04	19,04
Al	1,64	1,75	1,93	1,78
Si	0,10	0,76	0,93	1,08
Mn	0,05			
Zr	0,05			
B	0,006			
C	0,080			
Sum	100,00	99,48	99,55	100,03

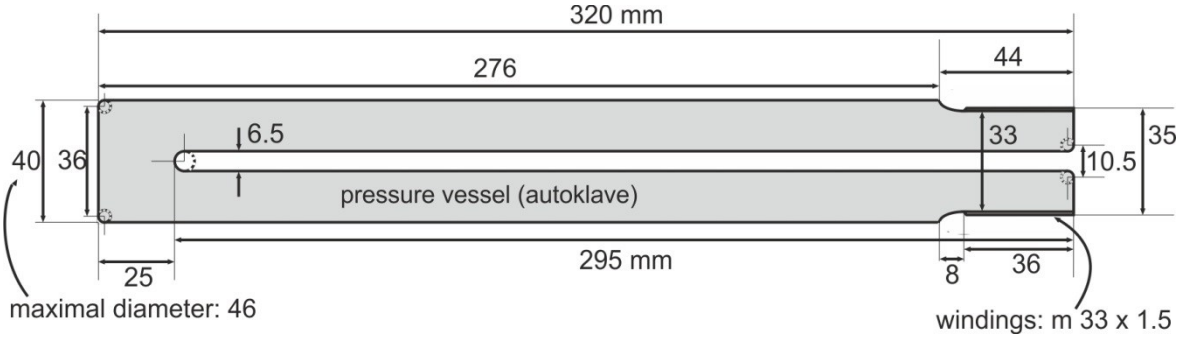

Fig. 8 Measures of the pressure vessel. (All measures are in millimeter)

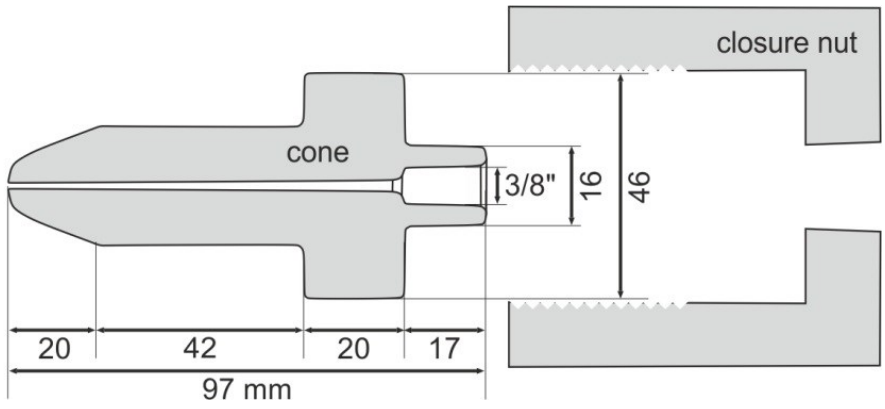

Fig. 9 Measures of the closing components. (All measures are in millimeter)

2.2.1.4 Pressure registration

Pressure transducers (type Eurotherm 2132) are kept at constant *T* (30 °C) to eliminate fluctuations in pressure-registration due to minor temperature changes, e.g. day and night temperature (Fig. 5 and 11). The pressure transducers are calibrated up to 700 MPa with a Heise dial gauge, which has an accuracy of 0.015 % of reading. During experimentation pressure is continuously logged (Fig. 11b). The pressure conditions are stabilized within 3 MPa during experimental run-times up to 40 days. Each autoclave can be controlled individually.

2.2.2 Temperature unit

2.2.2.1 Temperature supply

Experimental temperatures are supplied by electronic furnaces. The maximum temperature of furnaces is 700 °C. The furnace temperature is controlled (**1**) by the computer software LabView (Fig. 11b "Tsoll" and c) and (**2**) by a safety system which is combined to the electronic control box (Fig. 12). The electronic control box is connected to the PC with a RS232 cable to the serial port. Each furnace can be controlled with individual temperatures.

2.2.2.2 Temperature measurement

Temperature is detected at three positions: (**1**) the furnace temperature is measured near the hot spot of the oven on the outside and is displayed on the monitor (Fig. 11c "T Regel"), (**2**) the temperature of the loaded sample is measured by an internal thermo-couple (Fig. 10 and 11a; displayed in Fig. 11b "T Autoklav"), and (**3**) one for the safety system, similar as (**1**). During the experiments temperature is continuously logged and is controlled by the computerized operating system with an uncertainty of 0.1 °C. The temperature conditions are stabilized within 2 °C during experimental run-times up to 40 days.

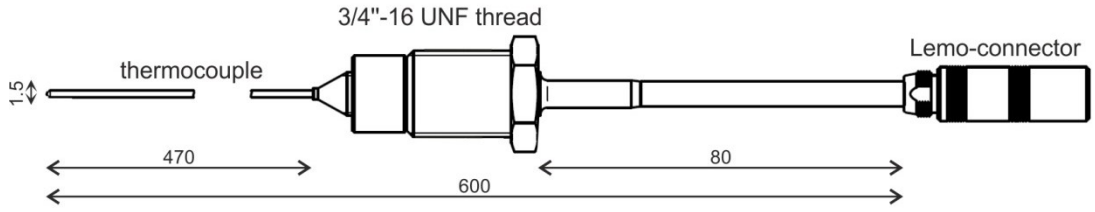

Fig. 10 Measures of a used thermocouple. Model T-Ma 15 G NiCr-Ni Type K
T_{max} = 800 °C, P_{max} = 700 MPa. (All measures are in millimeter)

2.2.2.3 Cooling system

The heated pressure vessel is cooled on the bottom by a vessel-surrounding water-cooling system (Fig. 4 and 11a).

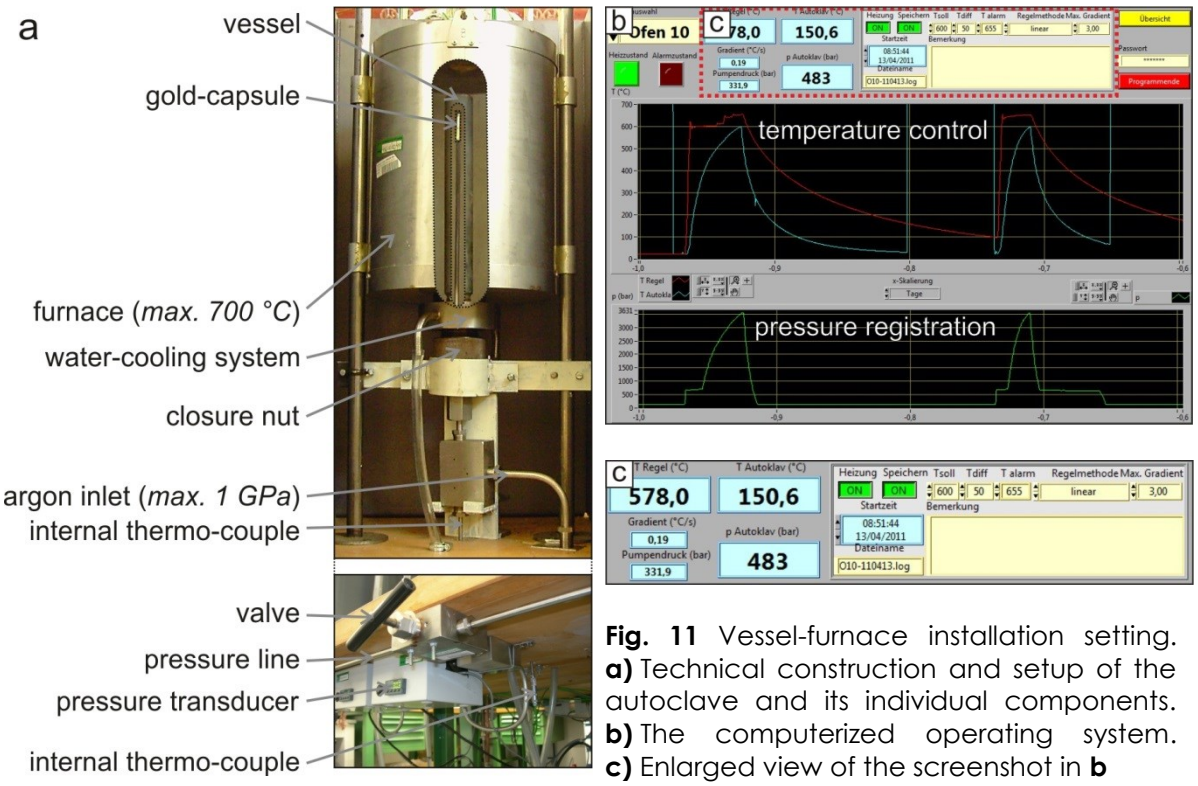

Fig. 11 Vessel-furnace installation setting. **a)** Technical construction and setup of the autoclave and its individual components. **b)** The computerized operating system. **c)** Enlarged view of the screenshot in **b**

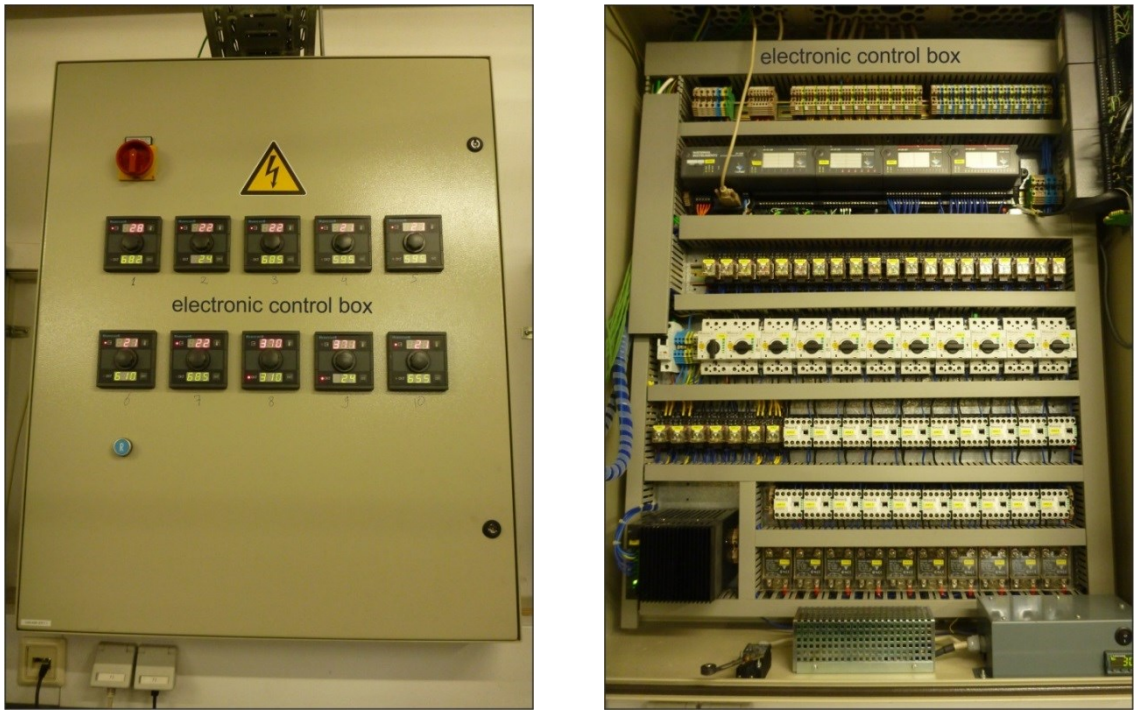

Fig. 12 Electronic control box which is interposed between the furnace and the computer software for digitalizing the electronic signal of the furnace

2.3 Material fatigue

According to the manufacturer the Ni-Cr alloy pressure vessels should withstand 700 °C and 1 GPa. A ten-year-old pressure vessel was cracked during an experiment at 400 °C and 600 MPa after the experimentation time of 5 days (Fig. 13).

As a possible cause of brittle deformation it is assumed that the advanced age of the used vessel was the main reason. Additionally it is assumed that the crack initiated at the cooler part (close to the water-cooled assembly) of the vessel.

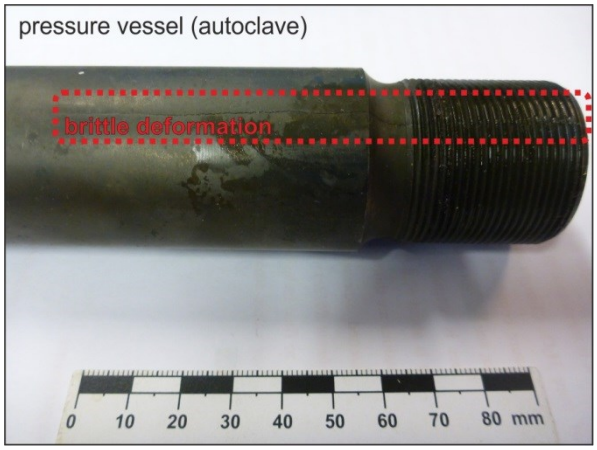

Fig. 13 Cracked pressure vessel after experimentation at ~650 MPa and 600 °C

3. Fluid inclusion modification by H_2O and D_2O diffusion: the influence of inclusion depth, size, and shape in re-equilibration experiments

Gerald Doppler • Ronald J. Bakker • Miriam Baumgartner

Contrib Mineral Petrol (2013) 165:1259–1274
DOI 10.1007/s00410-013-0857-6
Received: 2 August 2012, Accepted: 25 January 2013, Published online: 14 February 2013

Abstract The mobility of H_2O and D_2O by diffusion through quartz is illustrated with H_2O-rich fluid inclusions synthesized at 600 °C and 337 MPa, within the α-quartz stability field. Inclusions are re-equilibrated at the same experimental conditions within a pure D_2O fluid environment. Consequently, a gradient in volatile fugacities is the only driving force for diffusion, in the absence of pressure gradients and deformation processes. Up to 100 individual inclusions are analyzed in each experiment before and after re-equilibration by microscopic investigation, microthermometry, and Raman spectroscopy. Changes in fluid inclusion composition are obtained from the ice-melting temperatures, and density changes are obtained from total homogenization temperatures. After 1-day re-equilibration, inclusions already contain up to 11 mol % D_2O. A maximum concentration of 63 mol % D_2O is obtained after 40-day re-equilibration. D_2O concentration profiles in quartz are determined from the concentration in inclusions as a function of their distance to the quartz surface. These profiles illustrate that deep inclusions contain less D_2O than shallow inclusions. At equal depths, a variety of D_2O concentration is observed as a function of fluid inclusion size: Small inclusions are stronger effected compared with large inclusions. A series of 19-day re-equilibration experiments are performed at 300, 400, 500, and 600 °C (at 337 MPa), at the same conditions as the original synthesis. The threshold temperature of diffusion is estimated around 450 °C at 337 MPa, because D_2O is not detected in inclusions from re-equilibration experiments at 300 and 400 °C, whereas maximally 26 mol % D_2O is detected at 500 °C. Our study indicates that the isotopic composition of natural fluid inclusions may be easily modified by re-equilibration processes, according to the experimental conditions at 600 °C and 337 MPa.

Keywords Fluid inclusions · Quartz · Diffusion · Re-equilibration · Experimental study · Hydrogen isotopes · D_2O · H_2O

Introduction

Most of the nominally anhydrous minerals within the Earth's crust and mantle can incorporate considerable and measurable amounts of hydrogen (e.g. Keppler and Smyth 2006). The major incorporated species is assumed to be hydroxyl, that is, OH^- (e.g. Keppler and Smyth 2006). Molecular H_2O is generally concentrated in specific nano to micrometer-sized isolated cavities within single crystals, but H_2O molecules can also be present at interstitial lattice positions. Cavities that exceed diameters of about 1 μm are usually known as fluid inclusions, which can be analyzed by optical means (e.g. Shepherd et al. 1985). Nominally

anhydrous quartz is a common host mineral of fluid inclusions, and the entrapped fluids are used in a widespread field of geological investigations (see Roedder 1984 and references therein). Knowledge of the properties of this fluid may contribute to reconstructions of pressure–temperature–time (*P–T–t*) histories of rock units in the Earth's crust and may contribute to understanding fluid–rock interactions. The interpretation of paleo-fluids in inclusions is among other assumptions based on the hypothesis that the entrapped inclusions remain their density and composition after entrapment. Fluid inclusion research is generally based on a closed-system assumption within nominal anhydrous minerals. However, there is experimental evidence that entrapped inclusions do not always behave as closed systems (e.g. Sterner and Bodnar 1989; Bakker and Jansen 1990, 1994; Diamond et al. 2010). Detailed studies on the distribution and properties of fluid inclusions in natural samples also suggest post-entrapment modifications (e.g. Audétat and Günther 1999; Ayllón et al. 2003). The experimental studies on modification of fluid inclusions in quartz are not conclusive, because the impact of individual parameters, such as temperature, gradients in concentration, gradients in pressure, fluid-quartz interactions, host mineral phase transitions (e.g. α–β quartz), and deformation, on modification processes are not yet fully unraveled (e.g. Bakker and Diamond 2003). Most experimental studies do not separate the influence of these individual parameters on modification processes. For example, fluid inclusions in experiments that have mimicked nearly isothermal decompression are effected by gradients in fluid composition, gradients in fluid pressure (i.e. in fluid densities), and inclusion wall deformation processes at variable hydrothermal pressures and slightly decreasing temperatures. Any modification of fluid properties in these inclusions results from applying all of these variables at once. In order to estimate the effect of individual parameters, it is essential to accumulate more experimental data of post-entrapment modifications of fluid inclusions by performing systematic experiments in which only one variable is adjusted, whereas the others remain constant.

The present study describes major parameters that play a significant role in H_2O and D_2O diffusion experiments. The mobility of hydrogen isotopes in nominally anhydrous crystals is of major importance for the interpretation of constrains on the origin of parental fluids from which ore forming minerals have grown (e.g. Giuliani et al. 1997). In this context, the determination of isotopic composition of fluid inclusions has recently increased in importance (e.g. Wilkinson 2001; Dublyanski and Spötl 2010). Any modification of the δD composition of natural fluid inclusions due to re-equilibration processes will result in inaccurate fluid source identification, especially in magmatic and metamorphic environments. There are no studies available that document in detail the efficiency of D_2O–H_2O diffusion through quartz that may affect δD values of fluid inclusions.

In the present study, only hydrothermal activity of H_2O as the entrapped species and D_2O as the external fluid phase at constant *P–T* conditions of 337 MPa and 300, 400, 500, and 600 °C leads to the diffusional driving force regarding to the gradient of the chemical potential. Each presented experiment in this study was exclusively performed under hydrothermal experimental conditions without any experimental stress component. In order to avoid any changes of the initially entrapped inclusions during the start and the end of the experiments, loading and unloading the autoclave (pressure vessel)

is performed at constant fluid density conditions (isochorically) exclusively in the α-quartz stability field. Previous re-equilibration experiments have been carried out in a widespread stability field of quartz, but probably without respect to the different crystallographic modifications of α-quartz and β-quartz (e.g. Sterner and Bodnar 1989; Vityk and Bodnar 1995). Contrary to assumptions of previous work (e.g. Sterner et al. 1995), non-decrepitative changes of inclusion properties are directly related to the combination of (1) depth within the crystal; (2) inclusions size; (3) temperature; and (4) time. The experiments demonstrate the major factors that cause the mobility of water through quartz under hydrothermal experimental conditions and, therefore, the experimental alteration of natural fluid inclusions as they are currently performed by the authors (Baumgartner et al. 2011; Bakker et al. 2012). The newly acquired data of the compositional changes result in new diffusion models and diffusion constants of H_2O and D_2O in quartz.

Experimental procedure

The hydrothermal laboratory at the University of Leoben is specially designed for the synthesis of fluid inclusions. There are 10 Nimonic IOS/René 41 autoclaves (Ni–Cr alloy) in a vertical position that are installed in a cold-seal system (see Kerrick 1987). The pressure medium is Argon and may reach values up to 1 GPa hydrothermal pressure. The external oven temperatures are maximally 700 °C. Temperatures are directly measured at the samples within the autoclaves with an internal thermocouple. Temperature is controlled by a computerized operating system during the experiment and is measured with an uncertainty of 0.1 °C. The pressure is monitored with pressure transducers, which are calibrated up to 700 MPa with a Heise dial gauge (accuracy is 0.015 % of reading). Both temperature and pressure are continuously logged.

The experimental work is designed to synthesize fluid inclusions in quartz of known V_m–x properties (i.e. molar volume and composition, respectively), morphological properties, and positions within the crystal. The quartz samples with initially synthesized pure H_2O fluid inclusions are exposed to a pure D_2O environment during the re-equilibration experiment at the same temperature and pressure conditions. Consequently, gradients in temperature and pressure or deformation conditions are not present during experimentation. Both, synthesis and re-equilibration experiments, are carried out under hydrothermal conditions. Due to a compositional gradient, that is, fugacity gradients of H_2O and D_2O between synthetic fluid inclusions and the external fluid phase during the re-equilibration experiments, diffusion of the two species through the quartz crystal is provoked.

Fluid inclusion synthesis

Inclusion-free natural Brazilian quartz crystals are used as starting material. Rods are drilled in specific crystallographic orientations of the quartz crystal, with an approximate length of 1 cm and diameter of 2.75 mm. The direction of drilling is parallel to the *c*-axis of the quartz crystal to minimize the influence of birefringence of the laser light in subsequent Raman spectroscopic analyses of fluid inclusions (Baumgartner and Bakker 2009). The quartz rods are partially cracked by a thermal shock after heating to 400 °C. A cracked quartz rod and a certain amount of ultra-pure water are loaded within an Au-capsule, that is, arc-welded on both sides to prevent any interaction with the autoclaves and the pressure medium Argon at experimental conditions. The synthesis is performed by healing fractures according to the method of Bodnar and

Sterner (1987).

The *P–T* conditions of the synthesis experiments are given in Table 1. All experiments are performed at 337 MPa and various temperatures, that is, 300, 400, 500, and 600 °C, within the α-quartz stability field (Hosieni et al. 1985). The selected conditions are purely arbitrary and represent crustal conditions at about 10 km depth and variable temperatures, as it may occur in different geothermal gradients. The experimental setup stabilizes the synthesis conditions within 2 °C and 3 MPa (Table 1), and fluid inclusions are synthesized within 19 days. The experiments are loaded and unloaded according to specific isochores of the fluid trapped in the newly formed inclusions (see Appendix A in ESM) to prevent stress conditions that may cause cracking of inclusions due to internal fluid over- or under-pressures. This can only be achieved by the use of internal thermocouples.

After the initial synthesis of aqueous fluid inclusions, the quartz rods are cut into disks with a thickness of approximately 0.5 mm. Subsequently, the disks are polished on both sides for microscopic, microthermometric, and Raman spectroscopic investigations. A relatively large number of fluid inclusions (up to 100, see Table 1) of each disk are analyzed to achieve statistical distributions of a variety in parameters such as sizes, shapes, and distances to the crystal surface, that is, depth within the quartz crystal (see Appendix B in ESM).

Re-equilibration of fluid inclusions

After various analyses of the initially synthesized fluid inclusions, the same quartz disks are subsequently used for re-equilibration experiments. The relatively fragile sample disks are placed in between two quartz spacers to prevent any damage by capsule deformation during re-equilibration. Instead of ultra-pure water, pure D_2O is added to the gold capsule in re-equilibration experiments. Loading as well as unloading of the pressure vessels is carried out again according to specific isochores such that the pressure in the initial fluid inclusions does not differ from the external pressure medium. The experimental *P–T* conditions of re-equilibration experiments are illustrated in Table 1 and do not differ from the original synthesis conditions. The experimental run-times vary from 1, 5, 19 to 40 days, and re-equilibration conditions are stabilized within 2 °C and 3 MPa (Table 1). After the re-equilibration experiments, composition (H_2O–D_2O mixture), density, and morphology are compared with the initially synthesized fluid inclusions.

Analytical methods

Morphological properties of each fluid inclusion are characterized by the total area and the perimeter by tracing digitally around the outside edges of the fluid inclusions at room temperature according to Bakker and Diamond (2006). The volumetric properties of individual phases (liquid/vapor ratio) are difficult to obtain; therefore, area fractions of the vapor bubble (α_{vap}) of each fluid inclusion have been digitally measured from two-dimensional images by tracing the outside edge of the total inclusion and by the outside rim of the vapor bubble at room temperature. The distance of fluid inclusions to the crystal surface is measured with an ordinary microscope table that is adjustable in the z-direction (Olympus BX60).

Homogenization and melting temperatures of the entrapped fluids are measured by using the LINKAM MDS 600 and LINKAM THMSG 600 heating–freezing stages, which are calibrated with synthetic fluid inclusions at -56.6 °C (melting of CO_2), 0.0 °C (melting of H_2O), and 374.0 °C (critical density of H_2O). The precision of measurements is ±0.1 °C around 0 °C and about ±0.3 °C in the range of 300–400 °C.

The reproducibility of all measurements is within ±0.1 °C.

The presence of H_2O and D_2O in fluid inclusions is detected by an ISA JobinYvon LABRAM confocal Raman spectrometer, using a frequency-doubled 120 mW Nd-YAG laser with an excitation wavelength of 532.2 nm. Raman spectra of both H_2O and D_2O are broad bands within a range of wavenumbers that do not interfere (Fig. 1), 2,900–3,800 and 2,100–2,800 cm^{-1}, respectively (see also Rull 2002). Therefore, the relative amounts of D_2O and H_2O in fluid inclusions can be directly obtained by comparing their relative band areas in a spectrograph. Standard solutions of known variable H_2O/D_2O ratios were measured by Baumgartner et al. (2011) and reveal a simple relationship between ratio and area fractions (Eq. 1)

$$x_{rel}(\mathrm{D_2O}) = \frac{a_{D_2O}}{a_{D_2O} + a_{H_2O}} \qquad (1)$$

where x_{rel} is the relation mole fraction of D_2O in binary D_2O–H_2O mixtures and *a* is the band area.

The Raman cross-sections of H_2O and D_2O do not need to be considered in this purely empirical relationship. The D_2O content of re-equilibrated synthetic fluid inclusion is directly calculated with this equation. The D_2O composition is compared with melting temperatures of the D_2O/H_2O mixture, and significant different melting temperatures T_m(SV→LV) of pure H_2O (0.0 °C) and pure D_2O (+3.8 °C) can be used to determine relative amounts of H_2O and D_2O from intermediate melting temperatures. Consequently, these temperature changes can be directly related to relative band areas in Raman spectra (Eq. 1), resulting in a simple equation to calculate H_2O/D_2O mole fractions from T_m values (Eq. 2)

$$x_{rel}(\mathrm{D_2O}) = \frac{T_m(fi)}{T_m^0(\mathrm{D_2O}) - T_m^0(\mathrm{H_2O})} \qquad (2)$$

where T_m is melting temperature in °C, fi is the solution in a specific fluid inclusion. The superscript *0* indicates the pure phase.

The properties of H_2O and D_2O fluids are calculated with equations of state, Haar et al. (1984) and Hill et al. (1982), respectively, that are available in the software package FLUIDS provided by Bakker (2003, and http://fluids.unileoben.ac.at).

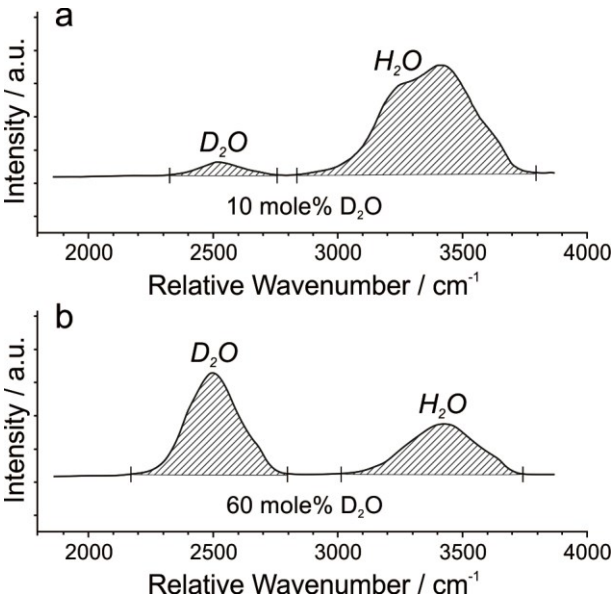

Fig. 1 Raman spectra of fluid inclusions (originally pure H_2O) after a re-equilibration experiment. Inclusion with 10 mol % D_2O (**a**) and inclusion with 60 mol % D_2O (**b**). The peak area is directly related to the relative amount of the fluid species

Fugacity, molar volume, and homogenization temperatures of H_2O and D_2O

Fugacity and molar volume calculations of pure H_2O in the initial synthesis are given in Table 1 (column f and h). Experiments *GMR002c* and *GMR004a*, *b*, and *c* have been performed at 600 °C and 337 MPa which corresponds to a molar volume of 25 $cm^3 \cdot mol^{-1}$ and a fugacity of 175.8 MPa. Additional three syntheses have been carried out at lower temperatures

and at approximately the same pressure. Synthesis *GMR008a* has been carried out at 500 °C which corresponds to a molar volume of 22.63 $cm^3 \cdot mol^{-1}$ and a fugacity of 120.5 MPa. Experiment *GMR007a* has been performed at 400 °C with a molar volume of 20.65 $cm^3 \cdot mol^{-1}$ and a fugacity of 68.42 MPa. The lowest temperature synthesis *GMR006a* has been performed at 300 °C which corresponds to a molar volume of 19.06 $cm^3 \cdot mol^{-1}$ and a fugacity of 28.74 MPa. The fugacity of H_2O in the external fluid in re-equilibration experiments is reduced to 0 MPa, due to the absence of H_2O in the capsule. H_2O fugacity within fluid inclusions and the D_2O fugacity in the capsule fluid during re-equilibration are illustrated in Table 1 (column f and i, respectively). Comparison of both fugacities indicates the similarities of both fluids at equal *P–T* conditions.

Table 1 Experimental conditions

a	b	c	d	e	f	g	h	i	j	k	l	m
Syntheses												
GMR002c	338.5	±2.8	600.2	±0.2	176.9	±1.8	24.97	-	-	-	19	100
GMR004a	336.0	±1.6	601.4	±2.0	176.0	±2.0	25.06	-	-	-	19	96
GMR004b	336.0	±1.6	601.4	±2.0	176.0	±2.0	25.06	-	-	-	19	100
GMR004c	336.0	±1.6	601.4	±2.0	176.0	±2.0	25.06	-	-	-	19	77
GMR006a	337.4	±1.5	300.3	±0.6	28.9	±0.3	19.06	-	-	-	19	15
GMR007a	337.6	±1.0	400.7	±0.6	69.0	±0.5	20.66	-	-	-	19	47
GMR008a	334.9	±2.0	500.1	±0.4	119.7	±1.0	22.67	-	-	-	19	98
Re-equil.												
R002c	336.9	±0.6	599.8	±0.3	175.7	±0.6	25.00	176.17	±0.55	24.91	5	94
R004a	337.3	±2.0	599.5	±1.6	175.8	±2.1	24.98	176.26	±2.14	24.89	19	90
R004b	335.9	±2.5	600.1	±0.9	175.3	±1.9	25.03	175.75	±1.96	24.94	1	100
R004c	336.1	±1.7	600.3	±0.4	175.4	±1.2	25.03	175.95	±1.25	24.94	40	33
R006a	336.7	±1.0	299.7	±0.8	28.6	±0.4	19.06	27.88	±0.36	19.09	19	12
R007a	336.8	±1.1	399.9	±0.8	68.3	±0.7	20.65	67.60	±0.68	20.76	19	30
R008a	337.2	±0.6	499.5	±0.8	120.3	±0.7	22.62	120.31	±0.65	22.68	19	91

a) Number and type of experiment (GMR = synthesis; R = re-equilibration)
b) Pressure (MPa)
c) Pressure variation (MPa)
d) Temperature (°C)
e) Temperature variation (°C)
f) H_2O fugacity (MPa; Haar et al., 1984; software from Bakker, 2003; http://fluids.unileoben.ac.at)
g) H_2O fugacity variation (MPa)
h) H_2O molar volume ($cm^3 \cdot mol^{-1}$; Haar et al., 1984; software from Bakker, 2003)
i) D_2O fugacity (MPa; Hill et al., 1982; software from Bakker, http://fluids.unileoben.ac.at)
j) D_2O fugacity variation (MPa)
k) D_2O molar volume ($cm^3 \cdot mol^{-1}$; Hill et al., 1982; software from Bakker, http://fluids.unileoben.ac.at)
l) Run-time (days)
m) Number of measured fluid inclusions

The equations of state for H_2O (Haar et al. 1984) and D_2O (Hill et al. 1982) are used to calculate isochores and homogenization temperatures (T_h) of fluid inclusions, from the experimental *P–T* conditions. At 600 °C and 337 MPa (experiments *GMR002c*; *GMR004a*, *b*, *c*; *R002c*; *R004a*, *b*, *c*), pure H_2O fluid inclusions homogenize in the liquid phase at 295.6 °C, whereas pure D_2O inclusions homogenize at 294.6 °C. The minor difference between these T_h values indicates that the isochores in both systems nearly coincide. At 500 °C and 337 MPa, the T_h values are 252.0 °C and 253.4 °C for H_2O and D_2O, respectively. The maximum difference in T_h values is obtained from 400 °C and 337 MPa experimental conditions: 193.4 °C for H_2O and 197.3 °C for D_2O. T_h values of 117.5 °C and 119.3 °C are calculated for H_2O and D_2O, respectively, from experimental conditions of 300 °C and 337 MPa.

Diffusion of H_2O and D_2O

The gradient in chemical potential of H_2O and D_2O between inclusions and the external capsule fluid is directly related to the fugacity gradient, an important parameter which effects bulk diffusion (e.g. Crank 1975). Relative free communication of fluid species between inclusions and external fluid through a quartz crystal would more or less instantaneously result in equalization of fugacities, according to the published theories of diffusion (see Bakker 2009). Extremely low solubility of H_2O in quartz is a major barrier for relative fast diffusion. It is expected that the imposed gradients in H_2O and D_2O fugacity in our experiments result in measurable changes in fluid inclusion density and composition. Bulk diffusion of fluid species in minerals is also controlled by temperature and time, which both may have a major impact on concentration profiles of fluid species in the quartz crystal. The influences of these parameters are investigated in a series of experiments in this study. The length of diffusion path (i.e. distance of fluid inclusions to the crystal surface) and fluid inclusion size are other parameters, which define the amount of inclusion alteration due to diffusion processes. In theory, diffusional changes in fluid inclusion composition are not related to changes in fluid inclusion morphology. The boundary conditions of the diffusion experiments in this study are defined by the geometry of the quartz sample, that is, a short cylinder, where H_2O and D_2O are able to enter the quartz in all directions: along the top or bottom plane and along the side (three-dimensional diffusion). The external fluid in the capsule is regarded as an infinite source and is wetting all sides of the quartz sample during the experimentation.

Experimental results

Up to 100 fluid inclusions of each experiment are photographed for identification purposes and for achieving the morphological properties, mainly the size and the inclusion shape. Each inclusion is analyzed by microthermometry and Raman spectroscopic methods. Each individual fluid inclusion is analyzed before and after re-equilibration (see Appendix B).

Initial experiments

The shapes of the originally synthesized fluid inclusions after 19 days of experimentation show a large variety (Fig. 2) according to the definition of Bakker and Diamond (2006). At 600 °C, about 90 % of all fluid inclusions are defined by a regular shape, varying between elongated and equant. However, the variation in inclusion shape is also large between the different samples that are used in the initial synthesis (c.f. Fig. 2a, b, and c).

Fluid inclusions are formed in the open volume limited by the micro-crack walls that were generated in quartz by thermal shock before experimentation; therefore, the size and shape of these cracks are important factors that determine this variability. At 500 °C (Fig. 2d), 85 % of all fluid inclusions have regular shapes. This percentage decreases further at lower experimental temperatures: 67 % at 400 °C (Fig. 2e) and only 60 % at 300 °C (Fig. 2f).

The measured fluid inclusions of all synthesis experiments (*GMR002c*; *GMR004a*, *b*, *c*; *GMR006a*; *GMR007a*; and *GMR008a*) reveal similar freezing and melting behavior (see Appendix B): Ice-melting temperatures vary between +0.1 and -0.1 °C in all measurements, which reflects the accuracy of microthermometry. The experiments at 600 °C and 337 MPa reveal average T_h of 293.2, 293.1, 292.7, and 293.8 °C (all within the liquid phase) for *GMR002c*, *GMR004a*, *b*, and *c*, respectively (Table 2, Fig. 3a). The variability in these temperatures is about ±5 °C. The experiments at 300, 400, and 500 °C reveal T_h's of 130.9, 200.8, and 254.3 °C for *GMR006a*, *GMR007a*, and *GMR008a*, respectively (Table 2).

The liquid–vapor ratio, that is, the volume fraction of the vapor phase in individual fluid inclusions at room temperatures and the measured homogenization temperatures, is compared in Fig. 3b. Both parameters are measures of the molar volume (or density) of fluid inclusions. According to Bakker and Diamond (2006), the area fraction (a_{vap}) of the vapor phase in two-dimensional images of regular-shaped fluid inclusions can be used as a measure of volume fraction. The T_h histogram (Fig. 3a) illustrates a relative narrow range with a mode (maximum frequency) between 293 and 294 °C and has passed the Shapiro–Wilk normality test (Shapiro and Wilk 1965); wherefore, a normal distribution of the T_h values can be recognized. The a_{vap} histogram (Fig. 3b) has a relative broad spread, between 15 and 40 %, with a mode between 20 and 25 %. The gray-shaded bar (26–27 %) in Fig. 3b indicates a_{vap} values that are calculated directly with homogenization temperatures (mode values) of this synthesis. The variability in shape of fluid inclusions results in a broad spread of a_{vap} values, and the statistical mode appears at slightly lower values than the calculated values from T_h. This observation is conform to the study of Bakker and Diamond (2006), who illustrated that irregular-shaped fluid inclusions always have smaller numbers on area fractions of vapor bubbles in two-dimensional images than on volume fractions. It also illustrates that T_h measurements result in more accurate molar volume estimations than area fraction measurements, if a reliable equation of state is available for the fluid system in inclusions that is able to transform these temperatures into molar volumes.

Morphological modifications of fluid inclusions after re-equilibration

Each sample in this study is re-equilibrated at the same pressure and temperature conditions as the initial synthesis to avoid any stress component in the crystal lattice surrounding the fluid inclusions. After re-equilibration, some of the inclusions show notable morphology changes (Figs. 2, 4). Originally synthesized irregular and elongated inclusions tend to become more equant and regular during re-equilibration process. Originally equant and regular inclusions tend to become negative crystal-shaped. The extend of morphological changes is dependent on the re-equilibration time. At 600 °C, after 5 days of re-equilibration (*R002c*, Figs. 2a, 4b), only relatively small changes in the shape distribution field can be detected and most fluid inclusions are

regular, either elongated or equant. More notable changes occur after a re-equilibration time of 19 days (*R004a*, Figs. 2b, 4c).

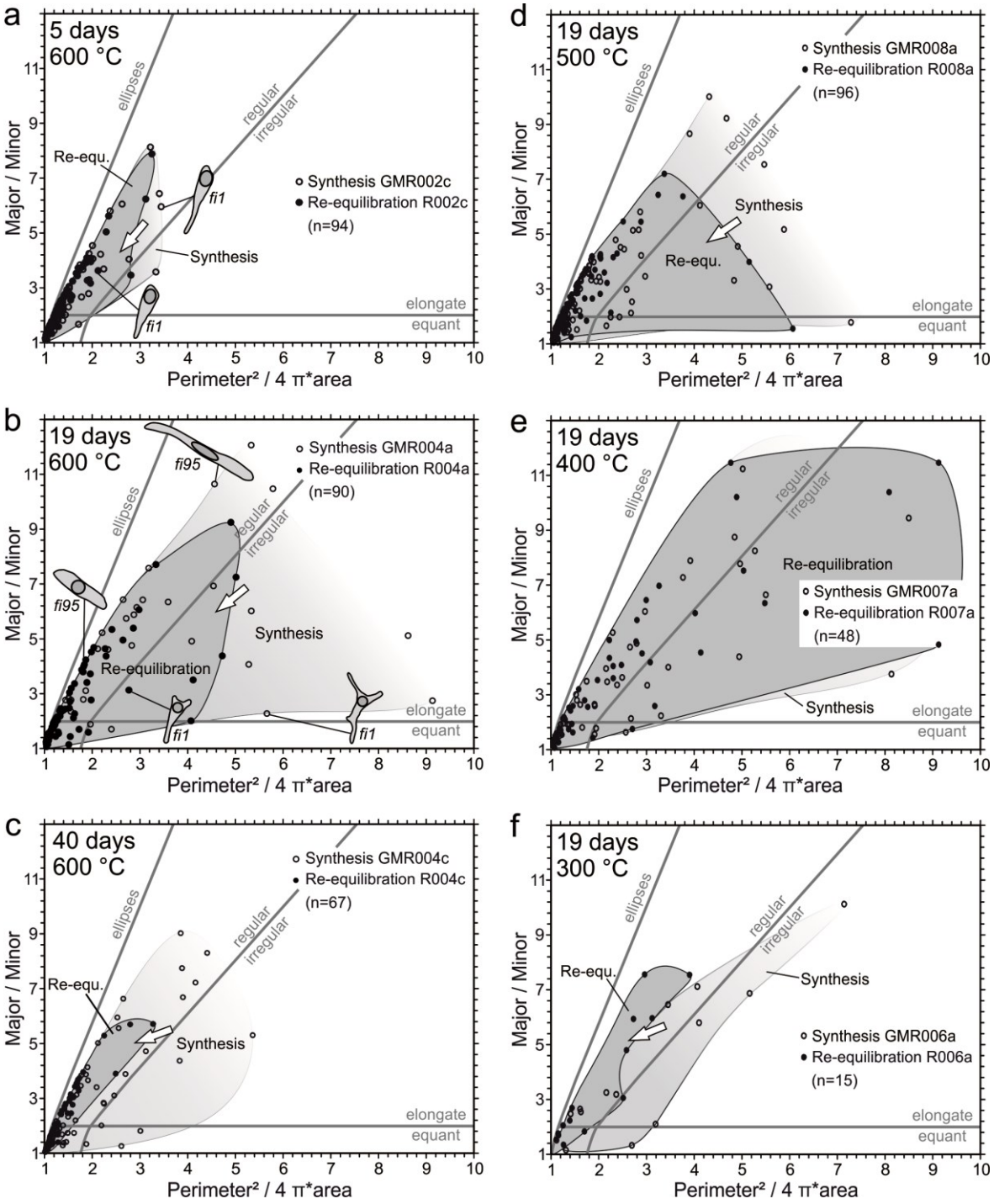

Fig. 2 Fluid inclusion shape classification diagrams of the experiments. The open circles are measurements after the original synthesis; the filled circles represent the same inclusions after re-equilibration. The run-times of the synthesis experiments are 19 days. Inclusion shapes at experimental conditions at 600 °C and 337 MPa are illustrated after 5 days (**a**), 19 days (**b**) and 40 days (**c**) of re-equilibration. Nineteen-day experimental run-times (re-equilibration experiments) are compared at different temperatures in **b** 600 °C, **d** 500 °C, **e** 400 °C, and **f** 300 °C. The open arrows indicate a general shift in fluid inclusion shape changes of the re-equilibrations. *fi1* in **a** illustrates the change in shape of an individual fluid inclusion at 600 °C, 337 MPa after 5 days re-equilibration. A much larger shift of individual *fi*'s is illustrated in **b**; *fi1* and *fi95*

Elongation and irregularity of fluid inclusions are clearly reduced toward more regular and equant shapes. The 40-day re-equilibration experiment (*R004c*, Figs. 2c, 4d) reveals the most regular fluid inclusions. After recrystallization of the inclusion walls in this re-equilibration experiment, the entire assemblage is defined as regular inclusions, with a maximum elongation of about 6 (major/minor ratio of best-fit ellipse, see Bakker and Diamond 2006).

The change in fluid inclusion shape after 19 days of experimentation is compared at a variety of temperatures: 300, 400, 500, and 600 °C (Figs. 2b, d–f, 4c, e–g). The amount of change of individual inclusions decreases to lower experimental temperatures. At 600 °C, the shape distribution field is clearly reduced after re-equilibration, whereas at 500 °C, the reduction is relatively less, and at 400 °C, there is no change in the shape distribution field (c.f. Fig. 2b, d, e). In contrast, at 300 °C (Fig. 2f), the shape distribution displays a relatively large reduction after re-equilibration. The low number of analyzed fluid inclusions (15) does not represent an extensive statistical examination and may cause a distortion of the shape distribution field.

Changes in total volume are not identified within two-dimension images of all analyzed fluid inclusions and can be excluded because of the absence of any stress or pressure gradients around inclusions. The dimensions of all fluid inclusions do not seem to have changed after re-equilibration.

Density and compositional changes of fluid inclusions after re-equilibration

Noticeable changes in H_2O-D_2O composition of initially synthesized inclusions are obtained in all re-equilibration experiments at 600 and 500 °C, whereas changes are not detected in experiments at 400 and 300 °C (all experimental data are presented in the Appendix B). Changes in composition of fluid inclusions are already detected after a relatively short re-equilibration time (e.g. 1 day, R004b). The changes are measured in terms of ice-melting temperatures and homogenization temperatures (Figs. 5, 6, 7).

At 600 °C (Fig. 5), four re-equilibration experiments were performed in 1 day (*R004b*), 5 days (*R002c*), 19 days (*R004a*), and 40 days (*R004c*). Fluid inclusions that have completely exchanged their H_2O content with D_2O at a constant total volume at experimental conditions must end up in the point at T_m(ice) = +3.8 °C and ΔT_h = –1.3 °C in Fig. 5. At an equal exchange rate of one molecule H_2O diffusing outward and one molecule D_2O diffusing inward, all possible pairs of T_m and T_h must be positioned on the inclined dashed line in Fig. 5. Minor amounts of D_2O (maximal 11 mol %) are already detected after 1 day of re-equilibration (Fig. 5a), as deduced from an increase of maximally 0.4 °C of T_m(ice). A decrease in bulk density is evidenced by an increase in T_h, with maximally +1.3 °C, which illustrates the loss of H_2O. These results prove that the gain of D_2O is a slower process than the loss of H_2O after 1 day. This unexpected shift becomes even more prominent after 5 days of experimentation (Fig. 5b): T_m(ice) reaches maximum values of +1.8 °C (47 mol % D_2O), illustrating diffusion of D_2O into fluid inclusions; and T_h values shift maximally to +4.9 °C, illustrating a loss in density, or a faster outward diffusion of H_2O than inward diffusion of D_2O. Inclusions with a low D_2O content, that is, lower T_m(ice), reveal a higher shift in T_h than inclusions with a high D_2O content. After 19 days of re-equilibration (Fig. 5c), D_2O contents have reached a maximum value of 63 mol %, corresponding to T_m(ice) of +2.4 °C. In contrast to the 5-day re-equilibration experiments, T_h's have a much lower positive shift and become even negative for inclusions

with higher D_2O contents. The temperature changes are approaching the equal exchange conditions, as continuous D_2O diffusion is slowly drawing level with the faster H_2O diffusion. After 40 days of re-equilibration (Fig. 5d), all microthermometric measurements are positioned on the mixing line between the two end members: starting conditions (0.0 °C) and the end point (+3.8, -1.3 °C). These four re-equilibration experiments at 600 °C illustrate that fluid inclusion modifications are not uniform, and a whole range of D_2O contents and density changes are detected for each experiment. Likely, the controlling factors for these changes are diffusion processes through quartz and depend on the size and distance to the grain boundary of individual inclusions. These re-equilibration experiments also illustrate that data obtained in relative short experimental run-times (less than 19 days) may lead to incorrect interpretations of processes, because changes in homogenization temperatures occur in the opposite direction.

Table 2 Homogenization temperatures from initial experiments and re-equilibration experiments, melting temperatures with corresponding D_2O content after re-equilibration

a	b	c	d	e	f	g	h	i	j
GMR002c	293.2	+4.6	-1.8	R002c	295.7	+4.9	-1.5	1.8	47
GMR004a	293.1	+2.5	-4.6	R004a	293.5	+2.4	-4.2	2.4	63
GMR004b	292.7	+3.1	-2.2	R004b	293.1	+3.1	-2.2	0.4	11
GMR004c	293.8	+3.0	-3.4	R004c	293.2	+1.9	-1.8	2.4	63
GMR006a	130.9	+5.9	-4.9	R006a	130.4	+6.1	-4.7	0.0	0
GMR007a	200.8	+4.2	-2.4	R007a	201.3	+2.3	-1.8	0.0	0
GMR008a	254.3	+5.1	-4.9	R008a	254.6	+4.6	-4.2	1.0	26

a) Synthesis experiment
b) Mean T_h (homogenization temperature) initial synthesis (°C)
c) Maximum T_h – mean T_h initial synthesis (°C)
d) Mean T_h – minimum T_h initial synthesis (°C)
e) Corresponding re-equilibration experiment
f) Mean T_h re-equilibration (°C)
g) Maximum T_h – mean T_h re-equilibration (°C)
h) Mean T_h – minimum T_h re-equilibration (°C)
i) Maximum T_m (melting temperature) re-equilibration (°C)
j) Maximum mole% D_2O

The re-equilibration experiment at 500 °C with a runtime of 19 days at 337 MPa (Fig. 6) shifts T_m(ice) to a maximum value of +1.0 °C, which corresponds to 26 mol % D_2O. The T_h increase to positive values with a maximum of +1.6 °C. The changes in microthermometric temperatures are much less compared with the experiments at 600 °C and 19 days run-time (c.f. Fig. 5c). At equal exchange conditions, all pairs of T_m and ΔT_h must be positioned on the mixing line between the starting point (0.0 °C) and the endpoint at T_m(ice) = +3.8 °C, ΔT_h = +1.4 °C, which corresponds to a complete replacement of H_2O by D_2O in fluid inclusions (inclined dashed line in Fig. 6). Similar to the experiment at 600 °C, ΔT_h changes to slightly higher values than expected from the mixing line, which illustrates again that H_2O is faster diffusing out of fluid inclusions than D_2O is diffusing in.

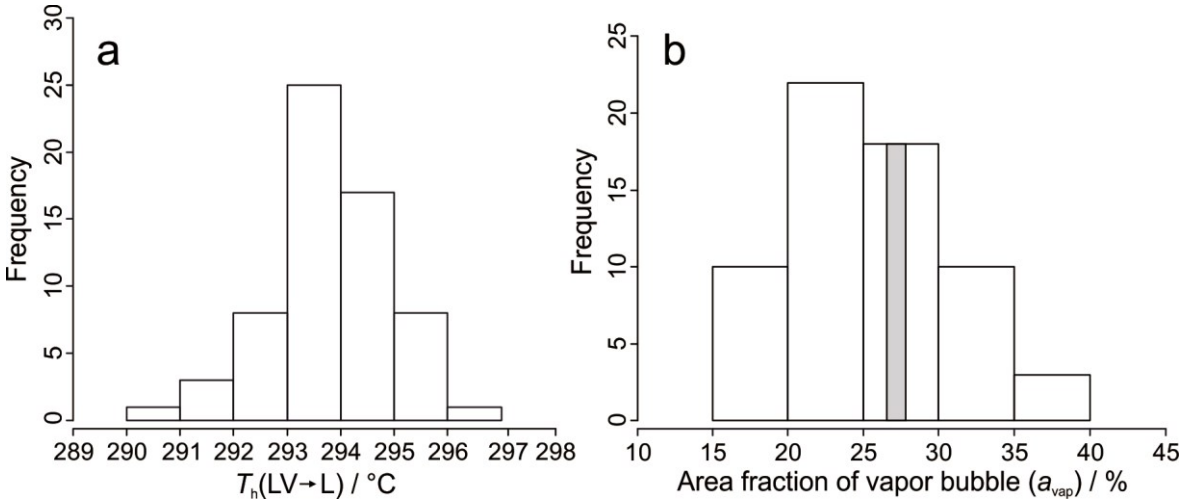

Fig. 3 The histograms (n = 63) are exemplarily illustrated based on the data of the experiment *GMR004c*. **a** The histogram shows the T_h range from 290.4 to 296.8 °C with a median of 293.7 °C and a mode of 293–294 °C. **b** Illustration of the a_{vap} with the broad spread between 15 and 40 % and the mode of 20–25 %. The gray-shaded bar shows the calculated a_{vap} value based on the T_h values of this synthesis illustrated in **a**. Detailed fluid inclusion properties are summarized in Table 2

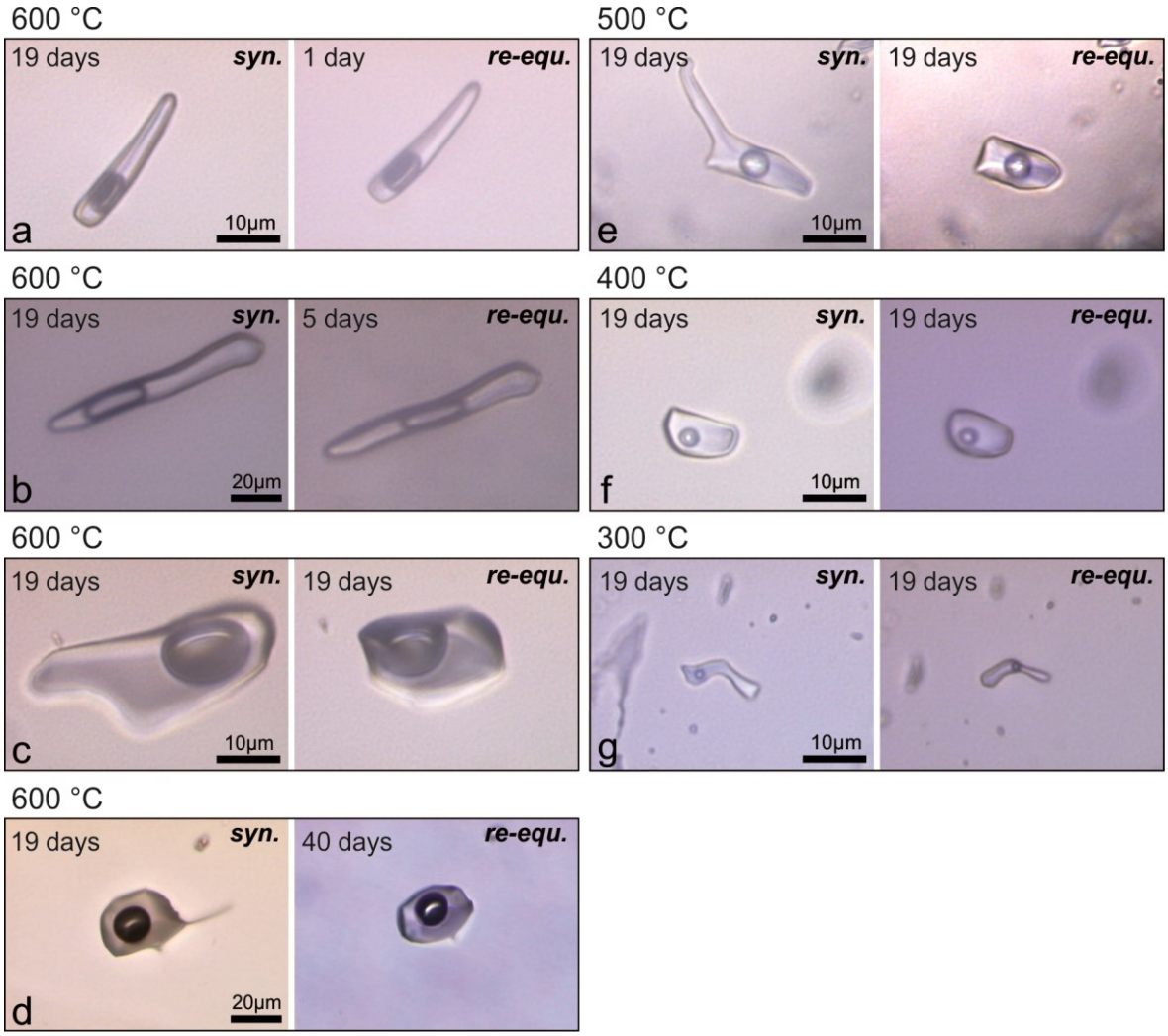

Fig. 4 Photomicrographs of the same inclusions before (syn. = synthesized) and after (re-equ. = re-equilibration) the re-equilibration experiment at 600 °C (**a–d**), 500 °C (**e**), 400 °C

(**f**), and 300 °C (**g**). Different run-times are illustrated at 600 °C: (**a**) 1 day; (**b**) 5 days; (**c**) 19 days; and (**d**) 40 days. The synthesis and re-equilibration experiments illustrated are **a** *GMR004b–R004b*, **b** *GMR002c–R002c*, **c** *GMR004a–R004a*, and **d** *GMR004c–R004c*. Experiments with equal re-equilibration times and different temperatures are shown in **e** *GMR008a–R008a*, **f** *GMR007a–R007a*, and **g** *GMR006a–R006a*

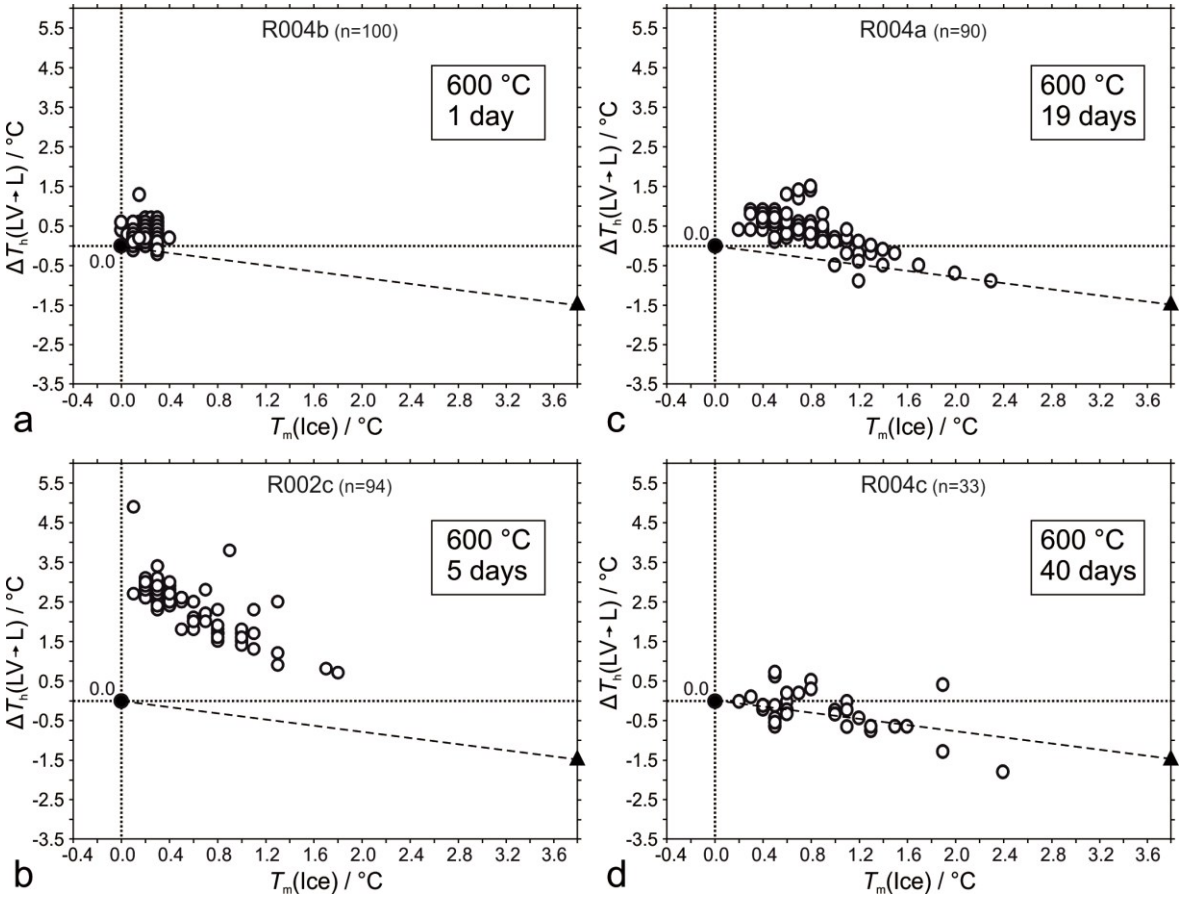

Fig. 5 Ice-melting temperatures and change in homogenization temperatures of re-equilibrated fluid inclusions at 600 °C and 337 MPa. **a** After 1 day of re-equilibration; **b** after 5 days of reequilibration; **c** 19 days of re-equilibration; and **d** after 40 days of experimentation. ΔT_h of -1.3 °C indicates the maximum negative shift of homogenization temperature with a fluid inclusion composition of 100 mol % D_2O, T_m(ice) = +3.8 °C, respectively. (see text for further detail)

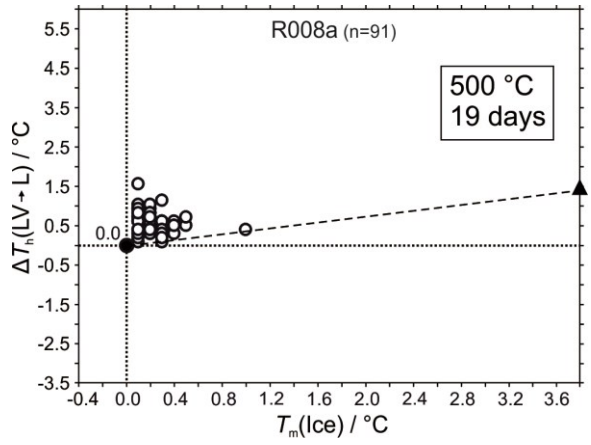

Fig. 6 Ice-melting temperatures and change in homogenization temperatures of re-equilibrated fluid inclusions at 500 °C and 337 MPa after 19 days of experimentation. ΔT_h of +1.6 °C indicates the maximum positive shift of homogenization temperature with a fluid inclusion composition of 100 mol % D_2O, T_m(ice) = +3.8 °C, respectively. (see text for further detail)

In respect to the temperature-depended diffusion phenomena, four experiments have been performed with the same run-times (19 days) at 337 MPa and at different temperatures: 300, 400, 500, and 600 °C (Fig. 7).

Considerably, changes in composition (up to 26 mol % D_2O) of the initially entrapped fluid are detected after re-equilibration at 500 °C, whereas at 600 °C, inclusions may contain up to 63 mol % D_2O. Compositional changes in fluid inclusions are not detected in the experiments at 300 and 400 °C. Consequently, it is expected that the threshold temperature of fluid inclusion re-equilibration is around 450 °C, whereas complete adjustment to external condition is obtained at temperatures above 650 °C.

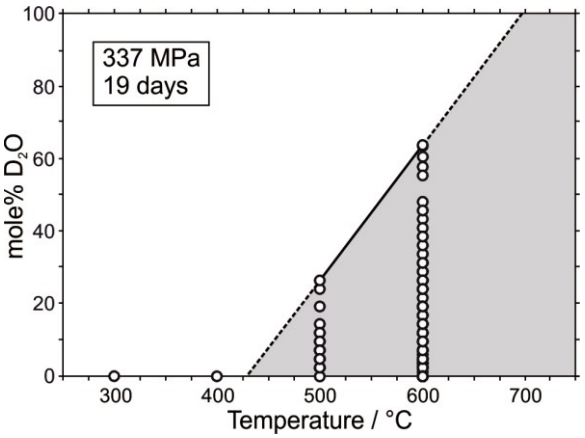

Fig. 7 D_2O contents (mole %) of fluid inclusions after the re-equilibration processes at 337 MPa and 19 days of experimentation time at 300, 400, 500, and 600 °C. The inclined solid line illustrates the maximum D_2O concentration in fluid inclusions. Extrapolation to lower temperatures (dashed line) indicates a threshold temperature of diffusion around 450 °C, whereas a complete exchange of D_2O is reached around 650 °C after 19 days of experimentation at 337 MPa. The gray area illustrates the range of D_2O concentration that is observed in the present experiments

Concentration profiles: depth and size relation

As the position of each investigated fluid inclusion within the quartz crystal is measured (see Appendix B), the accordant composition can be plotted in concentration profiles that are related to the depth, considering the distance to the crystal surface (i.e. top or bottom of the short quartz cylinder). Data of the experiment at 600 °C (Fig. 8) illustrate that at specific depths variations in D_2O concentration can be measured in terms of T_m(ice), and that an envelope can be constructed which indicates the limit of maximum concentration. With increasing distance to the crystal surface, the maximum concentrations of D_2O in re-equilibrated fluid inclusions are decreasing. After 1 day of re-equilibration at 600 °C (Fig. 8a), deep inclusions reveal the same concentration of D_2O as shallow inclusions, and a relatively flat maximum concentration profile can be drawn, with the maximum T_m(ice) at +0.4 °C (10 mol % D_2O). Concerning the longer run-time experiments at 600 °C (5, 19, and 40 days in Fig. 8b–d), a shift of the respective envelope is recorded. After longer run-times, the shallow inclusions reach maximum compositional change (approaching a pure D_2O content) earlier than deep inclusions. For example, inclusions at about 225 µm depth reach a maximum D_2O concentration (39 mol % D_2O) corresponding to T_m(ice) = +1.5 °C after 40 days (Fig. 8d), whereas inclusions at about 110 µm depth reach this concentration already after 19 days (Fig. 8c). Inclusions at 100 µm depth display a continuous increase in maximum T_m(ice) values from +0.4, +1.0, +1.6 to +2.4 °C after 1, 5, 19, and 40 days, respectively. It should be noted that at specific depths, the D_2O concentrations vary between a maximum value, which defines the envelope, and a minimum value. This minimum D_2O concentration is only slowly shifting to higher values at higher experimentation run-times (c.f. Fig. 8b, c). The range of values indicates that there is another important parameter

that defines the concentration of D_2O in re-equilibrated fluid inclusions, in addition to the path-length of diffusion.

The envelopes of maximum D_2O concentration are summarized in the concentration profile in Fig. 9a to illustrate the development of the profile by direct comparison of different experimental run-times.

In addition, Fig. 9b illustrates the temperature effect for equal run-time experiments (19 days). The envelope at 500 °C reaches much lower T_m(ice) values at a specific depth than the envelope at 600 °C. Changes in composition are not detected at 300 and 400 °C at any depth (Fig. 7).

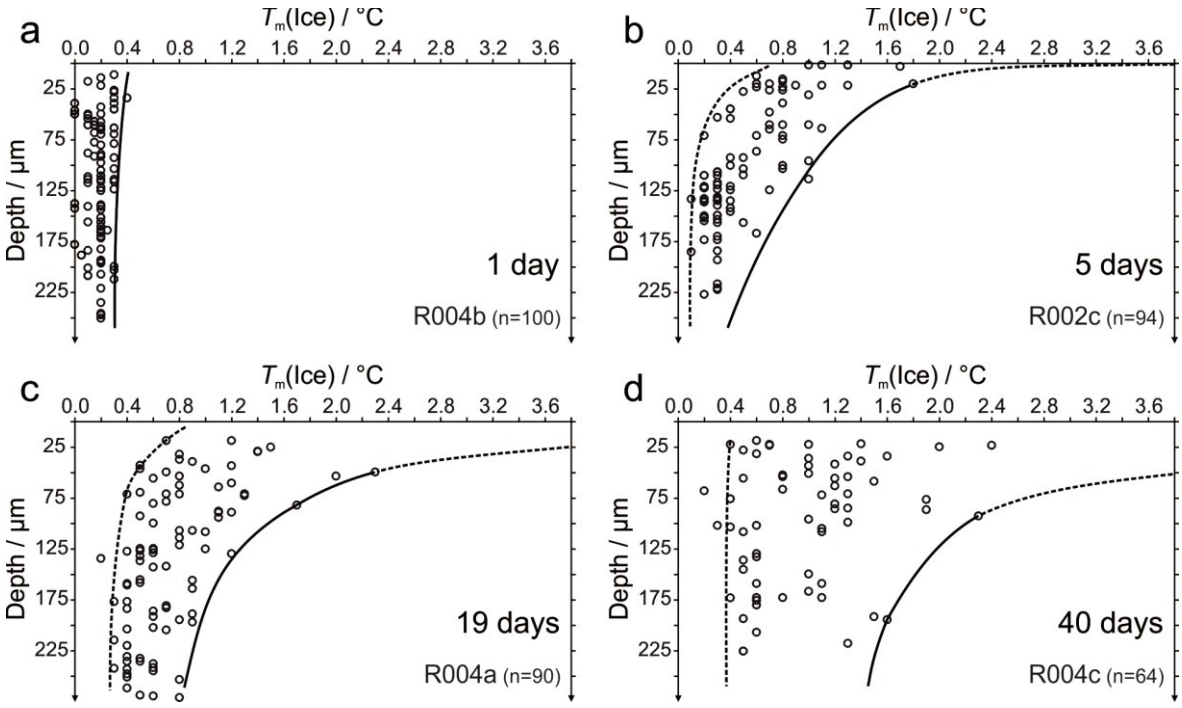

Fig. 8 Concentration profiles in terms of T_m(ice) values after re-equilibration of fluid inclusions at 600 °C and 337 MPa after **a** re-equilibration time of 1 day (*R004b*); **b** re-equilibration time of 5 days (*R002c*); **c** re-equilibration time of 19 days (*R004a*); and **d** re-equilibration time of 40 days (*R004c*). The dashed and solid curves indicate the boundary of maximum and minimum melting temperatures. Each experiment shows the effect of depth, that is, distance of fluid inclusion to the crystal surface

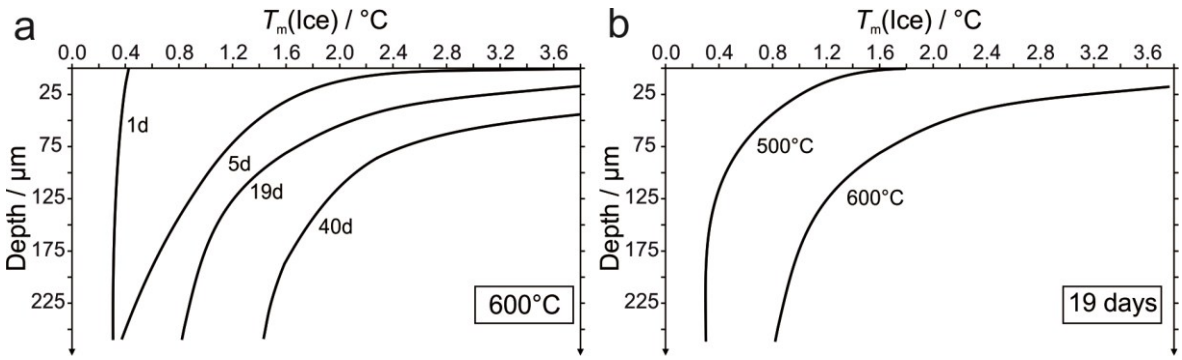

Fig. 9 Maximum concentration profiles (solid lines) in terms of T_m(ice) values at 600 °C and 337 MPa; **a** with variable experimental run-times (1, 5, 19, and 40 days). The concentration profiles are shifting to higher T_m(ice) values with progressing experimentation time. **b** a comparison of maximum concentration profiles at 600 and 500 °C with 19-day experimental run-time

The second parameter that influences the concentration profile is the size of fluid inclusions. The size of inclusions at approximately equal depth is plotted against their T_m(ice) value for the experiment at 600 °C and 337 MPa in Fig. 10. Variable concentrations at equal depth as shown in Fig. 8c for 19 days run-time are reflecting the size of fluid inclusions: Small inclusions have a higher D_2O content than large inclusions (Fig. 10a). This is clearly illustrated by fluid inclusions at approximately 75 µm depth (interval 69–80 µm) and 25 µm depth (interval 19–29 µm) after the re-equilibration experiment (Fig. 10a). Inclusions at ±25 µm depth show a less variable D_2O content, that is, smaller inclusions are only slightly enriched in D_2O compared with larger inclusions, but have much higher D_2O concentrations than inclusions at 75 µm depth. The smallest inclusions have the highest D_2O concentrations and are similar in both depth intervals, which indicate that these inclusions re-equilibrate in a similar way independent from the distance to the surface. After 40 days of re-equilibration (Fig. 10b), the D_2O content at all depths is similar and mainly dependent on the size of the fluid inclusions. The inclusions at approximately 25 µm depth (interval 20–29 µm) have a larger variation in D_2O content than the inclusions from the 19 days experiment and reach much higher values (up to 63 mol % D_2O). Inclusions at 100 µm depth (interval 96–105 µm) in the 40-day experiment (Fig. 10b) have similar concentrations as inclusion from the 19-day experiment (c.f. 75 µm depth, Fig. 10a), however, within a much larger range of inclusion sizes.

Discussion

Diffusion model

The mobility of H_2O and D_2O through quartz crystals at constant temperature and pressure conditions is visualized at about 337 MPa and 500–600 °C in this study. The isotopic composition of fluid inclusions is relatively easily changed at these temperatures, without opening (cracking) or deforming the inclusion walls. The fugacity gradients of both H_2O and D_2O are the only active driving forces in these re-equilibration experiments of fluid inclusions. Diffusion of fluid components through a solid quartz crystal, as interstitial particles or substitute particles, is the only process that is triggered by this gradient in our experiments, according to Fick's law. Several types of diffusion within quartz are described in the literature (see Bakker 2009 and reference therein). Diffusion of H_2O along dislocation lines (''pipe diffusion'') or other crystal defect structures is supposed to play an important role in re-equilibration experiment with additional pressure gradients that result in local deformation adjacent to fluid inclusions (e.g. Bakker and Jansen 1990, 1994; Audétat et al. 1999). This type of diffusion can be excluded in our experiments due to the absence of pressure gradients. Other types of diffusion can be summarized as bulk diffusion, which includes ''self-diffusion'' (e.g. Farver and Yund 1991) and ''tracer-diffusion'' (e.g. Kronenberg et al. 1986). It is assumed that bulk diffusion is the dominant process in our experiments. A variety of parameters that play a significant role in bulk diffusion processes are as follows: (1) gradient in chemical potentials of fluid components (i.e. concentration gradients) between inclusions and external pore fluids; (2) temperature and pressure; (3) experimental run-times; (4) distance of inclusions to crystal surfaces; and (5) inclusion size. These are exactly the parameters that are measured and defined in our experiments; consequently, our data can be used to calculate diffusion coefficients in a mathematical model

as illustrated by Bakker (2009). Diffusion coefficients can be used to calculated concentration profiles of fluid components in quartz and fluid inclusions at variable temperatures and selected experimental runtimes. Moreover, concentration profiles can be calculated at a geological time scale, because diffusion constants are time-independent.

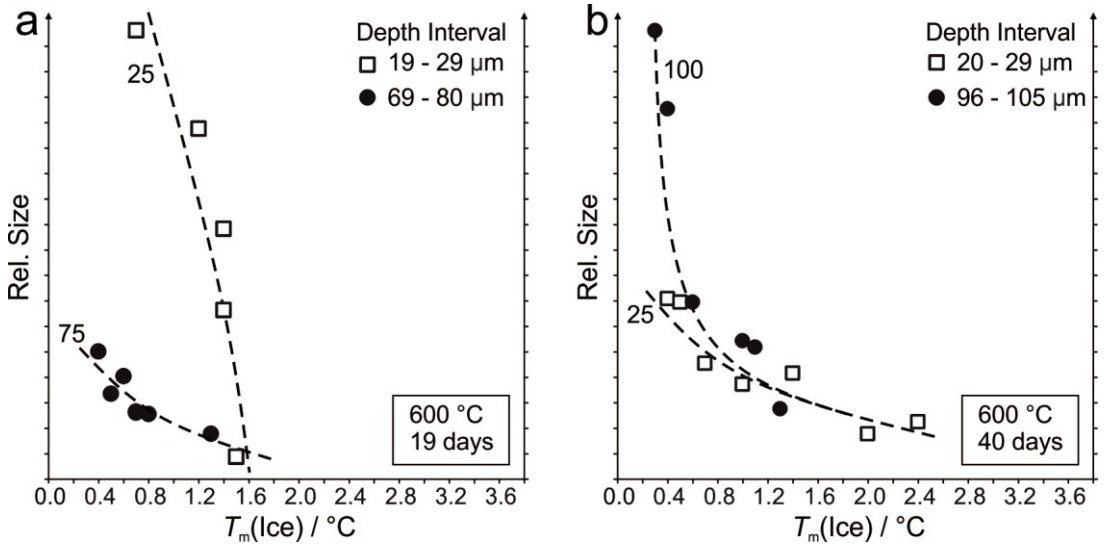

Fig. 10 T_m(ice) values versus relative size of fluid inclusions of the re-equilibration experiment *R004a* (**a**) at 600 °C and 19-day run-time and *R004c* (**b**) at 600 °C and 40 days runtime. Inclusions are selected at approximately 25 and 75 µm depth in **a**, and at approximately 25 and 100 µm depth in **b**. The dashed lines illustrate general trends in concentration dependent on inclusion size at constant depths

The bulk diffusion model developed by Bakker (2009) is used to determine the diffusion coefficient of H_2O and D_2O. It is assumed that the solubility of H_2O and D_2O is similar in quartz (4.4 µmol per Si), and both have similar diffusion coefficient. Furthermore, it is assumed that the fluid mixture of H_2O and D_2O in inclusions behaves like an ideal mixture at experimental condition, in order to be able to determine the individual fugacity coefficients of H_2O and D_2O. The geometry of our quartz crystal (short cylinder) differs from a spherical crystal in the model of Bakker (2009); however, the use of a three-dimensional diffusion model is preferred in our approach, and the deviating geometries have only a minor effect on the estimated concentration profiles. Concentration profiles are calculated for a 5-µm-diameter fluid inclusion after 1 and 19-day experimentation run-time at 600 °C and 337 MPa (Fig. 11a), by varying the diffusion coefficient until a similar profile is obtained as illustrated in Fig. 8a, c. The hypothetical concentration profiles in Fig. 11a are consistent with our experimental data by using a diffusion coefficient of about 10^{-14} m^2 s^{-1}. Minor differences after 1 day of experimentation can be explained by the difference in H_2O and D_2O diffusion coefficients. Our experimental data evidence that H_2O is faster diffusing than D_2O, which is mainly noticeable in short run-time experiments (Fig. 5). After 19 days of experimentation, the concentration profile that is calculated with the same diffusion coefficient fits even better our experimental data and is not anymore affected by small difference in H_2O and D_2O diffusion coefficients. The value of the H_2O diffusion coefficient in our experiments is a factor 100 lower than the values estimated for hydrogen diffusion in the β-quartz field at higher temperatures and pressures (see Bakker 2009 and references therein).

The experimentally determined variable D_2O concentration in fluid inclusions at equal depth is mainly defined by fluid inclusions size: Small inclusions are richer in D_2O than large inclusions (Fig. 10). The fluid inclusion size parameter is tested with the bulk diffusion model that is used in the previous paragraph to estimate the diffusion coefficient. At 600 °C and 19-day experimentation runtime, the modeled D_2O concentration at 75 µm and 50 µm depth has a minor variation as a function of inclusion size, which confirms the observation that larger inclusions are less affected than smaller inclusions (Fig. 11b).

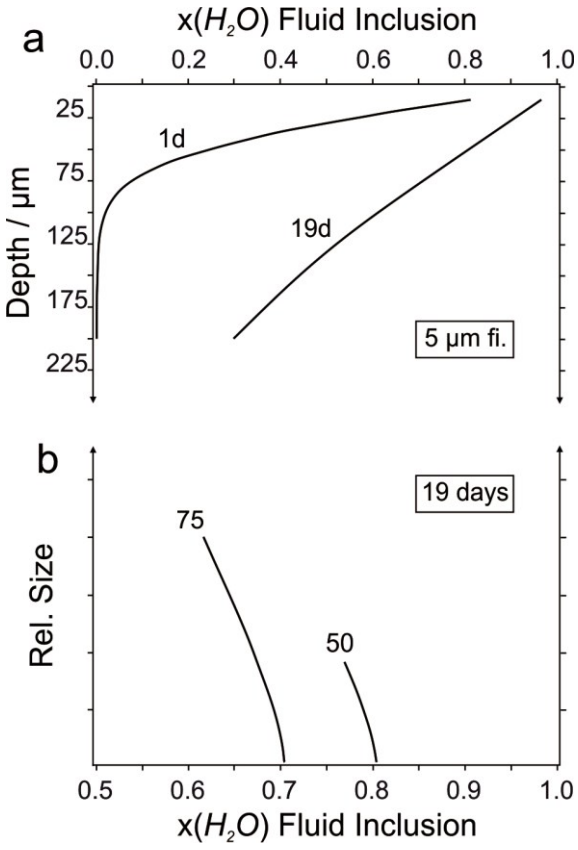

Fig. 11 H_2O concentration profiles calculated according to the bulk diffusion model of Bakker (2009). **a** for 5-µm-diameter fluid inclusions after 1 and 19 days of experimentation; **b** after 19 days of experimentation and variable inclusion sizes at 50 lm depth and 75 µm depth. (see text for further details)

However, the amount of change in D_2O content does not correspond to our observations (c.f. Fig. 11b, 10). The bulk diffusion model is based on specific boundary conditions, which include geometry definition, radial non-steady state diffusion, infinite external fluid source, solubility of H_2O in quartz, and a distribution coefficient (*K*) that defines the partitioning of D_2O/H_2O in quartz and fluid inclusions (see Appendix A in Bakker 2009). The *K* coefficient has a major impact on the calculation of D_2O concentrations in fluid inclusions. The value of *K* was theoretically estimated (see Bakker 2009) and related to the partial molar volume of H_2O in quartz. The *K* coefficient can also be related to fluid inclusion size, and preliminary calculations have indicated that concentration profiles as illustrated in Fig. 10 can be reproduced with the same diffusion coefficient that was estimated in the previous paragraph (10^{-14} m^2 s^{-1}). Modeling of the *K* coefficient will be presented in following studies.

Natural fluid inclusions

The results of our study illustrate that fluid inclusions can be re-equilibrated in relatively short experimental runtimes at elevated temperatures and pressures. The hydrogen isotope composition of fluid inclusions can be adjusted instantaneously to external fluid conditions in a geological time scale. It is important to emphasize the differences between experimental work and processes that may occur in natural rock. Our experimental studies are focused on the effect of one parameter, that is, fugacity gradient, and the experimental setup is designed to optimize processes that are induced by this gradient, whereas other parameters remain constant. The experiments have illustrated what a fugacity gradient can provoke in seemingly isolated fluid cavities within anhydrous crystals. In natural rock, the porosity is defining the existence of a

fluid phase, and natural quartz grains are not completely surrounded by pore space with an infinite fluid source. The porosity decreases with increasing depth, therefore, sedimentary rocks have a larger fluid source than metamorphic and magmatic rocks. Size and shape of the pores, in addition to the network of pores, define the availability of the external fluid source in natural rock. Pores may cover 50 area % of the quartz surface in sedimentary rock and down to a few percentages (or less) in metamorphic rock. Diffusion of external fluids into quartz grains can only occur at pore–grain interfaces and will mainly effect those inclusions that are closer to this interface, whereas inclusions near grain–grain interfaces may not be effected. Otherwise, a threshold temperature of about 450 °C at 337 MPa is identified for diffusion processes in this study, which become more efficient at higher temperatures. In other words, sedimentary rocks have a large fluid source available, but temperatures may not reach values for efficient fluid inclusion re-equilibration, whereas metamorphic rocks contain sufficient heat but have low porosities. Nevertheless, interpretation of hydrogen isotope analyses of fluid inclusions in metamorphic and magmatic rocks must include the possibility of fluid inclusion re-equilibration.

Other re-equilibration experiments

The significance of fluid inclusion re-equilibration is already considered since the first knowledge on fluid inclusion properties (e.g. Brewster 1845). The first experimental evidence that fluid inclusions may be affected by changes in fluid density and the development of inclusion haloes is given by Lemmlein (1956), Leroy (1979), and Pecher (1981). The processes that have been proposed in the literature to change the properties of fluid inclusions are as follows: (1) diffusion; (2) recrystallization; (3) stretching; (4) deformation; and (5) decrepitation. The driving forces of these processes are heat, concentration gradients, and pressure gradients. Re-equilibration studies of fluid inclusions are mainly performed with a pressure gradient, that is, a pressure difference between fluid inclusions and an external fluid pressure medium (e.g. Sterner and Bodnar 1989; Bakker and Jansen 1990; Vityk and Bodnar 1995). Occasionally, these experiments have been combined with a concentration gradient, that is, a gradient in chemical potentials between fluid components in fluid inclusions and the external fluid. The observed changes in fluid inclusions (i.e. shape, density, and composition) are defined by the sum of all these processes that are activated by these driving forces. However, the effect of individual processes cannot be quantified because these experiments include abundant independent and unrestrained parameters. For example, isothermal decompression of quartz samples with pure H_2O fluid inclusions results in internal overpressures, which may cause stretching, deformation, and decrepitation (e.g. Sterner and Bodnar 1989). The decompression is also accompanied with a change in fugacities in the experimental capsule fluids, which may cause diffusion. Fugacity gradients are intensified if the composition of the capsule fluid is modified. Density and compositional changes of fluid inclusions are caused by these simultaneously operating processes, but it is not possible to identify the importance of individual processes in these experiments, and there is no unambiguous relationship between cause and result.

Sterner et al. (1995), Bakker and Diamond (2003), and Bakker (2007) provide the only examples of re-equilibration experiments at constant temperature and pressure with exclusively gradients in fluid shape by

component fugacities. The re-equilibration experiments in Sterner et al. (1995) are all performed within the β-quartz stability field at high temperatures and 300 MPa and short run-times (4 days). The lack of sufficient information and data presented, in addition to a number of inconsistencies, does not allow re-evaluation of these results. Bakker and Diamond (2003) and Bakker (2007) provided systematic studies on reequilibration of fluid inclusions as a result of gradients in chemical potentials at constant pressure and temperature. A similar experimental setup is applied in the present study: The number of possible processes that may play a role in re-equilibration experiments is reduced and changes in fluid density and composition can be directly related to changes in homogenization and melting temperatures, due to the availability of accurate equations of the fluid state (H_2O and D_2O). Moreover, experimental conditions are within the a-quartz stability field, to exclude any fluid inclusion changes that are induced by the α–β phase transition of quartz.

Conclusions

Synthetic H_2O-rich fluid inclusions in quartz have been re-equilibrated in a pure D_2O pore fluid environment at 600 °C and 337 MPa. A gradient in fugacity is superimposed in the experimental setup in order to provoke diffusion of H_2O and D_2O, whereas other parameters such as pressure gradient and deformation are excluded. In addition, experiments at 500, 400, and 300 °C with a constant pressure of about 337 MPa are performed to estimate the efficiency of temperature on diffusion processes.

The original synthesized fluid inclusions reveal only minor morphological changes, which are mainly determined experimentation time. Re-equilibration experiments at 40 days reveal more equant to negative crystal shape inclusions than 1 or 5-day experiments. A total volume increase or decrease could not be detected in individual fluid inclusions.

The effect of diffusion through quartz is illustrated by the change in H_2O–D_2O composition of fluid inclusions at nearly equal densities. The D_2O content in fluid inclusions is obtained from ice-melting temperatures, whereas changes in density are obtained from total homogenization temperatures.

At 600 °C and 337 MPa, 1- and 5-day re-equilibrations illustrate that H_2O is faster diffusing out of inclusions than D_2O is diffusing into inclusions. This process also results in a decrease in density of these inclusions. After 19- and 40-days re-equilibration, D_2O concentration reaches values up to 63 mol %, whereas the density is restored to original values that correspond to the experimental temperature–pressure conditions.

The 19-day re-equilibration experiments are performed at 300, 400, 500, and 600 °C, and a constant pressure of 337 MPa. Maximum D_2O concentration at 600 °C is about 63 mol %, whereas at 500 °C, values are obtained of maximally 27 mol %. D_2O is not detected in fluid inclusions at 300 and 400 °C re-equilibration experiments.

Concentration profiles of D_2O content within quartz are obtained from measured distances between inclusions and crystal surface. Shallow inclusions reach faster higher D_2O concentrations than deep inclusions. However, a range of D_2O concentrations is observed at equal depths, which is defined by the size of the inclusions. Small inclusions have higher D_2O concentrations than large inclusions at equal depth. The concentration profiles are used to estimate a diffusion coefficient for D_2O and H_2O of about 10^{-14} m^2 s^{-1} at 600 °C

and 337 MPa, that is, with the α-quartz stability field.

Natural fluid inclusions that are used to measure hydrogen isotopic compositions in order to identify fluid sources can be affected by diffusion processes, and pore fluid compositions may totally control inclusion compositions at high temperatures and pressure. The absence of pore fluids in metamorphic rock, and the relative low temperature and pressure conditions in sedimentary rock may prevent any diffusion processes.

Acknowledgments We would like to thank two anonymous reviewers, and the Austrian Research Fund (FWF) for financial support (project no. P 22446-N21).

Communicated by J. Touret

Electronic supplementary material The online version of this article (doi:10.1007/s00410-013-0857-6) contains supplementary material, which is available to authorized users.

4. The influence of the α–β phase transition of quartz on fluid inclusions during re-equilibration experiments

Gerald Doppler • Ronald J. Bakker

LITHOS 198–199 (2014) 14–23
DOI 10.1016/j.lithos.2014.03.018
Received: 19 December 2013, Accepted: 16 March 2014, Published online: 29 March 2014

Abstract The influence of the α–β quartz phase transition on the properties of fluid inclusions was investigated experimentally. The experiments were designed to have no gradients in pressure and fugacity between fluid inclusions and pore fluid. Deformation due to pressure differences were also excluded in this study. H_2O-rich fluid inclusions with similar densities were synthesized in quartz at approximately 625 °C and 280 MPa in the α-quartz stability field, and at approximately 675 °C and 320 MPa in the β-quartz stability field. The experimental setup prevented any pressure differences during loading and unloading of the experiments. These inclusions were re-equilibrated at the same temperature–pressure–fluid conditions, and changes in total homogenization temperature and ice melting temperature were recorded. Fluid inclusions are sensitive monitors of fluid conditions during entrapment, which record minor variation in temperature and pressure and display a corresponding distribution pattern in homogenization temperatures. Fluid inclusions re-equilibrated in the α-quartz stability field were not affected by changes in density. Fluid inclusions re-equilibrated in the β-quartz stability field revealed density loss of −0.6% at 320 MPa to −3.0% at 280 MPa, which was caused by the α-β quartz phase transition. Consequently, density loss, which is probably caused by the formation of micro-cracks at the transition from α- to β-quartz, is more efficient at lower pressures. In addition, re-equilibration experiments were performed with a pure D_2O pore fluid, to investigate diffusion processes at these experimental conditions. Diffusion of D_2O is more efficient in β-quartz stability field, and may result in near total exchange of the original H_2O content within only 19 days. Fluid inclusions re-equilibrated in the α-quartz stability field contain only half the amount of D_2O within the same experimentation run time, up to 53 mol% D_2O.

Keywords Fluid inclusions · α-β quartz · diffusion · re-equilibration · experimental study · H_2O/D_2O

4.1. Introduction

Phase changes of polymorphic minerals result in a variety of changes in physical and chemical properties, such as molar volume and heat capacities (e.g. Heuer and Nord, 1976), which may also affect hosted fluid inclusions. SiO_2 can crystallize in a variety of polymorphs at varying temperature and pressure, where α-quartz is stable at relative shallow crustal conditions and β-quartz at higher temperatures in deep rock (e.g. Hosieni et al., 1985). Fluid inclusions in α-quartz are important research objects (e.g. Samson et al., 2003), and their formational conditions can be interpreted from careful analysis of their fluid properties (composition and density) based on the closed-system assumption after trapping (e.g. Roedder, 1984). Some experimental work that addressed

this assumption was performed within the β-quartz stability field (Sterner and Bodnar, 1989; Vityk and Bodnar, 1995, 1998), whereas changes of synthetic fluid inclusions within the α-quartz field were investigated by Bakker and Diamond (1999), Bakker and Jansen (1990, 1991, 1994), and Doppler et al. (2013).

Textural information utilizing the distribution, morphology and surroundings of natural fluid inclusion is a major line of evidence for identifying the occurrence of post-entrapment changes in natural rock (e.g. Audétat and Günther, 1999; Ayllón et al., 2003). Diamond et al. (2010) and Tarantola et al. (2010) investigated experimentally changes in natural fluid inclusions that were imposed to deviatoric stress within the α-quartz stability field close to the phase transition boundary.

The effect of the α-β quartz phase change on fluid inclusion properties during these experiments was not identified or systematically analyzed in these experimental studies and changes were only assigned to temperature and pressure of hydrothermal pore fluids. Consequently, these studies cannot identify definitely the individual processes that are independent of the α-β quartz transition, which may cause fluid inclusion alteration. Decrepitation experiments (e.g. Hladky and Wilkins, 1987) illustrated a relative intense acoustic emission at about the α-β quartz phase boundary at atmospheric pressures, interpreted to correspond to changes in the Young's modulus of quartz. The change in elasticity is most probably not accompanied with an acoustic effect during heating a quartz grain, because the effect is irreversible (pers. comm. B. Kingsley) and most likely to be related to the decrepitation of all smaller-sized fluid inclusions in a sample. Hall and Bodnar (1989) carried out decrepitation experiments on heated natural fluid inclusion samples at room pressures in order to determine decrepitation profiles. They suggested that only small inclusions do not decrepitate until the quartz α-β transition temperature of 573 °C. Schmidt-Mumm (1991) identified the process of formation and propagation of micro-cracks as the origin of acoustic emission. Fluid inclusion decrepitation is only partly responsible for this emission, whereas the massive emission around the quartz α-β transition at 573 °C was suggested to result mainly from stress induced twinning according to the Dauphiné law (Laughner et al., 1979). Branlund and Hofmeister (2007) discovered a change of thermal diffusivity near 573 °C that is associated with the α-β quartz transition. The authors recognized exceeding thermal diffusivity of β-quartz that is most probably due to the expansion of the crystal lattice after crossing the phase boundary.

The present study is focused on the effect of the α-β quartz phase transition on the properties of H_2O-rich synthetic fluid inclusions at higher pressures. Three types of experiments are performed: 1. Fluid inclusions are synthesized at specific conditions in the α-quartz stability field close to the transition, and re-equilibrated at the same conditions (i.e. temperature, pressure and a H_2O fluid). 2. A similar experiment is conducted within the β-quartz stability field, where it must be noted that loading and unloading of experiments must occur through the α-quartz stability field. 3. Similar experiments within the α-quartz and β-quartz stability field, with a D_2O fluid instead of a H_2O pore fluid during the re-equilibration experiments (see also Doppler et al., 2013) are performed to demonstrate diffusion. All synthesis and complementary re-equilibration experiments are carried out at the same temperature and pressure to have equal thermal activities and to exclude possible deformation. Re-equilibration experiments at the same

conditions on either side of the α-β quartz phase transition will illustrate solely the effect of the phase transition on properties of fluid inclusions. Differences in chemical potential such as fugacity gradients between internal and external fluid represent an important parameter that affects bulk diffusion through a crystal (e.g. Bakker, 2009; Crank, 1975). In the case of higher pore fluid-fugacities relative to the fluid-inclusions in the host crystal, diffusion into the crystal is expected. Reverse fluid movement behavior would occur if internal fluid fugacity is higher compared to the pore fluid fugacity. As the ambient *P-T* conditions are controlled by the computerized laboratory equipment and the composition of the loaded fluid species are well known, fluid fugacities can be easily calculated using the appropriate equations of state (e.g. Haar et al., 1984; Hill et al., 1982). By using pure D_2O during re-equilibration experiments, a gradient in chemical components is imposed, whereas the thermochemical properties are similar to H_2O.

4.2. Experimental procedure and analytical methods

4.2.1. High P–T apparatus

Each experiment was synthesized and subsequently re-equilibrated in the hydrothermal laboratory at the University of Leoben. There are 10 Nimonic IOS/René 41 (Ni–Cr alloy) autoclaves installed, in a vertical position, as a cold-seal system similar to Kerrick (1987). Argon was used as the pressure medium ranging up to 1 GPa hydrothermal pressure. Temperature ranging up to 700 °C is induced by external furnaces. The sample temperature within the autoclaves is measured with an internal thermocouple directly monitoring and recording temperatures of the Au capsule, pre-loaded with the experimental material, consisting of partly cracked quartz rods and H_2O or D_2O. Temperature is controlled by a computerized operating system during the experiment and is measured with an uncertainty of 0.1 °C. Pressure is measured via pressure transducers, calibrated up to 700 MPa with a Heise dial gauge with an accuracy of 0.015%. Both temperature and pressure are continuously logged. The experimental setup stabilizes the synthesis conditions within 2 °C and 3 MPa during the experimental run-time of 19 days.

4.2.2. Fluid inclusion synthesis

Inclusion-free Brazilian quartz crystals were selected as starting material. Rods with a length of approximately 1 cm and a diameter of 2.75 mm are drilled along the quartz *c*-axis. The quartz rods are partially cracked by a thermal shock after heating to 400 °C. Arc-welded Au capsules are used as containers during the experiments to prevent interaction with the autoclaves and the Ar-gas during the experiments. The capsules are loaded with the cracked quartz rod and approximately 0.07 g of ultra-pure H_2O. The synthesis is performed by healing fractures according to the method of Bodnar and Sterner (1987). The experimental *P-T* conditions of each experiment are given in Table 1 and Appendix A, and are illustrated in Figs. 1 and 2. All experiments are performed with a run-time of 19 days. The experiments are loaded and unloaded along specific isochores of the entrapped fluid to prevent stress that may cause deformation or cracking of inclusions due to internal fluid over- or under-pressure. Internal thermo-couples monitor the experimental *P-T* conditions and provide the possibility to adjust conditions to obtain the desired fluid density. After the initial synthesis experiments the quartz rods are cut into disks and subsequently polished on both sides to a thickness of

approximately 0.5 mm for subsequent equilibration experiments. microthermometric analyses and re-

Table 1 Experimental conditions and fluid properties of initial synthesis experiments (synth.) and corresponding re-equilibration experiments (re-equ.).

Experiment	P [a]	$\pm P$ [b]	T [c]	$\pm T$ [d]	f [e]	$\pm f$ [f]	V_m [g]	No. [h]
Blank H_2O–H_2O								
synth. *GMR009b*	279.2	0.9	624.8	±0.7	154.1	±0.8	27.5	47
re-eq. *R009b*	281.3	0.7	624.9	±0.3	155.5	±0.5	27.4	49
synth.*GMR010b*	322.5	0.8	674.8	±0.6	204.4	±0.9	27.5	58
re-eq. *R010b*	319.9	1.0	675.2	±0.3	202.8	±0.8	27.6	45
α–quartz H_2O–D_2O								
synth.*GMR009a*	279.2	0.9	624.8	±0.7	154.1	±0.8	27.5	68
re-eq. *R009a*	278.7	2.3	624.9	±0.5	154.0*	±1.4	27.5*	63
β–quartz H_2O–D_2O								
synth. *GMR010a*	322.5	0.8	674.8	±0.6	204.4	±0.9	27.5	100
re-eq. *R010a*	321.1	1.1	674.8	±0.9	203.8*	±1.2	27.3*	94
synth. *GMR013a*	280.3	1.1	674.7	±0.5	175.6	±1.0	29.2	60
re-eq. *R013a*	279.4	0.9	674.7	±0.7	175.2*	±0.9	29.0*	60

[a] Pressure (MPa)
[b] Pressure variation (MPa)
[c] Temperature (°C)
[d] Temperature variation (°C)
[e] Fluid fugacity (in MPa) of H_2O (Haar et al., 1984) and *D_2O (Hill et al., 1982) calculated with software from Bakker (2003; http://fluids.unileoben.ac.at)
[f] Fluid fugacity variation (MPa)
[g] Fluid molar volume (in $cm^3 \cdot mol^{-1}$) of H_2O (Haar et al., 1984) and *D_2O (Hill et al., 1982) calculated with software from Bakker (2003; http://fluids.unileoben.ac.at)
[h] Number of measured fluid inclusions
* D_2O fluid

4.2.3. Re-equilibration of fluid inclusions

After microscopic and microthermometric investigations the same quartz disks were used for re-equilibration experiments. Quartz disks were loaded in gold capsules supported by two quartz rods of the same diameter on both sides to prevent any damage of the relative fragile sample. Two re-equilibration experiments were performed with pure H_2O (experiments *R009b* and *R010b*; Table 1 and Appendix A) and are designed to have similar conditions as the original synthesis experiment. Three re-equilibration experiments were performed by using pure D_2O as the quartz surrounding medium (experiment *R009a*; *R010a*; *R013a*; see Table 1). Also here loading and unloading of the hydrothermal pressure vessels was performed according to specific isochore to minimize any pressure gradients between the synthesized fluid inclusions and the external fluid. The experimental *P-T* conditions of each re-equilibration experiment are shown in Table 1 and illustrated in Figs. 1 and 2. Each re-equilibration experiment was carried out with a run-time of 19 days. The pressure and temperature conditions are stabilized within 2 °C and 3 MPa.

After the re-equilibration experiments the same fluid inclusions from the initial synthesis were re-examined to compare inclusions density, composition and morphology and to detect changes in these parameters.

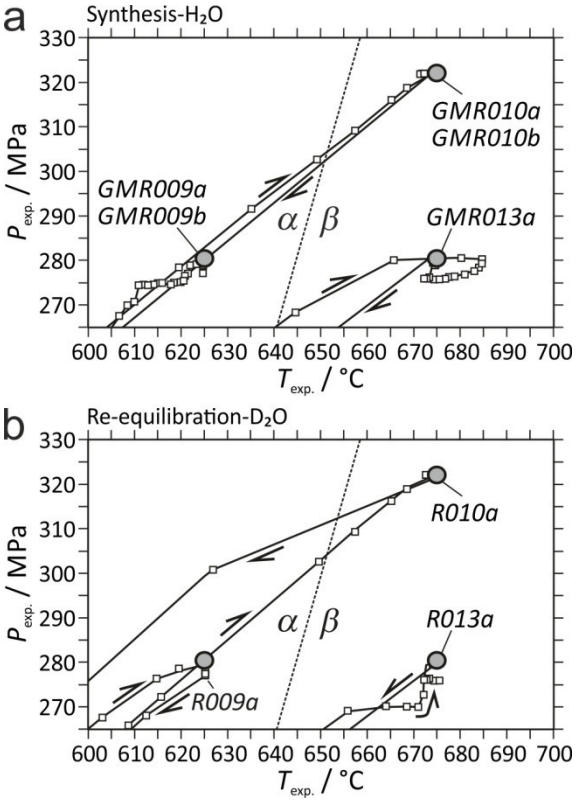

Fig. 1. Experimental *P-T* conditions based on the computerized logging-system of the hydrothermal laboratory. The curves illustrate the loading (upward arrows) and unloading (downward arrows) of the sample conditions with a logging interval of 5 min (filled squares). (a) Conditions of the initial synthesis experiments with H_2O fluid and (b) conditions of the complementary re-equilibration experiments with D_2O fluid. The gray filled circles illustrate the average experimental conditions (see Table 1).

4.2.4. Microthermometry and optical analysis of shape, size and distribution within the quartz disk

Fluid inclusion properties of each individual fluid inclusion were characterized and analyzed as described in Doppler et al. (2013). Each assemblage (pre- and post-equilibration) was analyzed by cataloging various properties of up to 100 fluid inclusions, i.e. 1) each inclusion was photographed for documenting the morphological properties such as shape and size, and for identification purposes; 2) depth below the crystal surface; 3) the fluid inclusion composition and density is analyzed by microthermometry and Raman spectroscopy. A compilation of several acquired parameters of each individual inclusion is added in Appendix B. Changes in morphology are based on the shape definitions according to Bakker and Diamond (2006). The shape changes of individual fluid inclusions after re-equilibration are defined according to the relative change in inclusion perimeter/area ratio in two dimensional images, and the relative change in the major/minor axis ratio of the best-fit ellipse. The volumes of individual phases (liquid/vapor ratio) were difficult to obtain; therefore, area fractions of the vapor bubble (a_{vap}) of each fluid inclusion were digitally measured from two-dimensional images by tracing the outside edge of the total inclusion and by the outside rim of the vapor bubble at room temperature. The distance of fluid inclusions to the crystal surface is measured with an optical microscope table that is adjustable in the *z*-direction (Olympus BX60). Both density and composition were obtained from homogenization and melting temperatures of the entrapped fluids, which were measured using a LINKAM MDS 600 and LINKAM THMSG 600 heating–freezing stages. The quality of the results of the Linkam MDS600 stage is determined by accuracy and precision of individual measurements. The instrument resolution of temperature measurements is 0.1 °C. The selection of thermodynamically determined temperatures of invariant points of phase changes measured in synthetic fluid inclusions with pure H_2O and a mixture of H_2O and CO_2, allows an excellent method to estimate the trueness of the stage. The precision of the stage is obtained from a series of

repeated measurements of the same parameter, e.g. the critical homogenization temperature of H_2O in synthetic fluid inclusions. Measurements of this standard within a period of six months (25 measurements) reveal an average critical temperature of 378.6 °C (not corrected by calibration), with a standard deviation of the sample of ±0.4 °C, whereas the standard error in mean is ±0.1 °C. The average melting temperatures of H_2O and CO_2 are +0.4 °C and −56.6 °C (not corrected by calibration), respectively, with standard deviations of sample of ±0.1 and ±0.2 °C, respectively, and standard error in mean of ±0.0 and ±0.1 °C, respectively. It must be noted that the precision of the measurement of one inclusion can only be obtained by multiple only be obtained by multiple measurements of the same object. It is assumed that the precision obtained from measurements of the standards is valid for measurements of individual fluid inclusions at similar temperatures. Knowledge of the exact temperatures of these invariant points, i.e. critical temperature of H_2O (374.0 °C), melting temperature of H_2O (0.0 °C) and CO_2 (−56.6 °C) is used for calibration, which is greatly improving the accuracy of individual measurements within the range of −56.6 to +374.0 °C. The D_2O composition was determined from the melting temperatures of the D_2O–H_2O mixtures (see Doppler et al., 2013), as defined by significant differences in melting temperatures T_m(SV ➔ LV) of pure H_2O (0.0 °C) and pure D_2O (+3.8 °C). Relative amounts of H_2O and D_2O are obtained from Eq. (1)

$$x_{rel}(\mathrm{D_2O}) = \frac{T_m(fi)}{T_m{}^0(\mathrm{D_2O}) - T_m{}^0(\mathrm{H_2O})} \quad (1)$$

where T_m is the melting temperature in °C, fi is the solution in a specific fluid inclusion. The superscript *0* indicates the pure phase. The presence of D_2O was also confirmed by Raman spectroscopy.

4.3. H_2O–D_2O fugacity, molar volume and calculated homogenization conditions

The fugacity and molar volume of pure H_2O and D_2O fluids were calculated with the equations of state of Haar et al. (1984) and Hill et al. (1982), respectively. These equations of state are included in the software package "FLUIDS" (Bakker, 2003; and http://fluids.unileoben.ac. at) in the programs "Loner HGK" and "Loner HCL". The equation of state for D_2O is limited to maximum values of 100 MPa and 600 °C, but was extrapolated to the experimental conditions in this study. Four experiments have been performed along the H_2O-isochore of 27.5 $cm^3 \cdot mol^{-1}$ (Table 1): two within the α-quartz stability field close to the transition conditions to β-quartz (*GMR009a* and *GMR009b*, Figs. 1 and 2), and two within the β-quartz stability field, just across the phase transition (*GMR010a* and *GMR010b*, Figs. 1 and 2). The calculated H_2O fugacities of these experiments are 154.1 MPa in the α-quartz stability field and 204.4 MPa in the β-quartz stability field (Table 1). In addition, one experiment in the β-quartz stability field was performed at similar temperatures as the previously mentioned experiments, but modified pressures, resulting in molar volume of 29.2 $cm^3 \cdot mol^{-1}$ (*GMR013a*, Fig. 1) with a corresponding H_2O fugacity of 175.6 MPa.

Homogenization conditions of the entrapped fluid in synthetic fluid inclusions were calculated by descending along the isochore from experimental conditions to the liquid–vapor curve, including isochore correction due to the thermal expansion and compressibility of the quartz host (Hosieni et al., 1985; and its rectification according to Sterner and Bodnar, 1991). The corrected isochores were calculated with the software "ISOC" (Bakker, 2003). Fluid inclusions from the initial synthesis experiments

GMR009a and *GMR009b* should theoretically homogenize at 320.5 ± 0.6 °C and have a molar volume of 27.05 ± 0.40 $cm^3 \cdot mol^{-1}$ at this temperature. Uncorrected isochores result in homogenization temperatures of 324.8 ± 0.6 °C. Although the molar volume of the fluid in the experiments *GMR010a* and *GMR010b* is similar to *GMR009a* and *GMR009b*, the theoretical homogenization temperature along the host mineral corrected isochore is 317.5 ± 0.5 °C, whereas the uncorrected isochore also results in T_h = 324.8 ± 0.5 °C. The corrected molar volume at homogenization conditions is 26.75 ± 0.40 $cm^3 \cdot mol^{-1}$. Theoretical homogenization conditions of experiment *GMR013a* according to corrected isochore is T_h = 332.3 ± 0.5 °C (corresponding to 28.40 $cm^3 \cdot mol^{-1}$). Uncorrected isochores result in Th of 337.9 ± 0.5 °C. Re-equilibration experiments with H_2O (*R009b* and *R010b*) are performed at the nearly the same conditions (Fig. 2) as the original synthesis experiments (*GMR009b* and *GMR010b*), and result in similar molar volumes, fugacities and theoretical homogenization temperatures. Re-equilibration experiments with D_2O at similar temperature and pressure in the α-quartz stability field (*R009a*) and the β-quartz stability field (*R010a* and *R013a*) do not show significant different values in molar volume, fugacities and T_h from the original experiment.

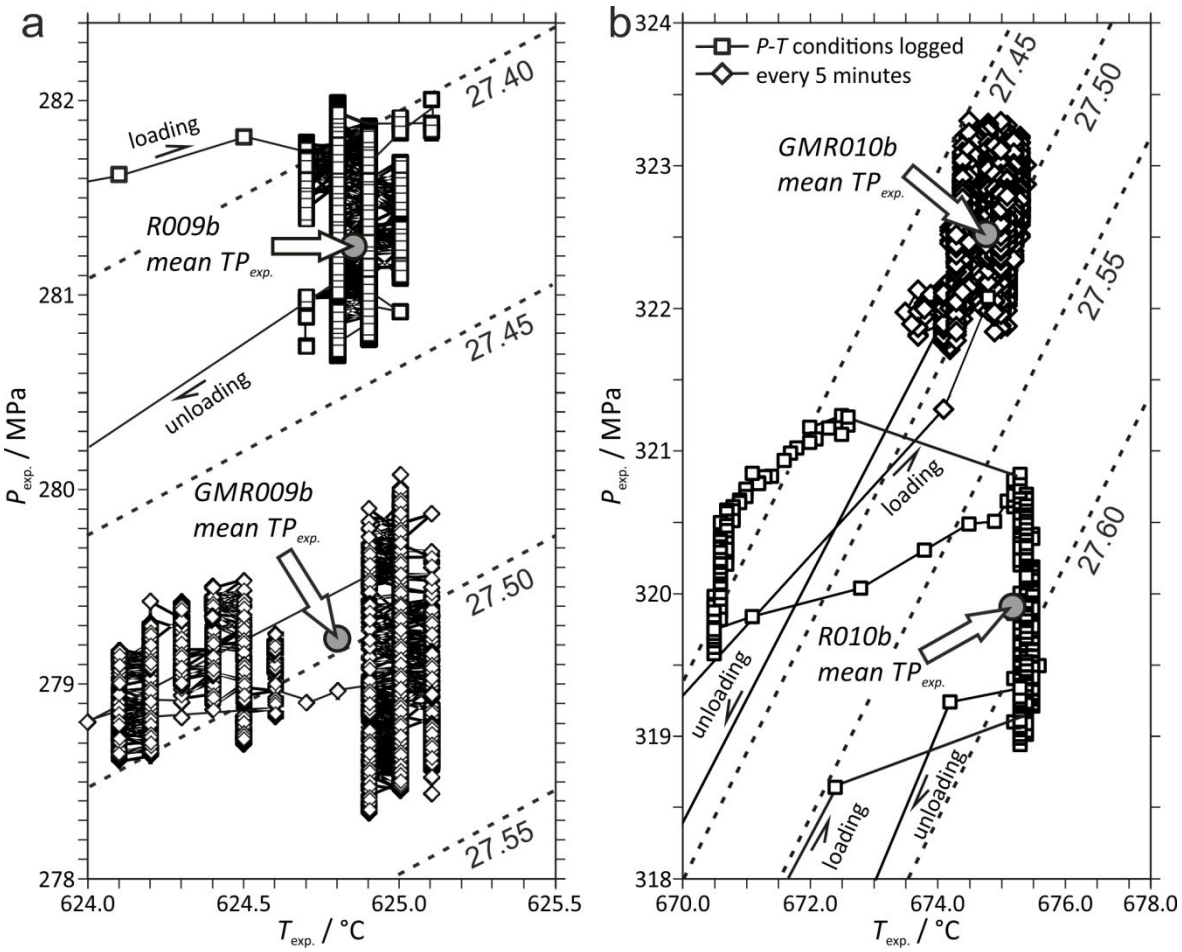

Fig. 2. Experimental pressure–temperature record of the blank experiments. The inclined dashed lines are isochores of pure H_2O (numbers in $cm^3 \cdot mol^{-1}$). (a) The experimental P_{mean} of synthesis *GMR009b* is 279.2 MPa at the T_{mean} of 624.8 °C (gray filled circle) within the α-quartz stability field. The experimental mean-conditions of the complementary re-equilibration *R009b* are 281.3 MPa and 624.9 °C. (b) The mean pressure of synthesis experiment *GMR010b* is 322.5MPa at T_{mean} of 674.8 °C within the β-quartz stability field. The complementary re-equilibration conditions of *R010b* are P_{mean} of 319.9 MPa and 675.2 °C.

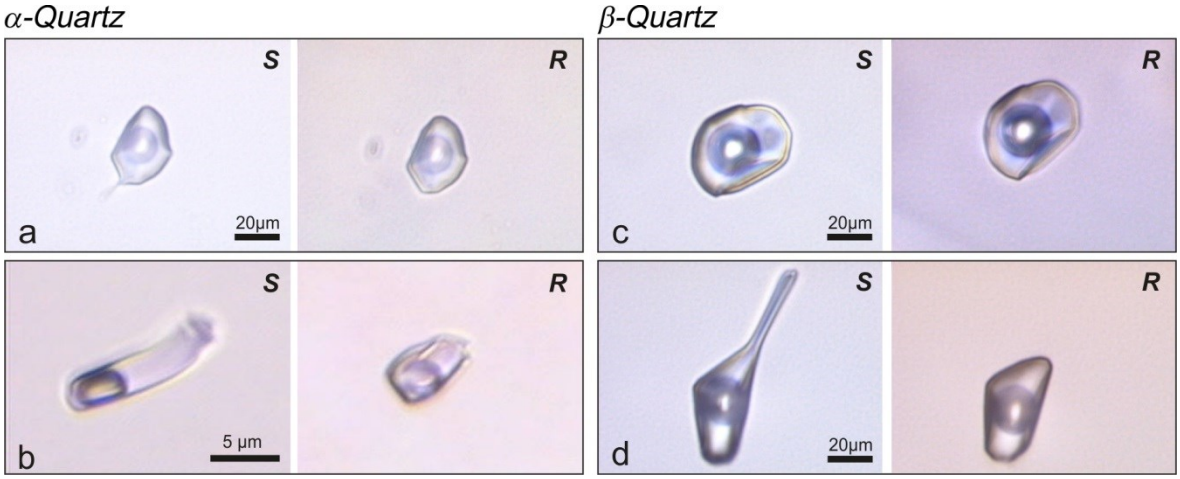

Fig. 3. Photomicrographs of the same inclusion before (*S* = synthesized) and after the blank re-equilibration experiments (*R* = re-equilibrated). Fluid inclusions of the experiments *GMR009b* and *R009b* are performed within the α-field (a and b); and fluid inclusion examples of *GMR010b* and *R010b* are carried out within the β-quartz stability field (c and d).

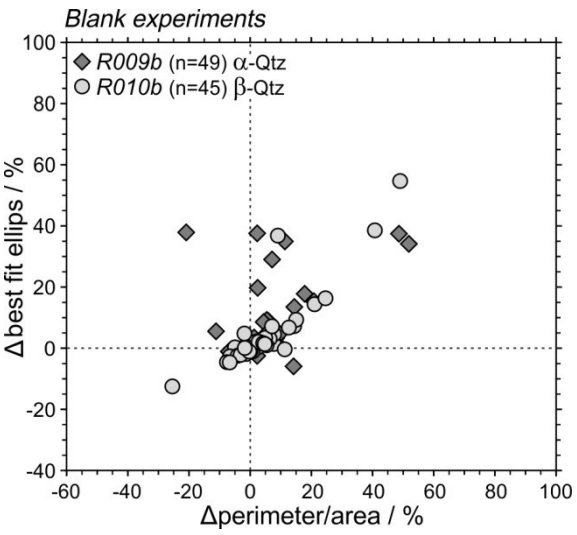

Fig. 4. Fluid inclusion shape diagram illustrating the magnitudes of shape changes during re-equilibration of the blank experiments. Terms are according to Bakker and Diamond (2006), see text for further details.

4.4. Experimental results

4.4.1. H_2O blank experiments

Most fluid inclusions synthesized in experiment *GMR009b* (α-quartz) displayed minor changes in morphology after re-equilibration (experiment *R009b*; Figs. 3a, b and 4).

The fluid inclusions are both equant and regular shaped or elongated and regular shaped. Initially the elongated fluid inclusions tend to become more equant after re-equilibration, and exhibit the highest magnitude in shape changes in Fig. 4. The inclusions that were originally equant and regular did not show shape change during re-equilibration. Morphological changes in the experiments *GMR010b* and *R010b* in the β-quartz stability field are similar to those changes in the α-quartz field (Figs. 3c, d and 4). However, the change in shape parameters in the β-quartz experiment exhibit slightly higher values than the α-quartz experiments (up to 60%).

Homogenization temperatures of the H_2O synthesis within the α-quartz stability field of experiment *GMR009b* reveal a mean T_h of 323.7 °C, a T_h mode between 323.0 and 323.5 °C, and a variation from 321.9 to 325.5 °C (Table 2 and Fig. 5a). Fig. 5a illustrates an irregular distribution of homogenization temperatures, i.e. the

mode is at lower temperatures than the temperature obtained from a best-fit Gaussian distribution function. Changes in density (and molar volume) were observed even for the blank experiments simply by measuring the homogenization temperature of the fluid inclusions. During α-quartz re-equilibration experiment *R009b* fluid inclusions altered to higher densities with a maximum shift in T_h up to −0.9 °C (see Fig. 6). Fluid inclusions with originally relatively low T_h have similar change in density as fluid inclusions with initially higher T_h. Experiment *GMR010b* was carried out within the β-quartz stability field and revealed a mean T_h of 322.0 °C with a variability of ±2.6 °C. The mode of the T_h distribution is between 322.0 and 323.0 °C (Table 2 and Fig. 5b). The T_h distribution of this experiment reveals a normal distribution (Gaussian). The change in T_h is opposite to the α-quartz experiment, and reaches values up to +2.5 °C for inclusions with originally higher densities, whereas inclusions with initially lower densities only change about +0.3 °C (Fig. 6).

Table 2 Homogenization temperatures of fluid inclusions from initial experiments and re-equilibration experiments, melting temperatures with corresponding D_2O content after re-equilibration.

Synth.	T_h [a]	Max [b]	Min [c]	Re-equ.	T_h [d]	Max [e]	Min [f]	Max. T_m [g]	%D_2O [h]
blank									
H_2O–H_2O									
GMR009b	323.7	+1.8	-1.8	*R009b*	323.2	+2.0	-1.7	0.0	-
GMR010b	322.0	+2.6	-2.6	*R010b*	323.2	+1.7	-1.5	0.0	-
α–quartz									
H_2O–D_2O									
GMR009a	323.7	+2.3	-2.4	*R009a*	322.3	+3.1	-1.9	2.6	68
β–quartz									
H_2O–D_2O									
GMR010a	322.9	+3.9	-2.0	*R010a*	321.1	+2.4	-4.4	3.7	97
GMR013a	337.3	+1.6	-1.5	*R013a*	335.2	+2.7	-2.3	3.6	95

[a] Mean T_h (homogenization temperature) initial synthesis (°C)
[b] Maximum T_h – mean T_h initial synthesis (°C)
[c] Mean T_h – minimum Th initial synthesis (°C)
[d] Mean T_h re-equilibration (°C)
[e] Maximum T_h – mean T_h re-equilibration (°C)
[f] Mean T_h – minimum T_h re-equilibration (°C)
[g] Maximum T_m (melting temperature) re-equilibration (°C)
[h] Maximum mole% D_2O

4.4.2. D_2O re-equilibration experiment in the α-quartz stability field

The majority of the synthesized fluid inclusions in the experiment *GMR009a* (α-quartz) display no appreciable change in the inclusions shape during re-equilibration (experiment *R009a; see* Figs. 7a and 8a). The synthesized fluid inclusions are both equant and regular or elongated and irregular. Initially elongated and irregular inclusions tended to become more equant and regular during re-equilibration. These inclusions show the highest magnitude (up to 80%) in shape changes for these experiments (Figs. 7 and 8).

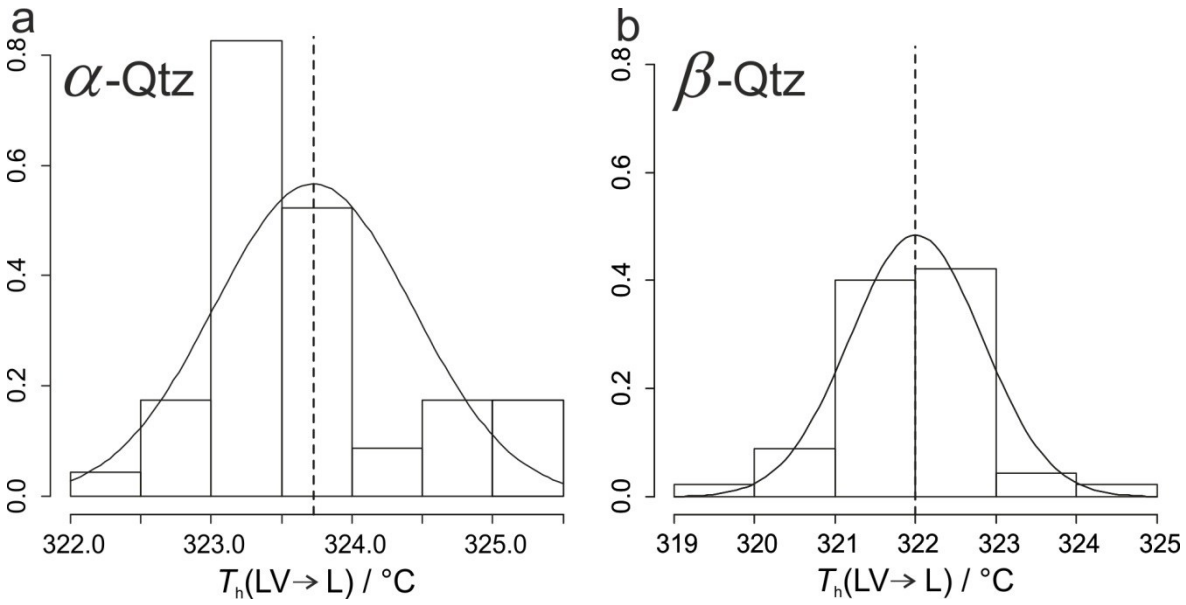

Fig. 5. Homogenization temperature histograms. (a) The α-quartz experiment (*GMR009b*) gives the range of T_h from321.9 to 325.5 °C with a median of 323.7 °C (dashed line) and a mode of 323.0 to 323.5 °C. (b) The histogram based on the data of the β-quartz experiment *GMR010b* gives the T_h range from 319.4 to 324.6 °C with a median of 322.0 °C (dashed line) and a mode of 322.0 to 323.0 °C. Both synthesis experiments show a normal distribution of the T_h values. Detailed fluid inclusion properties are summarized in Table 2 and in Appendix B.

Homogenization temperatures of the synthesized H_2O inclusions of the a-quartz experiment *GMR009a* reveal a mean T_h of 323.7 °C with a variation of 321.3 to 326.0 °C (see Table 2). Density changes (and molar volume changes) were measured using the changes in the homogenization temperatures of the re-equilibrated fluid inclusions. During α-quartz re-equilibration experiment *R009a*, fluid inclusions altered to higher densities with a maximum shift in T_h up to −2.4 °C (Fig. 9a). Changes in fluid inclusion composition after re-equilibration with D_2O are calculated from the positive melting temperatures via Eq. (1) and are illustrated in Fig. 9. Experiment *R009a* reveals a maximum T_m(ice) of +2.6 °C which corresponds to 68 mol% D_2O (Fig. 9a). The long dashed line in Fig. 9a represents the expected changes in T_h with increasing D_2O content as illustrated by increased T_m(ice). Re-equilibrated fluid inclusions in experiment *R009a* show a distribution of T_m and T_h which correspond to the expected composition.

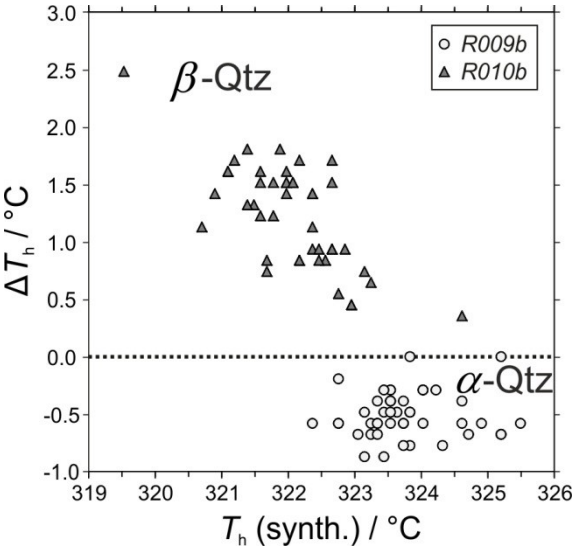

Fig. 6. Homogenization temperature of the initial synthesis (experiment *GMR009b* and *GMR010b*) versus the change in T_h of the complementary re-equilibration experiments *R009b* and *R010b*. α illustrates the experiment in the α-quartz stability field, and β in the β-quartz stability field.

4.4.3. D_2O re-equilibration experiment in the β-quartz stability field

Fluid inclusions which were synthesized in the β-quartz stability field (experiment *GMR010a* and *GMR013a*) display similar changes in morphology after re-equilibration (experiment *R010b* and *R013b*; Figs. 8b and 10).Originally equant and regular inclusions display limited shape changes compared to fluid inclusions which are originally elongated and irregular.

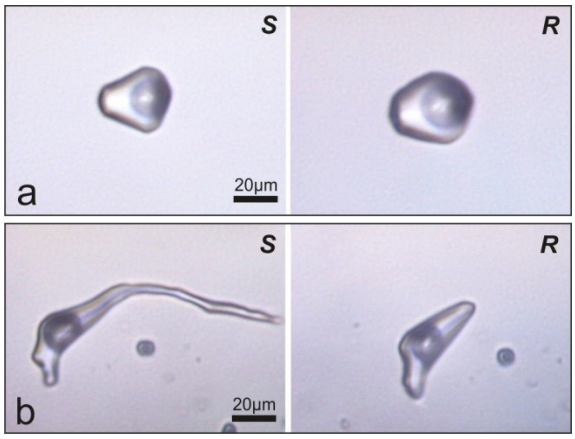

Fig. 7. Photomicrography of the same inclusions before (*S* = synthesized, *GMR009a*) and after re-equilibration experiments in D_2O (*R* = re-equilibrated, *R009a*) which are performed in the α-quartz field. Fluid inclusion with minor shape changes is illustrated in (a) and major shape changes in (b).

The distribution of the magnitude in shape changes during re-equilibration illustrates comparable values considering the stability field of quartz (α versus β-quartz; Fig. 8a and b). The synthesized H_2O inclusions of the experiment *GMR010a* display a mean T_h of 322.9 °C with a variation of 320.9 to 326.8 °C (Table 2). Homogenization temperatures of the fluid inclusions in experiment *GMR013a* display a mean T_h of 337.3 °C with a variation between 335.8 and 338.9 °C (Table 2). After re-equilibration in the β-quartz stability field density (and molar volume) changes were determined by measuring lower homogenization temperatures compared to the initial experiments. Both, experiment *R010a* and experiment *R013a* illustrate density increase (Fig. 9b), corresponding to a maximum shift in T_h of up to −3.0 °C and −3.4 °C, respectively. After re-equilibration with pure D_2O, the maximum ice melting temperature of experiment *R010a* is +3.7 °C which corresponds to a fluid inclusion composition of about 97 mol% D_2O. The maximum T_m(ice) value of the β-quartz experiment *R013a* is comparable to *R010a* with T_m values up to +3.6 °C. The long dashed lines in Fig. 9 illustrate the expected combination of

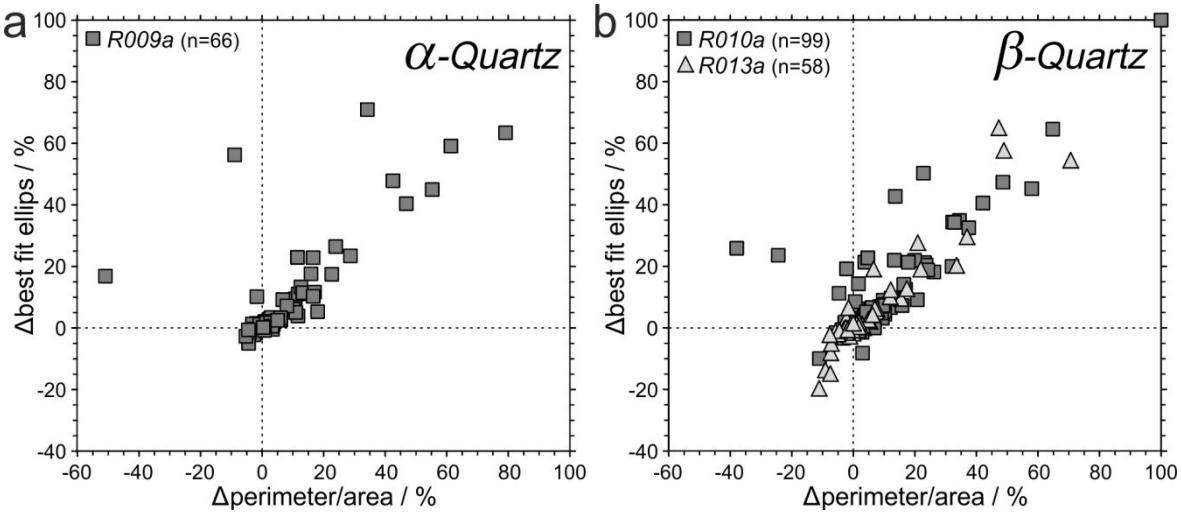

Fig. 8. Fluid inclusion shape diagram illustrating the magnitudes of shape changes of the re-equilibration experiment in the α-quartz stability field with D_2O in (a) and in the β-quartz stability field with D_2O in (b). Terms are according to Bakker and Diamond (2006), see text for further details.

homogenization temperature and melting temperature. The calculated T_h for inclusions that completely exchanged their H_2O content for D_2O in experiment *R010a* is 319.2 °C which corresponds to a ΔT_h of −5.6 °C (calculated with software package "FLUIDS"; Bakker, 2003). For the experiment *R013a* a maximum shift in T_h after total reequilibration with D_2O is expected with a ΔT_h of −7.0 °C derived by a calculated T_h of 338.1 °C. The measurements from *R009a* in the α-quartz stability field are approximately according to the expected trend in combinations of T_h and T_m, whereas *R010a* and *R013a* in the β-quartz stability field illustrate notably higher values of T_h than expected at selected T_m values.

4.5. Discussion

4.5.1. Morphological changes of fluid inclusions

According to the original assumptions only minor morphological changes of fluid inclusions can be observed after the presented reequilibration experiments. Morphological changes are almost identical in α-quartz and β-quartz. The morphological change rate is independent of the quartz modification. Fluid inclusions tend to reach negative crystal shape during elevated hydrothermal *P-T* conditions without respect to the quartz modification and without stress components. Irregular and elongated fluid inclusions show the highest shape change during reequilibration. Morphological changes are independent of the pore fluid ratios H_2O/D_2O. The magnitude of fluid inclusions shape change is mainly temperature dependent and consistent with the results of Doppler et al. (2013).

4.5.2. Distribution pattern of T_h in H_2O blank experiments

The measured homogenization temperatures of the α-quartz experiment *GMR009b* reveal an irregular distribution as illustrated in Fig. 5a. The corresponding histogram of the logged experimental pressure conditions (Fig. 11a) shows a similar irregular distribution, which deviates from a normal (Gaussian) distribution pattern. Therefore, the measured T_h of

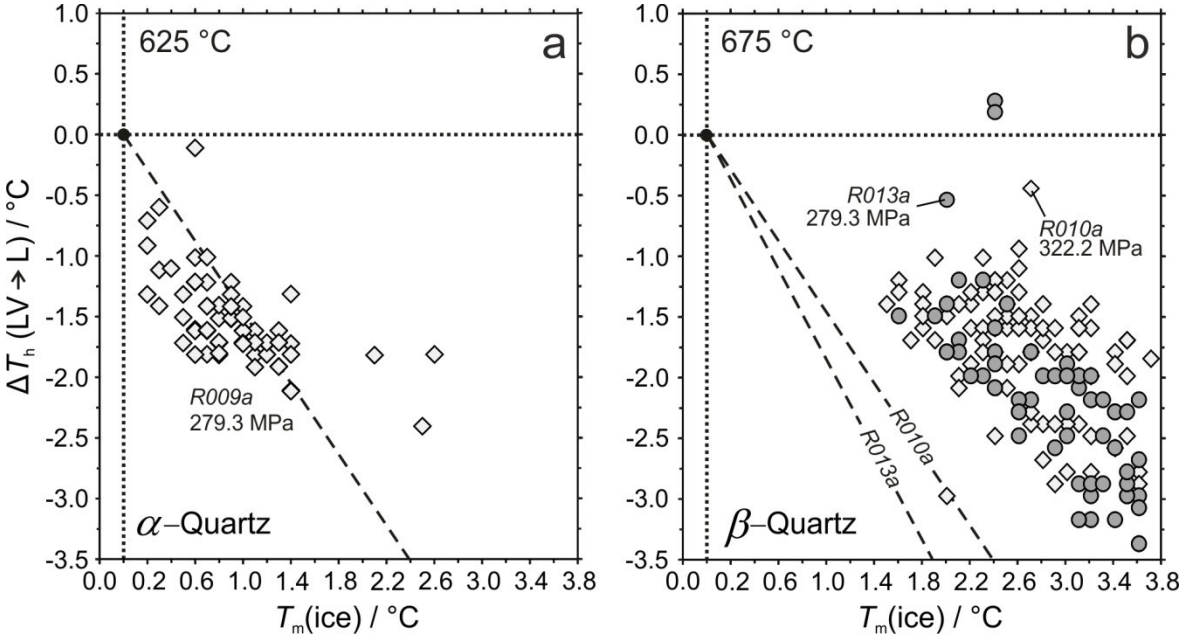

Fig. 9. Melting temperature of ice versus changes in homogenization temperature after the re-equilibration experiments *R009a* (a), *R010a* (b), and *R013a* (b) with D_2O.

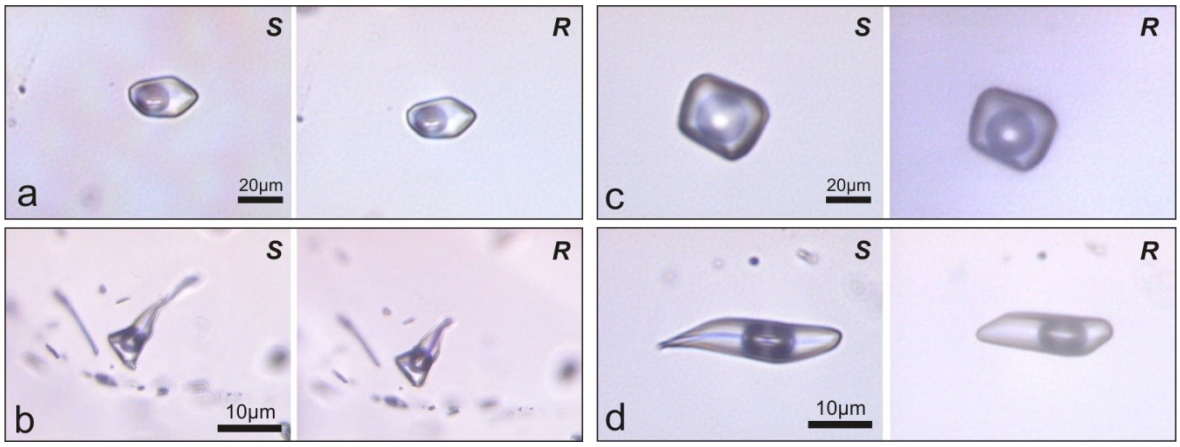

Fig. 10. Photomicrographs of the same inclusion before (*S*= synthesized) and after the re-equilibration experiments (*R* = re-equilibrated) with D_2O. Fluid inclusions of the experiments *GMR010a*, *R010a* (a and b) and *GMR013a* and *R013a* (c and d) are performed within the *β*-field.

a fluid inclusion assemblage clearly reflects fluctuations in experimental *P-T* conditions, and the fluid inclusion assemblage sensitively stores the ambient formation conditions. This can also be deduced from the second H_2O blank experiment *GMR010b* performed in the *β*-quartz field (c.f. Figs. 5b and 11b); both, the experimental conditions record of pressure and the measured T_h are normally distributed (Gaussian distribution). This phenomenon also illustrates that fluid inclusions are continuously synthesized during the entire experimental run-time and not at a specific moment of experimentation. In natural rock, the distribution pattern of Th in a fluid inclusion assemblage that did not re-equilibrate or change its properties after trapping must correspond to a variation in trapping conditions, probably caused by slightly varying pore fluid pressure.

4.5.3. Shift in T_h in H_2O blank experiments

According to the experimental variation in experiment *GMR009b* in the *α*-quartz stability field (Fig. 2a), the molar volume of the entrapped fluid may vary between 27.47 and 27.54 $cm^3 \cdot mol^{-1}$. The measured T_h (Fig. 5a), which directly reflect molar volumes, are slightly lower than the calculated T_h of "uncorrected" isochores (see paragraph 3), but significantly higher than T_h of "corrected" isochores. Consequently, isochore correction according to the compressibility and expansion of quartz result in overestimated density calculations. The complementary re-equilibration experiment *R009b* was performed at approximately 2 MPa higher pressures, with a variation in molar volume of 27.39 to 27.44 $cm^3 \cdot mol^{-1}$. These slightly lower molar volumes result in minor modifications of T_h, i.e. a change of −0.2 to −1.3 °C. The observed changes in T_h (Fig. 6) agree with these theoretical predictions.

Experiment *GMR010b* in the *β*-quartz stability field records a variation in molar volumes between 27.45 and 27.52 $cm^3 \cdot mol^{-1}$ (Fig. 2b), similar to the previously mentioned experiment in the *α*-quartz stability field. Although molar volumes are similar, the expected T_h are about 3 °C lower than in experiments *GMR009b*, due to a larger correction of isochores that originate in the *β*-quartz stability field. The observed T_h values are in fact slightly lower, but still exceed those values expected from full correction calculations. Again, the application of compressibility and expansion of quartz according to the model of Hosieni et al. (1985) result in overestimated densities. The complementary re-equilibration

experiment *R010b* was performed at approximately 2 MPa lower pressures, corresponding to a variation in molar volumes of 27.56 to 27.63 $cm^3 \cdot mol^{-1}$ (Fig. 2b). Homogenization temperatures should theoretically increase by +0.9 to +1.6 °C reflecting these slightly different experimental conditions. However, the observed changes in T_h range up to +2.5 °C, which must correspond to an additional process caused by leakage of the fluid inclusions. This process is considered to be the α-β transition of quartz that induced a series of micro-cracks or enhanced local diffusion of H_2O, resulting in a lower density. The relative change in density is only about −0.6% at a hydrothermal pressure of 320 MPa.

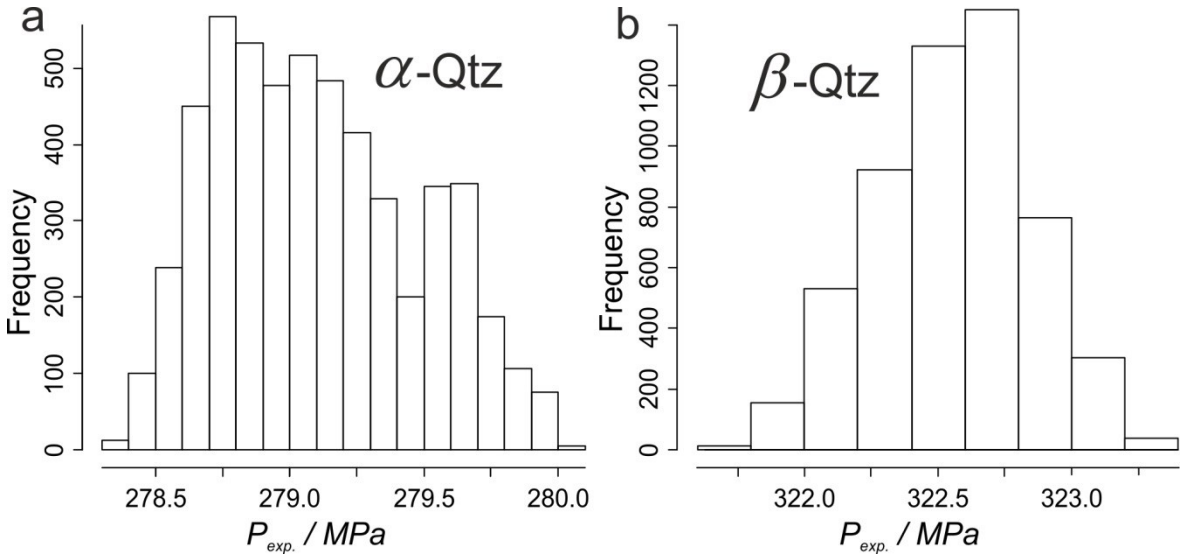

Fig. 11. Experimental pressure histograms. (a) The α-quartz experiment (*GMR009b*) gives the range of $P_{exp.}$ from 278.3 to 280.1 MPa with the mean value of 279.2 MPa (dashed line). (b) The histogram based on the data of the β-quartz experiment *GMR010b* gives the $P_{exp.}$ range from 321.7 to 323.3MPa with a mean value of 322.5MPa (dashed line). The β-quartz experiments show a normal distribution of the experimental pressure values. Detailed experimental condition properties are summarized in Table 1 and in Appendix A.

4.5.4. Compositional and density changes in re-equilibration experiments with D_2O

Re-equilibration experiments with D_2O (*R009a*, *R010a*, and *R013a*) at the same temperature and pressure, result in efficient diffusion processes ofH_2O out of the inclusions and D_2O into the inclusions. These results are consistent with the experiments of Doppler et al. (2013). The mobility of both components is clearly illustrated by changes in ice melting temperature of individual inclusions (Table 2, Fig. 9). Mixing of H_2O and D_2O at constant experimental conditions also results in changes in homogenization temperatures. The combined changes of T_m(ice) and T_h with increasing fraction of D_2O is illustrated in Fig. 9.

The synthetic fluid inclusion assemblage from the re-equilibration experiment in the α-quartz stability field (*R009a*) display changes in both T_m(ice) and Th consistent with the theoretical predictions (Fig. 9a). Therefore, the exchange of H_2O and D_2O according to the induced fugacity gradients is the only process responsible for changes in the fluid inclusions and the variation in change depends on the size and the position of inclusions in the host relative to the re-equilibrating fluid.

The re-equilibration experiment in the β-quartz stability field (*R010a*) with the

same molar volume as in the α-quartz stability field results in larger shifts in T_m(ice) and T_h (Fig. 9b). The maximum T_m(ice) is +3.7 °C which indicates a nearly total exchange of H_2O and D_2O in the relative short experimental run time of 19 days. However, the expected shift in T_h due to this process is much higher than the observed T_h in the sample (Fig. 9b). In other words, the observed homogenization temperature is higher than expected from H_2O and D_2O diffusion alone. The relative change in density in experiment *R010a* according to these considerations is about −1.5%. Again, the α-β transition of quartz must have induced a total volume increase postulated again to be via the formation of micro-cracks around individual inclusions, resulting in a lower density.

The theoretically predicted changes in T_m(ice) and T_h is larger in re-equilibration experiment *R013a* (Fig. 9b) in the β-quartz stability field at the same temperature compared to the experiment *R010a* at lower pressures (280 MPa). The observed changes in temperature are similar to those measured in *R010a*. Consequently, the change in Th is much more dramatic after the diffusion process that exchanges H_2O and D_2O. Therefore, the density loss due to the α-β transition of quartz is more efficient at lower pressures, and reaches relative values up to −3.0% in experiment *R013a*. The increase of loss towards lower pressures is consistent with observations at room pressures, where decrepitation of fluid inclusions at the α-β transition causes a total loss of the fluid content in inclusions (e.g. Hall and Bodnar, 1989).

4.5.5. Comparison with previous re-equilibration experiments that are affected by the α-β quartz transition

Four phenomena have been identified by a number of fluid inclusion researchers that can affect fluid inclusions composition and density in quartz at high temperature. These are: 1) fugacity gradient; 2) pressure gradient; 3) α-β quartz transition; and 4) microstructure. All of these factors promote diffusion of fluid components (mainly H_2O) through the crystal lattice and promote decrepitation, leakage, or incomplete decrepitation. Our study illustrates the effect of only the α-β quartz transition on the diffusion of H_2O and D_2O as a water tracer. Although fluid inclusion changes are clearly enhanced if the α-β quartz transition is crossed, mainly at relative lower pressures, while these changes become less pronounced at increasing pressures. Most of the re-equilibration experiments published by Sterner and Bodnar (1989) were performed in the β-quartz stability field. Pure H_2O synthetic fluid inclusions were subjected to high internal overpressures (up to 400 MPa) simultaneously with high gradients in H_2O fugacity. Moreover, the α-β quartz transition was crossed in most experiments. The results were mainly analyzed in terms of general changes in homogenization temperatures of a fluid inclusion assemblage, without knowledge of changes in individual inclusions. Internal overpressure and the α-β quartz transition may result in uncontrolled total volume increase of fluid inclusions (incomplete decrepitation), and over-fugacity results in diffusion of H_2O out of the inclusions. Each of these processes result in the observed decrease in H_2O density in fluid inclusions, but the individual contribution of each process cannot be quantified. At the selected temperatures of the experimentation (700 to 900 °C), diffusion is a highly efficient process for fluid component transfer through the quartz lattice (Doppler et al., 2013). Diffusion of H_2O according to the imposed gradients resulted in a decrease of internal pressure in addition to the loss of H_2O, calculated with the software "ReqDif" (Bakker, 2009). At equilibrium condition, i.e. when the internal and external

fugacities of H_2O are equal; the initial internal overpressure is converted into an internal under-pressure, unlike the considerations of Sterner and Bodnar (1989). In addition the experiments with internal under-pressures (Sterner and Bodnar, 1989) are submitted to similar processes. However, diffusion of H_2O into the inclusions according to fugacity gradients is not able to produce an internal overpressure (see Bakker, 2009).

Re-equilibration experiments with synthetic fluid inclusions (10 mass % NaCl) from Vityk and Bodnar (1995) that simulate "nearly isothermal decompression" or "nearly isothermal compression" were performed at the exact temperature–pressure conditions of the α-β quartz transition. The set-up of the Vityk and Bodnar (1995) experiments did not allow any direct comparison of specific fluid inclusions before and after re-equilibration, because individual inclusions were not characterized prior to re-equilibration. The stepwise temperature and pressure changes result in inclusions entrapment at multiple conditions, during the variable re-equilibration conditions. The results were mainly given in terms of texture (morphology of fluid inclusion assemblages) and expected general changes in homogenization temperatures of a fluid inclusion assemblage, according to the empirical equations of Bodnar and Vityk (1994). These experiments were subjected to huge gradients in H_2O fugacity, which must have resulted in diffusion at these conditions. NaCl is assumed to remain immobile, consequently, a change in salinity must have occurred, but was not reported. Similar to the experiments of Sterner and Bodnar (1989), H_2O fugacity gradients, pressure gradients and the α-β quartz transition may have affected the properties of the synthetic inclusions, but the individual contribution to the change in homogenization temperatures (molar volume) of each of these phenomenon is unknown.

4.5.6. Implications for the interpretation of natural fluid inclusions

The α-β quartz transition may occur in metamorphic rocks that are formed at amphibolite and granulite facies, in addition to contact metamorphism. Fluid inclusions that are trapped under these conditions in quartz may be subjected to density loss due to α-β quartz transition during exhumation of the rock. Our experimental work has illustrated that the density loss is only about −0.5% at 320 MPa hydrostatic pressures, and rapidly increases towards lower pressures. Consequently, the α-β quartz transition does not affect fluid densities at higher pressure, at metamorphic conditions that occur in subduction zones and continental orogenic belts. However, the retrograde segment of a specific *P-T-t* path (pressure-temperature-time) for a rock may follow a decreasing temperature during uplift and erosion, which may reach conditions below 300 MPa around 600 °C. Fluid inclusions in quartz in these rocks are most certainly affected by density-loss due to the α-β quartz transition.

4.6. Conclusions

Potential effects of the α-β quartz phase transition on the properties of fluid inclusions were investigated by re-equilibration experiments with synthesized H_2O-rich inclusions. Fluid inclusions were synthesized in the α-quartz and β-quartz stability fields with equal molar volumes, close to the phase transition. Complementary re-equilibration experiments were performed at the same experimental pressure and temperature to avoid pressure gradients, fugacity gradients and deformation. Therefore, any changes in fluid properties of the

inclusions were caused only by the α-β quartz transition.

Shape changes are independent of the used fluid composition, either H_2O or D_2O. The majority of the originally regular and equant fluid inclusions reveal only minor changes in shape after re-equilibration. Only elongated and irregular fluid inclusions are affected by shape changes, and reach relative values of 55% and 60% in shape parameters in the α-quartz and β-quartz re-equilibration experiments, respectively. Re-equilibration experiments with pure H_2O demonstrate only minor changes in fluid inclusion properties in the α-quartz stability field. These experiments also reveal the sensitivity of changes in fluid inclusion density due to minor changes in experimental conditions. Fluid inclusions properties are significantly changed to lower densities after the re-equilibration experiment in the β-quartz, due to the α-β quartz phase transition. The magnitude of the hydrothermal pressure affects the amount of density loss. At 320 MPa, a density loss of approximately −0.6% is observed, whereas density loss up to 3.0% is measured at 280 MPa after 19 days of experimentation.

Additional fugacity gradients were induced with pure D_2O re-equilibration experiments. The mobility of both H_2O and D_2O at the same conditions illustrates the efficiency of diffusion processes within 19 days. Fluid inclusions contain up to 53 mol% D_2O after the re-equilibration experiment in the α-quartz stability field, but up to 97 mol% D_2O after re-equilibration in the β-quartz stability field. The observed changes in homogenization temperatures illustrate that density loss due to the α-β quartz phase transition is an additional process that affects inclusions from the β-quartz re-equilibration experiments, and that the density-loss caused by the α-β quartz phase transition is more efficient at lower pressures.

Acknowledgments

We would like to thank the Austrian Science Fund (FWF) for financial support (project no. P 22446-N21). Alfons van den Kerkhof and an anonymous reviewer are thanked for their fruitful critics and suggestions. Comments from M. Scambelluri (editor) clearly improved the manuscript.

Supplementary data to this article can be found online at http://dx.doi.org/10.1016/j.lithos.2014.03.018.

5. Modification in fluid inclusion salinity during re-equilibration experiments at constant experimental *P-T*

Gerald Doppler • Ronald J. Bakker

Chemical Geology (in preparation)
Submission for revision: estimated in August 2014

Abstract The mobility of different fluid species by diffusion through quartz crystals was investigated using synthetic fluid inclusions. Both, the initial synthesis experiments and the subsequent re-equilibration experiments were performed at unique *P–T* of 337 MPa and 600 °C within the α–quartz stability field. Different series of synthesis and re-equilibration experiments were performed: **1)** pure H_2O inclusions re-equilibrated "*blank*"; **2)** pure H_2O inclusions re-equilibrated with external H_2O–NaCl mixture; **3)** H_2O–NaCl inclusions re-equilibrated with external water; and **4)** H_2O–NaCl inclusions re-equilibrated "*blank*". The salt experiments were performed using different brine concentrations, e.g. 19.8 mass % NaCl, 16.3 mass % NaCl, 10 mass % NaCl. It could be proved that post entrapment fluid inclusion shape changes are more dominant in pure H_2O inclusions, compared to minor shape changes of brine-inclusions which increase the solubility of the surrounding quartz. Pure H_2O inclusions which were faced to brine during re-equilibration lost water according to the induced water fugacity gradient. Fluid inclusion salinity was increasing during re-equilibration, whereas density was decreasing. Re-equilibrated H_2O-NaCl inclusions which were faced to pure H_2O during re-equilibration revealed a reverse diffusion behavior after experimentation of 5 days, 19 days, and 40 days. Water moved against the induced water fugacity gradient after 5 days. Inclusions of these assemblages lost water, with increasing T_h and decreasing T_m(ice). Re-equilibration of synthesized pure H_2O inclusions with external brine could prove that NaCl is not diffusing through quartz at the chosen *P–T*; T_m(ice) did not change, even after 40 days of experimentation. This experimental study shows that morphology, salinity, and density of entrapped fluid inclusions can be easily changed after entrapment in natural rocks at crustal conditions of 10 km depth and at a standard geothermal gradient.

Keywords Fluid inclusions · quartz · diffusion · re-equilibration · experimental study · H_2O–NaCl fluid

5.1. Introduction

Fluid inclusions are important indicators of rock forming conditions (Shepherd et al., 1985), and knowledge about possible post-entrapment modifications of fluid properties are of major importance to fluid inclusion studies. These were discussed by prior authors, e.g. Barker (1995), Küster and Stöckhert (1997), Audétat and Günther (1999), and Ayllón et al. (2003) for natural fluid inclusions. Their argumentation is mainly based on the textural analyses of individual fluid inclusions and a large variety in homogenization and dissolution temperatures in a single fluid inclusion assemblage. It does not provide information about processes, timing, and driving force of

modifications.

Water and salt are major components in natural fluids that are observed in fluid inclusions in most types of rocks. These inclusions are often hosted by quartz, which is a nominally anhydrous mineral. However, the amount of water in quartz crystals is defined by structural OH groups and nano-scale water clusters, in addition to fluid inclusions (Johnson, 2006; Bakker, 2009; and references therein). The presence of salt is restricted to fluid inclusions.

Experimental re-equilibration studies on synthetic H_2O-NaCl fluid inclusions in natural quartz were presented by various authors (Sterner and Bodnar, 1989; Sterner et al., 1995; Vityk and Bodnar, 1995 and 1998). These experiments do not allow the identification of the effect of individual parameters on modification, such as fugacity gradients, pressure gradients, deformation, and α–β quartz phase transition (see also Doppler and Bakker, 2014). For example, Sterner and Bodnar (1989) performed experiments at 700 °C and various pressures with gradients in pressure (internal over- and under-pressures) and H_2O fugacity gradients. Both gradients were simultaneously applied during 7-day re-equilibration experiments, which took partly place in the β–quartz stability field. Sterner et al. (1994) performed re-equilibration experiments at constant temperature and pressure with highly saline synthetic fluid inclusions in argon and pure H_2O. The results of this study are not sufficiently elucidated, and the incompletely presented data does not allow an unambiguous interpretation. Moreover, most of the illustrated results are inconsistent and cannot be reproduced according to the lack of an explicit experimental setup description. The experiments of Vityk and Bodnar (1995, and 1998) were performed exactly at the α–β quartz phase transition. Their experimental setup does not allow a direct comparison of individual fluid inclusions before and after re-equilibrations, but is based on a bulk analysis of T_h values in distribution diagrams. The stepwise unloading of these experiments causes the formation of multiple generations of fluid inclusions with a variety of inclusion densities, and each generation is subject to different re-equilibration conditions. Histograms do not provide information about the modification of Th values of individual fluid inclusions, and a large part of the data in these histograms may correspond to synthesized inclusions, and not to re-equilibrated inclusions.

Properties of various synthetic pure H_2O and H_2O-NaCl fluid inclusions are described for the experiments presented in this study, before and after re-equilibration. Experiments were performed exclusively at constant temperature and pressure conditions (337 MPa and 600 °C) exclusively within the α–quartz stability field, for evaluating only the effect of H_2O-fugacity gradients on fluid inclusion modifications. The gradient in fugacity (or chemical potential) causes bulk diffusion of a component such as water through a homogeneous anhydrous medium such as quartz (Crank 1975, Bakker 2009, Doppler et al. 2013). Therefore, water diffusion in the form of molecular H_2O, and OH ions through quartz is expected in our experiments. NaCl is assumed not to diffuse through the quartz crystal at the chosen conditions. Experimental runtime varies between 5, 19 and 40 days to investigate time-dependent parameters, such as diffusion.

5.2. Experimental procedure

5.2.1. Hydrothermal laboratory

All experiments were carried out in the hydrothermal laboratory at the University of Leoben (Austria). The laboratory provides a high

temperature-pressure apparatus that enables conditions of maximum 1 GPa hydrothermal pressure and 700 °C. The device is constructed with 10 Nimonic IOS/René 41 autoclaves (Ni–Cr alloy) in a vertical position, with a cold-seal system (e.g. Kerrick 1987). Argon is used as pressure medium that is compressed by a high-pressure pump system. Pressure transducers monitored a pressure variation of 2 MPa during the experiments. The transducers are calibrated up to 700 MPa with a Heise dial gauge with an accuracy of 0.015 % of reading. External furnaces induce the appropriate temperature conditions. The temperature is measured by an internal thermocouple that allows direct monitoring and registration of the sample temperature with an uncertainty of 0.1 °C. Temperature during the experimental run was stabilized within 2 °C. The internal thermocouple allows direct controlling experimental temperature conditions during loading and unloading according to specific fluid isochores. Experimental pressure and temperature were continuously logged by the computerized system. Each experiment in the present study, both synthesis and the complementary re-equilibration were exclusively performed under hydrothermal conditions without any temperature and pressure gradients or deviatoric stress.

5.2.2. Fluid inclusion synthesis

Fluid inclusions were synthesized according to the method of Bodnar and Sterner (1987). Natural inclusion-free Brazilian quartz crystals were used as starting material. Cores with a length of approximately 1 cm and a diameter of 2.75 mm were drilled along the quartz *c*–axis. These cores were partially cracked by thermal shock after heating to 400 °C. Arc-welded gold capsules were used as containers which were loaded with the quartz core and pure H_2O , 19.8 mass % NaCl, 16.3 mass % NaCl, or 10.0 mass % NaCl. The induced cracks of the quartz cores entrapped the surrounding fluid by fracture-healing processes during the synthesis experiment. Experimental *P–T* conditions of each experiment are given in Table 1. Loading and unloading the experiments were performed along specific isochores of the entrapped fluid (Fig. 1) to prevent any stress that could cause cracking and deformation of inclusions due to internal fluid over- or under-pressure. Each synthesis experiment was carried out with a run-time of 19 days. The quartz cores were cut into approximately 0.5 mm thick disks, which were then polished on both sides to estimate morphological, volumetric and microthermometric properties of the original fluid inclusions (Appendix A).

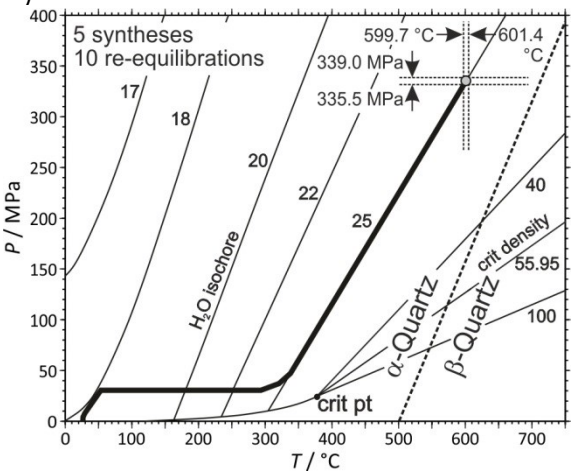

Fig. 1 Experimental *P–T* conditions of the initial synthesis and complementary re-equilibration experiments based on the computerized logging-system of the hydrothermal laboratory. The thick curve illustrates the loading and unloading of the experimental conditions with a logging interval of 5 minutes. Thin solid lines are isochores of pure H_2O. crit pt is the critical point of pure H_2O, and the isochore of the critical molar volume (55.95 $cm^3 \cdot mol^{-1}$) is also illustrated. The dashed line illustrates the α–β phase transition of quartz.

5.2.3. Re-equilibration of fluid inclusions

The same quartz disks were used for re-equilibration experiments at similar temperature and pressure conditions (Table 1). Two quartz rods, one below and one above the relatively fragile analyzed quartz disk in the gold capsule prevented any damages during the re-equilibration experiment. Pure H_2O, and aqueous mixture with 19.8 mass % NaCl, 16.3 mass % NaCl, and 10.0 mass % NaCl were added to the gold capsule in re-equilibration experiments. Loading and unloading of the pressure vessels was performed again along the specific isochore of the entrapped fluid with the intention to prevent any fluid over- or underpressure within the inclusions and to obtain the same experimental temperature and pressure. Re-equilibration experiments were carried out with variable run-times from 5, 17, 19, 34 to 40 days. After the re-equilibration experiments dissolution temperature of ice (salinity), homogenization temperature (density) and inclusions morphology (two-dimensional analysis) were compared to these properties of the initially synthesized fluid inclusions.

Table 1 Experimental conditions and fluid properties of initial synthesis experiments (*GMR*) and corresponding re-equilibration experiments (*R*).

Experiment	H_2O [a]	NaCl [a]	Days	P [b]	T [c]	f [d]	V_m [d]	V_m [e]
GMR003c	100	-	19	336.7 ± 1.3	600.7 ± 0.8	176.1 ± 1.2	25.02 ± 0.05	-
R003c	80	20	40	339.0 ± 1.5	600.4 ± 0.6	157.4 ± 1.4	24.16 ± 0.03	23.69 ± 0.03
GMR004d,g	100	-	19	336.0 ± 1.6	601.4 ± 2.0	176.0 ± 2.0	25.06 ± 0.09	-
R004d	80	20	19	337.4 ± 1.0	600.2 ± 0.5	156.5 ± 0.8	24.18 ± 0.02	23.71 ± 0.02
R004g	100	-	19	337.6 ± 1.6	599.7 ± 0.8	176.1 ± 1.4	24.98 ± 0.06	-
GMR005a,b,c	80.2	19.8	19	336.9 ± 1.6	600.2 ± 0.9	156.2 ± 1.3	24.19 ± 0.04	23.72 ± 0.04
R005a	100	-	19	336.4 ± 1.6	599.9 ± 1.0	175.4 ± 1.6	25.01 ± 0.06	-
R005b	100	-	40	336.3 ± 1.2	600.2 ± 0.4	175.5 ± 0.9	25.02 ± 0.04	-
R005c	100	-	5	332.7 ± 0.6	600.5 ± 0.4	173.5 ± 0.6	25.12 ± 0.03	-
GMR011a	90	10	19	337.4 ± 0.6	599.8 ± 0.3	163.5 ± 0.5	24.42 ± 0.02	24.17 ± 0.02
R011a	100	-	19	338.2 ± 1.0	600.4 ± 0.5	176.8 ± 0.9	24.98 ± 0.04	-
GMR014a,b,c	83.7	16.3	19	337.5 ± 0.7	600.1 ± 1.2	159.3 ± 0.9	24.26 ± 0.04	23.84 ± 0.04
R014a	100	-	40	338.5 ± 0.7	599.7 ± 0.8	176.6 ± 0.9	24.96 ± 0.04	-
R014b	83.7	16.3	17	336.5 ± 1.0	599.9 ± 0.4	158.7 ± 0.7	24.23 ± 0.01	23.86 ± 0.01
R014c	83.7	16.3	34	337.6 ± 1.3	599.8 ± 0.5	159.2 ± 1.0	24.21 ± 0.01	23.84 ± 0.01

a) Composition in mass %
b) Experimental pressure in MPa
c) Experimental temperature in °C
d) H_2O fugacity (in MPa) and fluid molar volume (in $cm^3 \cdot mol^{-1}$) calculated with Haar et al. (1984) for pure H_2O fluids and with Anderko and Pitzer (1993) for H_2O–NaCl mixtures, using the software *Loner HGK* and *Loner AP*, respectively (from R. J. Bakker, *http://fluids.unileoben.ac.at*)
e) Fluid molar volume (in $cm^3 \cdot mol^{-1}$) of H_2O–NaCl mixtures calculated with Driesner (2007), using the software *AqSo DH* (from R. J. Bakker, http://fluids.unileoben.ac.at)

5.2.4. Optical analysis and microthermometry

Each quartz disk was investigated by microscopic examinations with an optical microscope Olympus BX60. Up to 100 fluid inclusions were photographed for analyzing shape, size and identification purposes (Appendix volumes at experimental conditions are

and identification purposes (Appendix A). The distance to the crystal surface of fluid inclusions was measured by focusing the inclusions with adjusting the z-direction of the microscope stage. Morphological aspects of fluid inclusions, i.e. (**1**) size and (**2**) shape were characterized by tracing digitally the outside edges of the inclusions at room temperature according to Bakker and Diamond (2006). Fluid properties, i.e. (**1**) composition and (**2**) density were analyzed by microthermometric investigations. Homogenization and dissolution temperatures of the entrapped fluids were measured by using the LINKAM MDS 600 and LINKAM THMSG 600 heating-freezing stages, which were calibrated with synthetic fluid inclusions at –56.6 °C (melting of CO_2), 0.0 °C (melting of H_2O), and 374.0 °C (critical density of H_2O). The resolution of temperature measurements was ±0.1 °C (see Doppler and Bakker, 2014).

5.2.5. Calculation of fluid properties

The properties of pure H_2O fluids were calculated with the equation of state from Haar et al. (1984) with the software *Loner HGK* (*http://fluids.unileoben.ac.at*). Fluid inclusions density (and molar volume) was calculated from homogenization temperatures T_h(LV → L). The salinity of H_2O-NaCl inclusions was calculated from dissolution temperatures of ice, T_m(ice), with the software *AqSo WHS* (Bakker, 2012; software available from: *http://fluids.unileoben.ac.at*) from the package *FLUIDS* (Bakker 2003). The software *Loner AP* and *AqSo DH* were used for calculating density, molar volume, fugacities and homogenization temperatures for H_2O-NaCl fluid mixtures, with the equations from Anderko and Pitzer (1993) and Driesner and Heinrich (2007), Driesner (2007), respectively (software available from: *http://fluids.unileoben.ac.at*). The calculated H_2O fugacity and molar volumes at experimental conditions are illustrated in Table 1.

Theoretical homogenization temperatures of fluid inclusions can be calculated from the experimental conditions of fluid entrapment (Table 1) with the selected equations of state. Pure H_2O fluids trapped in the synthesis experiment *GMR003c* should homogenize at 296.2 ± 0.8 °C, which correspond to the calculated molar volume of 25.02 ± 0.05 $cm^3 \bullet mol^{-1}$ at experimental conditions. This homogenization temperature is corrected to 292.6 ± 0.8 °C according to the volumetric properties of the quartz host (Hosieni et al. 1985), which result in a molar volume modification of the entrapped fluid of 24.77 ± 0.05 $cm^3 \bullet mol^{-1}$ at T_h. The synthesis experiments *GMR004d* and *g* should reveal homogenization temperatures of 293.2 ± 1.5 °C.

The theoretical homogenization temperatures of H_2O-NaCl inclusions (19.8 mass % NaCl) from synthesis experiments *GMR005a*, *b*, and *c* are calculated at 329.7 ± 1.2 °C, according to the purely empirical equations from Driesner and Heinrich (2007) and Driesner (2007). The relative quartz host contraction along the isochore towards homogenization conditions is about 0.6 vol. %, which result in a minor correction of the molar volume to 23.58 ± 0.04 $cm^3 \bullet mol^{-1}$ at T_h. The synthesis experiments *GMR014a*, *b* and *c* with 16.3 mass % NaCl aqueous fluid inclusions should reveal homogenization temperatures of 324.2 ± 1.0 °C. The fluid inclusions with 10.0 mass % NaCl from synthesis experiment *GMR011a* should have homogenization temperatures of 314.5 ± 0.4 °C.

5.3. Experimental results

5.3.1. The H_2O blank re-equilibration experiment

The so called "blank" re-equilibration

experiment with pure H_2O was performed with the same fluid species for both the original synthesis (*GMR004g*) and the complementary re-equilibration (*R004g*) at same temperature and pressure, to check if the experimental setup is able to influence the properties of fluid inclusions. Pure H_2O fluid inclusions were synthesized at 601.4 ± 2.0 °C and 336.0 ± 1.6 MPa and subsequently re-equilibrated at 599.7 ± 0.8 °C and 337.6 ± 1.6 MPa (Table 1, Fig. 1). Most of the synthesized inclusions have a regular-equant shape, whereas some are regular-elongated (Fig. 2a).

Most fluid inclusions did not change their shape after 19 days of re-equilibration. Significant changes in fluid inclusions density due to deformation processes that may be induced by pressure gradients between fluid inclusions and pore fluid during loading and unloading the experiments were not observed. Homogenization temperatures of the pure H_2O synthesis *GMR004g* reveal a mean Th of 292.8 °C (Table 2, Fig. 3a), and variation of FWHM (full with at half maximum) from 291.4 to 294.1 °C, which illustrates the homogeneity of this fluid inclusion assemblage.

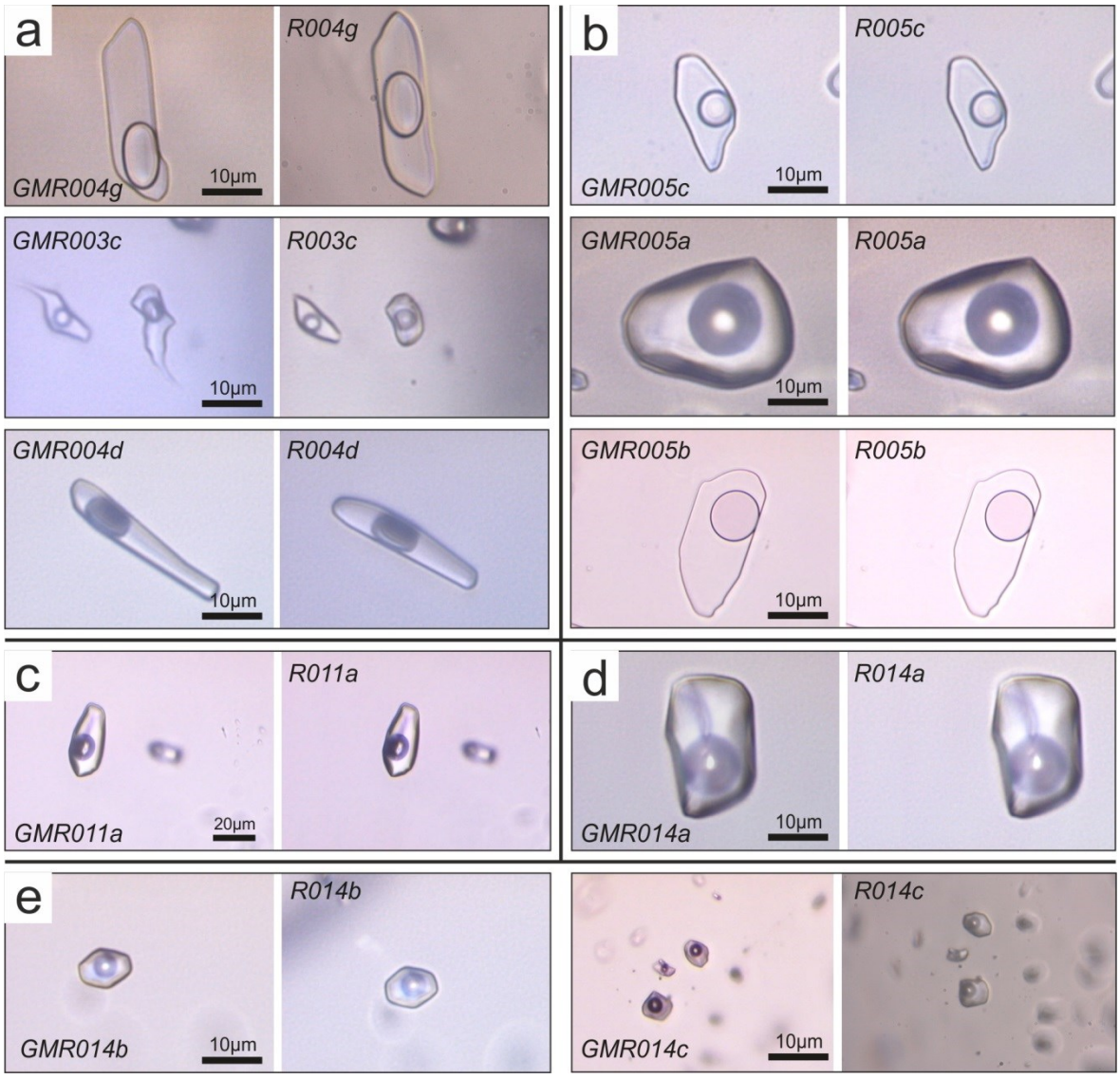

Fig. 2 Photomicrographs of the same inclusions before (*GMR*) and after the re-equilibration (*R*) experiments. a) *R004g*: H_2O blank; *R003c*: 20 mass % NaCl; and *R004d*: 20 mass % NaCl. b) *R005c*: 5d H_2O; *R005a*: 19d H_2O; and *R005b*: 40d H_2O. c) *R011a*: 19d H_2O; d) *R014a*: 40d H_2O; and e) *R014b*: 17d 16.3 mass % NaCl blank; and *R014c*: 34d 16.3 mass % NaCl blank.

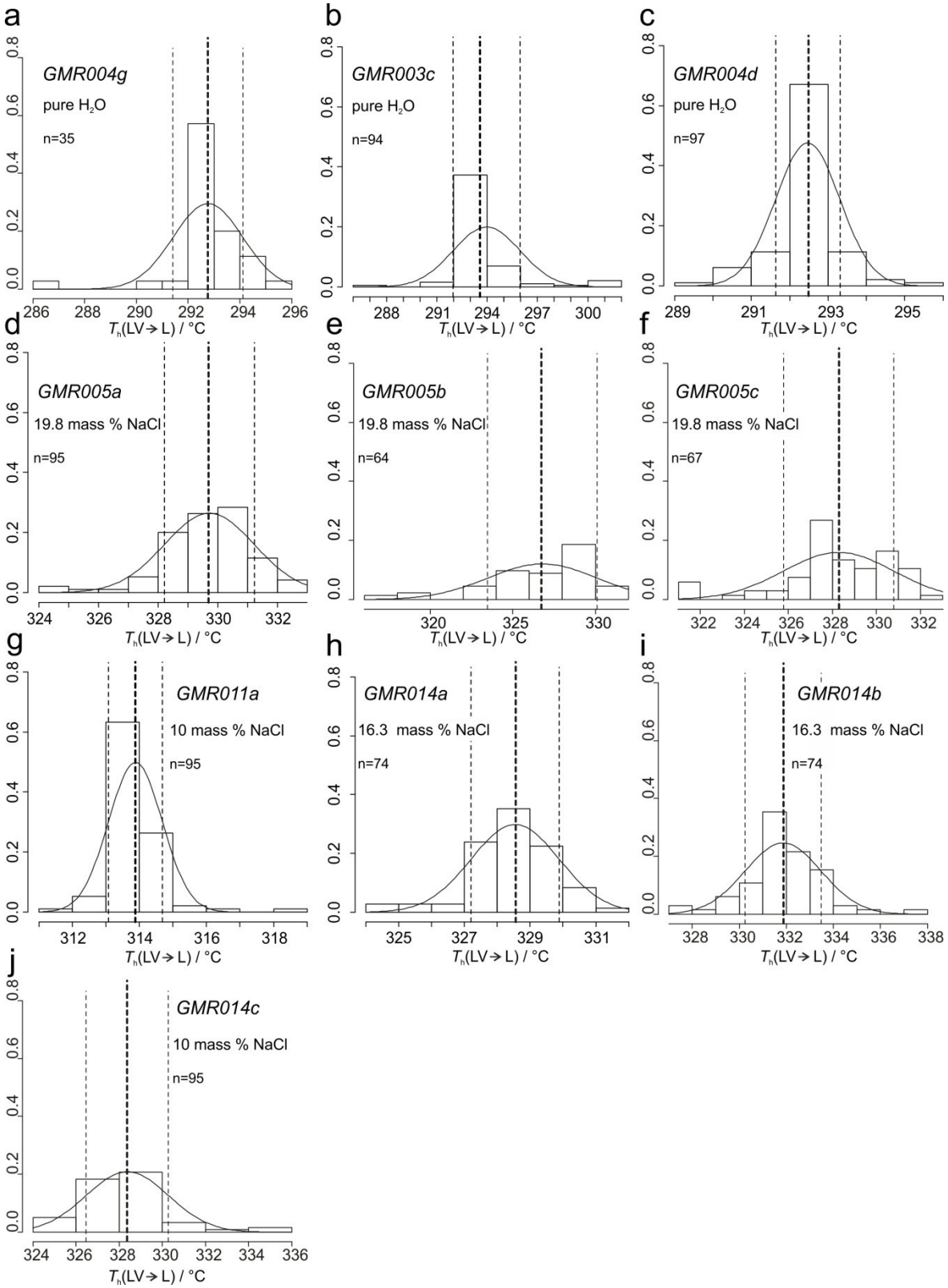

Fig. 3 Homogenization temperature histograms of initial synthesis experiments. The distribution is modelled according Gaussian distribution function (software *R version 2.7.0*). The thick dashed lines are the mean T_h, the thin dashed lines represent the FWHM. See text and Appendix B for further information.

Table 2 Fluid inclusion properties before (initial syntheses *GMR*) and after the re-equilibration experiment (*R*).

Synth.	*n* [a]	T_h [b]	*Range* [c]	T_m [d]	*Variation*	*Re-eq.*	*n* [a]	T_h [b]	*Range* [c]	T_m [d]	*Variation*
GMR003c	97	293.6	287.6/301.8	0.0	±0.1	*R003c*	84	294.7	292.2-296.9	0.0	±0.1
GMR004d	100	292.5	289.5/295.6	0.0	±0.1	*R004d*	68	294.4	292.3-297.6	0.0	±0.1
GMR004g	35	292.8	286.5/295.2	0.0	±0.0	*R004g*	34	292.2	286.2 295.3	0.0	±0.1
GMR005a	100	329.7	324.4/332.8	−16.5	±0.2	*R005a*	87	333.1	328.1-336.4	−18.9	±1.7
GMR005b	100	326.9	316.0/330.8	−16.9	±0.3	*R005b*	64	337.1	327.6-342.1	−21.1	±1.1
GMR005c	70	328.3	321.5/332.1	−16.5	±0.0	*R005c*	67	326.5	319.6-332.4	−17.1	±1.0
GMR011a	97	313.9	311.8/318.8	−6.6	±0.1	*R011a*	96	312.4	310.7-314.5	−7.2	±0.4
GMR014a	71	328.5	327.8/331.9	−12.4	±0.0	*R014a*	67	335.3	331.8-338.4	−16.0	±2.0
GMR014b	65	331.9	327.0/337.2	−12.2	±0.1	*R014b*	60	328.4	324.7-333.5	−12.8	±0.5
GMR014c	60	328.4	324.9/335.1	−12.3	+0.0	*R014c*	34	337.0	323.0-331.4	−12.8	±0.5

a) Number of measured fluid inclusions
b) Mean T_h (homogenization temperature) in °C
c) Minimum and maximum T_h in °C
d) Mean T_m (ice dissolution temperature) in °C

This temperature corresponds to the calculated values according to the equation of state from Haar et al. (1984). After re-equilibration (*R004g*), the mean Th is 292.2 °C, varying between +3.1 and –6.0 ˚C (Table 2). The experimental setup, i.e. the intended experimental temperature and pressure corresponds to the measured properties of fluid inclusions. Direct comparison of individual synthesized and re-equilibrated fluid inclusions (Fig. 4a) indicates that the multiple isochoric loading and unloading of the experiments does not affect these properties.

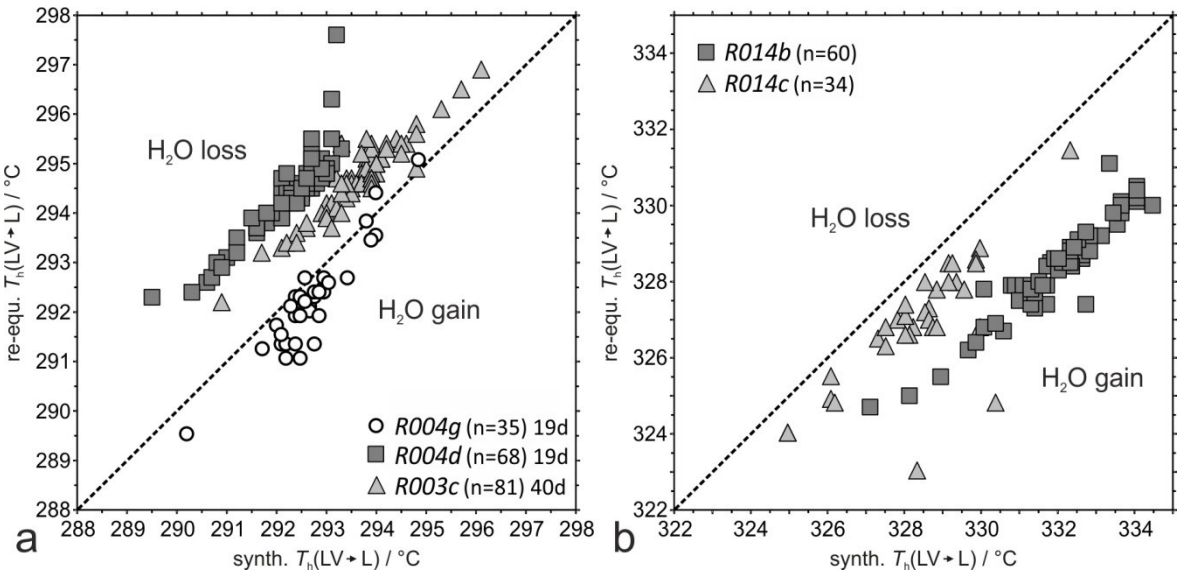

Fig. 4 Homogenization temperatures before and after re-equilibration. a) Two H_2O syntheses re-equilibrated with 20 mass % NaCl for different run-times (19 days for experiment *R004d* and 40 days for *R003c*). Experiment *R004g* is the result of "blank" re-equilibration with pure H_2O for 19 days. b) Two 16.3 mass % NaCl syntheses blank re-equilibrated with 16.3 % with two different run-times (17 days for experiment *R014b* and 34 days for *R014c*).

5.3.2. Pure H_2O fluid inclusions re-equilibrated in 20 mass % NaCl

Re-equilibration of pure H_2O inclusions in a brine with 20 mass % NaCl (experiments *R003c* for 40 days and *R004d* for 19 days) should give insights whether NaCl can diffuse into fluid inclusions through the quartz disk and H_2O can diffuse out of fluid inclusions according to gradients in fugacity. These processes would modify the density and composition of the originally synthesized inclusions, which can be verified by measuring a modification in dissolution temperature of ice due to increased salinity, and a modification in homogenization temperature due to H_2O loss.

Originally irregular fluid inclusions (*R003c*; Fig. 2a) and elongated inclusions (*R004d*; Fig. 2a) tended to reach "ideal shape" during the re-equilibration process, and demonstrate large modifications in shape parameters (Fig. 5). Considering the different experimental run-times no substantial differences in magnitude of shape changes could be observed between the long term *R003c* and the short term *R004d* (Fig. 5). The maximum post entrapment shape change was noticed after 19 days of re-equilibration (*R004d*) with a modification of 90 % in perimeter/area ratio and in elongation.

The fluid inclusions measured after the 40 days re-equilibration experiment (*R003c*) shows a maximum shape change of 80 %.

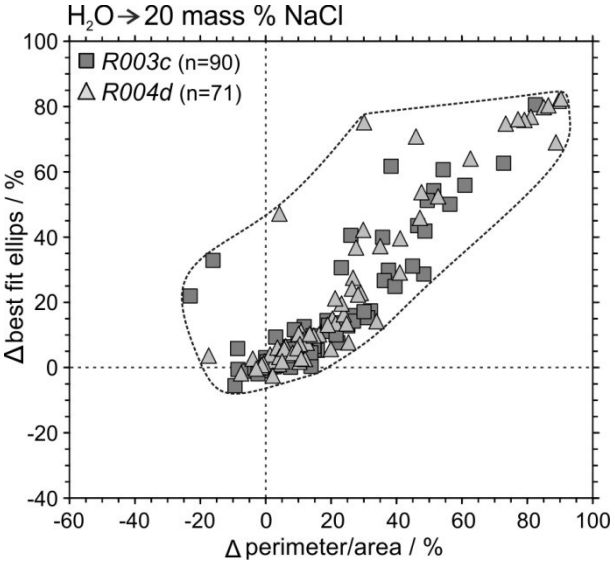

Fig. 5 Fluid inclusion shape change diagrams of pure H_2O fluid inclusions, that were re-equilibrated with 20 mass % NaCl for 19 days (experiment *R004d*) and 40 days for (*R003c*). 'Δ best fit ellipse' and 'Δ perimeter/area' are defined as the relative change in the ratio major/minor of the best fit ellipse and the relative change in the ratio perimeter/area (see Bakker and Diamond, 2006).

The homogenization temperatures of the pure H_2O synthesis experiments *GMR003c* and *GMR004d* reveal a regular T_h distribution (Gaussian distribution) for both experiments as illustrated in Figures 3b and c and Table 2. The mean T_h of experiment *GMR003c* was 293.6 °C, with a variation of FWHM from 292.0 to 296.0 °C and *GMR004d* showed a mean T_h of 292.5 °C with a variation in FWHM from of 291.7 to 293.2 °C which correspond to the expected temperatures according to calculated values from experimental conditions: 292.6 ± 0.8 ˚C and 293.2 ± 1.5 ˚C, respectively. The original dissolution temperature of all pure H_2O inclusions is 0.0 °C (Table 2). A modification of Tm(ice) was not observed after re-equilibration with a 20 mass % NaCl fluid in 19 days (*R004d*) nor 40 days (*R003c*). Therefore, pure H_2O inclusions were not enriched in NaCl at 600 °C and 337 MPa. However, T_h of fluid inclusions were modified to higher values during re-equilibration in both experiments (Table 2, Fig. 4a), which correspond to lower densities and a loss of H_2O. The maximum positive shift in T_h for the 40 days re-equilibration experiment *R003c* was +2.1 °C. T_h of the 19 days experiment *R004d* shifted to a maximum ΔT_h of +4.4 °C. The loss of H_2O is expected according to the gradients in fugacity between fluid inclusions and pore fluid (Table 1).

5.3.3. Fluid inclusions with 19.8 mass % NaCl re-equilibrated in pure H_2O

Synthesized 19.8 mass % NaCl inclusions (*GMR005a*, *b*, and *c*) were re-equilibrated in pure H_2O at various experimental run-times: for 5 days (*R005c*), for 19 days (*R005a*), and for 40 days (*R005b*). It is expected that H_2O will diffuse into fluid inclusions according to the fugacity gradient at 600 °C and 337 MPa (Table 1). Consequently, fluid inclusions will be enriched in H_2O and become less saline whereas the density will increase. These modifications can be deduced from variations in T_m(ice) and Th. Modifications in fluid inclusion salinity and density should progress with increasing re-equilibration time according to the principles of diffusion.

Most fluid inclusions that have been synthesized with 19.8 mass % NaCl in the experiments *GMR005a*, *b*, and *c* showed regular and equant shapes and did not change the morphology significantly after re-equilibration (Fig. 2b). Inclusions already developed a negative crystal shape after 5 days of synthesis, and the perfection of this shape does not provide any driving force for shape-modifications during re-equilibration.

The original synthesized fluid inclusions in the experiments *GMR005a*, *b*, and *c* reveal ice dissolution temperatures of –16.5 ˚C, which correspond to 19.8 mass% NaCl (Table 2). After 5 days of re-equilibration (*R005c*) at constant temperature and pressure, the mean Tm(ice) was modified to –17.1 °C, varying between 319.6 and 332.4 °C, corresponding to a salinity of 20.3 ±

0.7 mass % NaCl (Table 2, Fig. 6). The increase in salinity is not consistent with the expected dilution due to H2O diffusion into fluid inclusions (cf. fugacity gradients, Table 1). After 19 days of re-equilibration (R005a), fluid inclusion compositions are further modified to higher salinities (21.6 mass % NaCl), as reflected by a mean T_m(ice) of –18.9 °C, varying between –17.2 and –20.2 °C (Table 2, Fig. 6). Finally, after 40 days of re-equilibration (*R005b*), T_m(ice) was further decreased to a mean value if –21.1 ˚C, varying between –19.2 and –22.2 °C (Table 2, Fig. 6), corresponding to a salinity of 23.1 ± 2.7 mass % NaCl.

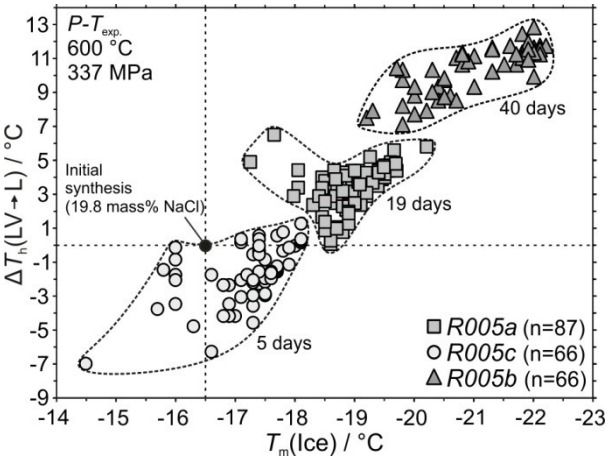

Fig. 6 Ice-melting temperatures and change in homogenization temperatures of initially 19.8 mass % NaCl inclusions after re-equilibration with pure H_2O and different experimental run-times. The zero-point indicates fluid inclusion properties after the initial synthesis of *GMR005a*, *b*, and *c*.

Total homogenization temperatures of 329.7 ± 3.1 °C, 326.9 ± 3.9 °C, and 328.3 ± 3.8 °C are obtained from synthesize experiments *GMR005a*, *b*, and *c*, respectively (Table 2, Fig. 3d, e, and f). These values are consistent with the calculated H_2O-NaCl fluid properties according to the experimental conditions. After 5 days of re-equilibration (*R005c*), the spread in T_h values was largely increased to a range of 319.6 to 332.4 °C (Table 2, Fig. 6), whereas most individual inclusions reveal a decrease in T_h, which correspond to a minor increase in density. This increase can only be obtained by adding H_2O to the inclusions by diffusion processes or by loss of total inclusion volume at constant temperature and pressures. However, the trend in modification of Th illustrates higher values for longer re-equilibration experiments (19 and 40 days). Experiment *R005a* (19 days) reveals an average T_h of 333.1 °C with a variation of 328.1 to 336.4 °C (Table 2, Fig. 6), whereas those values increased to an average of 337.1 °C and a variation of 327.6 to 342.1 °C after 40 days of re-equilibration (*R005b*) (Table 2, Fig. 6). The increase in T_h correspond to a decrease in fluid inclusion density, consequently, inclusions in the long-term experiments must have lost fluid components according to diffusional processes.

Comparison of changes in T_h and T_m(ice) of individual fluid inclusions (Fig. 6) demonstrates that preferential H_2O loss at constant temperature (600 ˚C) and pressure (336 MPa) is increasingly important for longer-term experiments. This process is directly deduced from the calculated increase in salinity and decrease in density of individual fluid inclusions. It must be noted that this process is not consistent with theoretical modifications according to the applied gradient in H_2O fugacity.

5.3.3.1. Concentration profiles: depth and size relation

As each investigated fluid inclusion was localized within the quartz disk, the accordant composition can be charted in concentration profiles that are related to the distance from the sample surface (Fig. 7a and Fig. 8a). All 19.8 mass % NaCl experiments which have been re-equilibrated in pure H_2O (*R005a*, *b* and *c*) with different run-times are plotted in these diagrams to illustrate the different magnitude of compositional and density changes. An envelope can be constructed to indicate the limit of maximum changes. Figure 7a

shows that similar to Figure 6 some inclusions of the short term experiment of 5 days for *R005c* shift to positive T_m(ice) whereas the majority shift to negative T_m(ice). Concerning the longer run-time experiments (19 days for *R005c* and 40 days for *R005b*), a shift of the corresponding envelope to negative values is recorded. No relation of magnitude of compositional change related to the distance to the crystal surface can be recorded (Fig. 7a).

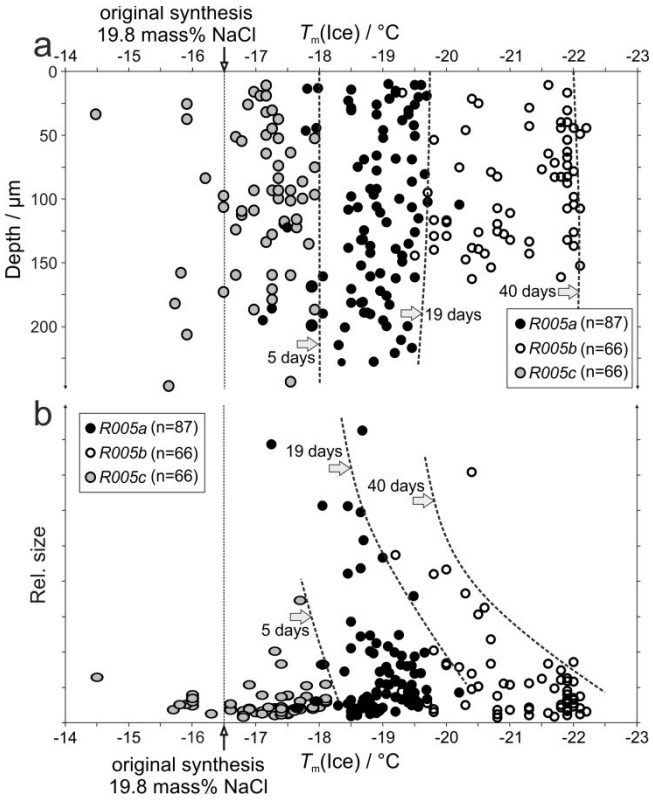

Fig. 7 Concentration profiles in terms of T_m(ice) of initially synthesized fluid inclusions with 19.8 mass % NaCl after re-equilibration in pure H_2O with different run-times. a) Dissolution temperatures of fluid inclusions plotted against inclusions distance to the crystal surface (Depth) and T_m(ice) as a function of inclusions size in (b).

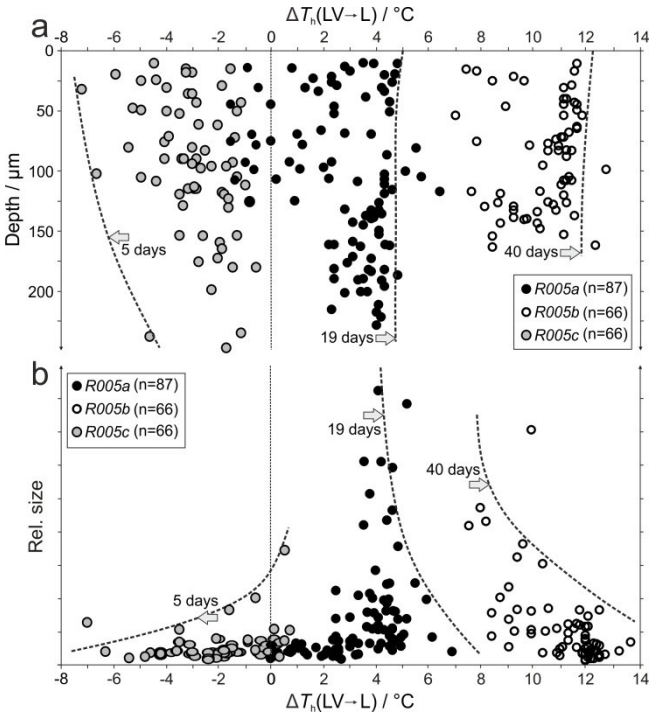

Fig. 8 Concentration profiles in terms of ΔT_h of initially synthesized fluid inclusions with 19.8 mass % NaCl after re-equilibration in pure H_2O with different run-times. a) Homogenization temperatures of fluid inclusions plotted against inclusions distance to the crystal surface (Depth) and T_h as a function of inclusions size in (b).

Fluid inclusions dissolution temperature is plotted against the relative inclusion size (Fig. 7b). A general shift of the corresponding envelope to negative T_m(ice) can be related to the different run-times of re-equilibration. The three envelopes indicate a size-dependency with a higher shift of smaller inclusions to lower T_m(ice) compared to larger inclusions which have a smaller shift (Fig. 7b).

As the diagram in Figure 6 illustrates a general negative shift in T_h of the 5 days experiment *R005c*, the corresponding envelope can be constructed in positive ΔT_h direction (Fig. 8a). Shallower inclusions of *R005c* changed more than deeper inclusions. Fluid inclusions of *R005a* (19 days) and *R005b* (40 days) shift to positive ΔT_h. No difference in magnitude of change can be observed concerning the inclusions depth for these two re-equilibration experiments (Fig. 8a).

Similar to Figure 7b a size-dependency of fluid inclusion modification can be observed concerning change in Th (Fig. 8b). The majority of short term re-equilibrated inclusions of *R005c* shift to negative

ΔT_h, where smaller inclusions show higher magnitudes of density change compared to larger inclusions. After 19 and 40 days of re-equilibration the respective envelope shifts to positive ΔT_h with the same characterized size dependency (Fig. 8b).

5.3.4. Fluid inclusions with 10 mass % NaCl re-equilibrated in pure H_2O

Fluid inclusions synthesized with 10 mass % NaCl (*GMR011a*) have regular-equant shapes (Fig. 2c), approximately negative-crystal shapes. After re-equilibration in 19 days (*R011a*), these inclusions do not reveal significant modifications in shape parameters (Fig. 2c), similar to the previously described fluid inclusions with 19.8 mass % NaCl.

The original T_m(ice) of all synthesized inclusions is –6.6 °C (Table 2), which are modified to an average value of –7.2 °C (10.7 mass % NaCl) and a variation of –6.8 to –7.5 °C after 19 days of re-equilibration in pure H_2O (Fig. 9). Again, these modifications are not corresponding to expected processes according to fugacity gradients, but illustrate the preferential loss of H_2O. The magnitude of modifications is similar to the short-term (5 days) re-equilibration experiment *R005c* with higher salinity inclusions.

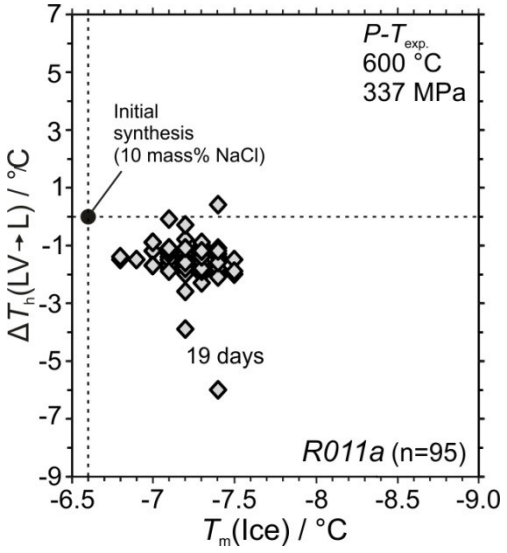

Fig. 9 Ice-melting temperatures and change in homogenization temperatures of initially 10 mass % NaCl inclusions after 19 days of re-equilibration with pure H_2O.

The mean T_h of fluid inclusions from the synthesize experiment *GMR011a* is 313.9 °C with a variation of 311.8 to 318.8 °C (Table 2, Fig. 3g), which is corresponding to the theoretical predicted values obtained from experimental conditions. After re-equilibration, the mean T_h is decreased to 312.4 °C with a much larger variation of 310.7 to 314.5 °C (Table 2). Individual fluid inclusions reveal significant modifications in T_h and T_m simultaneously (Fig. 9), with up to 7 degrees decrease in T_h and up to 1 degree decrease in T_m.

5.3.5. Fluid inclusions with 16.3 mass % NaCl re-equilibrated in pure H_2O

Synthesized fluid inclusions with 16.3 mass % NaCl (*GMR014a*) have regular and equant shapes (approximately negative-crystal shape) and do not modify their shape parameters after 40 days of re-equilibration in pure H_2O (*R014a*, Fig. 2d).

All the original synthesized fluid inclusions have T_m(ice) of –12.4 °C (Table 2), which corresponds to a salinity of 16.3 mass % NaCl. This temperature decreases significantly, up to –4.5 degree in individual inclusions, after 40 days of re-equilibration (*R014a*), resulting in an average value of –16.0 °C (19.4 mass % NaCl) and a variation of –14.0 to –16.5 °C (Table 2, Fig. 10). The magnitude of modification is similar to the 19 days re-equilibration experiments with 19.8 mass % NaCl inclusions (*R005a*).

The average T_h in experiment *GMR014a* is 328.5 °C with a variation of 327.8 to 331.7 °C (Table 2, Fig. 3h), which corresponds to the predicted fluid properties according to the experimental conditions. After re-equilibration in pure H_2O at constant temperature and pressure (*R014a*), T_h values were modified to an average value of 335.3 °C and a larger variation of 331.8 to 338.4 °C (Table 2,

Fig. 10). The modification of T_h and T_m in individual fluid inclusions (Fig. 10) illustrates that preferential loss of H_2O must have occurred, in contrast to the expected diffusion of H_2O in to fluid inclusions, according to fugacity gradients.

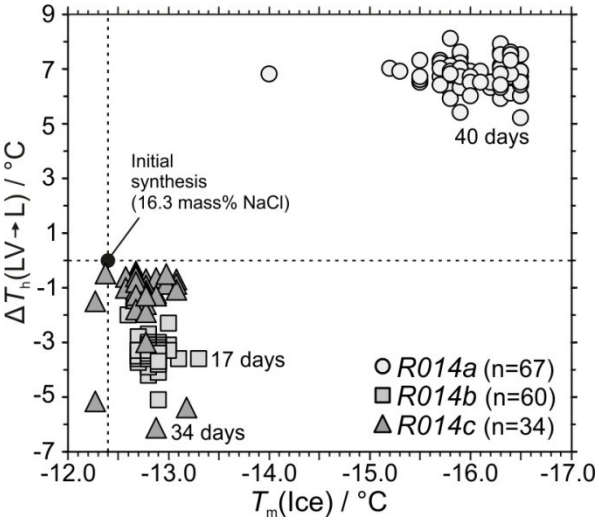

Fig. 10 Ice-melting temperatures and change in homogenization temperatures of initially 16.3 mass % NaCl inclusions. Circles show fluid inclusions re-equilibrated with pure H2O. Squares and triangles illustrate fluid inclusions after blank re-equilibration with 16.3 mass % NaCl for two different experimentation times.

5.3.6. Fluid inclusions blank re-equilibration with 16.3 mass % NaCl

Synthesized fluid inclusions containing 16.3 mass % NaCl (*GMR014b* and *GMR014c*) have equant and regular shapes (Fig. 2e) and do not change their shape properties during blank re-equilibration in a 16.3 mass % NaCl fluid even after 17 days (*R014b*) nor after 34 days (*R014c*, Fig. 2e).

The mean dissolution temperature of the synthesized fluid inclusions of the experiment *GMR014b* is –12.2 °C (Table 2), which corresponds to a salinity of 16.2 mass % NaCl. Fluid inclusions of synthesis experiment *GMR014c* reveal a T_m(ice) of –12.3 °C (Table 2) which corresponds to 16.2 mass % NaCl. After re-equilibration with the same fluid as it was used for the initial synthesis no changes in fluid inclusion density and composition should be expected. After blank re-equilibration in the 16.3 mass % NaCl fluid the mean T_m(ice) for both experiments shifted to –12.8 °C (Table 2, Fig. 10). The variation in T_m(ice) of the 17 days re-equilibration experiment *R014b* is –12.6 to –13.3 °C. After re-equilibration for 34 days of experiment *R014c* T_m(ice) varies from –12.3 to –13.2 °C.

The mean Th of synthesized fluid inclusions of *GMR014b* reveals 331.9 °C with a variation of 327.0 to 337.2 °C (Table 2, Fig. 3i). After 17 days of re-equilibration T_h shifted to a lower mean value of 328.4 °C with a variation of 324.7 to 333.5 °C (Table 2, Fig. 4b, Fig. 10). Experiment *GMR014c* has an average Th of 328.4 °C with a variation of 324.9 to 335.1 °C (Table 2, Fig. 4b, Fig. 3j). After 34 days of re-equilibration T_h shifted to a mean of 337.0 °C with a variation of 323.0 to 331.4 °C.

The negative shift in T_m(ice) and positive shift in T_h (Fig. 10) of both experiments (*R014b* and *c*) is similar to the changes in fluid inclusions of experiment *R011a* (Fig. 9).

5.4. Discussion

Fugacity gradients of fluid components and fluid pressure differences between inclusions and pore fluid are the driving forces in the performed re-equilibration experiments at constant *P-T*. Potential changes and modifications of synthetic fluid inclusions of previous experiments were discussed in Doppler et al. (2013) and Doppler and Bakker (2014). Comparable re-equilibration experiments on natural fluid inclusions were carried out by Baumgartner et al. (2014).

Experiment *R004g*

The measured properties of fluid inclusions correspond to the intended experimental temperature and pressure. Multiple isochoric loading and unloading of the experiments

may slightly affect the homogenization temperature according to the lower surrounding pore fluid density in the capsule during re-equilibration. The trend to slightly lower T_h's after re-equilibration is according to the experimental conditions and is due to the difference in water fugacity.

Experiments *R004d* and *R003c*

In contrast to the original assumptions only minor differences in magnitude of shape change can be observed concerning the different re-equilibration run-times of 19 days for *R004d* and 40 days for experiment *R003c*, respectively. The relatively high shape changing rates up to 90 % in Δ(perimeter/area), and around 80 % in Δ(best fit ellipse) could be developed by the tendency to reach negative crystal shapes concerning the inclusion walls.

Re-equilibration of pure H_2O fluid inclusions with a 20 mass % NaCl fluid would result in an increase in T_h towards 304 °C, if the H_2O fugacity inside the inclusions is modified to the external value of 157.4 MPa (see Table 1). Diffusion of H_2O according to the fugacity gradient would result in a molar volume increase to 25.87 $cm^3 \bullet mol^{-1}$, which is a loss of 3.3 mole%. This would also result in a pressure decrease inside the inclusions towards 305 MPa at 600 °C. Therefore, the diminution of a fugacity gradient through diffusion processes is producing a pressure gradient between inclusions and pore fluid. It is assumed that a pressure gradient of about –32 MPa, which is defined as pressure inside – pressure outside, will not be able to trigger deformation processes that may account for different types of re-equilibration. It is remarkable to observe that the changes in T_h values are larger for the 19 days experiment (*R004d*) than for the 40 days experiments (*R003c*). Diffusion of H_2O is the first parameter that affects the properties of these inclusions, but with increasing equalization of fugacities the pressure gradient becomes a parameter of major importance. The first parameter causes T_h values to increase, whereas the internal underpressure is causing T_h values to decrease in longer experiments to adapt the fluid inclusion properties to the external temperature and pressure, similar to the results of Sterner and Bodnar (1989), but in contrast to the experiments of Sterner et al. (1995) where only diffusion processes were assumed to modify fluid inclusions.

Experiments *R005a, b, and c*

No shape changes could be observed after re-equilibration experiments in pure H_2O. Using NaCl mixtures for synthetic fluid inclusions the solubility of quartz is increasing, resulting in no detection of shape changes after re-equilibration in pure water.

Fluid inclusions synthesized with 19.8 % NaCl show a time related trend of compositional change. The changes in T_h and T_m show a systematic development with experimental run-time of the re-equilibrated fluid inclusions (Fig. 6). Changes in composition and density of fluid inclusions were already detected after 5 days of experimentation (experiment *R005c*). Most of the re-equilibrated fluid inclusions reveal a decrease in T_h with a maximum shift of –7.0 °C, which may correspond to decreasing salinity. Consequently to the dilution of the entrapped brine the melting point must result in a shift of T_m (maximum –14.5 °C). However, most inclusions reveal an opposite shift in T_m to lower values (to a minimum of –18.1 °C), indicating a relative loss of H_2O, against the water fugacity gradient (Table 1). Some negative T_m shifting inclusions show higher T_h values (maximum ΔT_h of +1.2 °C), which indicate a decrease of fluid density.

Figure 6 visualizes that no fluid inclusions increased both, T_m and T_h. A positive shift in T_h (max. ΔT_h of +6.4 °C) and negative shift in T_m (down to

–20.2 °C) was more prominent for inclusions that have been re-equilibrated with 19 days in experiment *R005a*. All fluid inclusions in R005a became more saline and decreased density. This effect is even much more prominent for the 40 days re-equilibration experiment *R005b* with a maximum ΔT_h of +12.7 °C and a minimum T_m of –22.2 °C (Fig. 6).

Concentration profiles of the max. values (T_m and ΔT_h) and illustrate the time-dependent relation on compositional fluid inclusion post-entrapment changes. Changes in composition are independent on fluid inclusions depth (distance to the crystal surface; Fig. 7 and 8). Magnitude of compositional change is related to the inclusions size. Smaller inclusions are more affected and show higher changes in post-entrapment changes than larger inclusions.

Experiment *R011a*

As described for the brine inclusions of experiments *R005a*, *b*, and *c* no shape changes can be detected after re-equilibration in pure water.

Fluid inclusions synthesized with 10 mass % NaCl that were re-equilibrated in pure H_2O show a comparable trend to the major number of inclusions of experiment *R005c*. Inclusions salinity is increasing to a calculated percentage of 11.1 % NaCl after 19 days of experimentation. All inclusions, except one outlier show negative shift in homogenization temperature.

Experiments *R014a*, *b*, and *c*

The long-time re-equilibration experiment *R014a* reveals a comparable trend in compositional change as it was detected for the experiment *R005b*. 40 days of re-equilibrated, originally 10 mass % NaCl containing inclusions, in pure water result in increasing salinity against the imposed water fugacity gradient. Th shifts to a positive $\Delta_{max.}$*(R014a)* value of +8.1 °C, whereas $\Delta_{max.}$*(R05b)* revealed +12.7. Magnitude of density change is related to the salt concentration within the initially synthesized fluid inclusions.

Against the original assumptions the "*blank*" re-equilibration experiments *R014b* and *R014c* reveal changes of fluid inclusions density and composition. Although no significant differences in fluid fugacity occurred during re-equilibration, each individual fluid inclusion slightly modified its composition and density. All fluid inclusions increased salinity comparably to experiment *R011a*. Both experiments tend to decrease Th after re-equilibration with different magnitudes of change. After 17 days of re-equilibration the mean ΔT_h tends to decrease back to the original mean value (Fig. 4b).

5.5 Conclusions

Synthetic pure H_2O and NaCl-H_2O bearing fluid inclusions in quartz have been re-equilibrated at the same experimental *P-T* conditions as they were chosen for the initial experiments at 337 MPa and 600 °C. Post-entrapment changes in fluid inclusion morphology could only be detected for pure H_2O containing inclusions. NaCl mixture increases the solubility of the fluid inclusion hosting quartz, thus no quartz-growth can modify the inclusions morphology.

To check if the experimental setup is able to influence the properties of fluid inclusions, three so-called "*blank*" re-equilibration experiments were performed. One assemblage was carried out by the use of pure H_2O. The measured properties of synthesized fluid inclusions correspond to the intended experimental *P-T* conditions. Comparison of fluid inclusion properties before and after the re-equilibration experiment indicates that the multiple isochoric loading and unloading of the experiments did not affect these properties. Only minor changes in fluid inclusion morphology could be observed for a few fluid

inclusions.

Two assemblages with synthesized 16.3 mass % NaCl were "*blank*" re-equilibrated with different experimental run-times. Both experiments shifted to negative T_h and increased salinity. The shorter experiment, performed with 17 days reveals higher ΔT_h compared to the long-term experiment which was performed with 34 days.

A series of re-equilibration experiments was performed with originally 19.8 mass % NaCl fluid inclusions. This experimental time-series was performed for 5, 19, and 40 days with the same experimental setup. Due to the imposed fugacity gradient of H_2O between the entrapped brine and the crystal surrounding pure H_2O it was expected, that water will diffuse into the inclusions with the effect of dilution of the salt concentration. After 5 days of re-equilibration some of the fluid inclusions were diluted, however the major amount of fluid inclusions increased the salinity. Both variations occur with decreasing T_h. Some fluid inclusions tend to increase T_h with increasing T_m. After 19 days of re-equilibration all fluid inclusions shift to negative Tm and positive T_h. This effect is more prominent in the long-term experiment with 40 days. Constructing concentration profiles with the maximum ΔT_h and maximum T_m it can be observed that no relation between magnitude of compositional change and the distance to the quartz crystal surface occur. However, the magnitude of compositional change is a function of the fluid inclusion size.

One experiment with synthesized 10 mass % NaCl was carried out comparably to the 19 days experiment with synthesized 19.8 mass % NaCl. After re-equilibration in pure water all fluid inclusions shifted to negative ΔT_h and negative T_m against the imposed fugacity gradient of water.

Acknowledgments

We would like to thank the Austrian Science Fund (FWF) for financial support (project no. P 22446-N21).

Supplementary data to this article is attached to this work on DVD.

6. General conclusion

Synthetic H_2O-D_2O-NaCl fluid inclusions in quartz have been re-equilibrated with several different pore fluids at constant *P-T*. The superimposed gradient in fugacity provokes diffusion of water-related species such as H_2O, D_2O, H_2, and O_2. The chosen experimental *P-T* ranges from 675 to 300 °C and 340 to 280 MPa which represents crustal conditions at about 10 km depth and a normal geothermal gradient.

During the first experiments pure H_2O and pure D_2O were used to estimate the efficiency of temperature on water diffusion processes. These re-equilibration experiments were performed at systematically selected temperatures at constant pressure. The threshold temperature of water diffusion through quartz could be found around 450 °C at 337 MPa. Synthesis of fluid inclusions was possible at relatively low temperature of 300 °C. Estimated *T*-dependent morphological changes of fluid inclusions could be observed by these experiments. Fluid inclusions tend to become ideal and regular shaped during ongoing re-equilibration. Water diffusion through quartz starts already after one day of experimentation at 600 °C and 340 MPa. These experiments were exclusively designed within the α-quartz stability field.

The effects of the α-β quartz phase transition on water diffusion through quartz were tested with re-equilibration experiments which were carried out near the phase transition. The experiments were designed between 625 and 675 °C with pressure between 320 and 280 MPa, both in the α-quartz and β-quartz stability field. It was found, that morphological changes of fluid inclusions are independent of the used pore fluid composition, either H_2O or D_2O. Only minor differences in magnitude of shape changes were detected concerning the quartz stability field. But changes in composition (H_2O and D_2O) and density of the fluid inclusions are more dominant in the β-quartz stability field. Water diffusion rates are significantly higher above the quartz phase transition inter alia due to bigger gaps in the quartz crystal lattice.

NaCl-H_2O bearing fluid inclusions were synthesized to investigate diffusion behavior of brines within quartz. Differently designed re-equilibration experiments showed that NaCl is immobile and does not diffuse through quartz at 600 °C and 340 MPa. Brine inclusions do not change their shape during re-equilibration due to their influence on quartz solubility. H_2O diffusion occurs both, accordingly to the imposed water fugacity gradient, and for some experiments against the fugacity gradient. So called "*blank*" experiments showed that fluid inclusions are sensitive monitors of fluid conditions during entrapment. Minor variation in experimental *P-T* is detectable by the distribution pattern in the measured homogenization temperatures.

This dissertation shows that post entrapment changes in fluid inclusions in quartz occur above 450 °C around 300 MPa already after 24 hours of experimentation time. Changes of fluid inclusion shape tend to process to be ideal and regular shaped (negative crystal shape). Water diffusion occurs according to the imposed fugacity gradient. The new insights gained from the present experimental study should support interpretations of natural fluid inclusions. Further re-equilibration experiments should be designed with similar high technical precision.

References

Audétat A, Günther D (1999) Mobility and H_2O loss from fluid inclusions in natural quartz crystals. Contrib Mineral Petrol 137:1–14

Ayllón F, Bakker RJ, Warr LN (2003) Re-equilibration of fluid inclusions in diagenetic-anchizonal rocks of the Ciñera-Matallana coal basin (NW Spain). Geofluids

Bakker RJ (2003) Package FLUIDS 1. Computer programs for analysis of fluid inclusion data and for modeling bulk fluid properties. Chem Geol 194:3–23

Bakker RJ (2007) Diffusion of fluids through quartz. Geochim Cosmochim Acta 71:A54

Bakker RJ (2009a) Re-equilibration of fluid inclusions: bulk-diffusion. Lithos 112:277–288

Bakker RJ (2009b) Package FLUIDS. Part 3. Correlations between equations of state, thermodynamics and fluid inclusions. Geofluids, vol. 9 (1), 63-74

Bakker RJ, Diamond LW (1999) Reequilibration of synthetic CO_2-H_2O fluid inclusions in quartz: isofugacity experiments. Terra Nostra, v. 99/6, 20-21

Bakker RJ, Diamond LW (2003) Fluid inclusion re-equilibration experiments in quartz: chemical potential gradients. Acta Mineralogica-Petrographica, Abstract Series 2:17–18

Bakker RJ, Diamond LW (2006) Estimation of volume fractions of liquid and vapor phases in fluid inclusions, and definition of inclusion shapes. Am Mineral 91:635–657

Bakker RJ, Jansen JBH (1990) Preferential water leakage from fluid inclusions by means of mobile dislocations. Nature 345:58–60

Bakker RJ, Jansen JBH (1991) Experimental post-entrapment water loss from synthetic CO_2-H_2O inclusions in natural quartz. Geochimica et Cosmochimica Acta, v. 55, 2215-2230

Bakker RJ, Jansen JBH (1994) A mechanism for preferential H_2O leakage from fluid inclusions in quartz, based on TEM observations. Contributions to Mineralogy and Petrology, v. 116, 7-20

Bakker RJ, Baumgartner M, Doppler G (2012) Diffusion of water through quartz: a fluid inclusion study. Goldschmidt 2012, Abstracts

Barker AJ (1995) Post-entrapment modification of fluid inclusions due to overpressure: evidence from natural samples. Journal of Metamorphic Geology 13-6 (737-750)

Baumgartner M, Bakker RJ (2009) Raman spectroscopy of pure H_2O and NaCl–H_2O containing synthetic fluid inclusions in quartz—a study of polarization effects. Mineral Petrol 95(1–2):1–15

Baumgartner M, Doppler G, Bakker RJ (2011) Preliminary results of experimental re-equilibration studies of natural H_2O–CO_2–NaCl bearing fluid inclusions in quartz. ECROFI-XXI, Abstracts, pp 44–45

Baumgartner, Bakker, Doppler (2014) Re-equilibration of natural H2O–CO2–salt-rich fluid inclusions in quartz—Part 1: experiments in pure water at constant pressures and differential pressures at 600 °C. Contrib Mineral Petrol 167:1017

Bodnar RJ, Sterner SM (1987) Synthetic fluid inclusions. In: Barnes HL, Ulmer GC (eds) Hydrothermal experimental techniques. Wiley, New York, pp 423–457

Bodnar RJ, Vityk MO (1994) Interpretation of microthermometric data for NaCl-H_2O fluid inclusions. In: De Vivo B. Frezzotti ML (eds) Fluid inclusions in minerals: methods and applications. Virginia Polytechnic Inst State Univ. Blacksburg. VA. 17-13 9

Branlund JM, Hofmeister AM (2007) Thermal diffusivity of quartz to 1,000°C: effects of impurities and the α–β phase transition. Phy Chem Minerals, 34:581–595

Brewster (1845) On the modification of the doubly refracting and physical structure of topaz, by elastic forces emanating from minute cavities. Philosophical Magazine Series 3, V. 31, 206:101–104

Crank J (1975) The mathematics of diffusion. Oxford science publications, Oxford

Diamond LW, Tarantola A, Stünitz H (2010) Modification of fluid inclusions in quartz by deviatoric stress. II: experimentally induced changes in inclusion volume and composition. Contrib Mineral Petrol 160:845–864

Doppler G, Bakker RJ, Baumgartner M (2013) Fluid inclusion modification by H_2O and D_2O diffusion: the influence of inclusion depth, size, and shape in re-equilibration experiments. Contrib Mineral Petrol, 165:1259–1274

Doppler G, Bakker RJ (2014) The influence of the α–β phase transition of quartz on fluid inclusions during re-equilibration experiments. Lithos 198-199:14-23)

Dublyanski VD, Spötl C (2010) Evidence for a hypogene paleohydrogeological event at the prospective nuclear waste disposal site Yucca Mountain, Nevada, USA, revealed by the isotope composition of fluid-inclusion water. Earth Planet Sci Lett 289(3–4):583–594

Farver JR, Yund RA (1991) Oxygen diffusion in quartz: dependence on temperature and water fugacity. Chem Geol 90:55–70

Giuliani G, France-Lanord C, Zimmermann JL, Cheilletz A, Arboleda C, Charoy B, Coget P, Fontan F, Giard D (1997) Fluid composition, δD of channel H_2O, and

$\delta^{18}O$ of lattice oxygen in beryls: genetic implications for Brazilian, Colombian, and Afghanistani Emerald deposits. Int Geol Rev 39(5):400–424

Haar L, Gallagher JS, Kell GS (1984) NBS/NRC steam tables. Hemisphere Publishing Corporation, Washington

Hall D, Bodnar RJ (1989) Comparison of fluid inclusion decrepitation and acoustic emission profiles of Westerly granite and Sioux quartzite. Tectonophysics, 168:283-296

Heuer AH, Nord Jr GL (1976) Polymorphic phase transitions in minerals. Electron Microscopy in Mineralogy, pp 274-303

Hill PG, MacMillan CRD, Lee V (1982) A fundamental equation of state for heavy water. J Phys Chem Ref Data 11(1):1–14

Hladky G, Wilkins RWT (1987) An evaluation of fluid inclusion decrepitometry using quartz from the Kingsgate molybdenite–bismuth deposits, New South Wales, Australia. N. Jb. Miner. Mh.,Stuttgart, 12:537–549

Hosieni KR, Howald RA, Scanlon MW (1985) Thermodynamics of the lambda transition and the equation of state of quartz. Am Mineral 70:782–793

Johnson EA (2006) Water in Nominally Anhydrous Crustal Minerals: Speciation, Concentration, and Geologic Significance. Reviews in Mineralogy & Geochemistry 62: 117-154

Keppler H, Smyth JR (2006) Water in nominally anhydrous minerals. Rev Mineral Geochem 62:5–8

Kerrick DM (1987) Cold-seal systems. In: Ulmer GC, Barnes HL (eds) Hydrothermal experimental techniques. Wiley, New York, pp 293–323

Kronenberg AK, Kirby SH, Aines RD, Rossman GR (1986) Solubility and diffusional uptake of hydrogen in quartz at high water pressures: implications for hydrolytic weakening. J Geophys Res Solid Earth (1978–2012), 91:12723–12741

KÜSTER M, STÖCKHERT B (1997) Density changes of fluid inclusions in high-pressure low-temperature metamorphic rocks from Crete: A thermobarometric approach based on the creep strength of the host minerals. - Lithos, 41, (151-167)

Laughner JW, Cline TW, Newnham RE, Cross LE (1979) Acoustic emissions from stress-induced dauphiné twinning in quartz. Physics and Chemistry of Minerals, Vol. 4, Issue 2, 129–137

Lemmlein GG (1956) Formation of fluid inclusions and their use in geological thermometry. Geochemistry 6:630–642

Leroy A (1979) Contribution to the evaluation of internal pressure in fluid inclusions when they decrepitate. Bull Min 102:583–593

Pecher A (1981) Experimental decrepitation and re-equilibration of fluid inclusions in synthetic quartz. Tectonophysics 78(1–4): 567–583

Roedder E (1984) Fluid Inclusions. Min Soc Am Rev in Min 12:644

Rull F (2002) Structural investigation of water and aqueous solutions by Raman spectroscopy. Pure Appl Chem 74(10):1859–1870

Samson I, Anderson A, Marshall D (2003) Fluid Inclusions: Analysis and Interpretation: Mineralogical Association of Canada Short Course Volume 32, 370 p

Schmidt-Mumm (1991) Low Frequency Acoustic Emission from Quartz upon Heating from 90 to 610 °C. Phys Chem Minerals (1991) 17:545-553

Shapiro SS, Wilk MB (1965) An analysis of variance for normality (complete samples). Biometrika 52:591–611

Shepherd TJ, Rankin AH, Alderton DHM (1985) A practical guide to fluid inclusion studies. Blackie, Glasgow-London

Sterner SM, Bodnar RJ (1989) Synthetic fluid inclusions. VII. Reequilibration of fluid inclusions in quartz during laboratory simulated metamorphic burial and uplift. J Metamorphic Geol 7:243–260

Sterner SM, Bodnar RJ (1991) Synthetic fluid inclusions. X: Experimental determination of P-V-T-X properties in the CO_2-H_2O system to 6 kb and 700 °C. American journal of science, 291, 1-54

Sterner SM, Hall LD, Keppler H (1995) Compositional re-equilibration of fluid inclusions in quartz. Contrib Mineral Petrol 119:1–15

Tarantola A, Diamond LW, Stünitz H (2010) Modification of fluid inclusions in quartz by deviatoric stress I: experimentally induced changes in inclusion shapes and microstructures. Contrib Mineral Petrol 160:825–843

Vityk MO, Bodnar RJ (1995) Textural evolution of synthetic fluid inclusions in quartz during reequilibration, with applications to tectonic reconstruction. Contrib Mineral Petrol 121:309–323

Vityk MO, Bodnar RJ (1998) Statistical microthermometry of synthetic fluid inclusions in quartz during decompression reequilibration. Contrib Mineral Petrol 132:149–162

Wilkinson JJ (2001) Fluid inclusions in hydrothermal ore deposits. Lithos 55:229–272

Appendix

A. Experimental conditions

A.a Experimental conditions of chapter 3

"*Fluid inclusion modification by H_2O and D_2O diffusion: the influence of inclusion depth, size, and shape in re-equilibration experiments*"

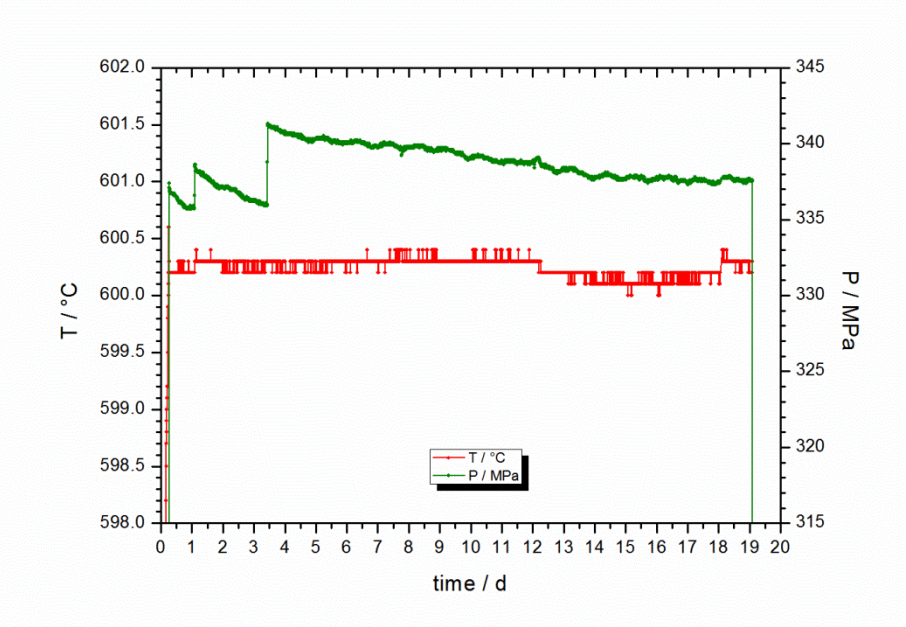
T / °C
P / MPa
time / d
602.0
601.5
601.0
600.5
600.0
599.5
599.0
598.5
598.0
345
340
335
330
325
320
315
0 1 2 3 4 5 6 7 8 9 10 11 12 13 14 15 16 17 18 19 20

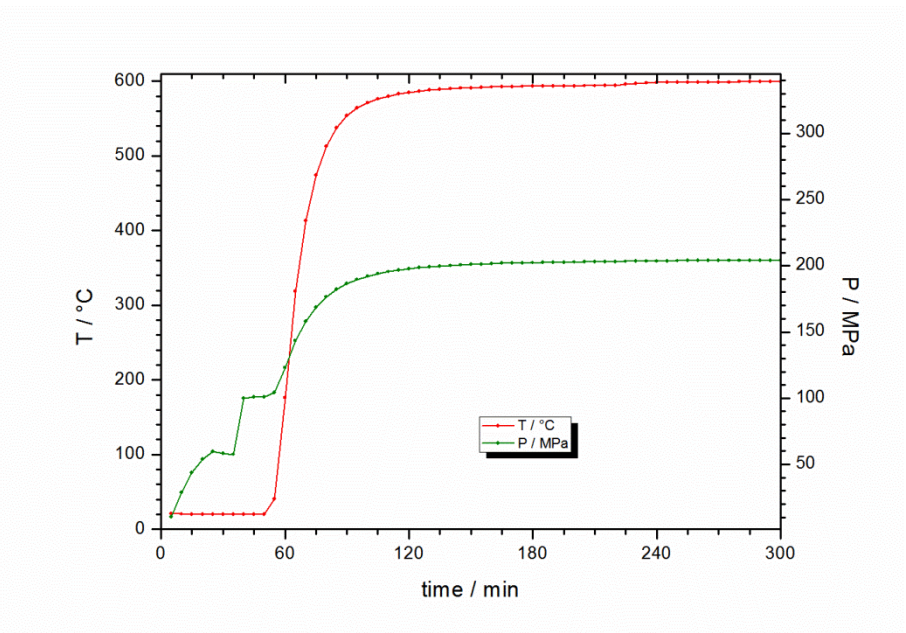
T / °C
P / MPa
time / min
600
500
400
300
200
100
0
300
250
200
150
100
50
0 60 120 180 240 300

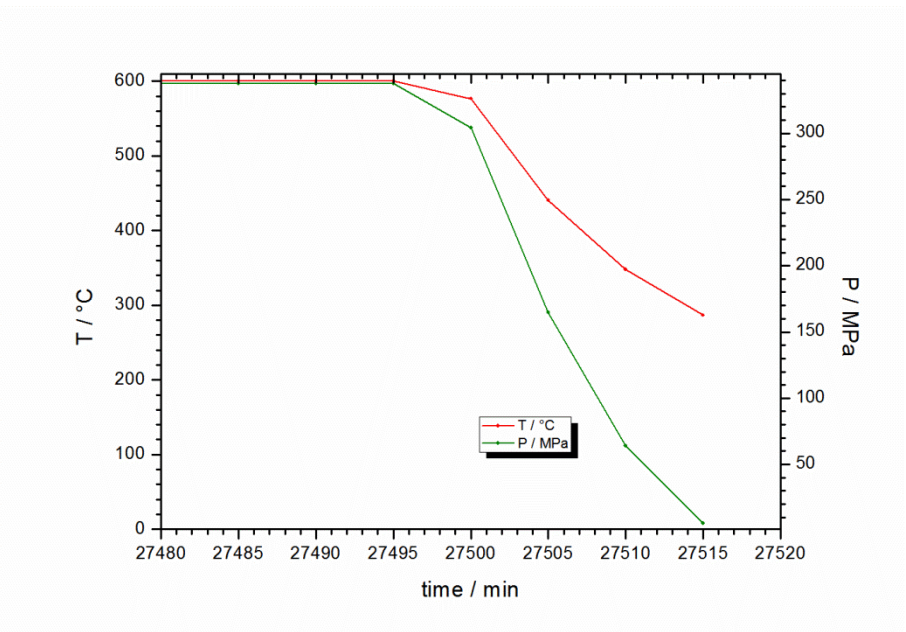
T / °C
P / MPa
time / min
600
500
400
300
200
100
0
300
250
200
150
100
50
27480 27485 27490 27495 27500 27505 27510 27515 27520

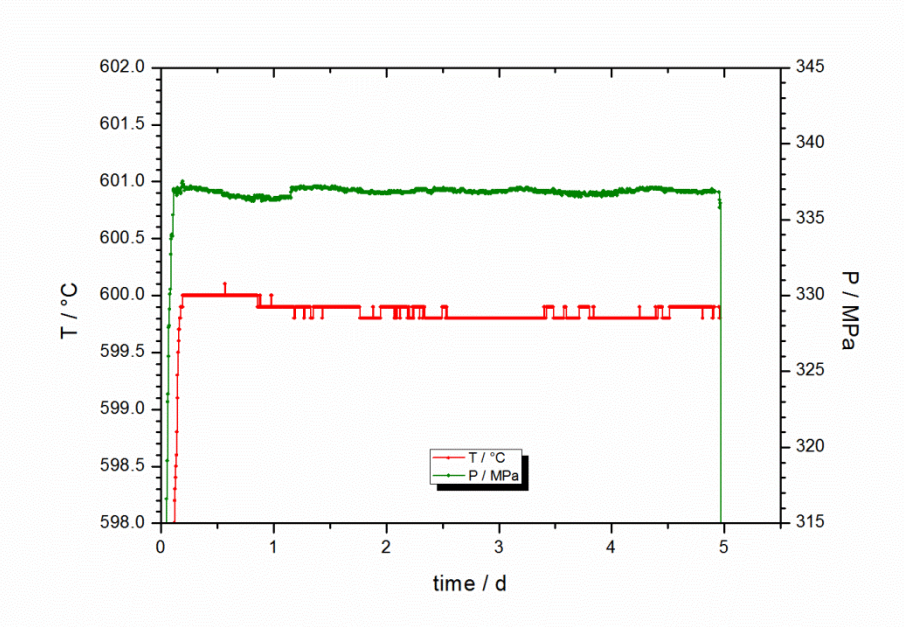
T / °C
P / MPa
time / d
602.0
601.5
601.0
600.5
600.0
599.5
599.0
598.5
598.0
345
340
335
330
325
320
315
0
1
2
3
4
5

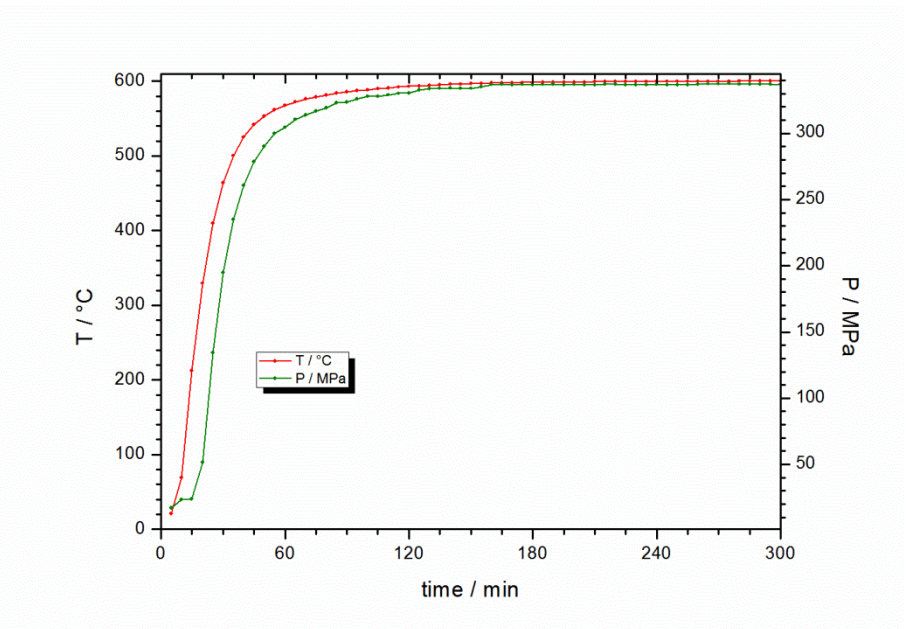
T / °C
P / MPa
time / min
600
500
400
300
200
100
0
300
250
200
150
100
50
0
60
120
180
240
300

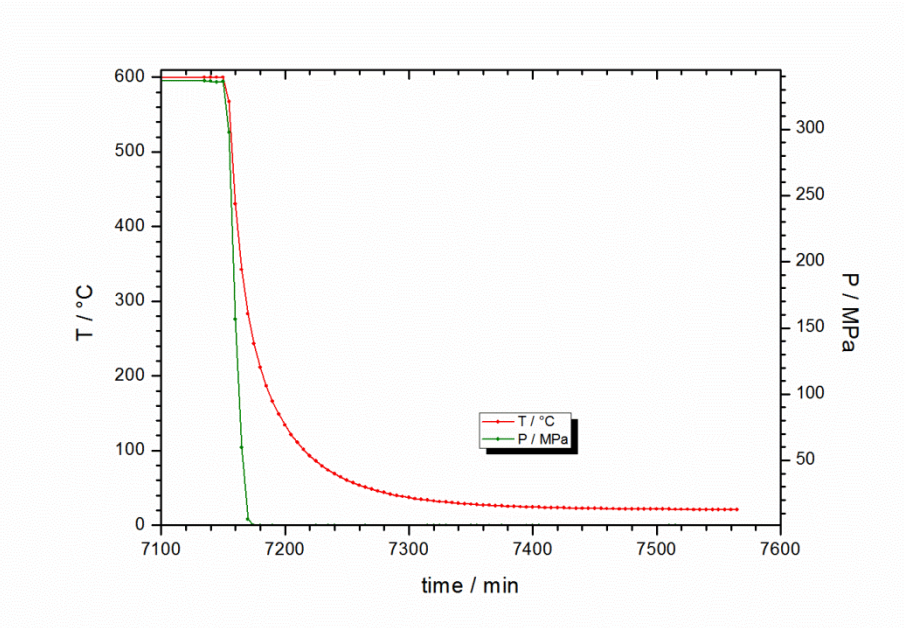
T / °C
P / MPa
time / min
600
500
400
300
200
100
0
300
250
200
150
100
50
7100
7200
7300
7400
7500
7600

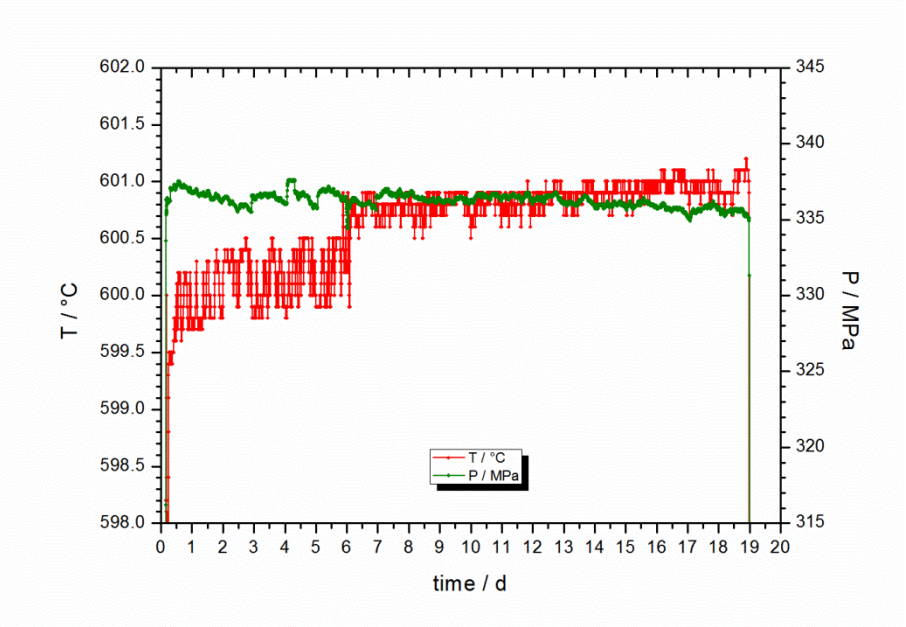
T / °C
P / MPa
time / d

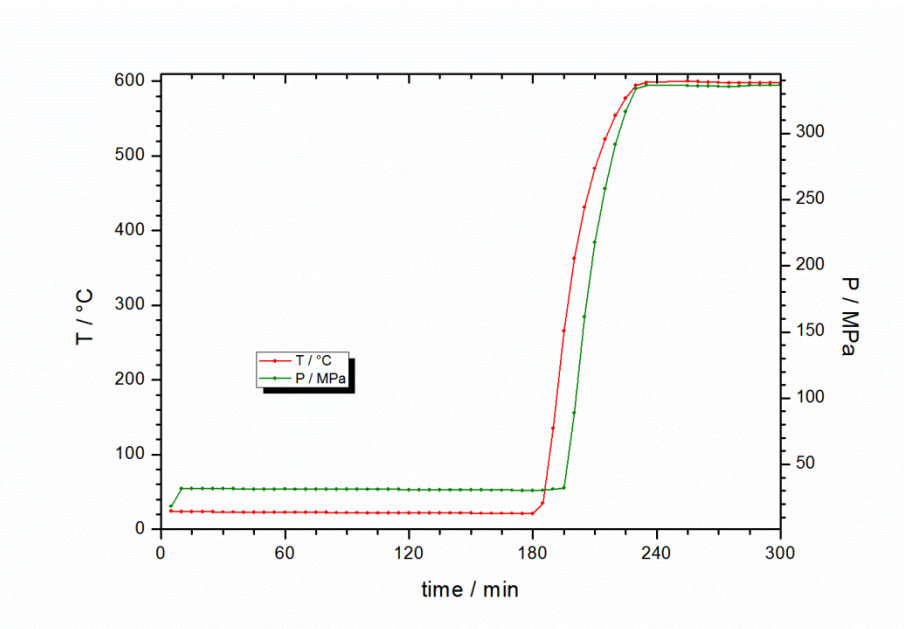
T / °C
P / MPa
time / min

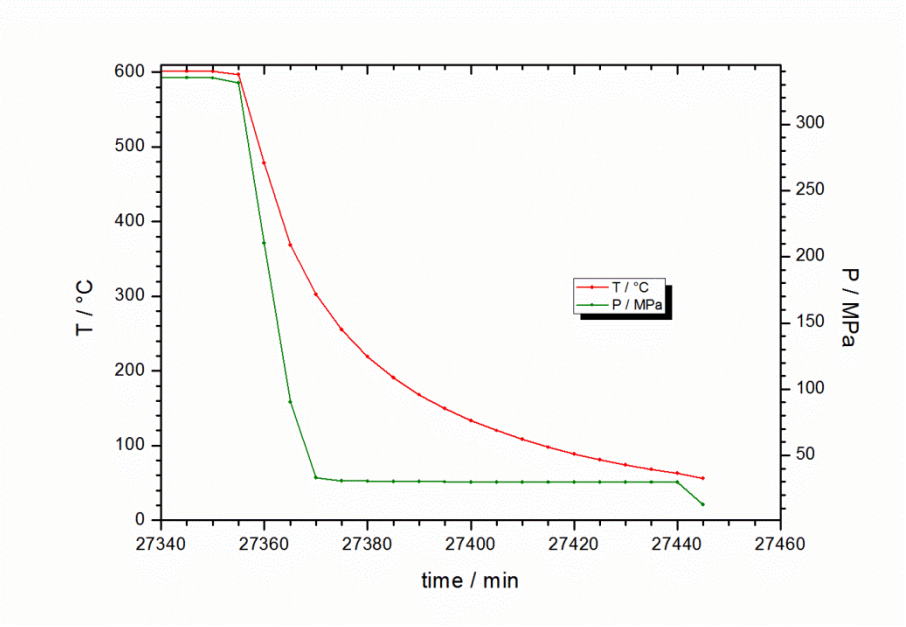
T / °C
P / MPa
time / min

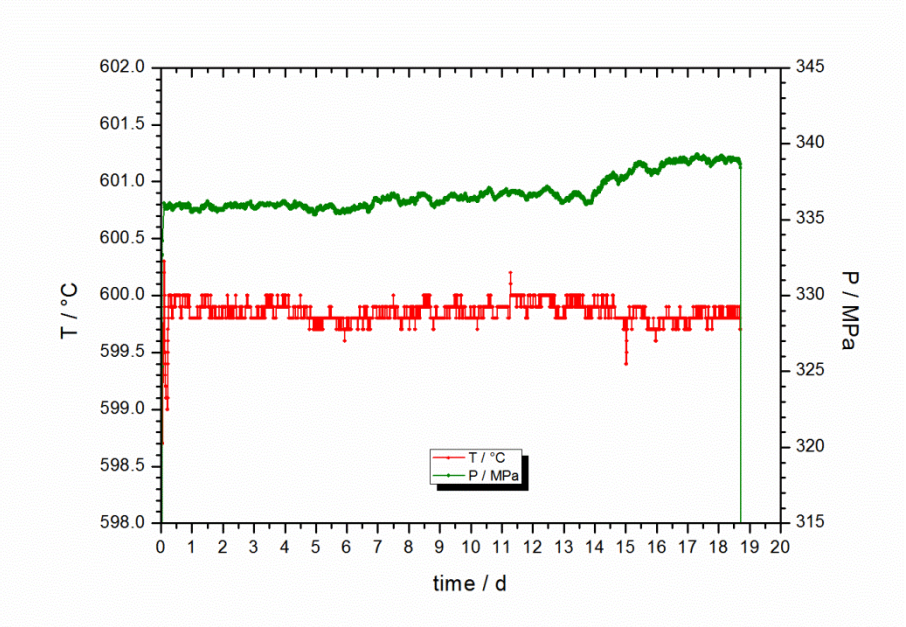
T / °C
P / MPa
time / d

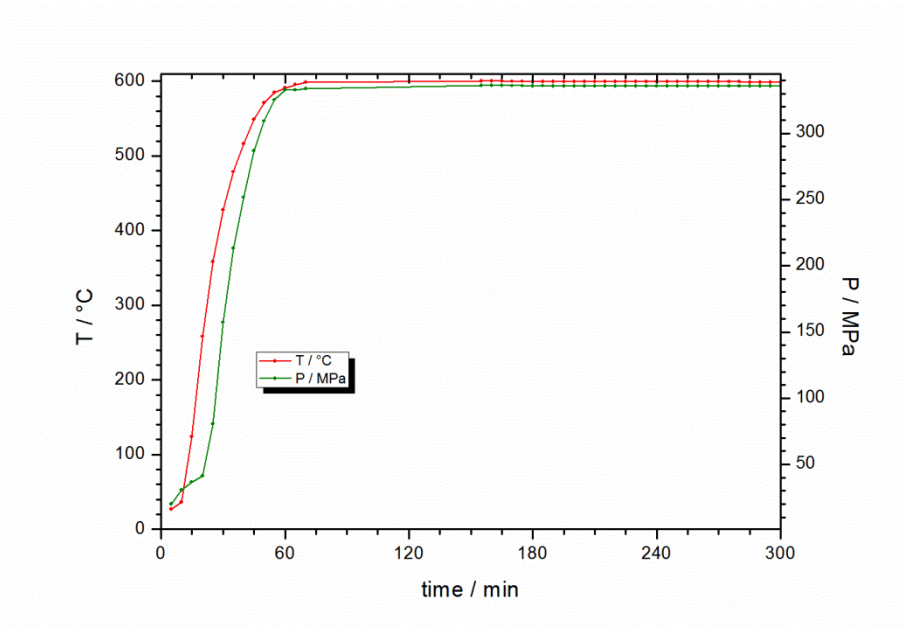
T / °C
P / MPa
time / min

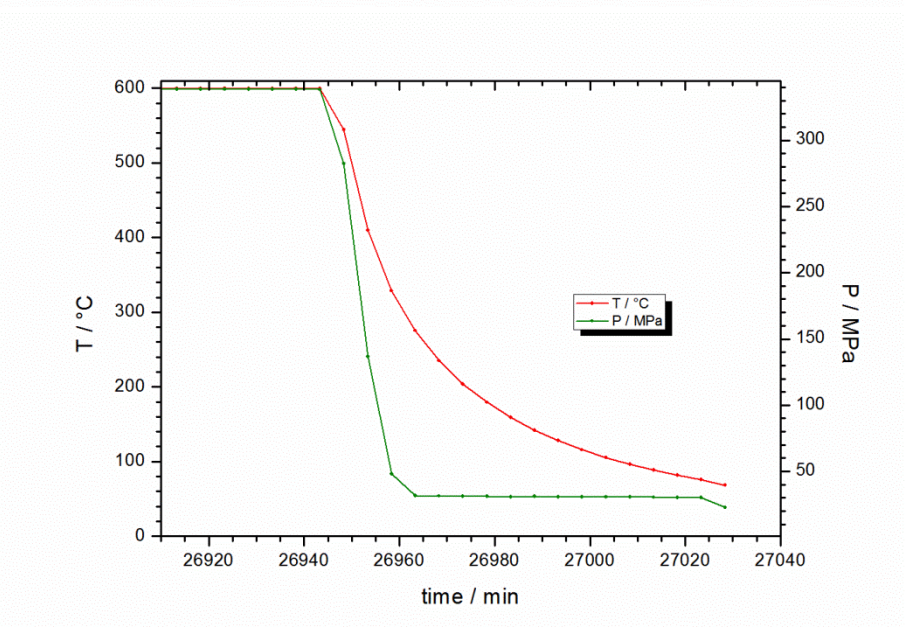
T / °C
P / MPa
time / min

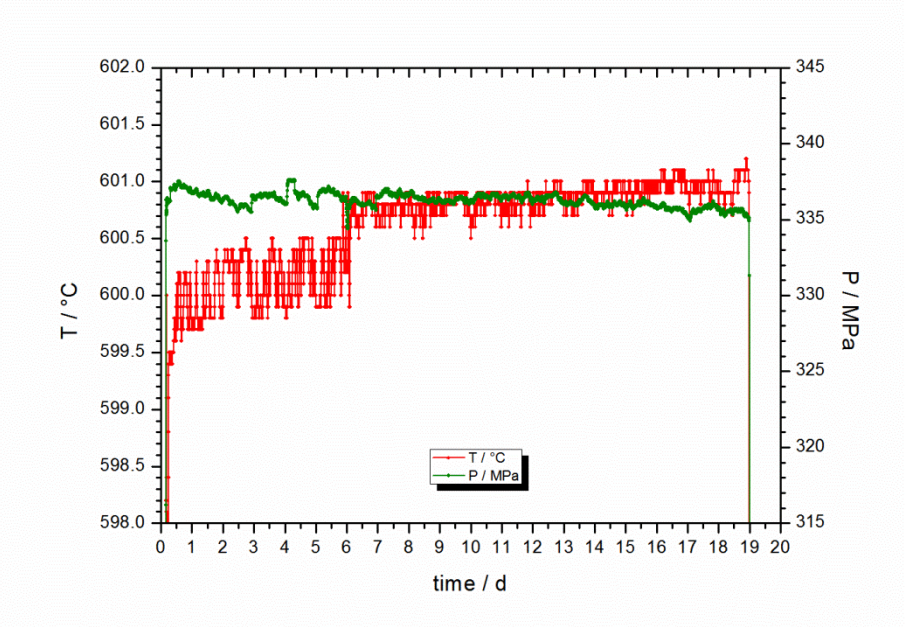
T / °C
P / MPa
time / d

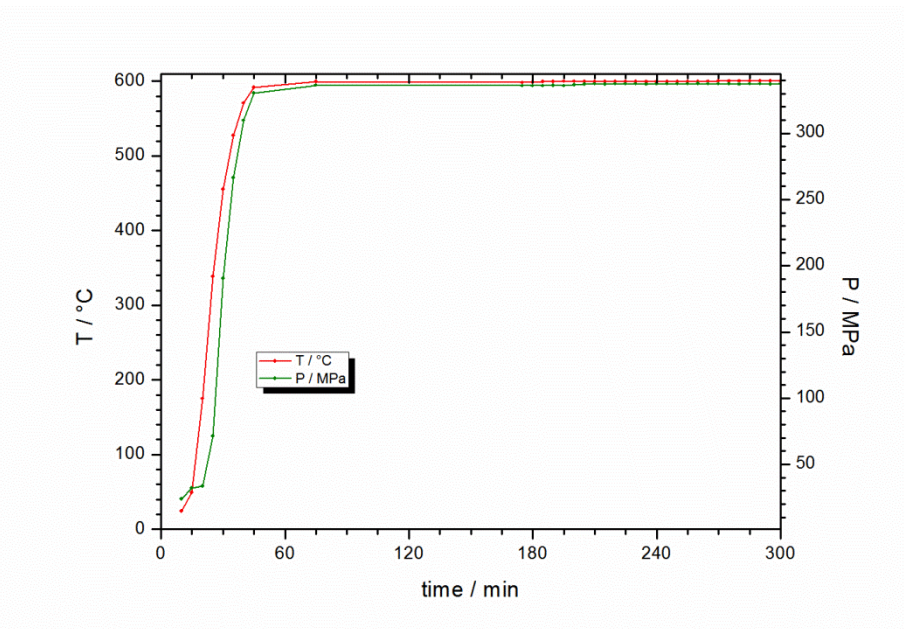
T / °C
P / MPa
time / min

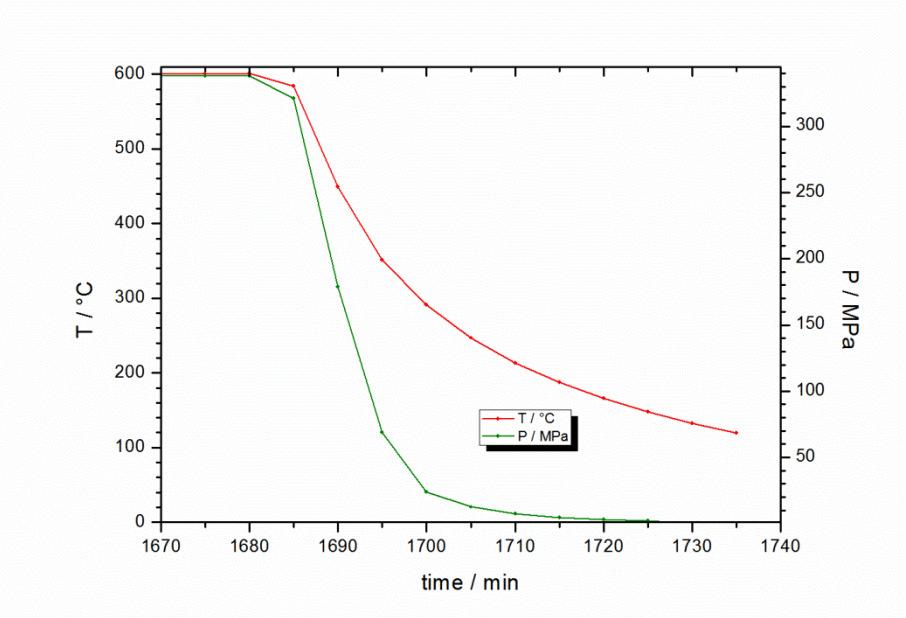
T / °C
P / MPa
time / min

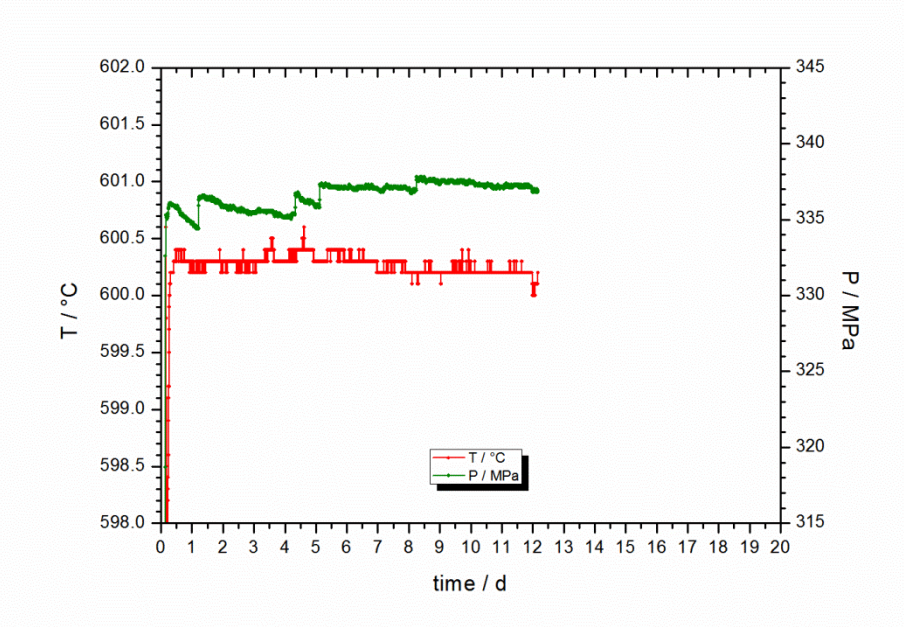

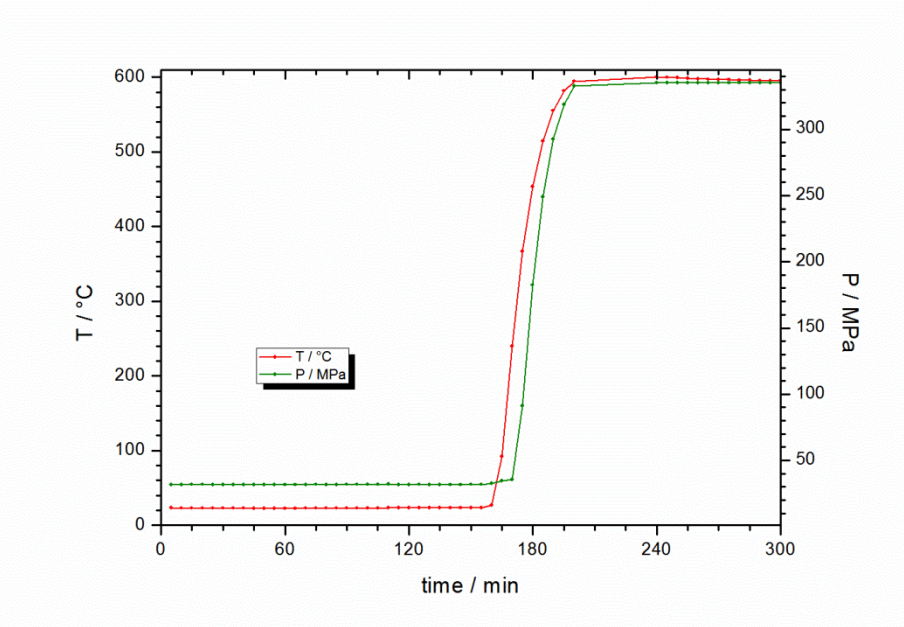

no log data of experimental unloading!

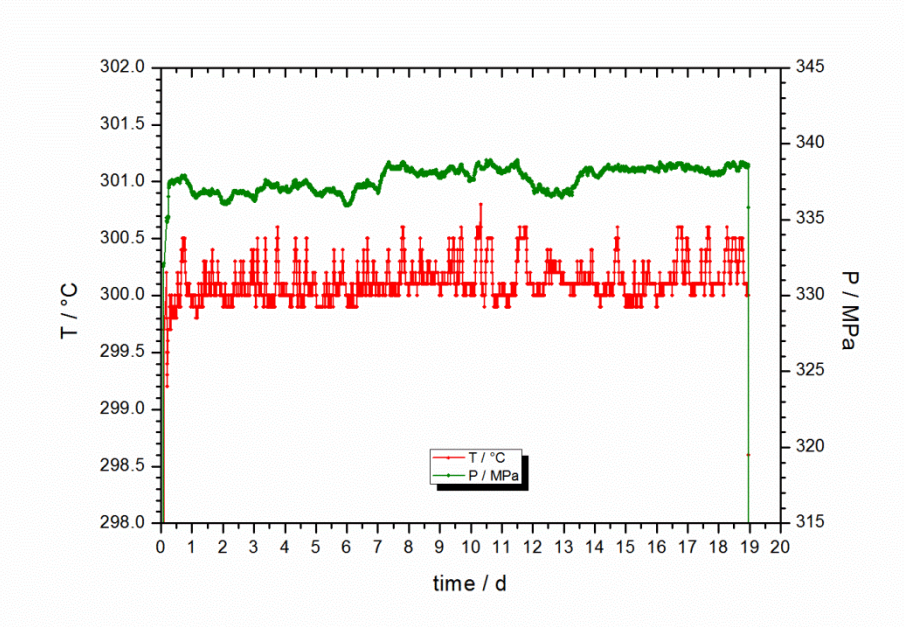
T / °C
P / MPa
time / d

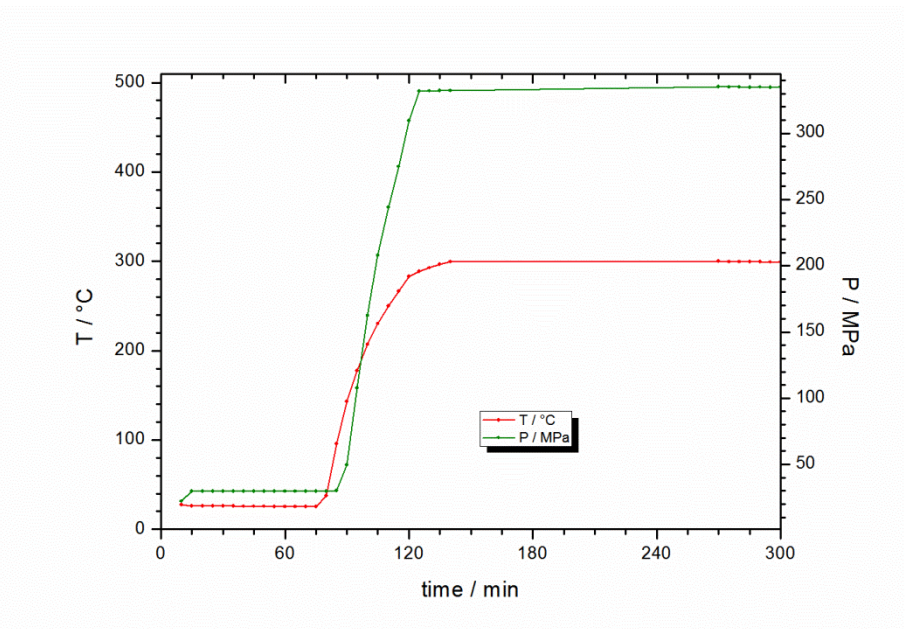
T / °C
P / MPa
time / min

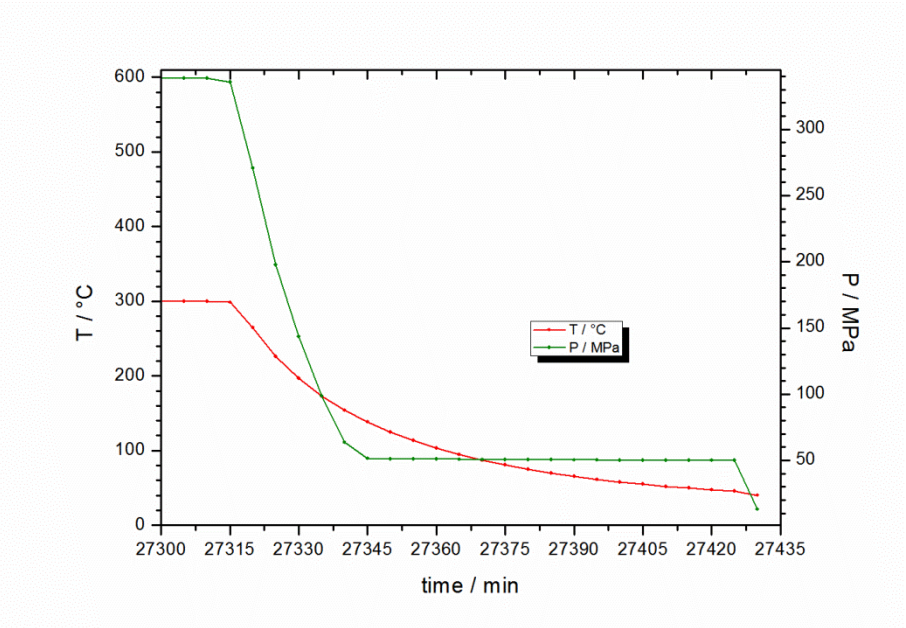
T / °C
P / MPa
time / min

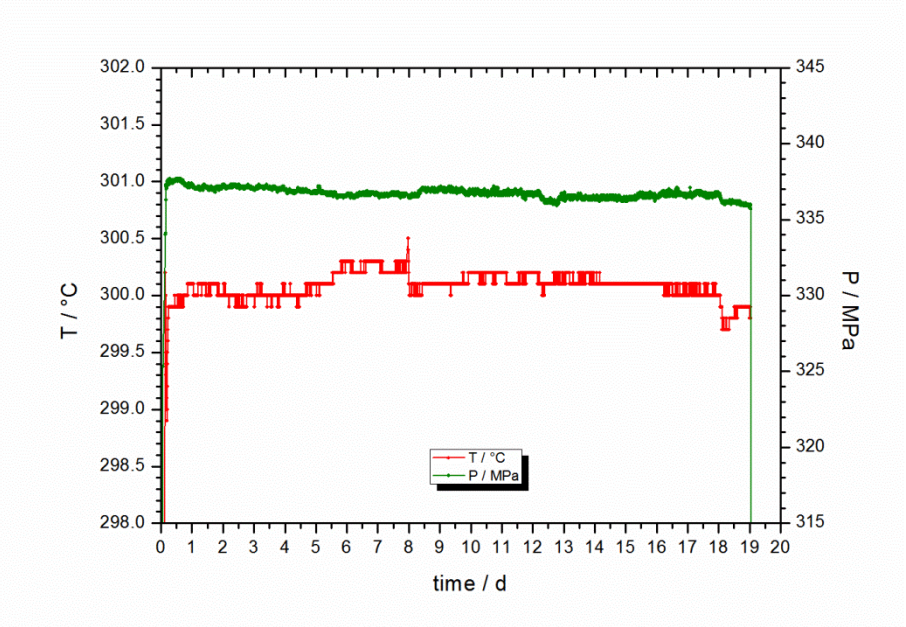
T / °C
P / MPa
time / d

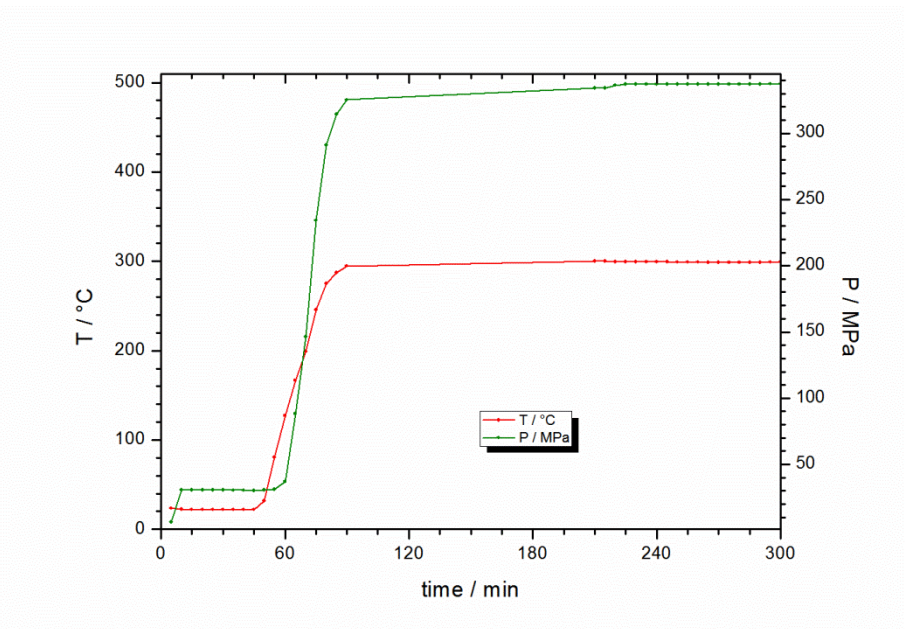
T / °C
P / MPa
time / min

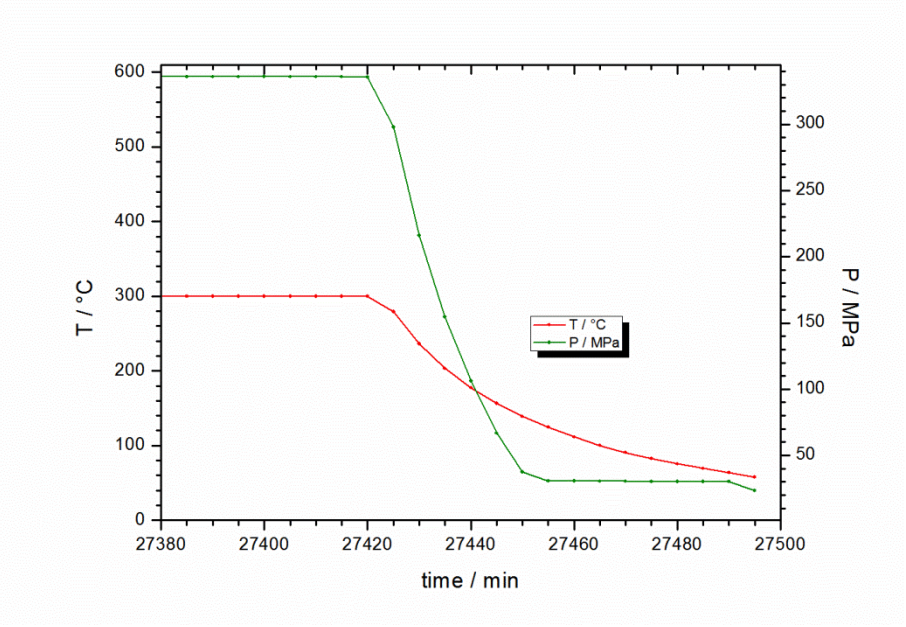
T / °C
P / MPa
time / min

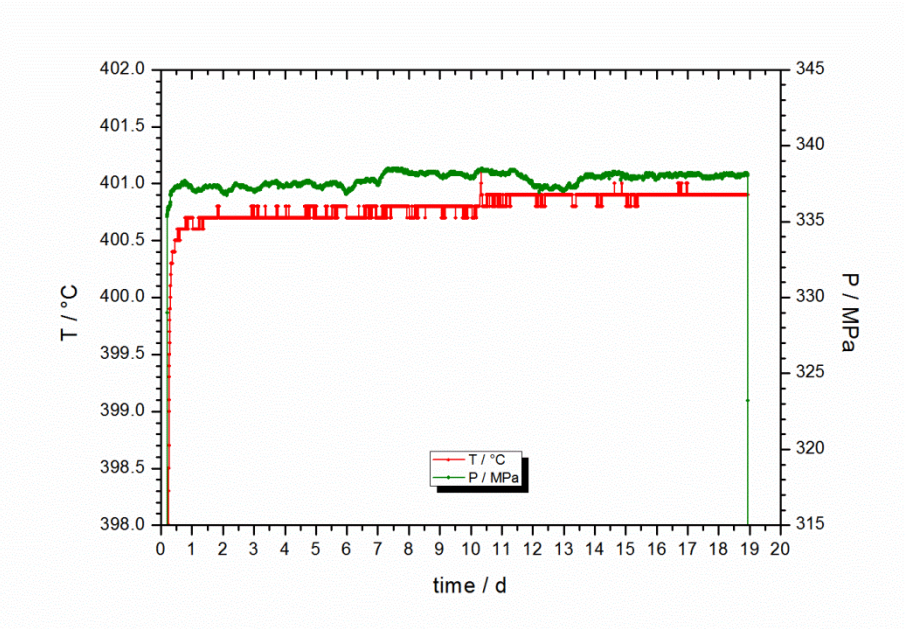
T / °C
P / MPa
time / d
T / °C
P / MPa

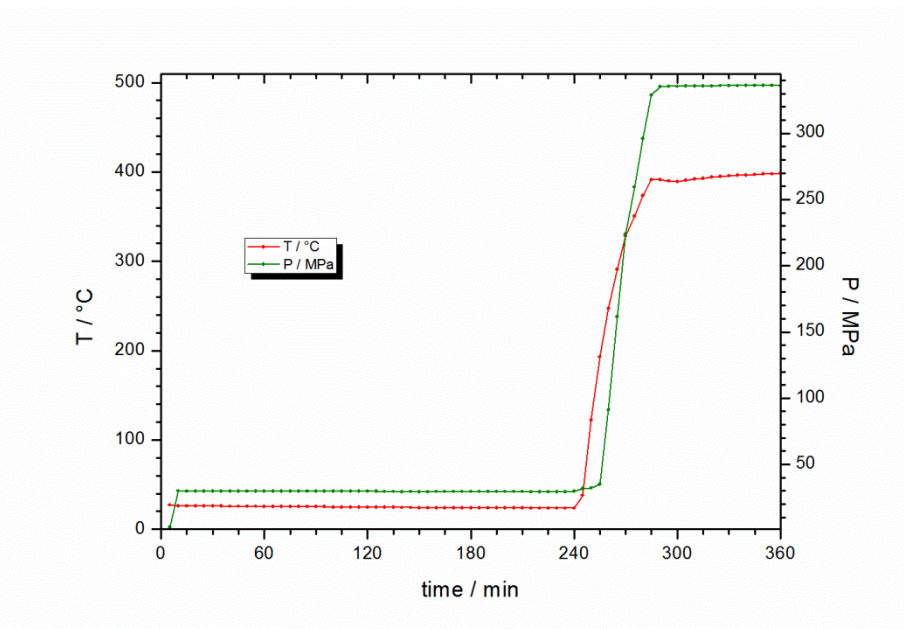
T / °C
P / MPa
time / min
T / °C
P / MPa

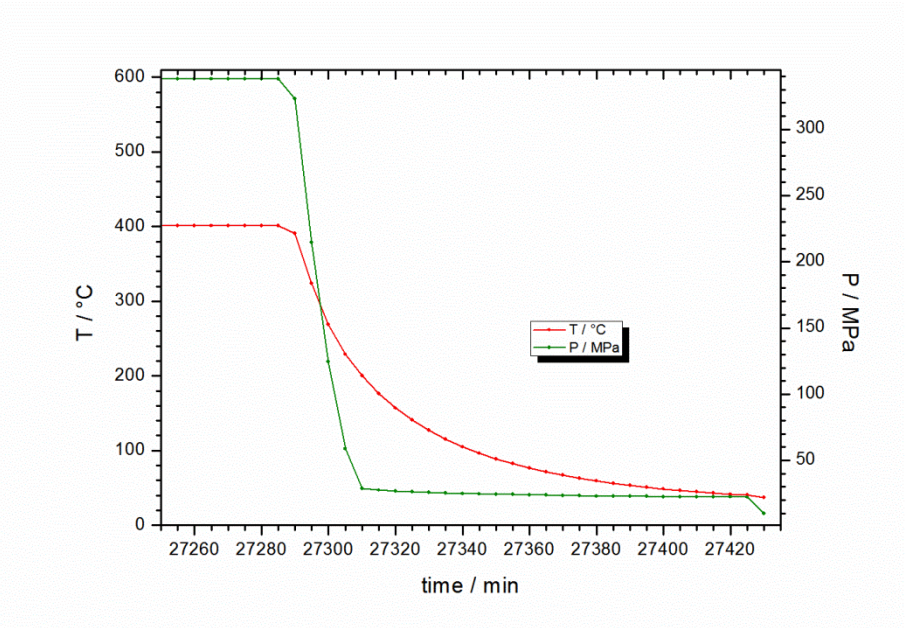
T / °C
P / MPa
time / min
T / °C
P / MPa

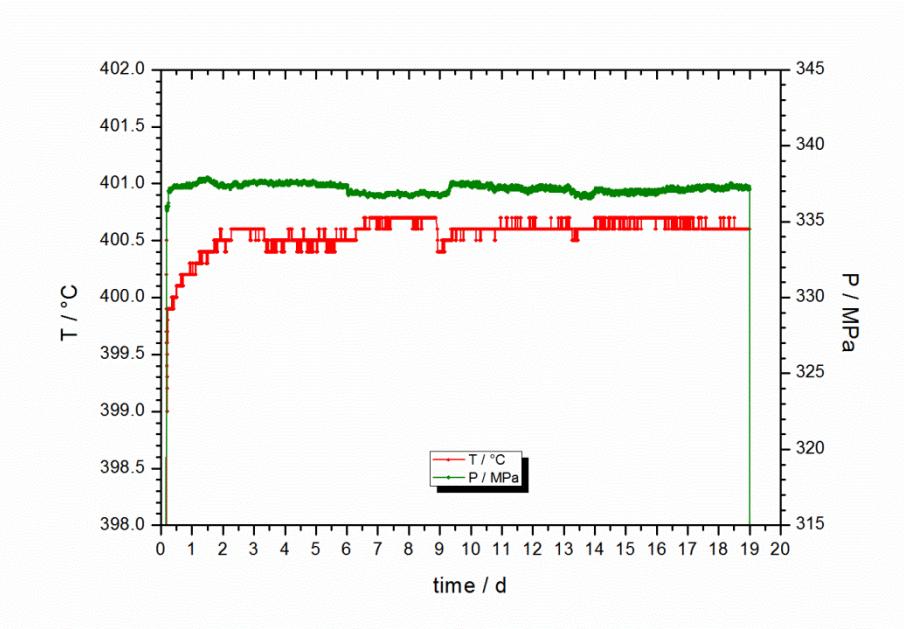
T / °C
P / MPa
time / d
402.0
401.5
401.0
400.5
400.0
399.5
399.0
398.5
398.0
345
340
335
330
325
320
315
0 1 2 3 4 5 6 7 8 9 10 11 12 13 14 15 16 17 18 19 20

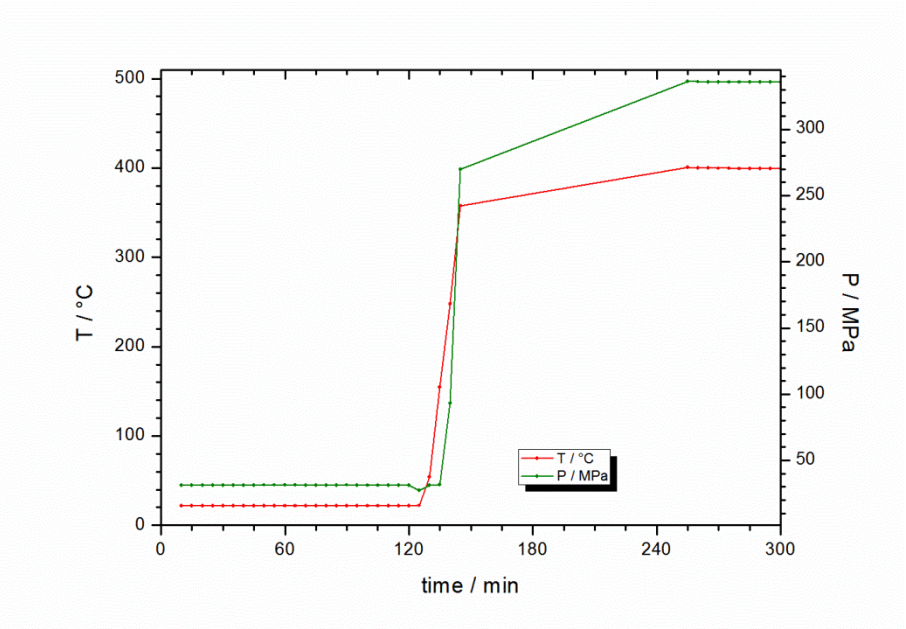
T / °C
P / MPa
time / min
500
400
300
200
100
0
300
250
200
150
100
50
0 60 120 180 240 300

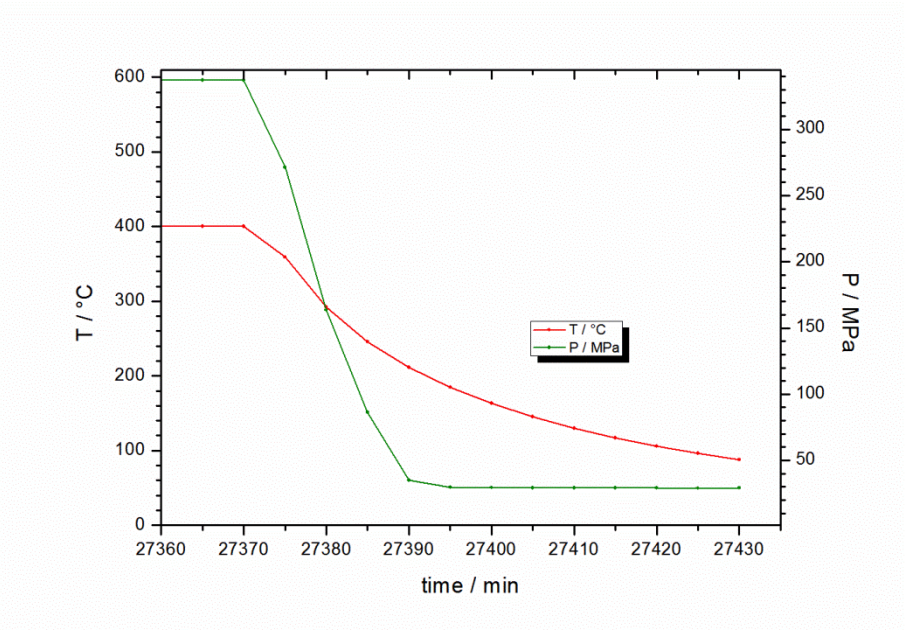
T / °C
P / MPa
time / min
600
500
400
300
200
100
0
300
250
200
150
100
50
27360 27370 27380 27390 27400 27410 27420 27430

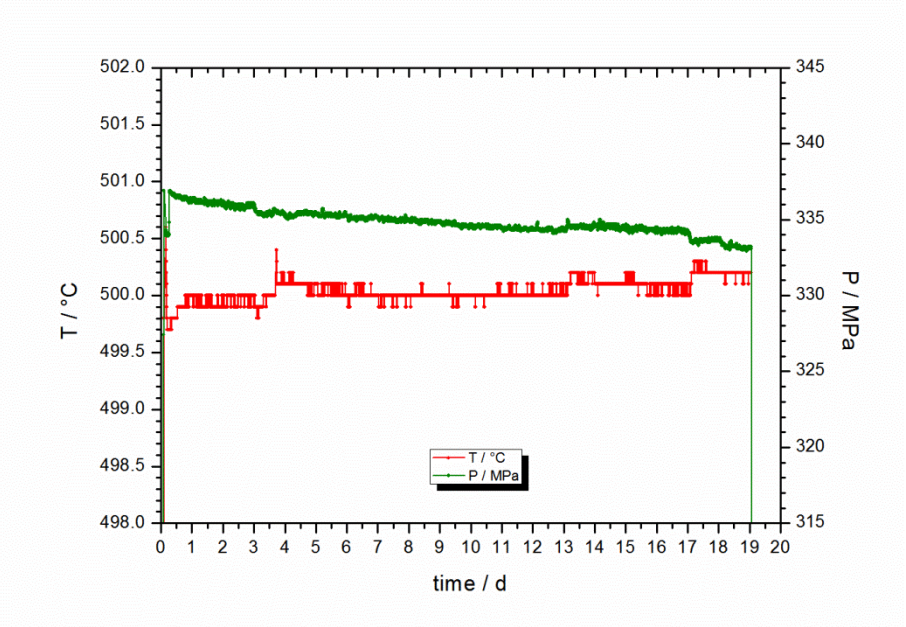
T / °C
P / MPa
time / d
T / °C
P / MPa

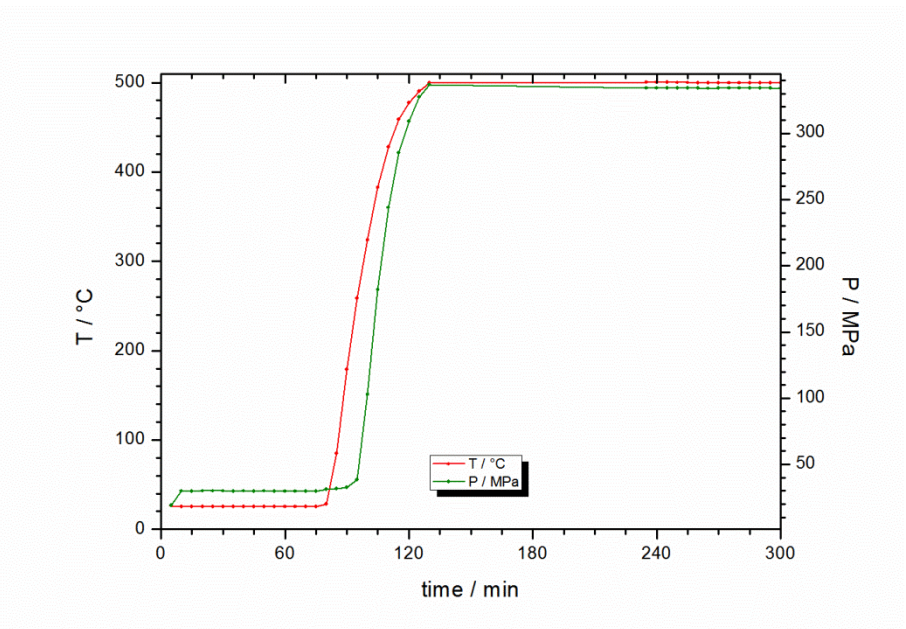
T / °C
P / MPa
time / min
T / °C
P / MPa

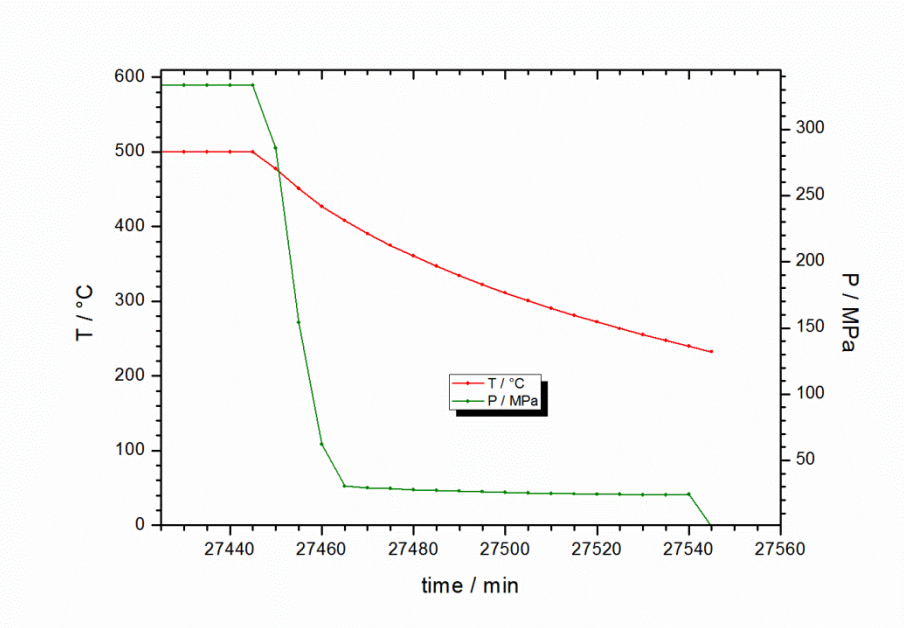
T / °C
P / MPa
time / min
T / °C
P / MPa

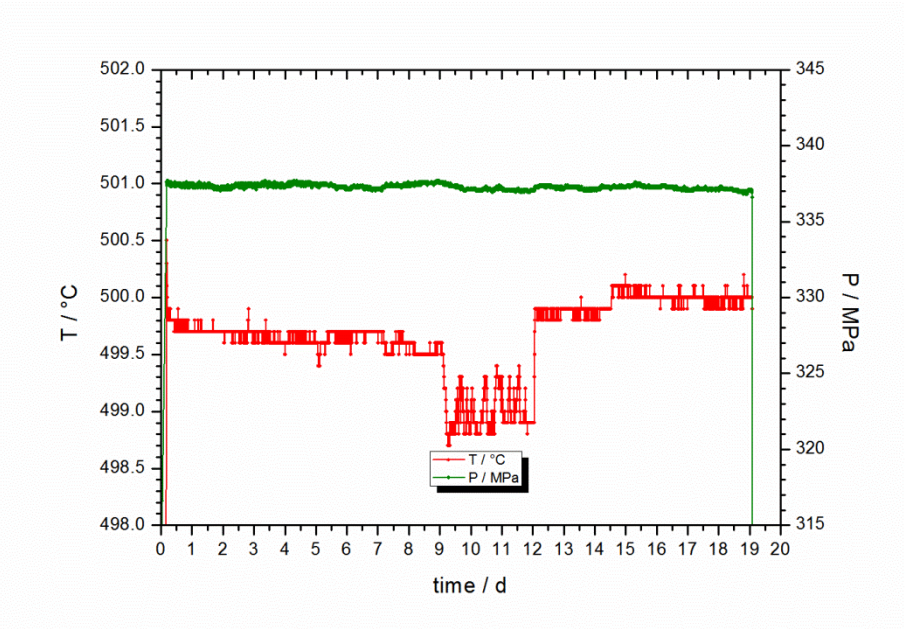
T / °C
P / MPa
time / d
T / °C
P / MPa

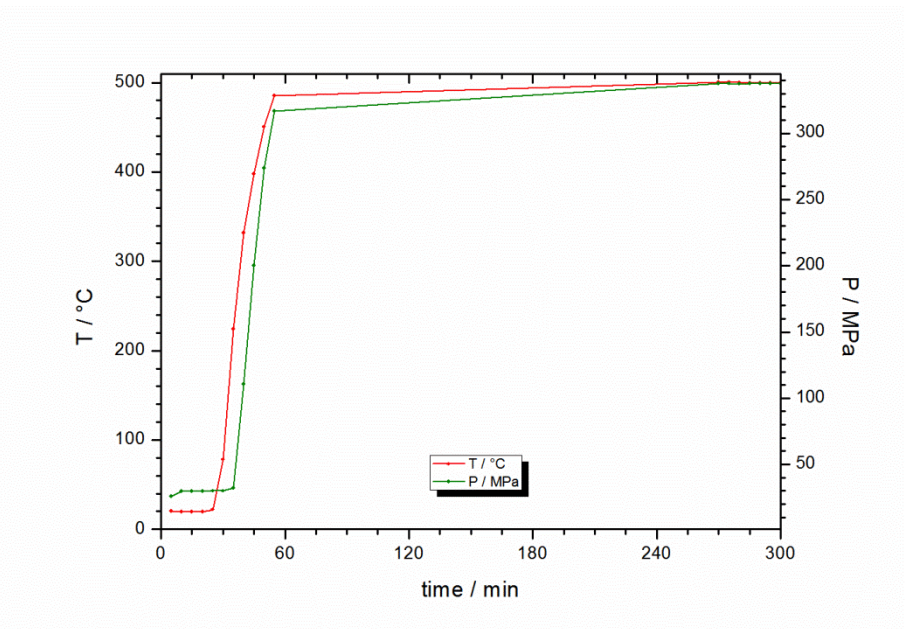
T / °C
P / MPa
time / min
T / °C
P / MPa

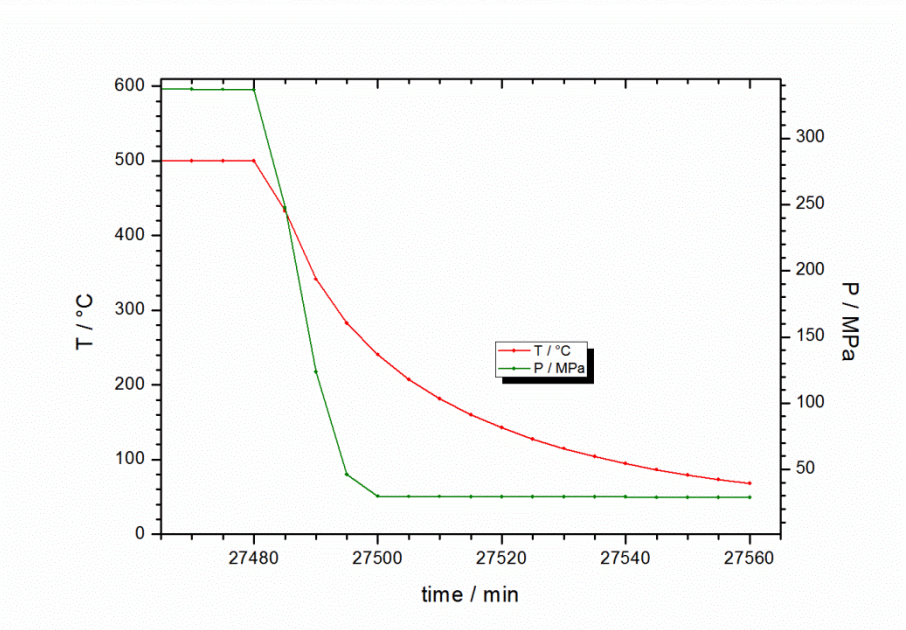
T / °C
P / MPa
time / min
T / °C
P / MPa

A.a.i Data set

All experimental records are attached as DVD to this work.

A.b Experimental conditions of chapter 4

"*The influence of the α–β phase transition of quartz on fluid inclusions during re-equilibration experiments*"

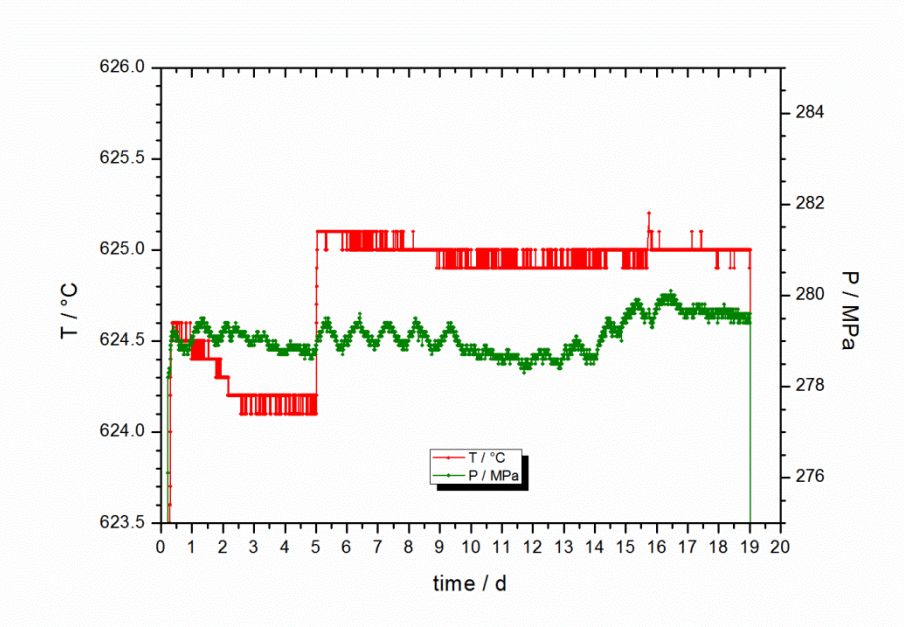
T / °C
P / MPa
time / d
626.0
625.5
625.0
624.5
624.0
623.5
284
282
280
278
276
0 1 2 3 4 5 6 7 8 9 10 11 12 13 14 15 16 17 18 19 20

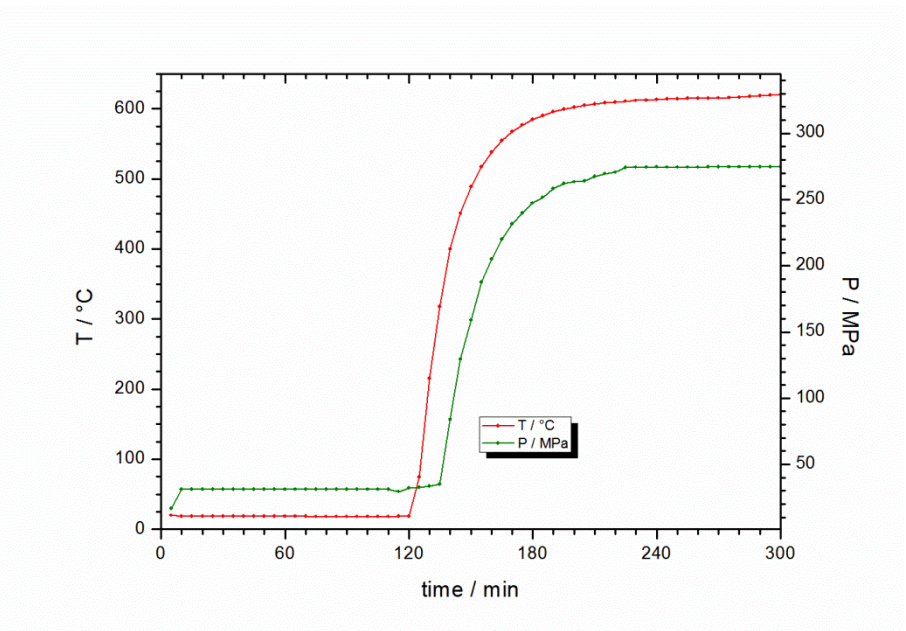
T / °C
P / MPa
time / min
600
500
400
300
200
100
0
300
250
200
150
100
50
0 60 120 180 240 300

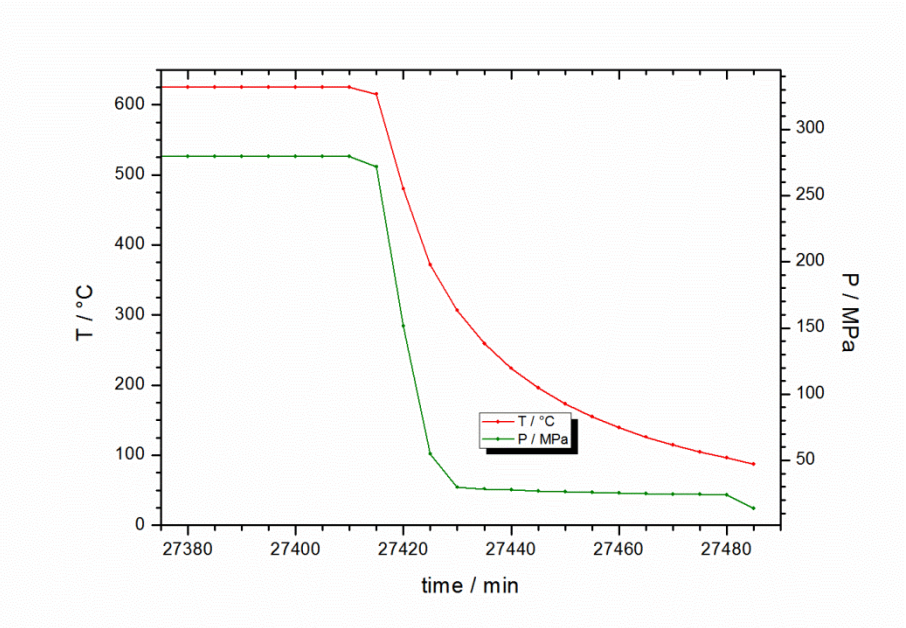
T / °C
P / MPa
time / min
600
500
400
300
200
100
0
300
250
200
150
100
50
27380 27400 27420 27440 27460 27480

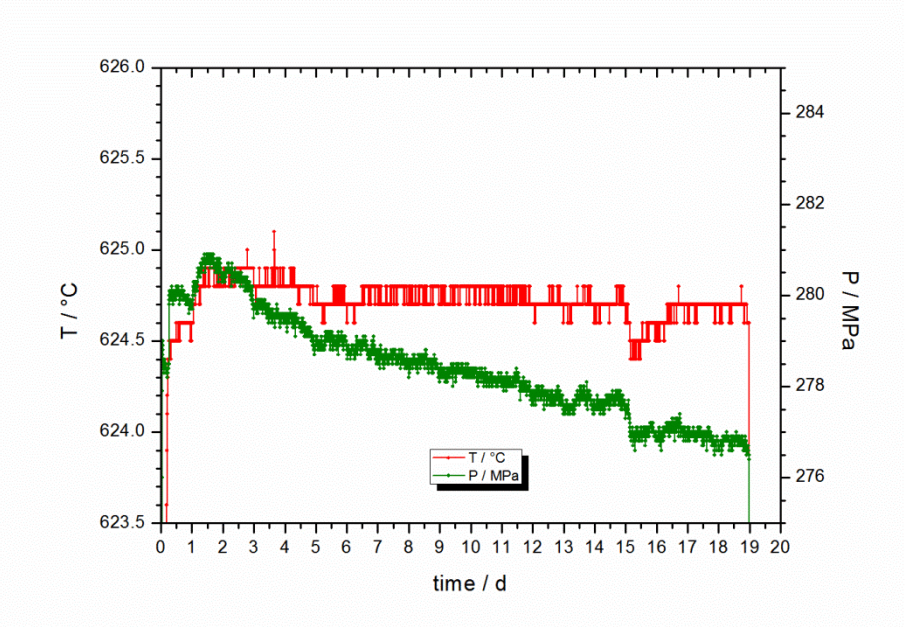
T / °C
P / MPa
time / d
626.0
625.5
625.0
624.5
624.0
623.5
284
282
280
278
276
0 1 2 3 4 5 6 7 8 9 10 11 12 13 14 15 16 17 18 19 20

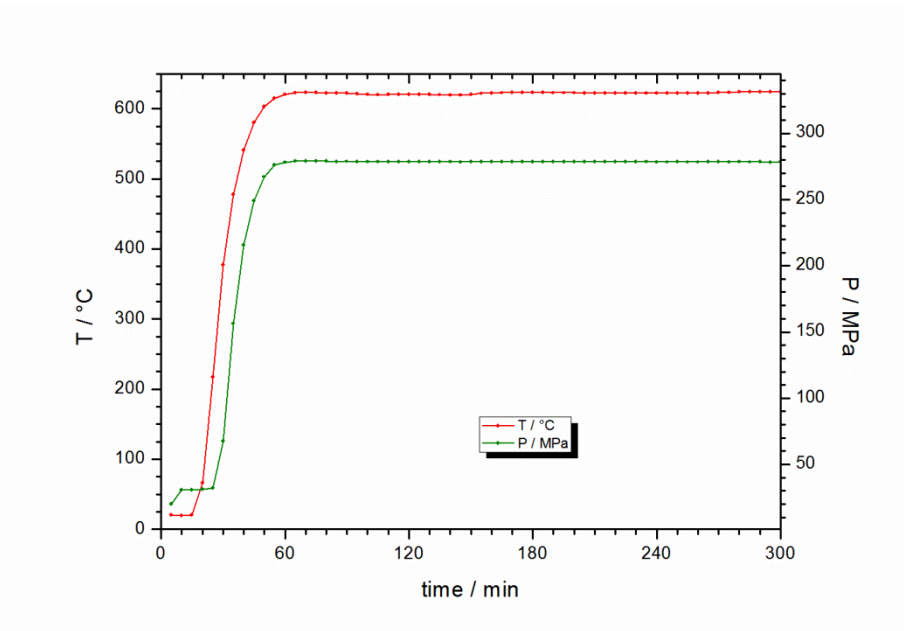
T / °C
P / MPa
time / min
600
500
400
300
200
100
0
300
250
200
150
100
50
0 60 120 180 240 300

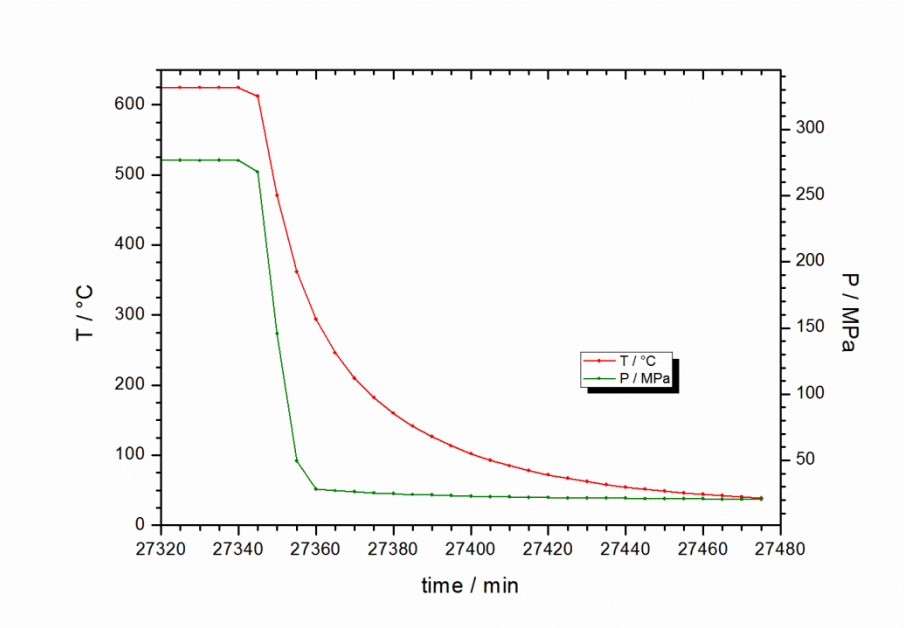
T / °C
P / MPa
time / min
600
500
400
300
200
100
0
300
250
200
150
100
50
27320 27340 27360 27380 27400 27420 27440 27460 27480

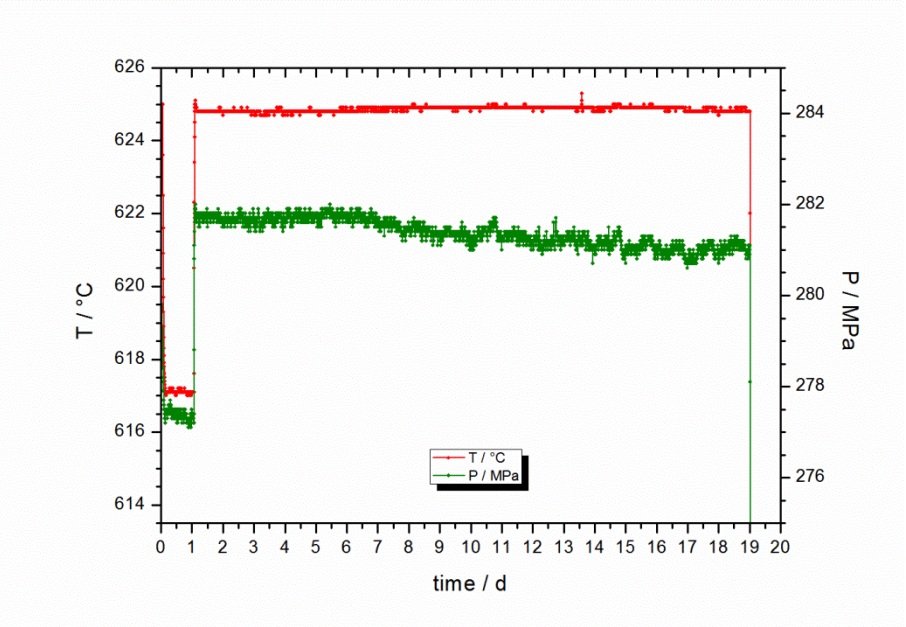
T / °C
P / MPa
time / d
626
624
622
620
618
616
614
284
282
280
278
276
0 1 2 3 4 5 6 7 8 9 10 11 12 13 14 15 16 17 18 19 20

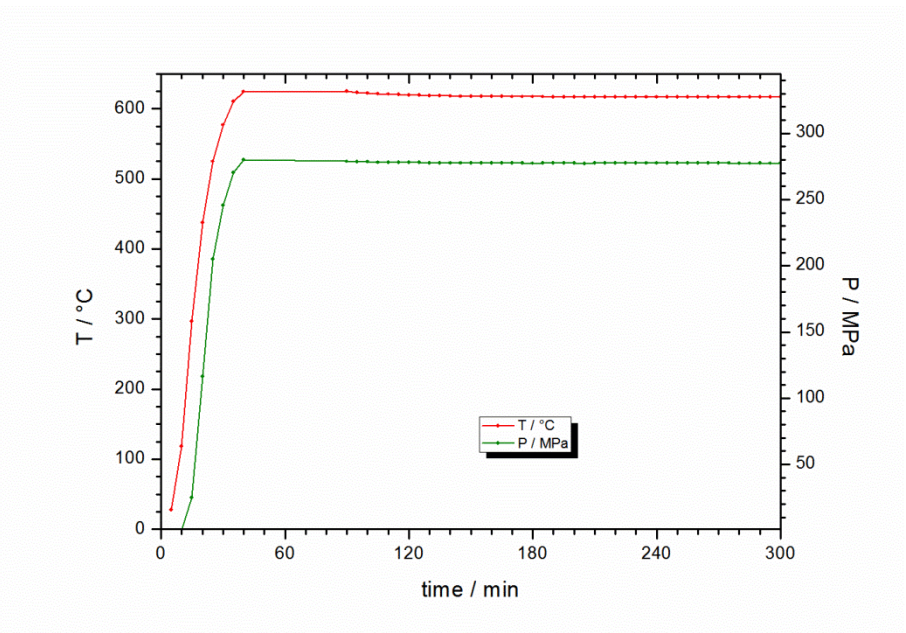
T / °C
P / MPa
time / min
600
500
400
300
200
100
0
300
250
200
150
100
50
0 60 120 180 240 300

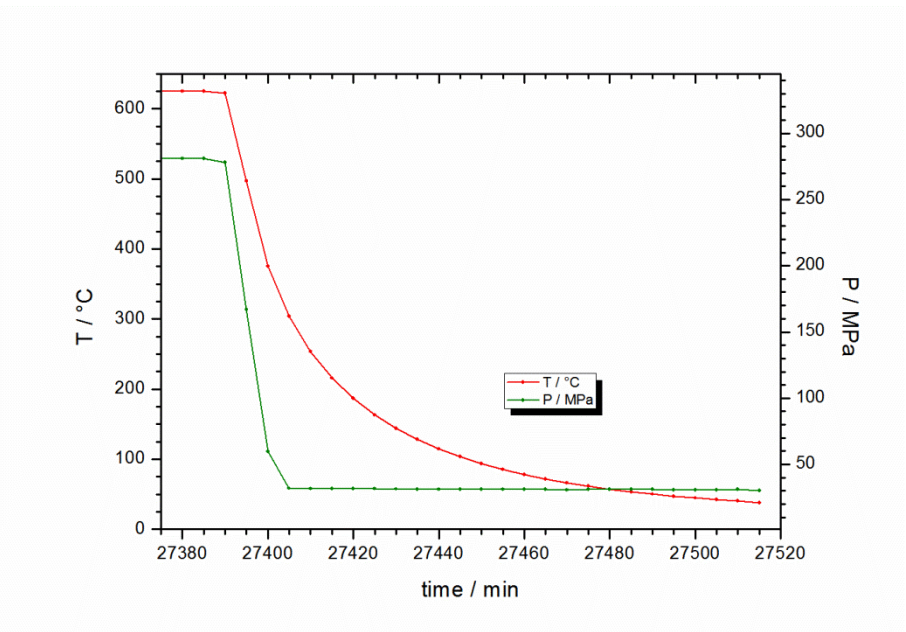
T / °C
P / MPa
time / min
600
500
400
300
200
100
0
300
250
200
150
100
50
27380 27400 27420 27440 27460 27480 27500 27520

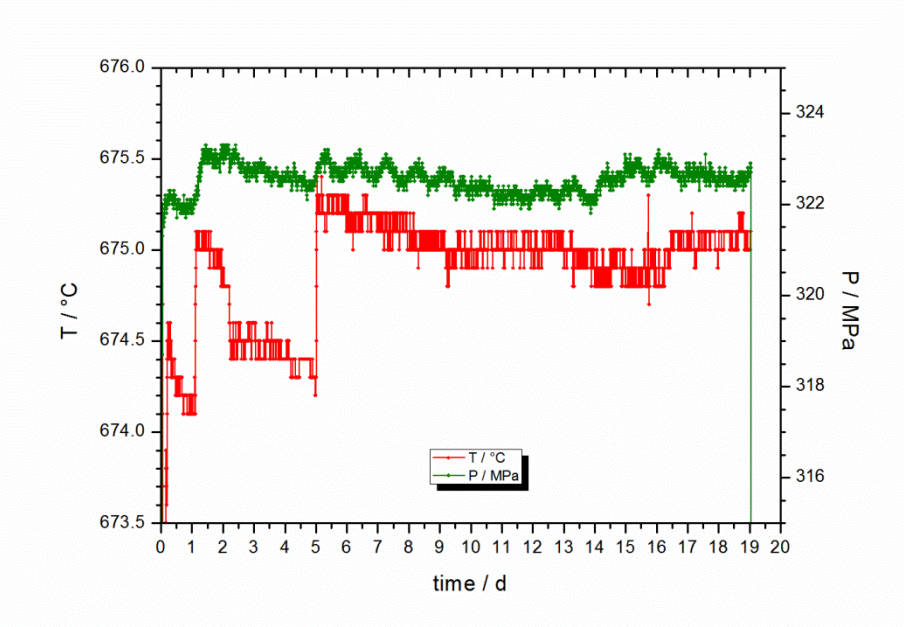
T / °C
P / MPa
time / d
676.0
675.5
675.0
674.5
674.0
673.5
324
322
320
318
316
0 1 2 3 4 5 6 7 8 9 10 11 12 13 14 15 16 17 18 19 20

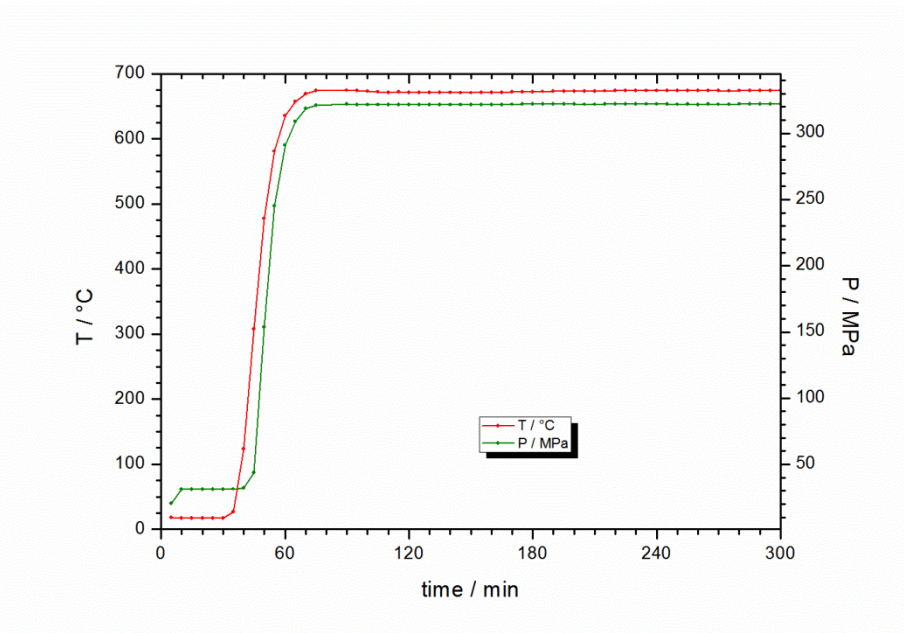
T / °C
P / MPa
time / min
700
600
500
400
300
200
100
0
300
250
200
150
100
50
0 60 120 180 240 300

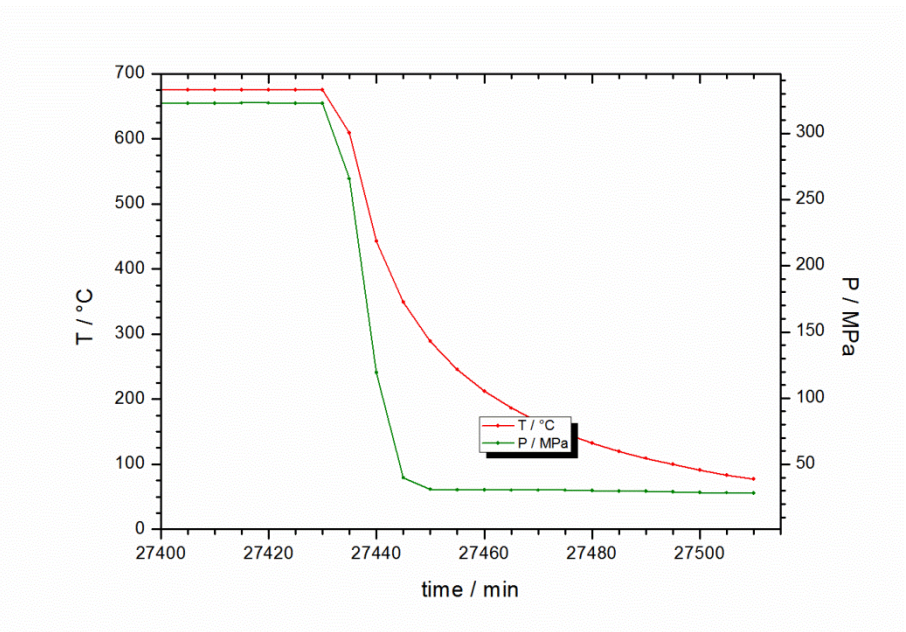
T / °C
P / MPa
time / min
700
600
500
400
300
200
100
0
300
250
200
150
100
50
27400 27420 27440 27460 27480 27500

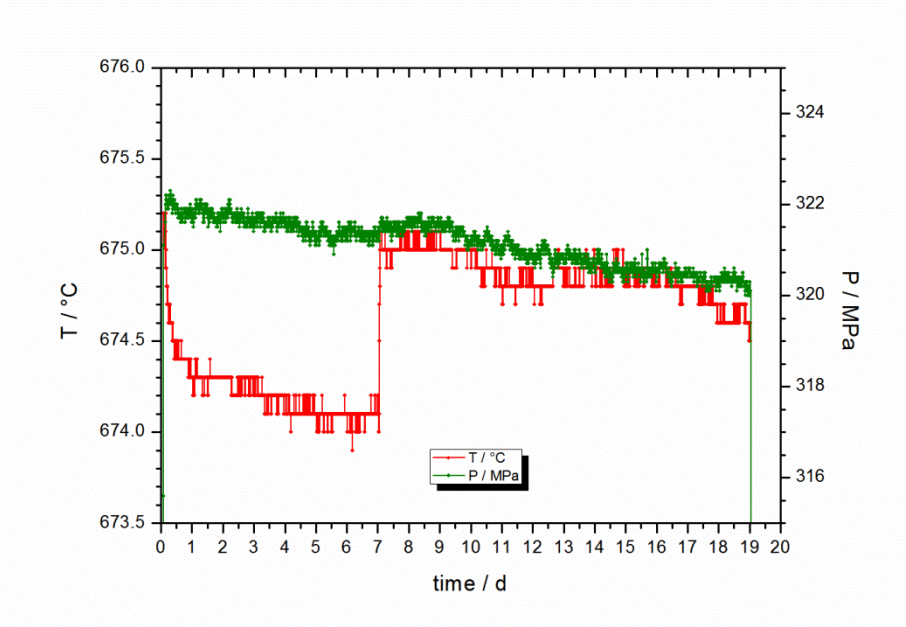
T / °C
P / MPa
time / d
676.0
675.5
675.0
674.5
674.0
673.5
324
322
320
318
316
0 1 2 3 4 5 6 7 8 9 10 11 12 13 14 15 16 17 18 19 20

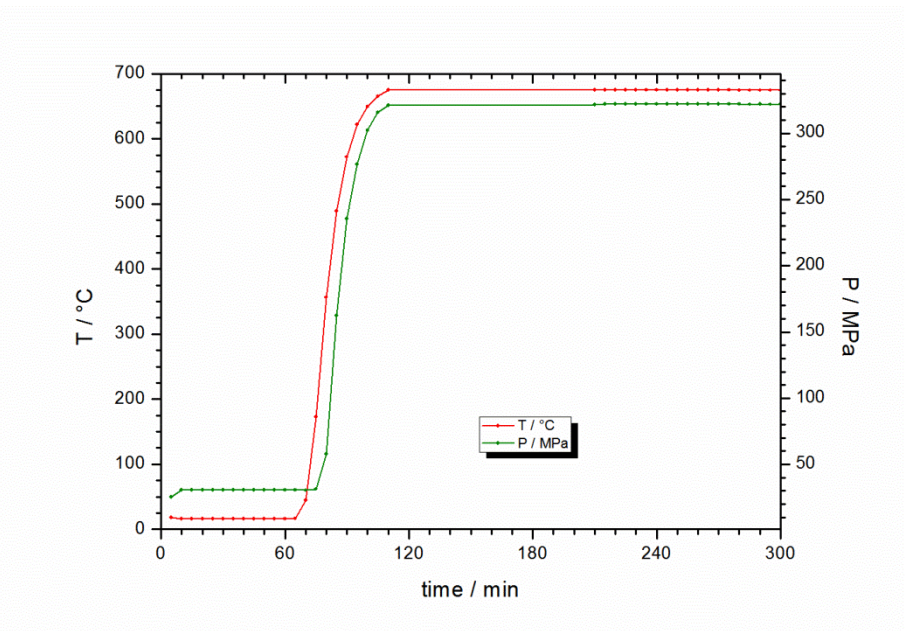
T / °C
P / MPa
time / min
700
600
500
400
300
200
100
0
300
250
200
150
100
50
0 60 120 180 240 300

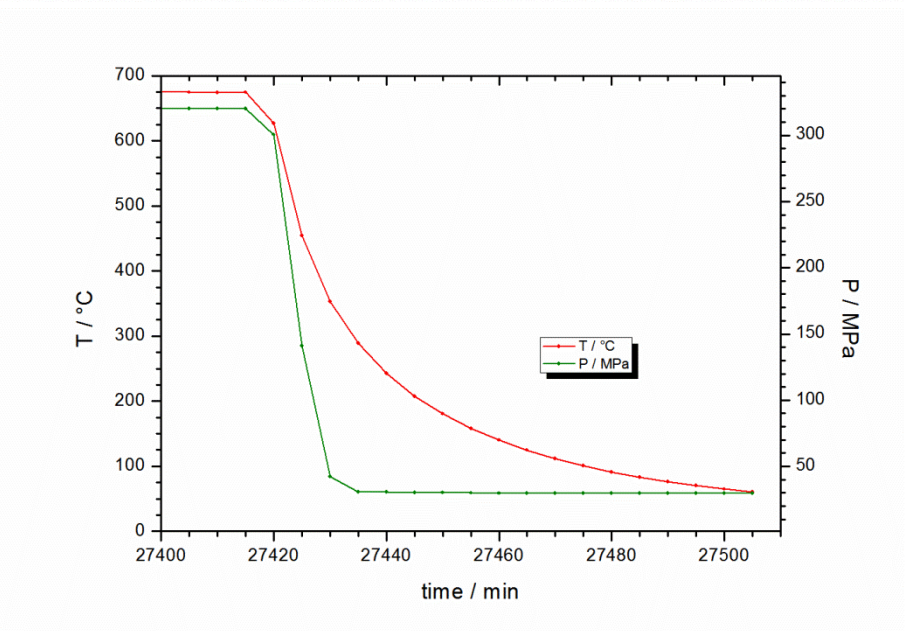
T / °C
P / MPa
time / min
700
600
500
400
300
200
100
0
300
250
200
150
100
50
27400 27420 27440 27460 27480 27500

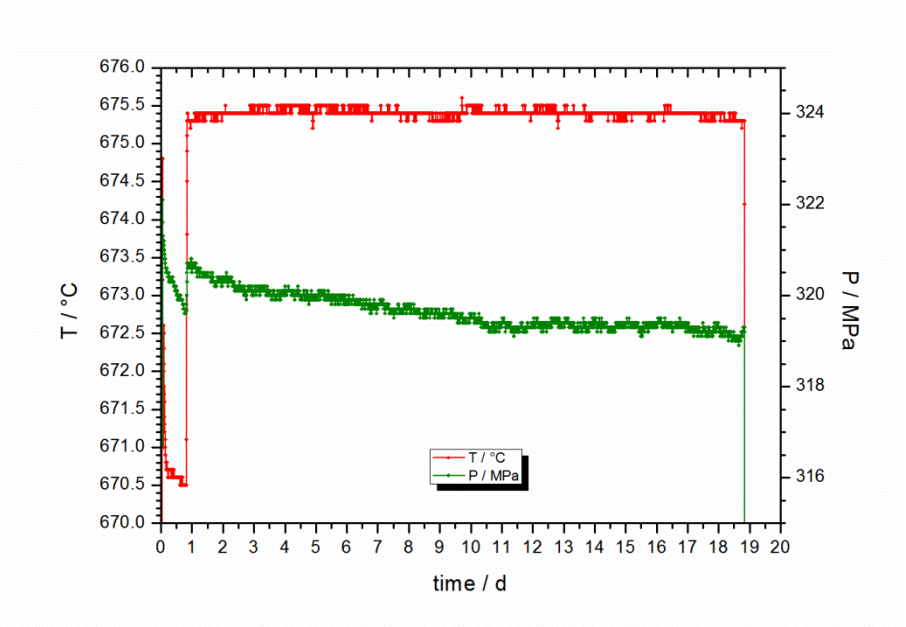
T / °C
P / MPa
time / d
T / °C
P / MPa

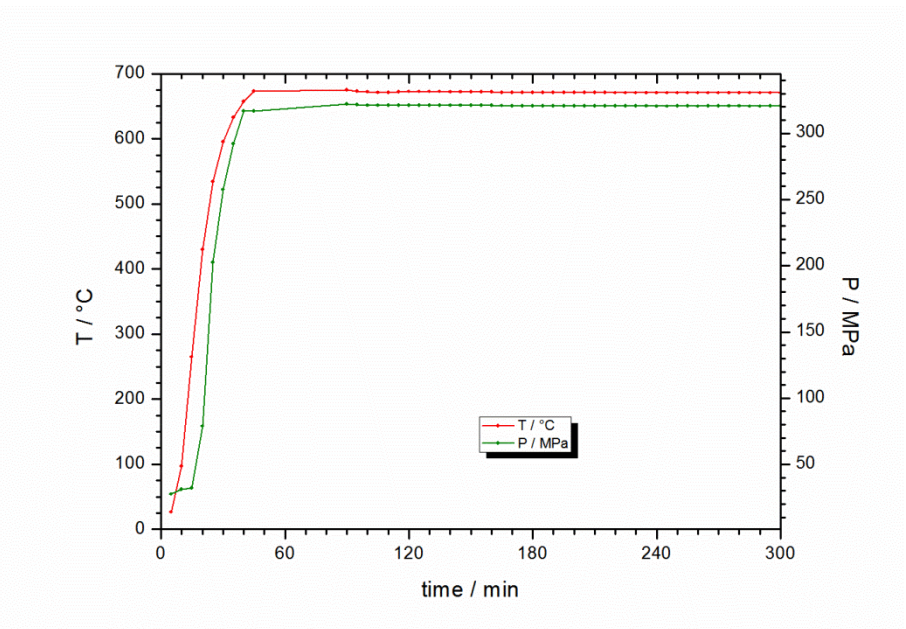
T / °C
P / MPa
time / min
T / °C
P / MPa

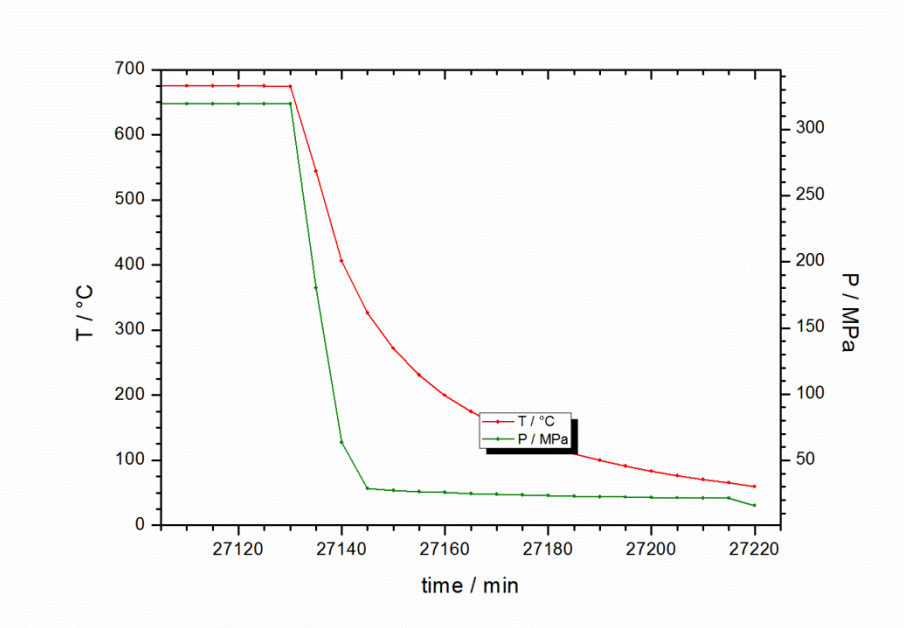
T / °C
P / MPa
time / min
T / °C
P / MPa

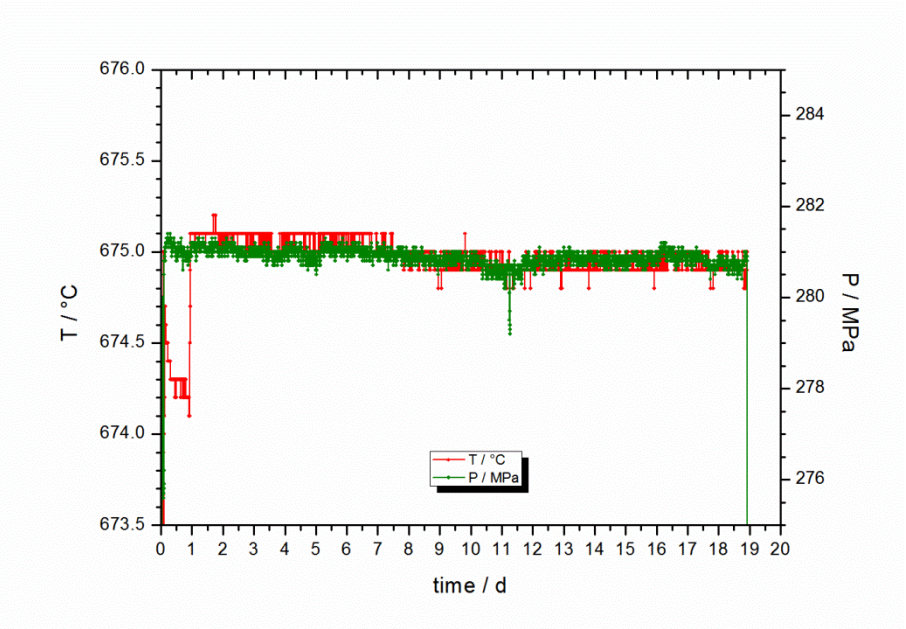
T / °C
P / MPa
time / d

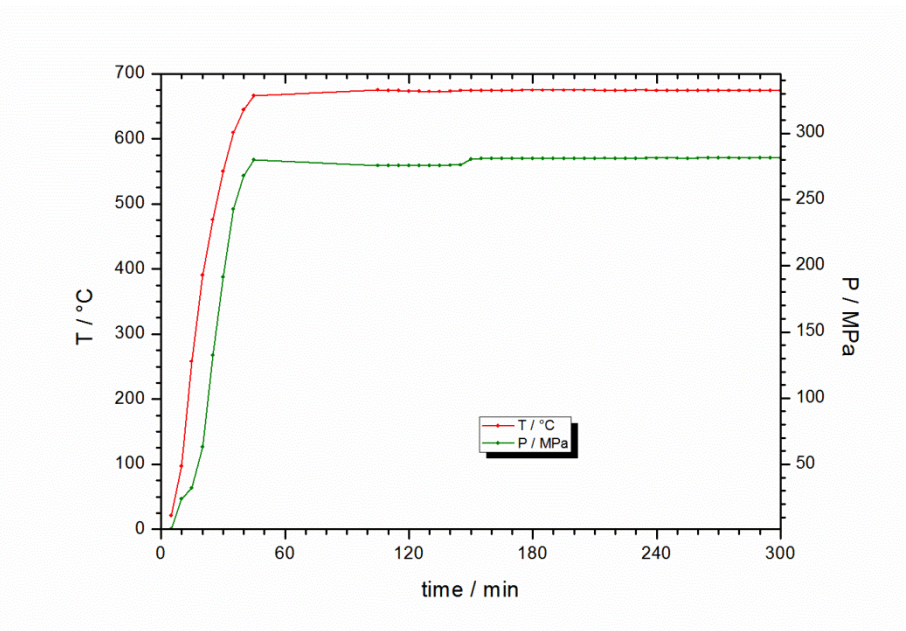
T / °C
P / MPa
time / min

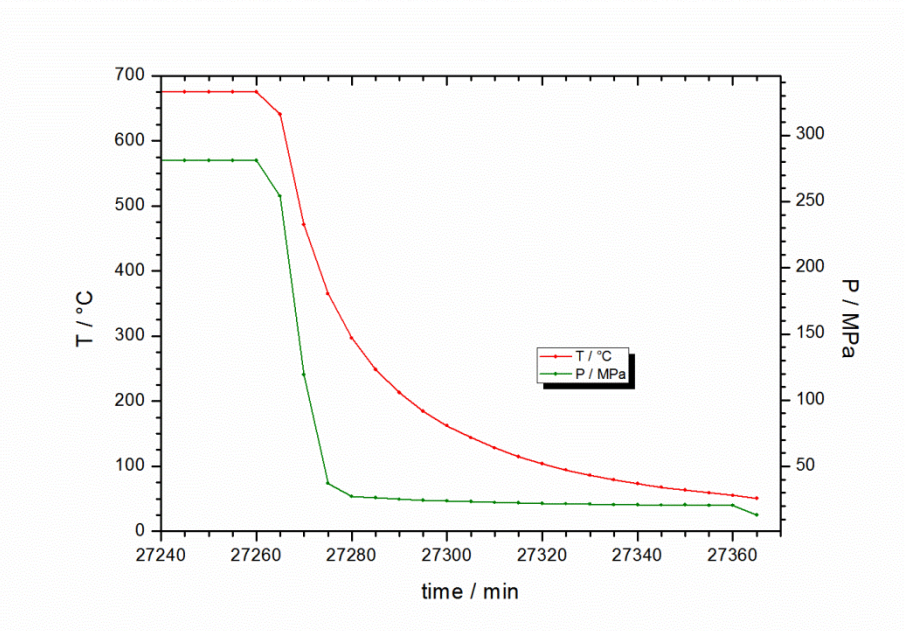
T / °C
P / MPa
time / min

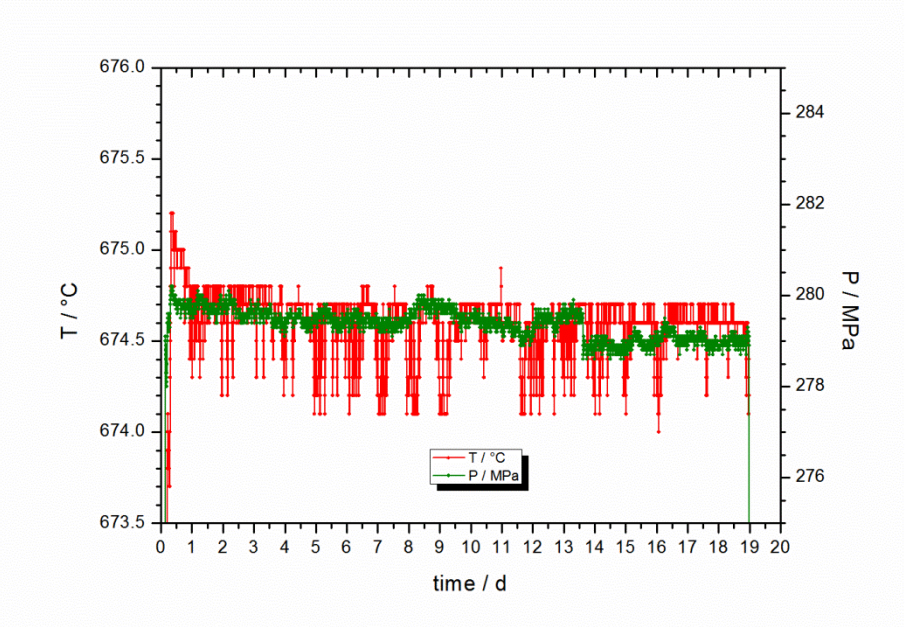
T / °C
P / MPa
time / d
676.0
675.5
675.0
674.5
674.0
673.5
284
282
280
278
276
0 1 2 3 4 5 6 7 8 9 10 11 12 13 14 15 16 17 18 19 20

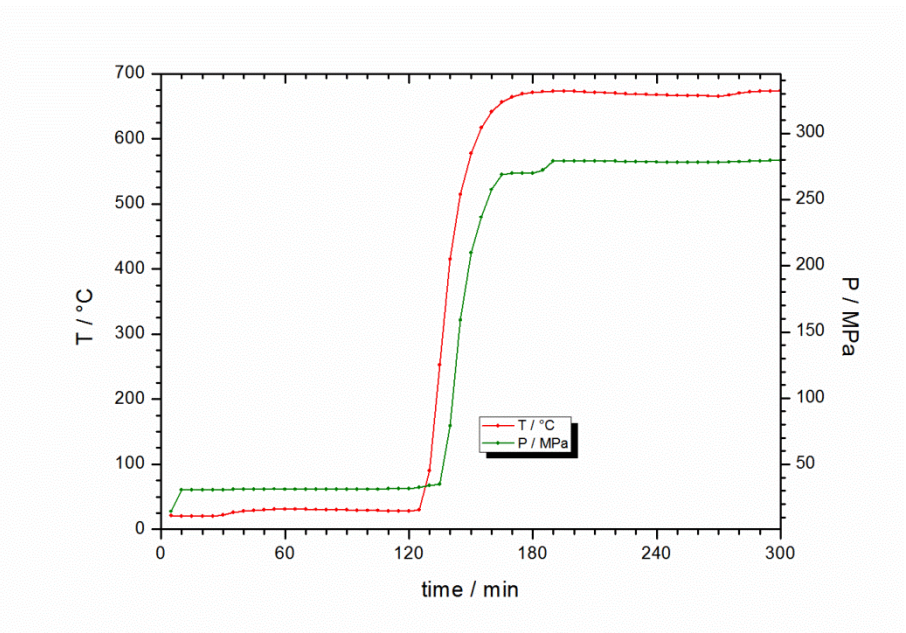
T / °C
P / MPa
time / min
700
600
500
400
300
200
100
0
300
250
200
150
100
50
0 60 120 180 240 300

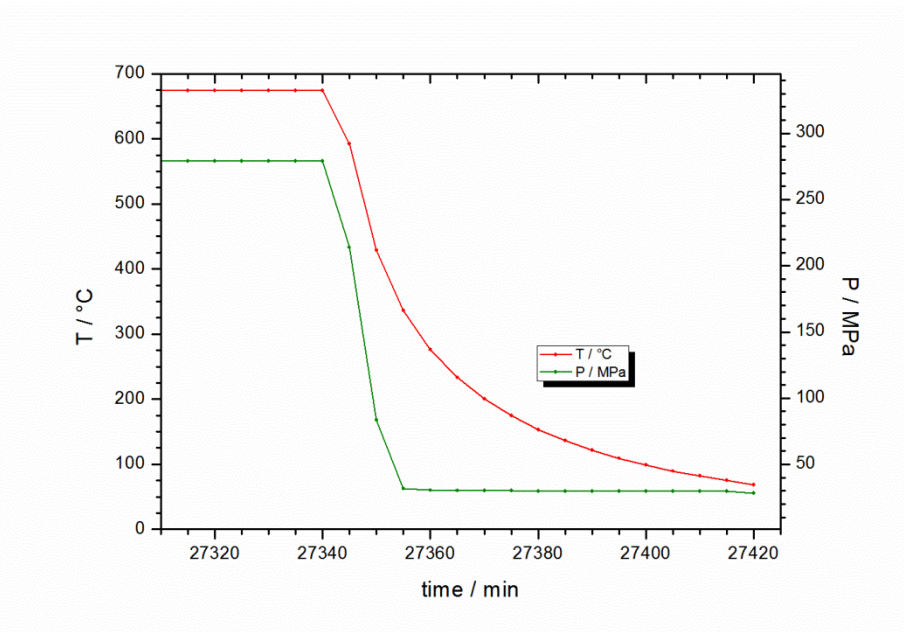
T / °C
P / MPa
time / min
700
600
500
400
300
200
100
0
300
250
200
150
100
50
27320 27340 27360 27380 27400 27420

A.b.i Data set

All experimental records are attached as DVD to this work.

A.c Experimental conditions of chapter 5

"*Modification in fluid inclusion salinity during re-equilibration experiments at constant experimental P-T*"

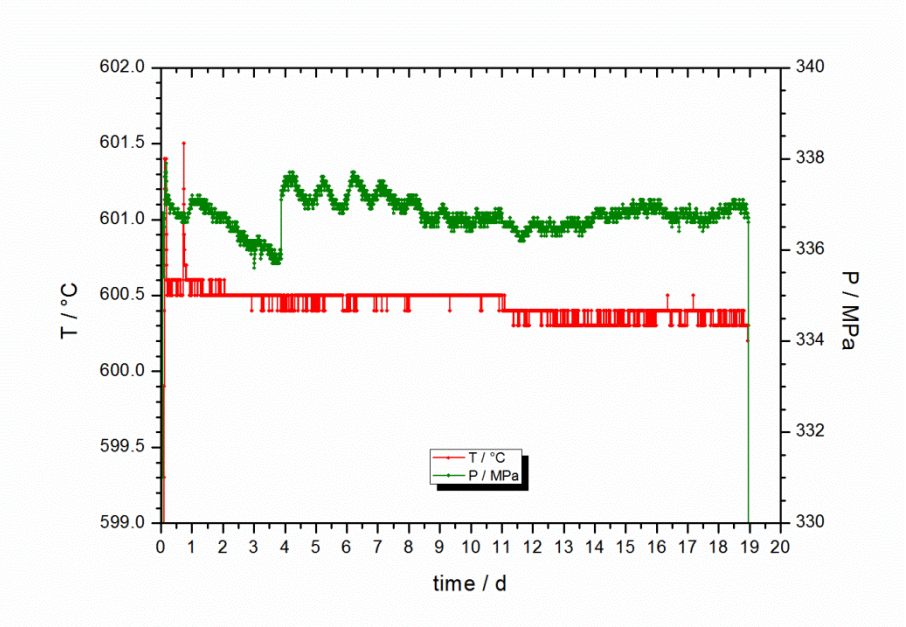
T / °C
P / MPa
time / d
T / °C
P / MPa

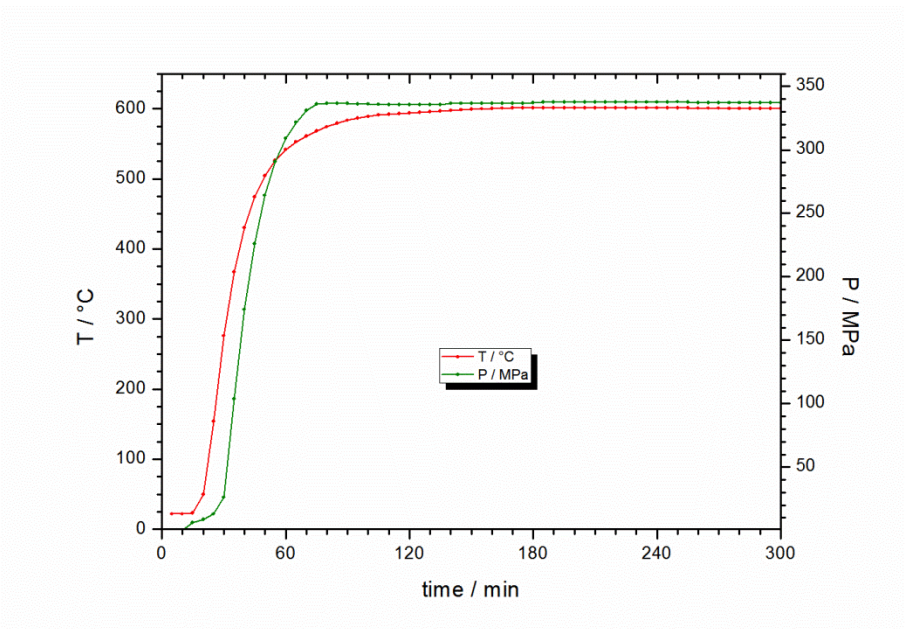
T / °C
P / MPa
time / min
T / °C
P / MPa

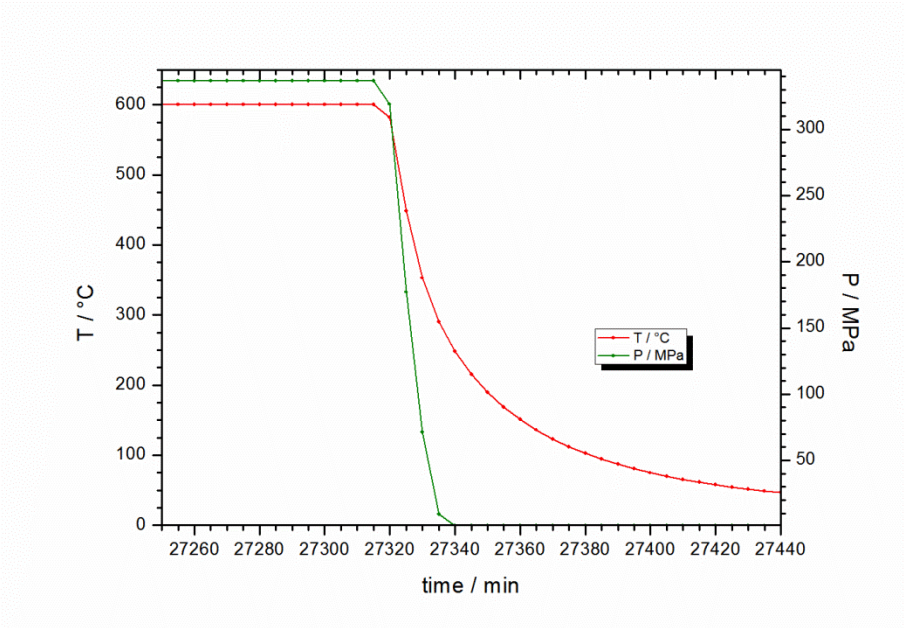
T / °C
P / MPa
time / min
T / °C
P / MPa

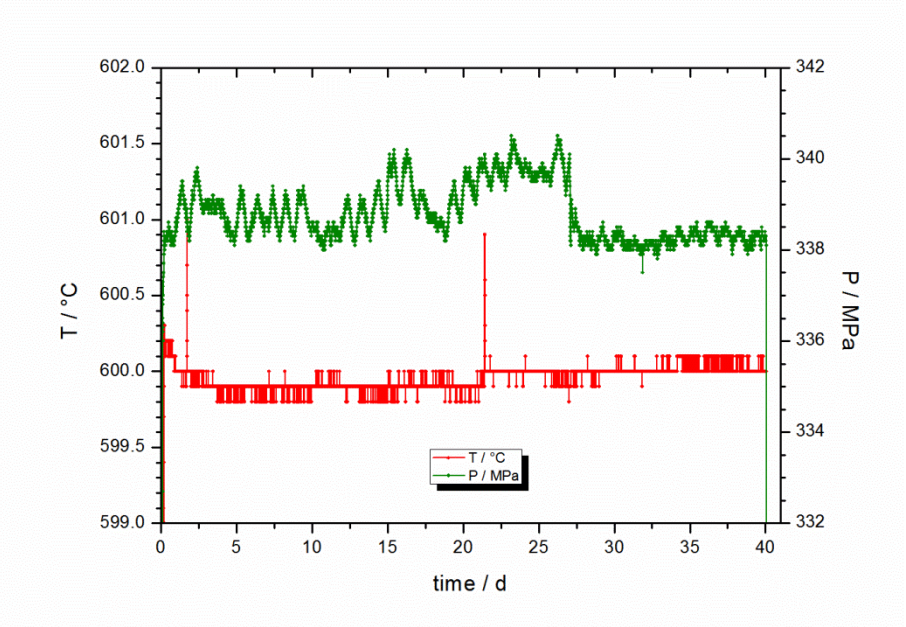
602.0
601.5
601.0
600.5
600.0
599.5
599.0
342
340
338
336
334
332
T / °C
P / MPa
0
5
10
15
20
25
30
35
40
time / d
T / °C
P / MPa

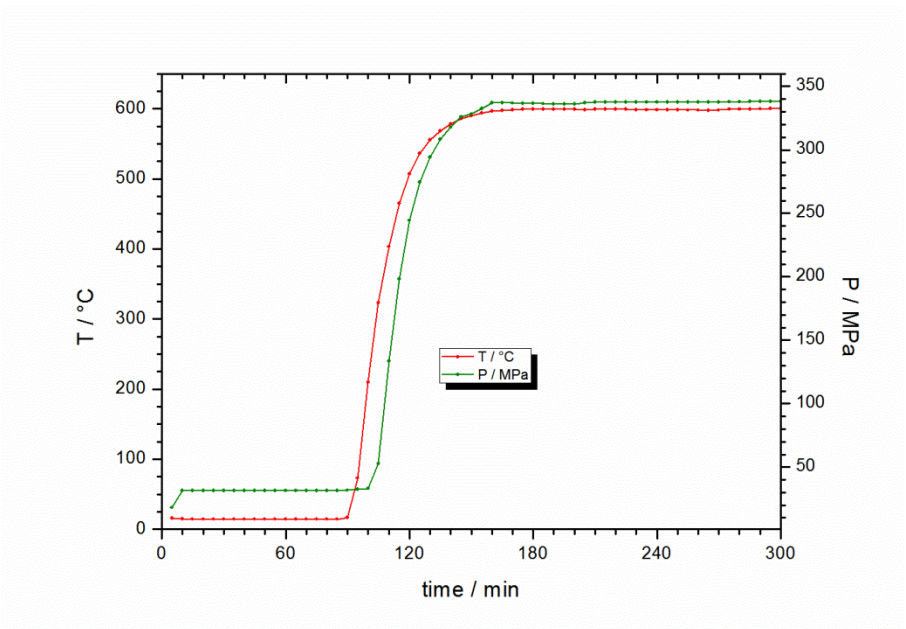
600
500
400
300
200
100
0
350
300
250
200
150
100
50
T / °C
P / MPa
0
60
120
180
240
300
time / min
T / °C
P / MPa

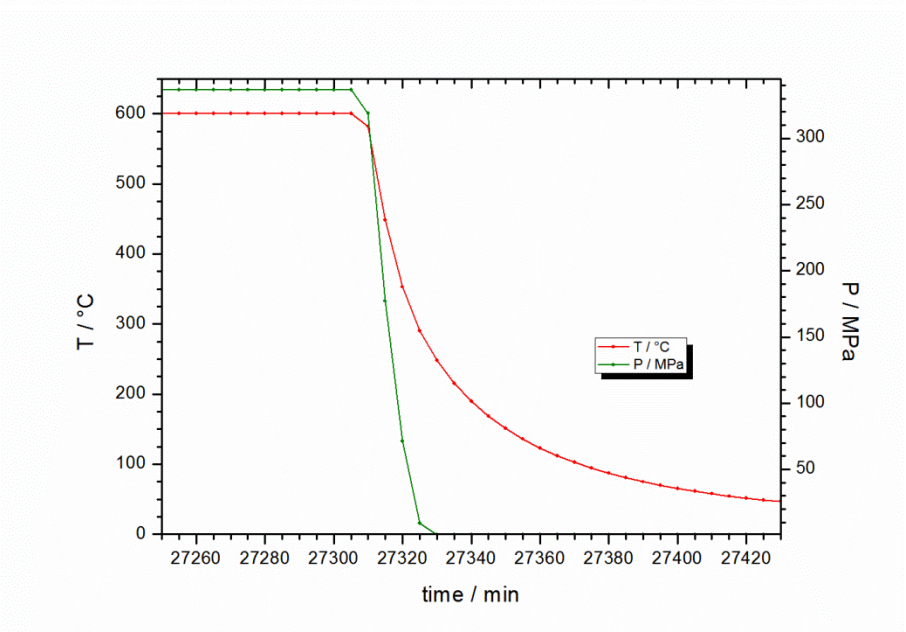
600
500
400
300
200
100
0
300
250
200
150
100
50
T / °C
P / MPa
27260
27280
27300
27320
27340
27360
27380
27400
27420
time / min
T / °C
P / MPa

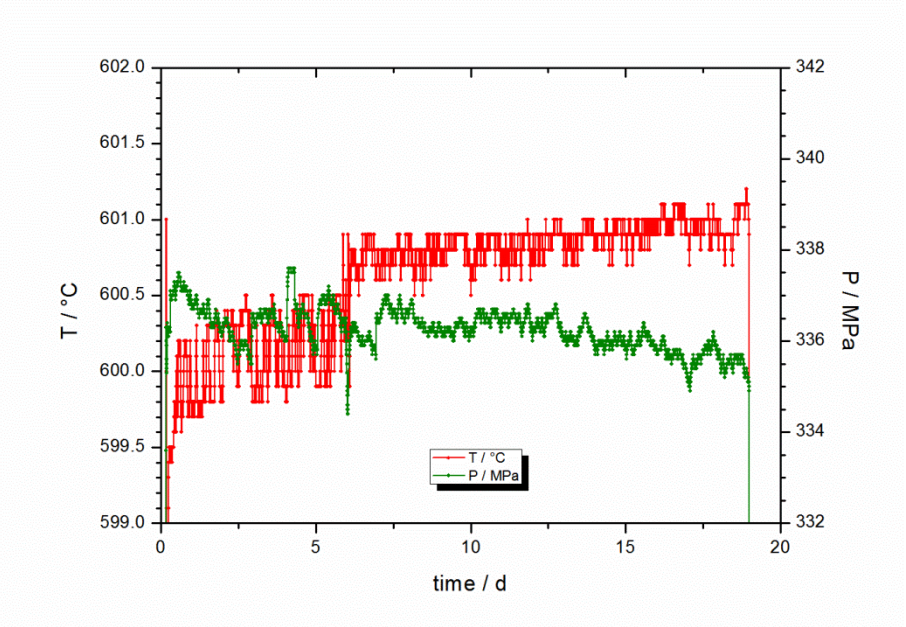
602.0
601.5
601.0
600.5
600.0
599.5
599.0
T / °C
342
340
338
336
334
332
P / MPa
0
5
10
15
20
time / d
T / °C
P / MPa

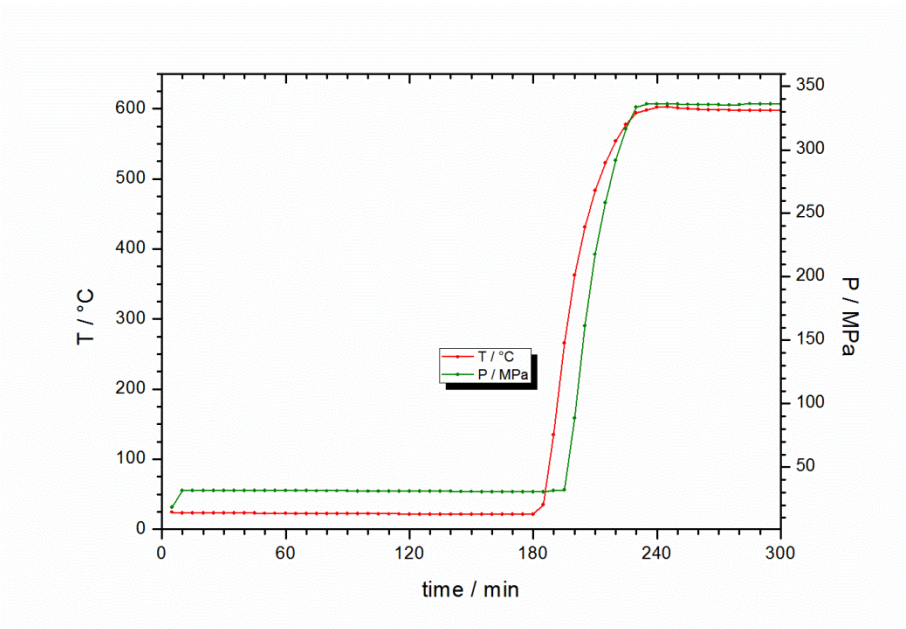
600
500
400
300
200
100
0
T / °C
350
300
250
200
150
100
50
P / MPa
0
60
120
180
240
300
time / min
T / °C
P / MPa

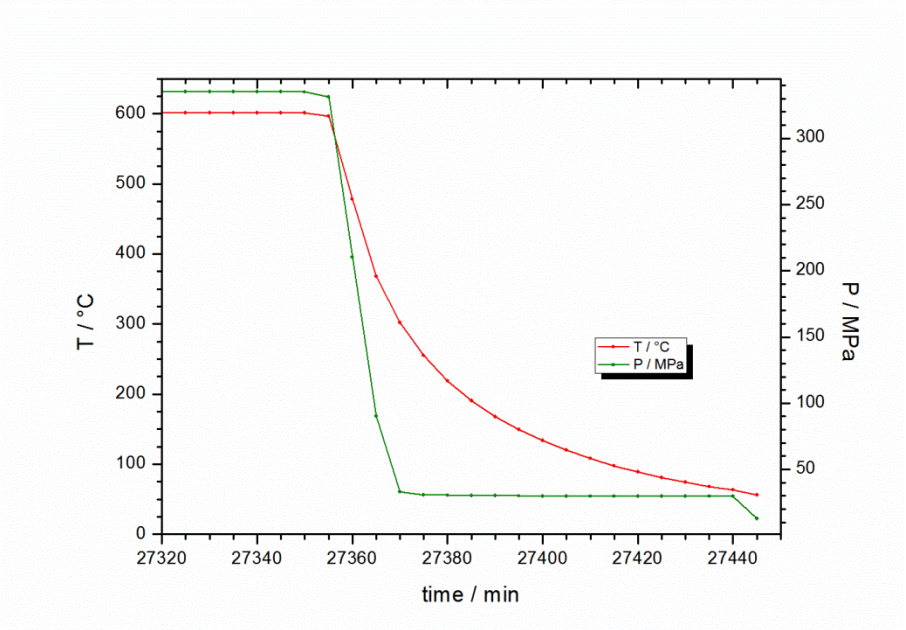
600
500
400
300
200
100
0
T / °C
300
250
200
150
100
50
P / MPa
27320
27340
27360
27380
27400
27420
27440
time / min
T / °C
P / MPa

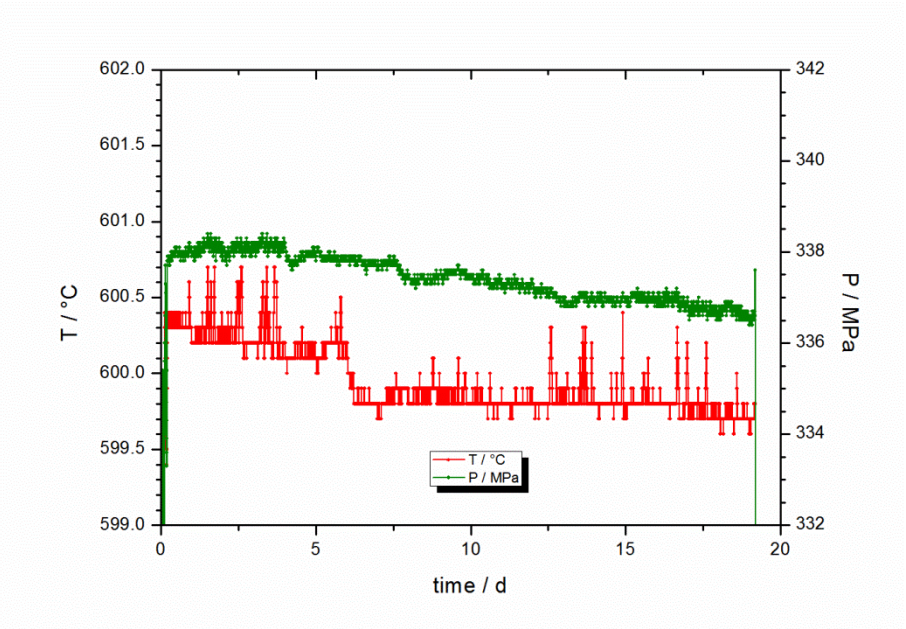
602.0
601.5
601.0
600.5
600.0
599.5
599.0
T / °C
342
340
338
336
334
332
P / MPa
0
5
10
15
20
time / d
T / °C
P / MPa

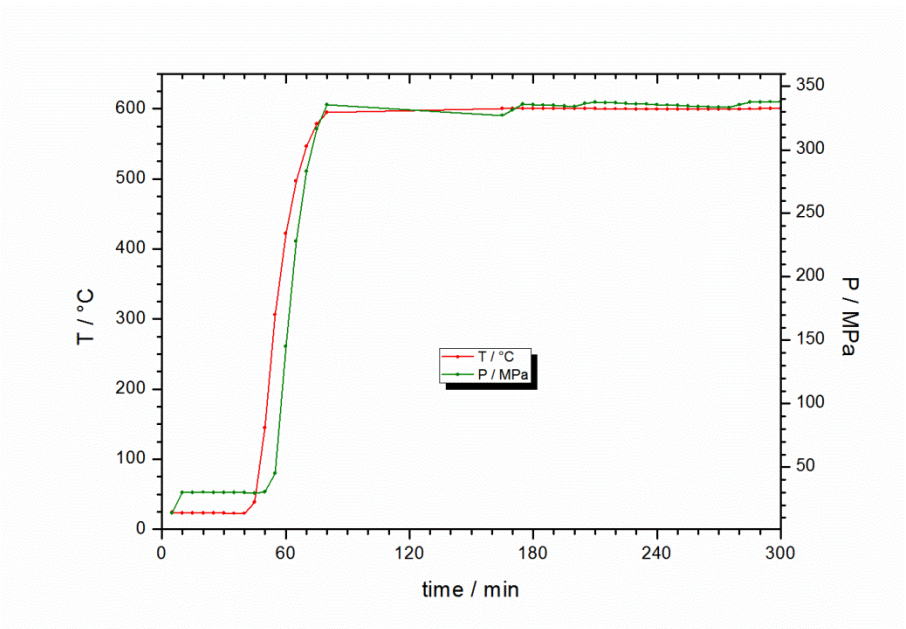
600
500
400
300
200
100
0
T / °C
350
300
250
200
150
100
50
P / MPa
0
60
120
180
240
300
time / min
T / °C
P / MPa

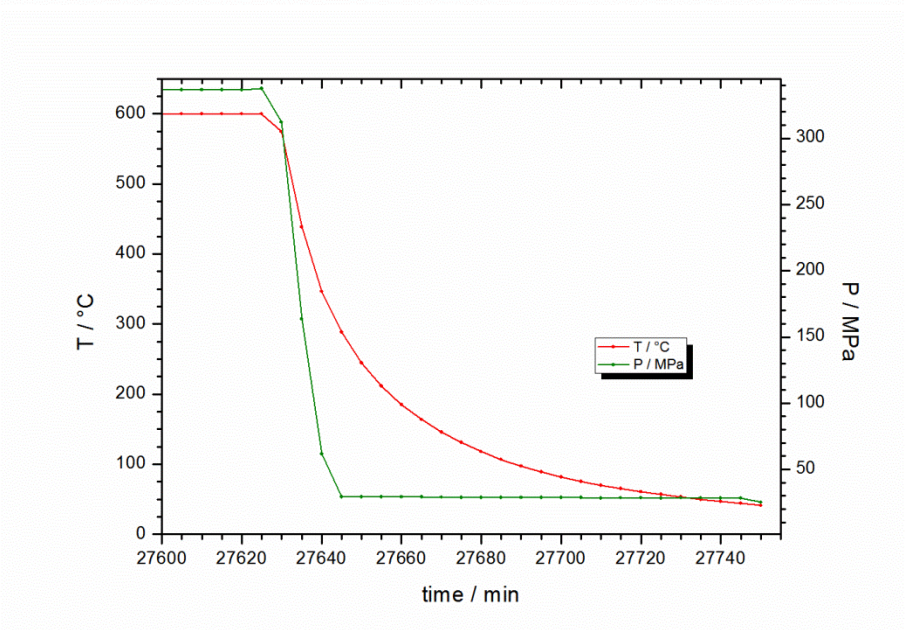
600
500
400
300
200
100
0
T / °C
300
250
200
150
100
50
P / MPa
27600
27620
27640
27660
27680
27700
27720
27740
time / min
T / °C
P / MPa

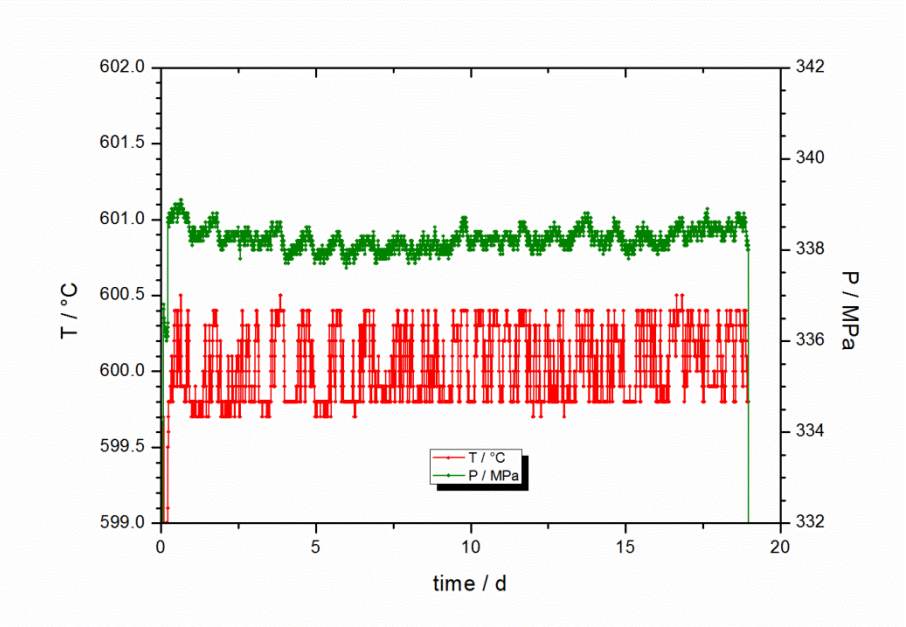
602.0
601.5
601.0
600.5
600.0
599.5
599.0
T / °C
342
340
338
336
334
332
P / MPa
0
5
10
15
20
time / d
T / °C
P / MPa

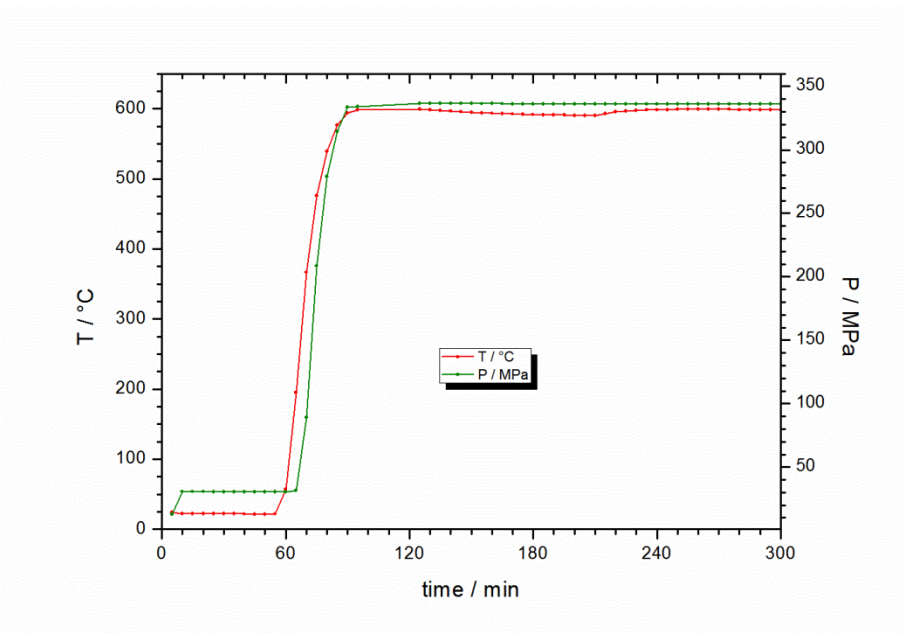
600
500
400
300
200
100
0
T / °C
350
300
250
200
150
100
50
P / MPa
0
60
120
180
240
300
time / min
T / °C
P / MPa

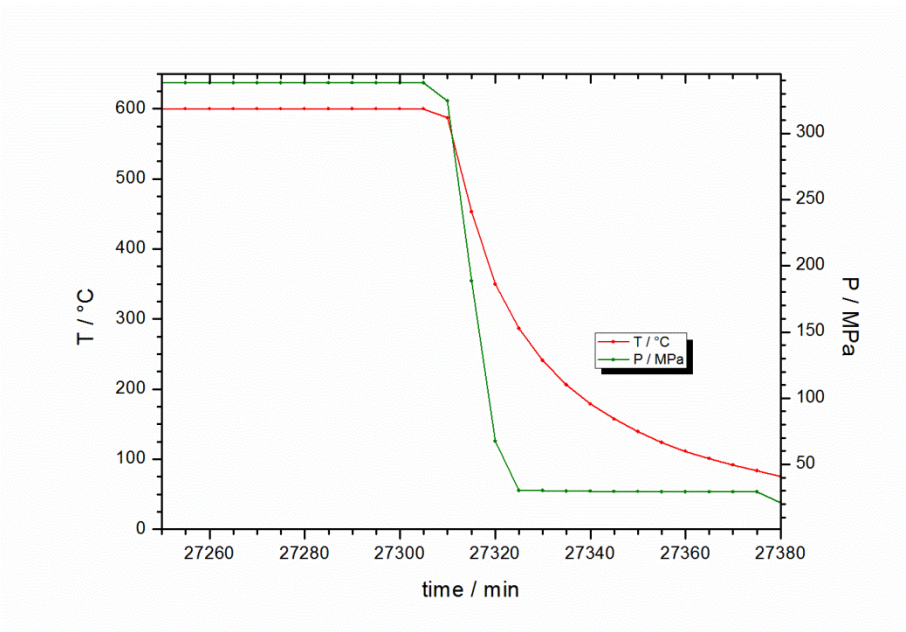
600
500
400
300
200
100
0
T / °C
300
250
200
150
100
50
P / MPa
27260
27280
27300
27320
27340
27360
27380
time / min
T / °C
P / MPa

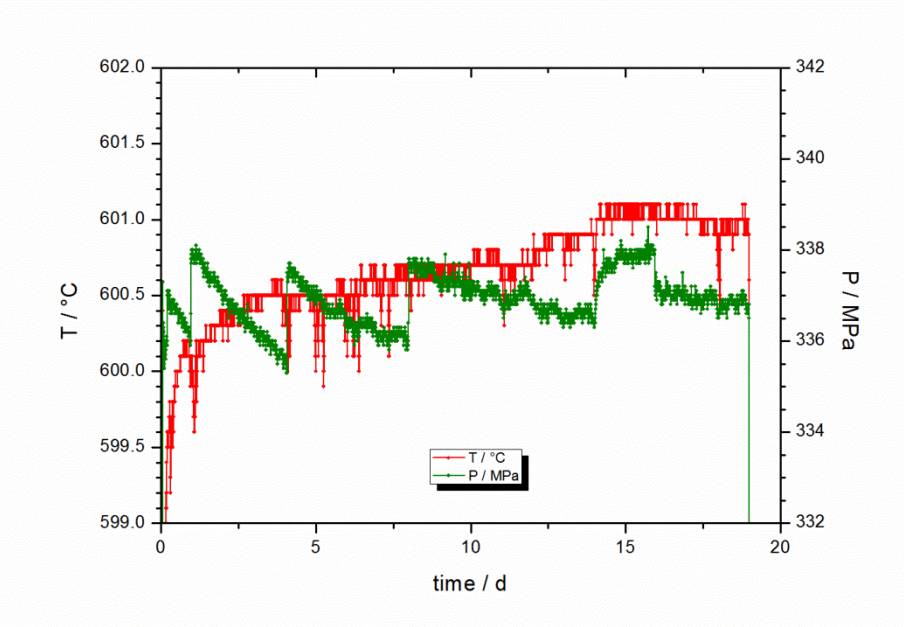
602.0
601.5
601.0
600.5
600.0
599.5
599.0
T / °C
342
340
338
336
334
332
P / MPa
0
5
10
15
20
time / d
T / °C
P / MPa

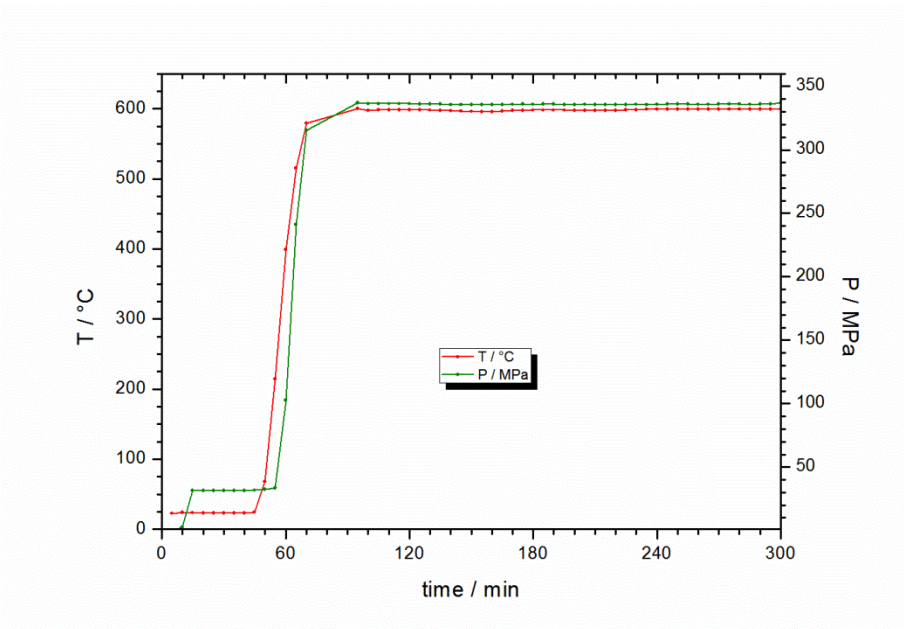
600
500
400
300
200
100
0
T / °C
350
300
250
200
150
100
50
P / MPa
0
60
120
180
240
300
time / min
T / °C
P / MPa

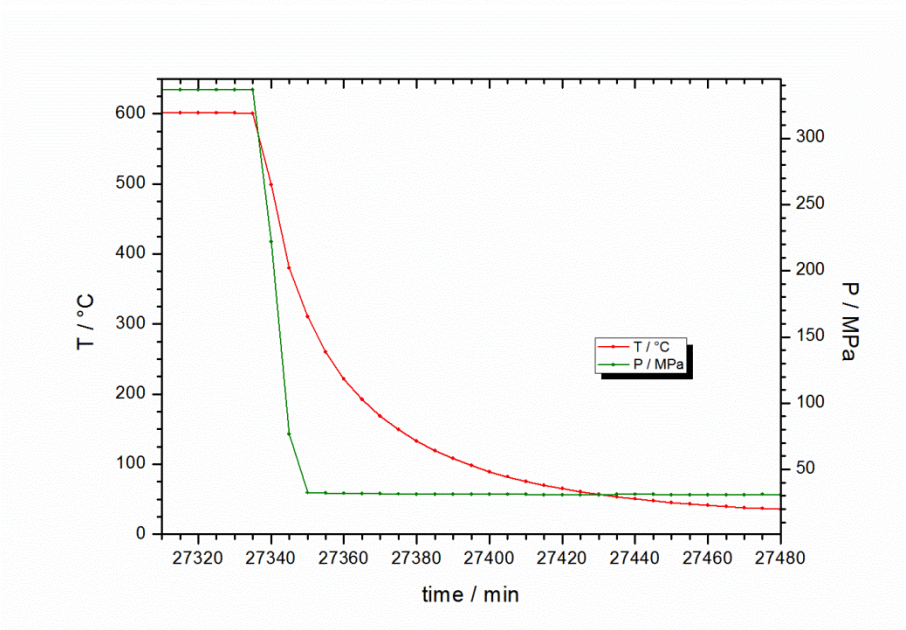
600
500
400
300
200
100
0
T / °C
300
250
200
150
100
50
P / MPa
27320
27340
27360
27380
27400
27420
27440
27460
27480
time / min
T / °C
P / MPa

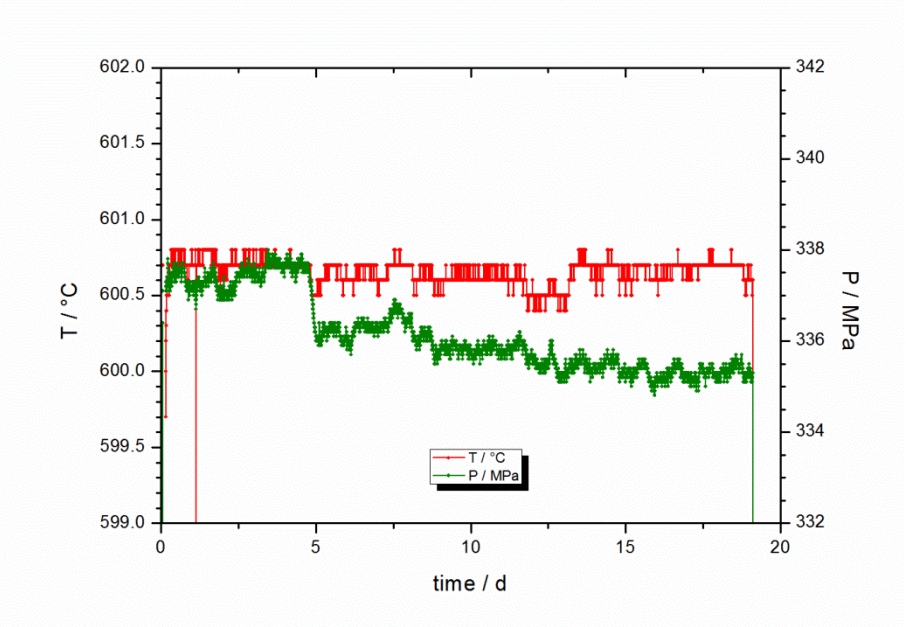
602.0
601.5
601.0
600.5
600.0
599.5
599.0
T / °C
342
340
338
336
334
332
P / MPa
0
5
10
15
20
time / d
T / °C
P / MPa

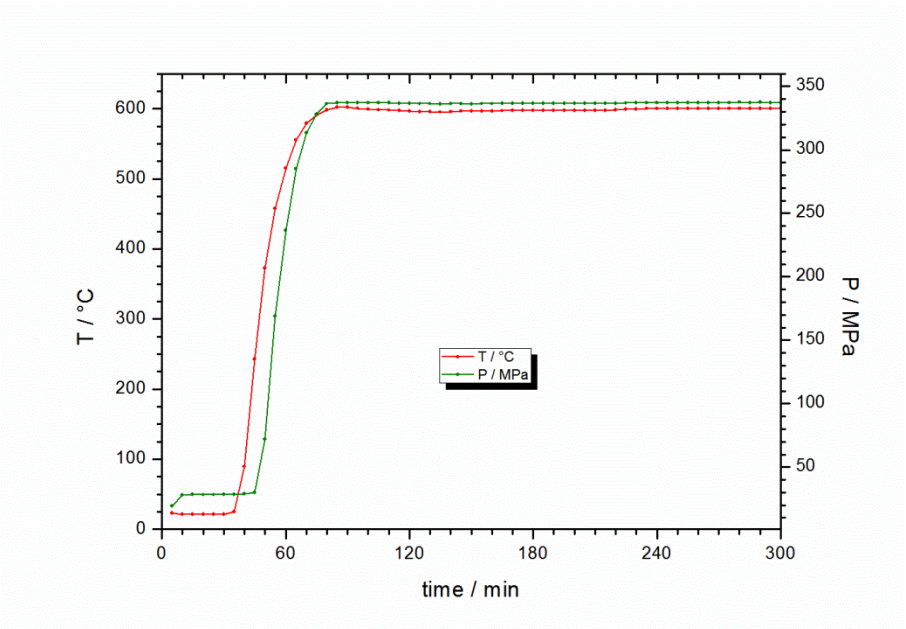
600
500
400
300
200
100
0
T / °C
350
300
250
200
150
100
50
P / MPa
0
60
120
180
240
300
time / min
T / °C
P / MPa

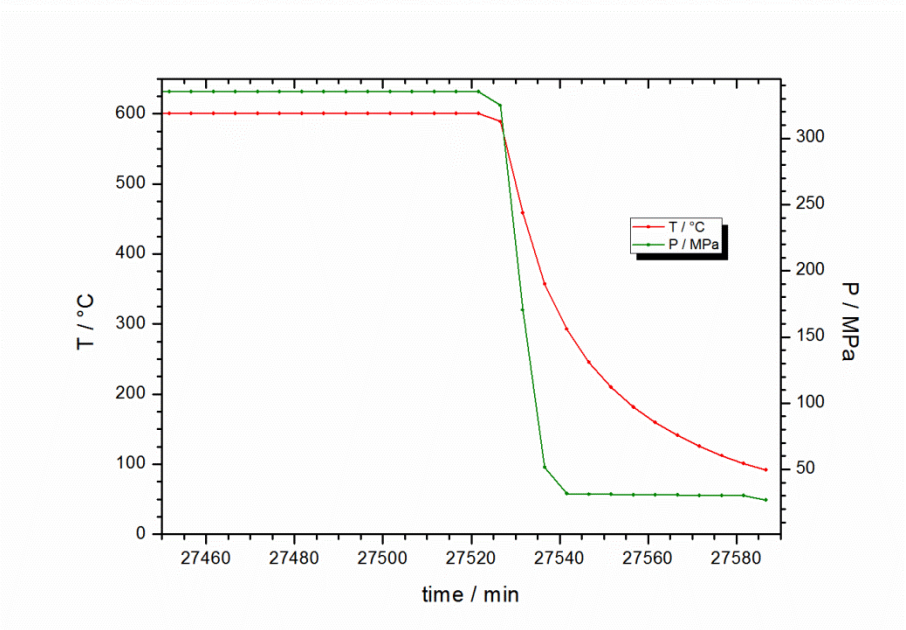
600
500
400
300
200
100
0
T / °C
300
250
200
150
100
50
P / MPa
27460
27480
27500
27520
27540
27560
27580
time / min
T / °C
P / MPa

no log data of experimental run!

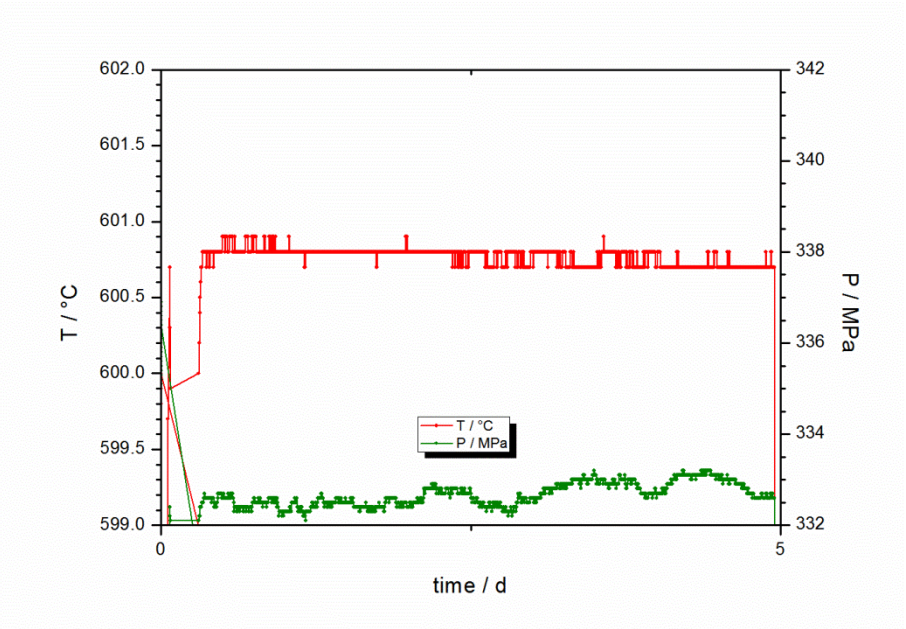
602.0
601.5
601.0
600.5
600.0
599.5
599.0
T / °C
342
340
338
336
334
332
P / MPa
0
5
time / d
T / °C
P / MPa

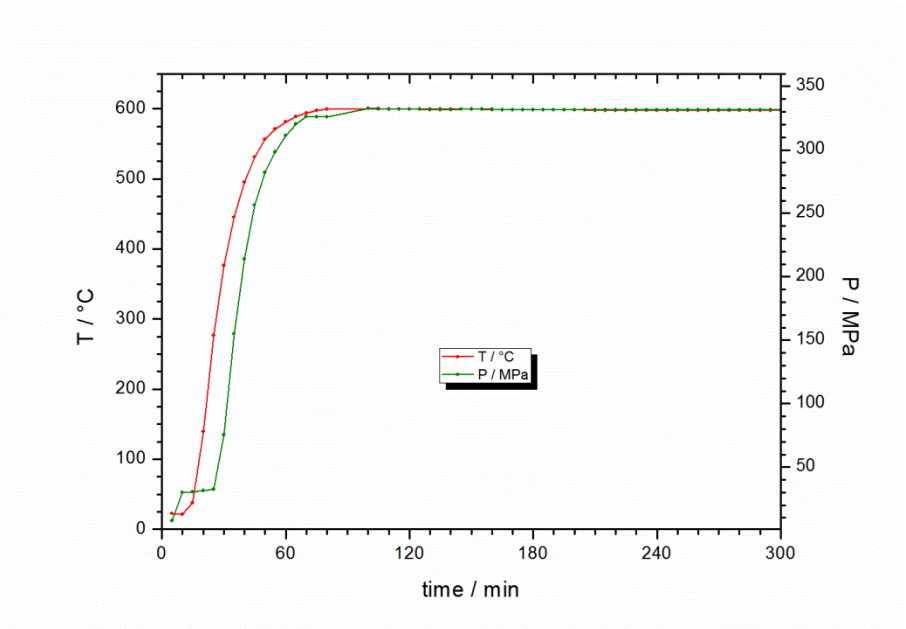
600
500
400
300
200
100
0
T / °C
350
300
250
200
150
100
50
P / MPa
0
60
120
180
240
300
time / min
T / °C
P / MPa

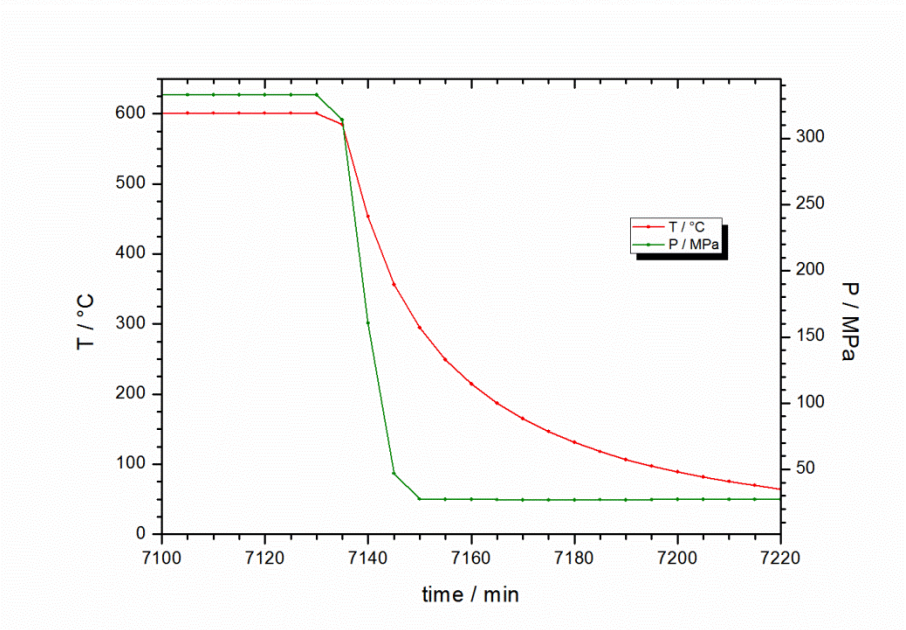
600
500
400
300
200
100
0
T / °C
300
250
200
150
100
50
P / MPa
7100
7120
7140
7160
7180
7200
7220
time / min
T / °C
P / MPa

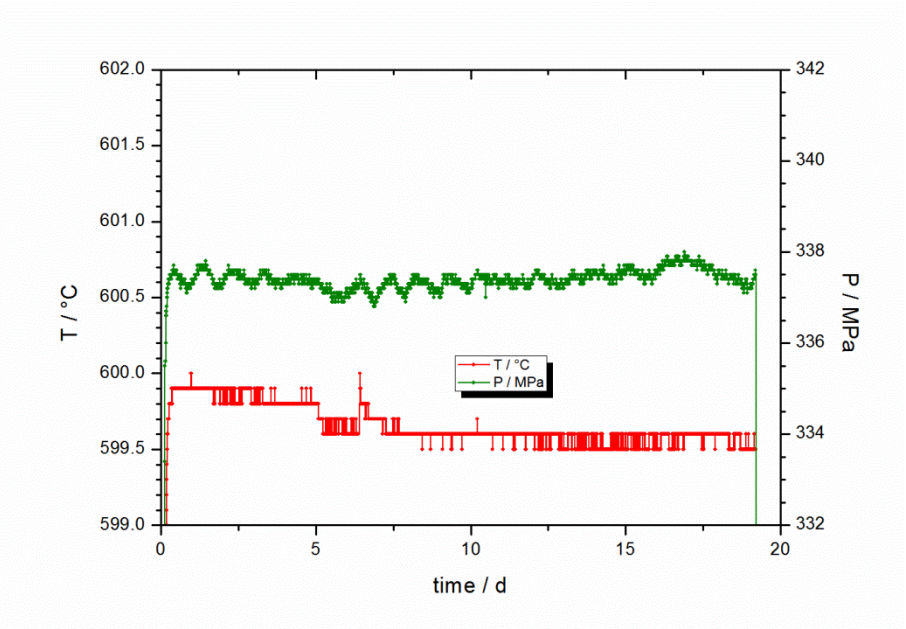
602.0
601.5
601.0
600.5
600.0
599.5
599.0
T / °C
342
340
338
336
334
332
P / MPa
0
5
10
15
20
time / d
T / °C
P / MPa

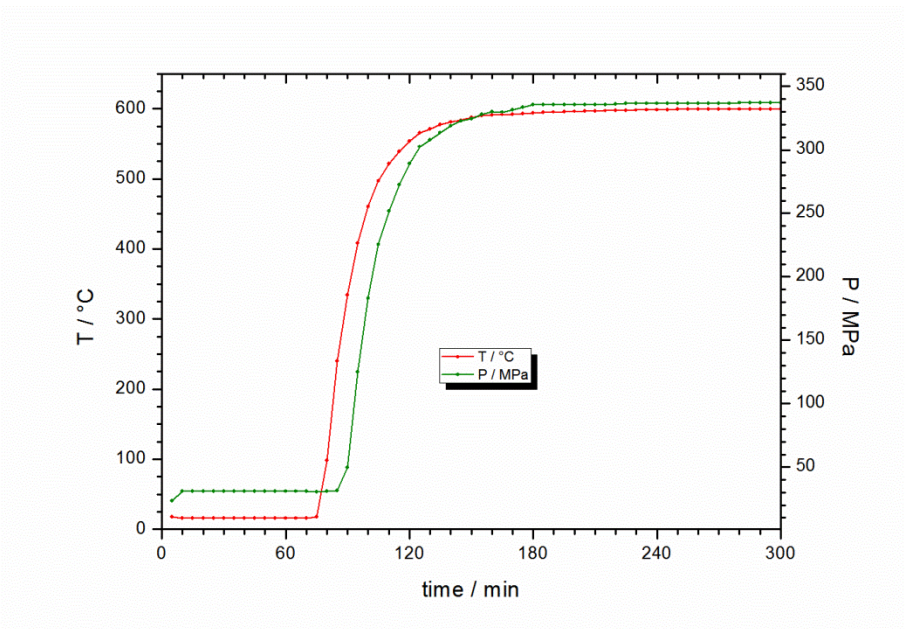
600
500
400
300
200
100
0
T / °C
350
300
250
200
150
100
50
P / MPa
0
60
120
180
240
300
time / min
T / °C
P / MPa

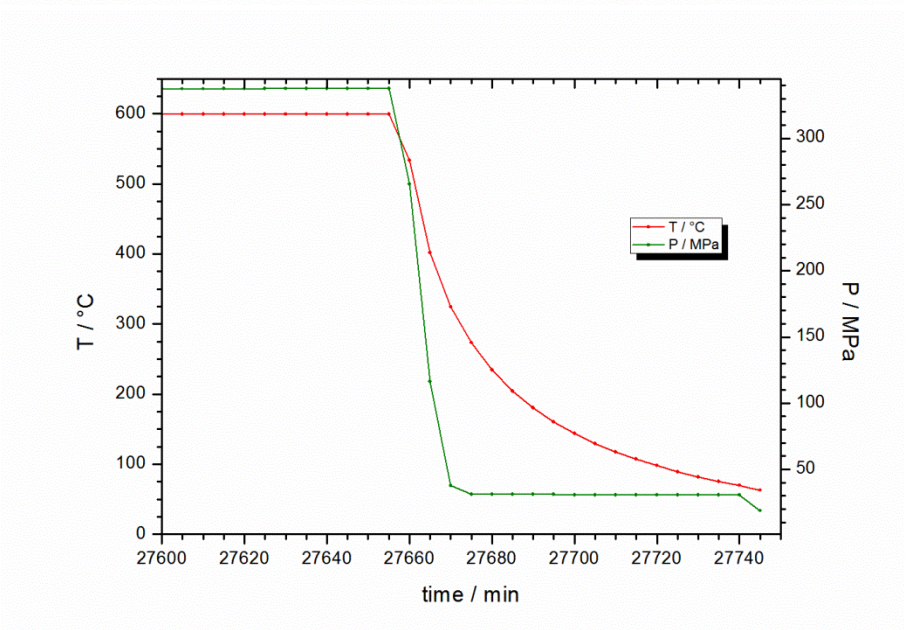
600
500
400
300
200
100
0
T / °C
300
250
200
150
100
50
P / MPa
27600
27620
27640
27660
27680
27700
27720
27740
time / min
T / °C
P / MPa

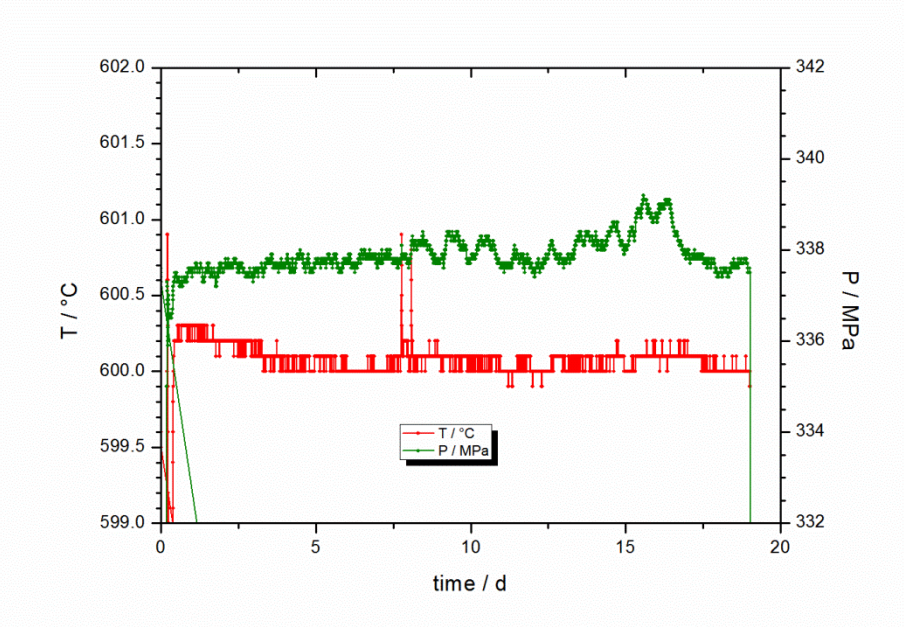
602.0
601.5
601.0
600.5
600.0
599.5
599.0
T / °C
342
340
338
336
334
332
P / MPa
0
5
10
15
20
time / d
T / °C
P / MPa

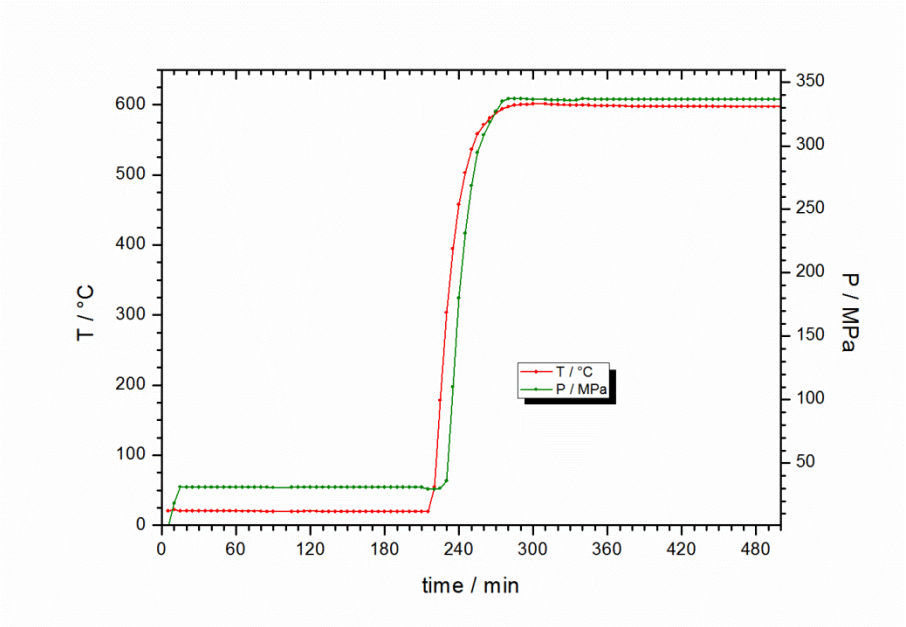
600
500
400
300
200
100
0
T / °C
350
300
250
200
150
100
50
P / MPa
0
60
120
180
240
300
360
420
480
time / min
T / °C
P / MPa

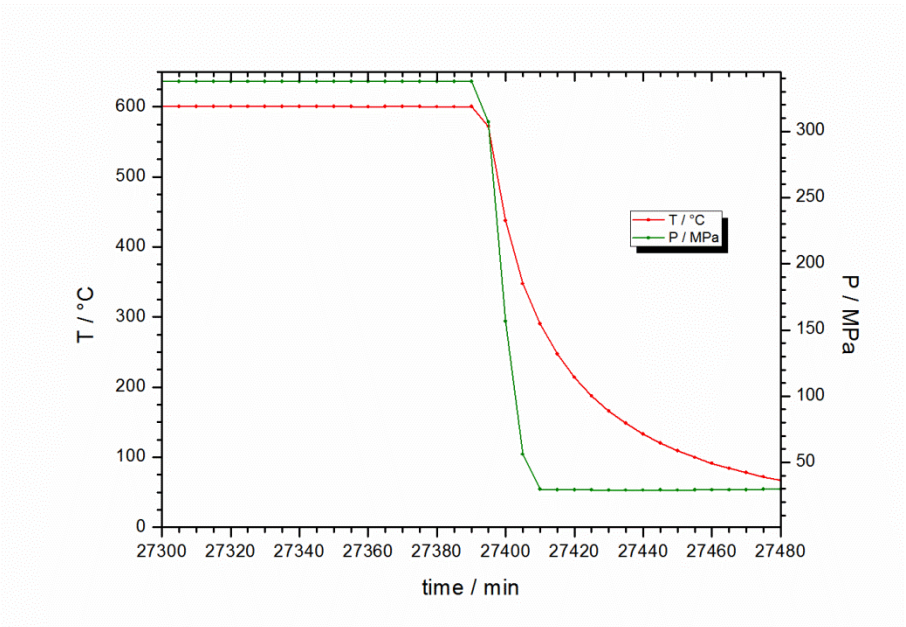
600
500
400
300
200
100
0
T / °C
300
250
200
150
100
50
P / MPa
27300
27320
27340
27360
27380
27400
27420
27440
27460
27480
time / min
T / °C
P / MPa

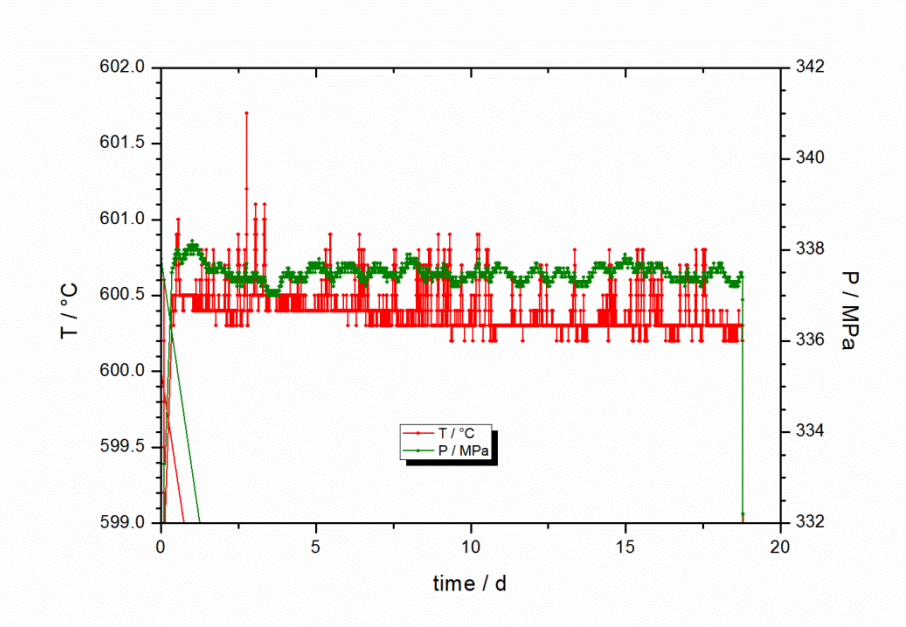
602.0
601.5
601.0
600.5
600.0
599.5
599.0
T / °C
342
340
338
336
334
332
P / MPa
0
5
10
15
20
time / d
T / °C
P / MPa

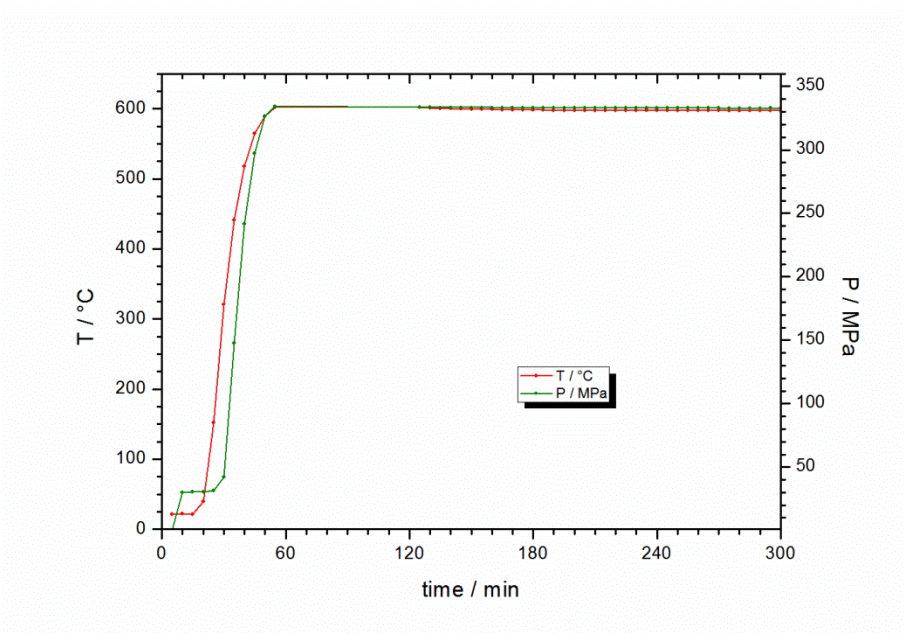
600
500
400
300
200
100
0
T / °C
350
300
250
200
150
100
50
P / MPa
0
60
120
180
240
300
time / min
T / °C
P / MPa

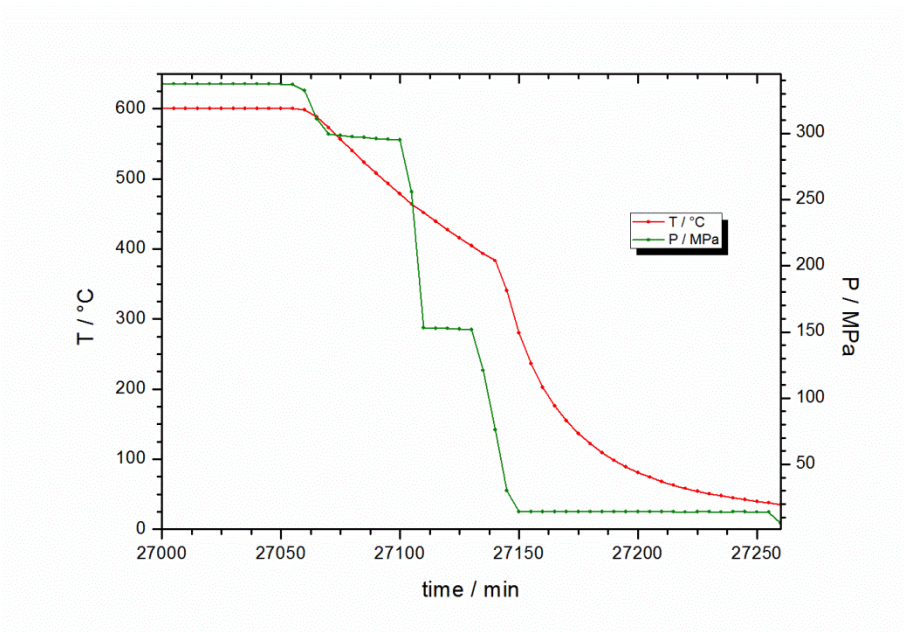
600
500
400
300
200
100
0
T / °C
300
250
200
150
100
50
P / MPa
27000
27050
27100
27150
27200
27250
time / min
T / °C
P / MPa

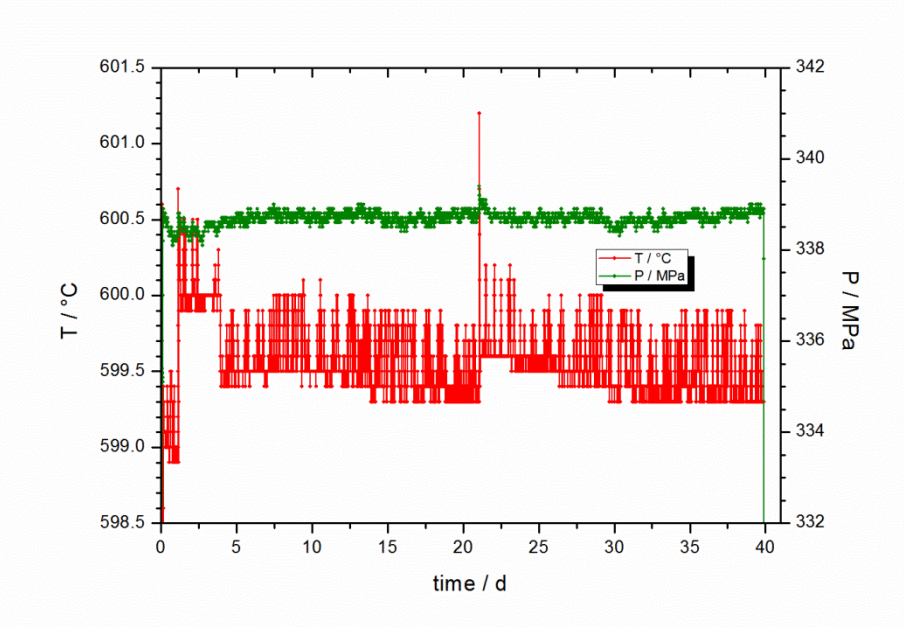
T / °C
P / MPa
time / d

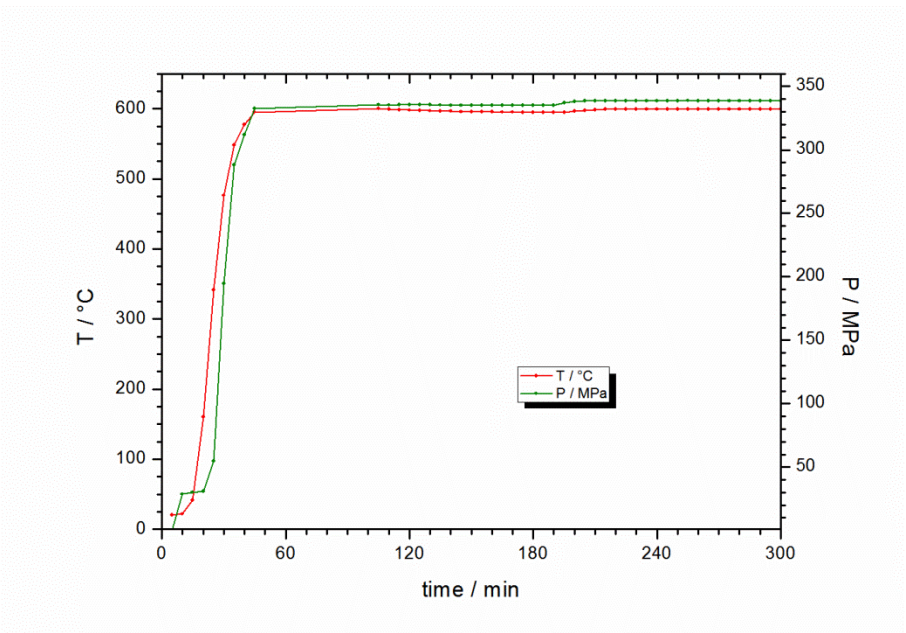
T / °C
P / MPa
time / min

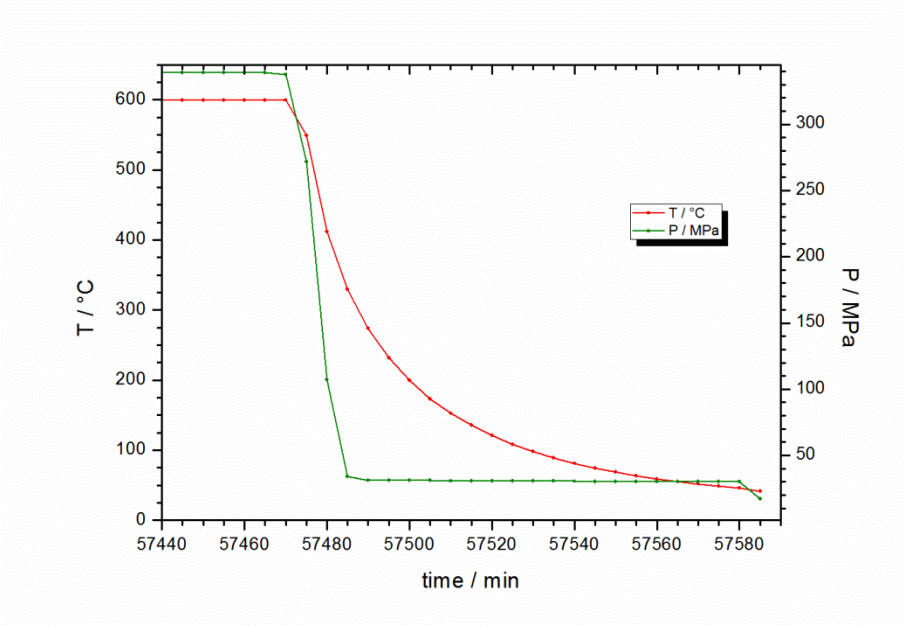
T / °C
P / MPa
time / min

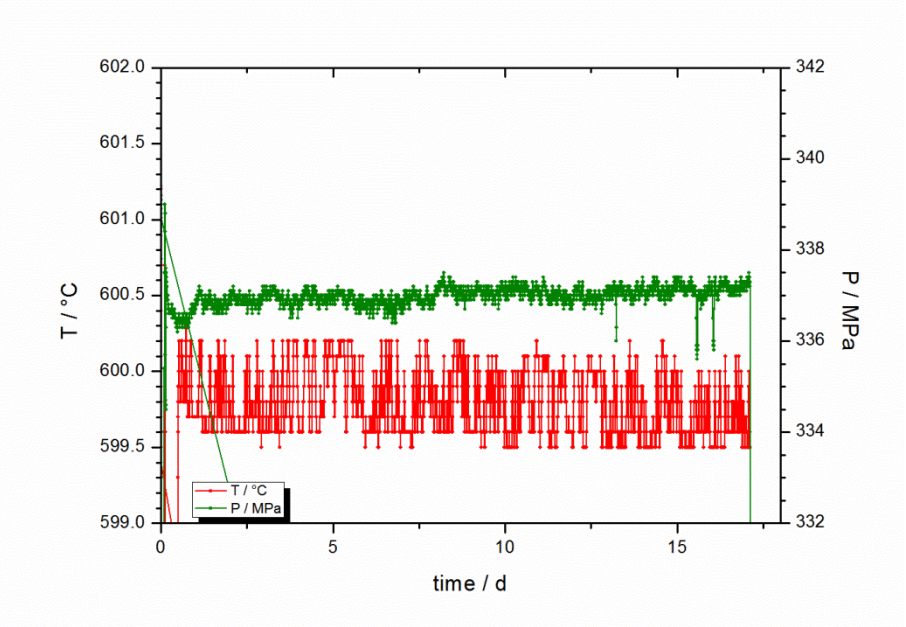
602.0
601.5
601.0
600.5
600.0
599.5
599.0
T / °C
342
340
338
336
334
332
P / MPa
0
5
10
15
time / d
T / °C
P / MPa

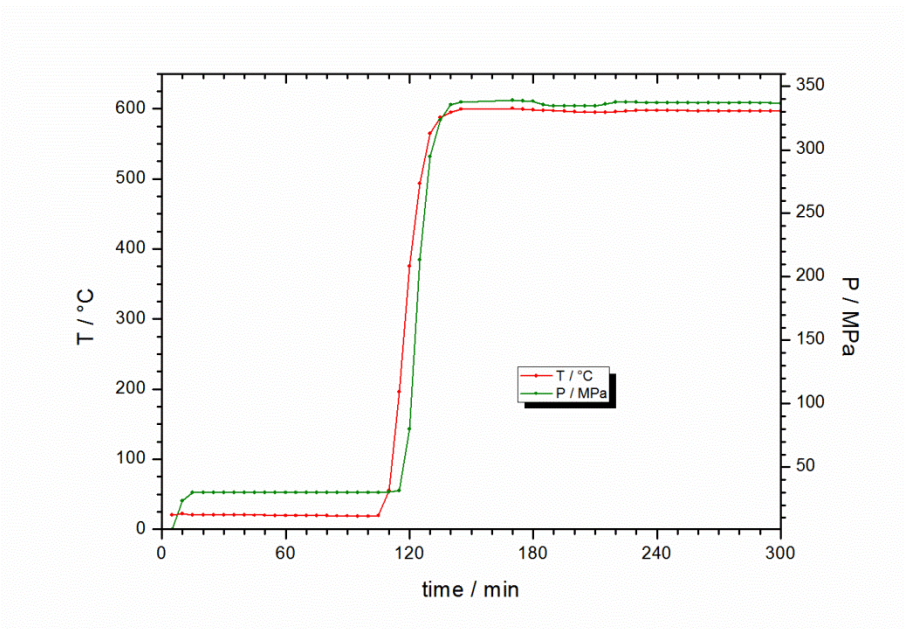
600
500
400
300
200
100
0
T / °C
350
300
250
200
150
100
50
P / MPa
0
60
120
180
240
300
time / min
T / °C
P / MPa

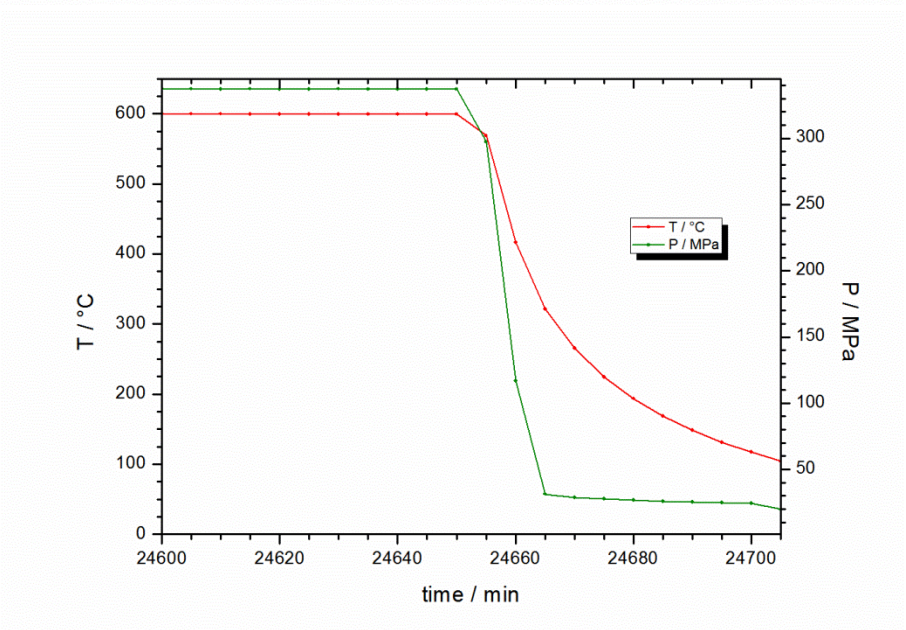
600
500
400
300
200
100
0
T / °C
300
250
200
150
100
50
P / MPa
24600
24620
24640
24660
24680
24700
time / min
T / °C
P / MPa

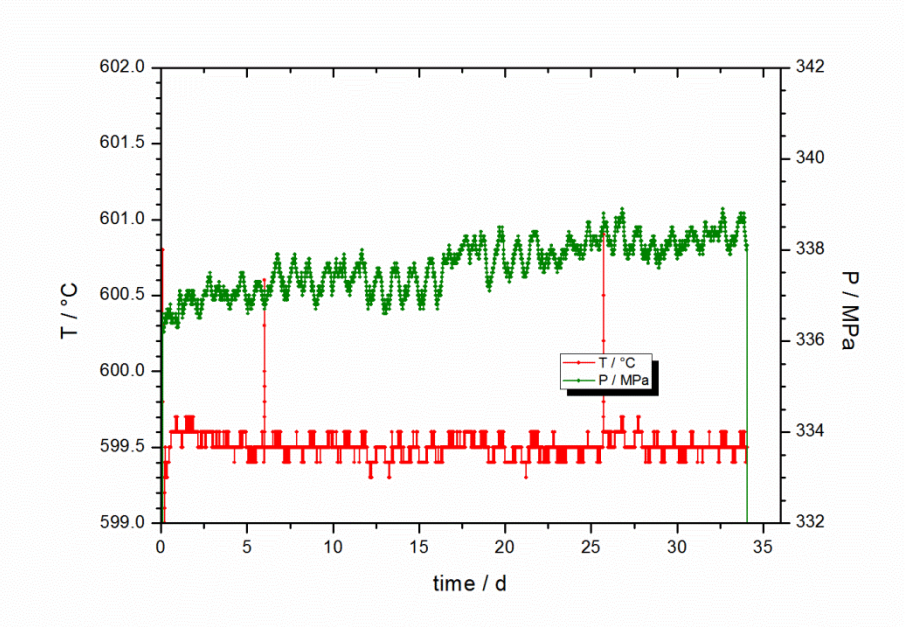
602.0
601.5
601.0
600.5
600.0
599.5
599.0
T / °C
342
340
338
336
334
332
P / MPa
0
5
10
15
20
25
30
35
time / d
T / °C
P / MPa

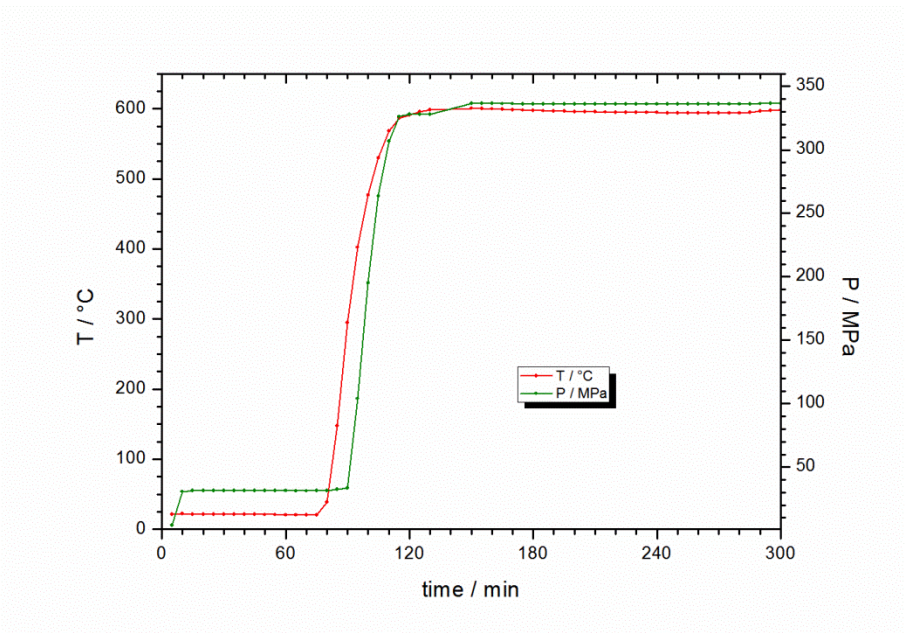
600
500
400
300
200
100
0
T / °C
350
300
250
200
150
100
50
P / MPa
0
60
120
180
240
300
time / min
T / °C
P / MPa

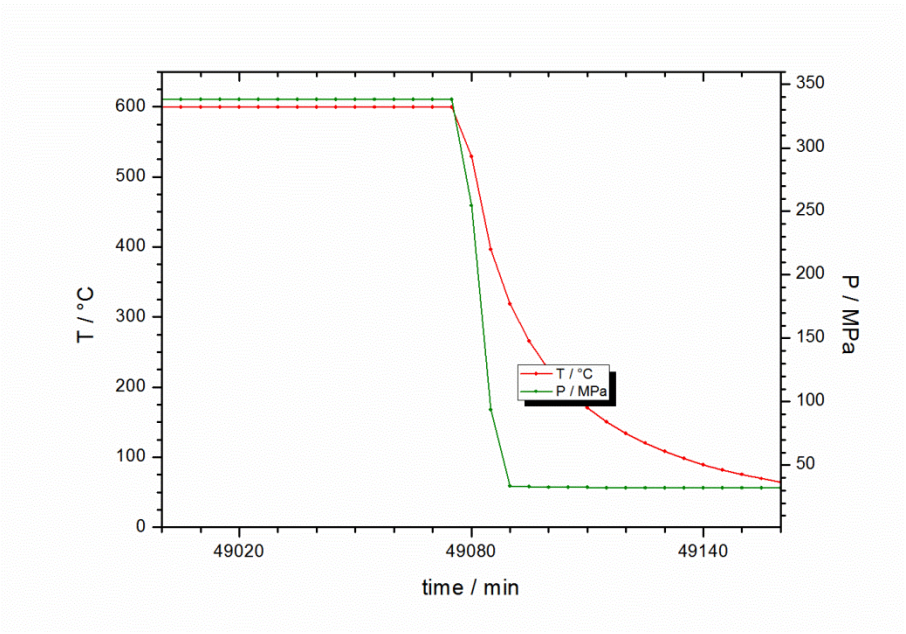
600
500
400
300
200
100
0
T / °C
350
300
250
200
150
100
50
P / MPa
49020
49080
49140
time / min
T / °C
P / MPa

B. Samples overview

B.a Close-up samples of chapter 3

"*Fluid inclusion modification by H_2O and D_2O diffusion: the influence of inclusion depth, size, and shape in re-equilibration experiments*"

GMR002c

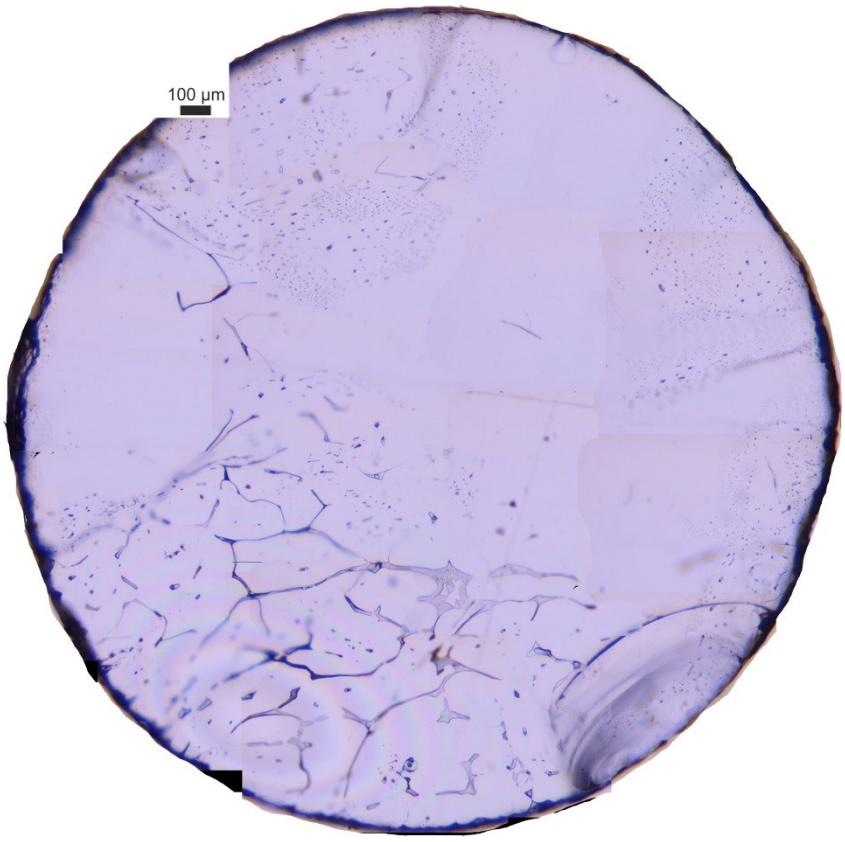

GMR004a

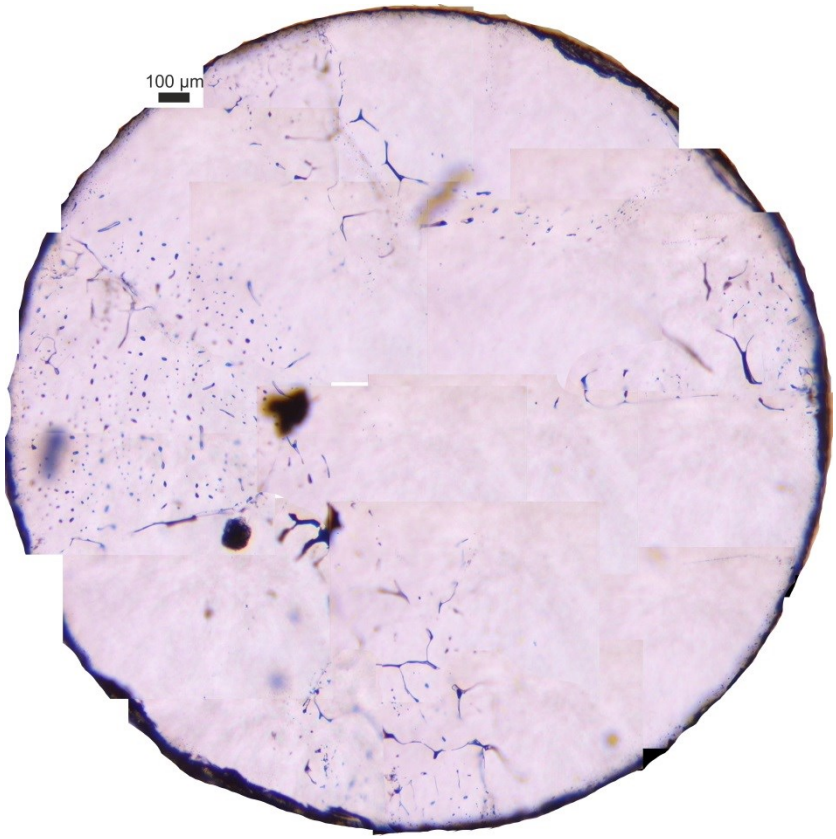

GMR004b

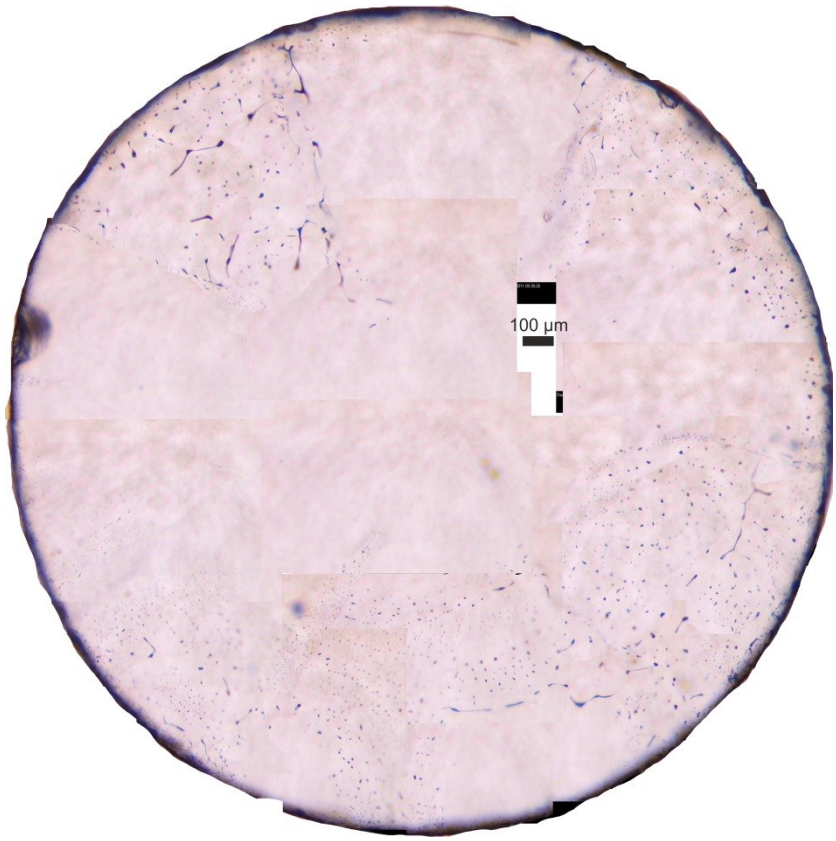

GMR004c

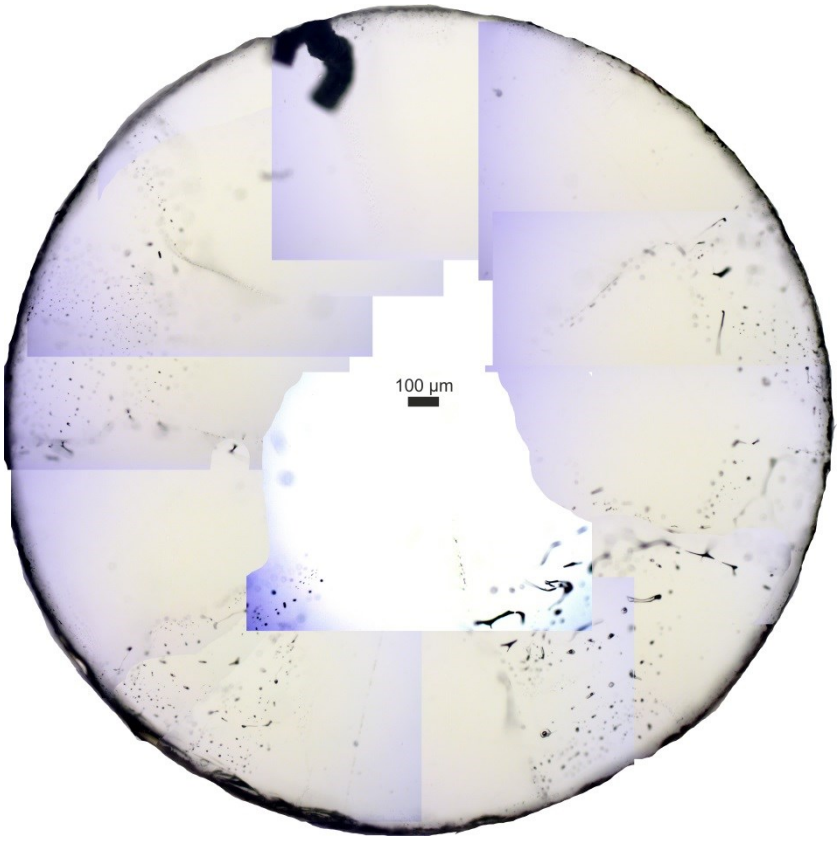

GMR006a

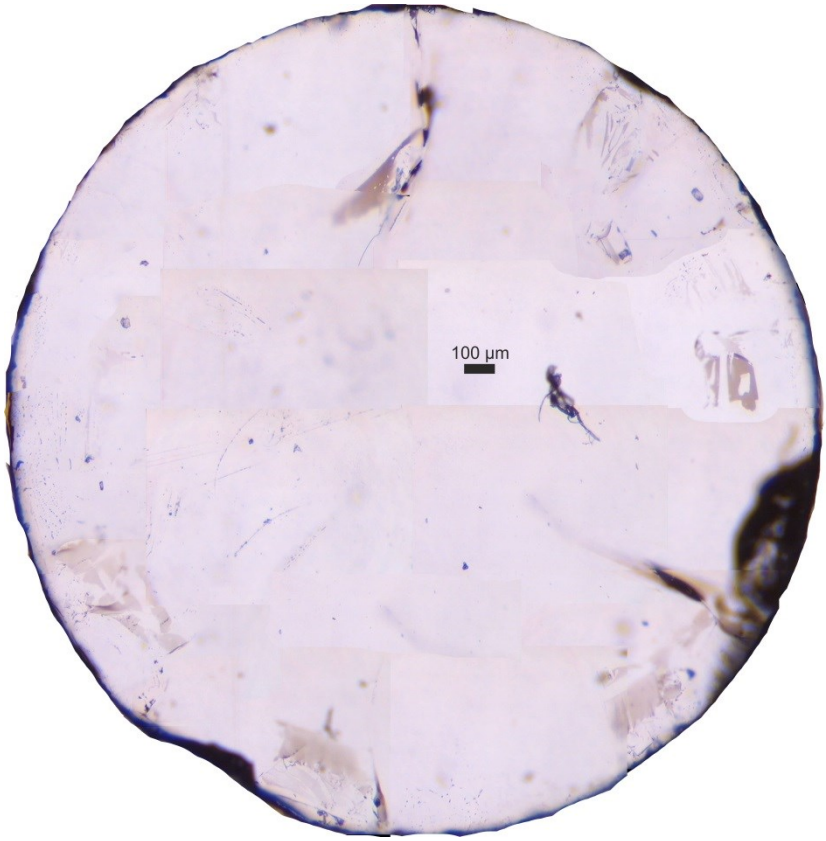

GMR007a

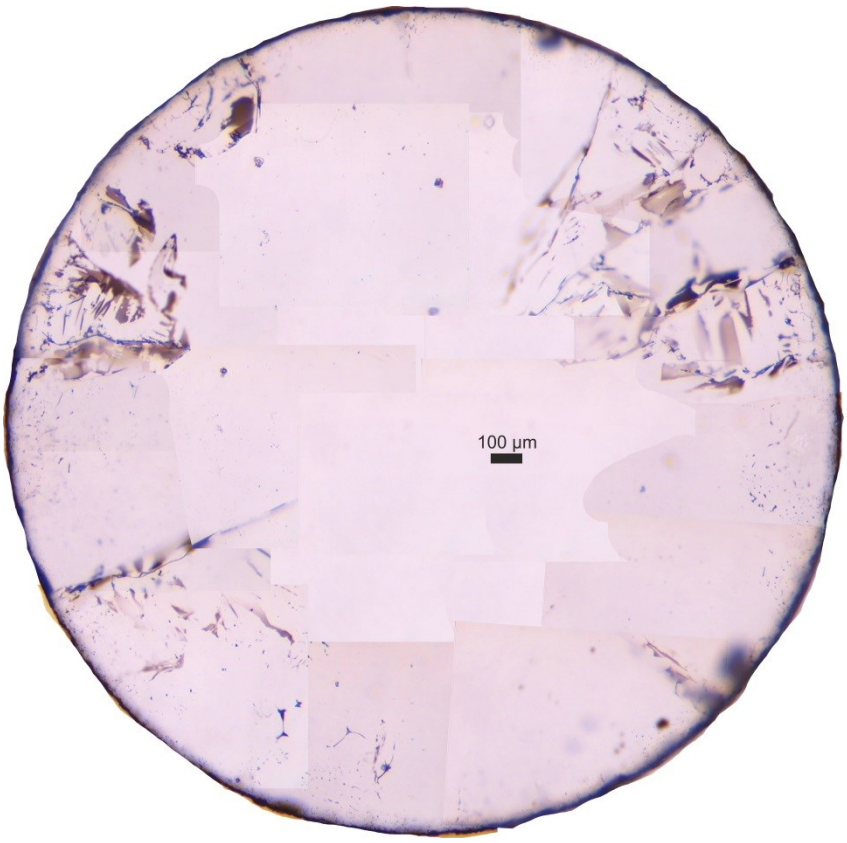

GMR008a

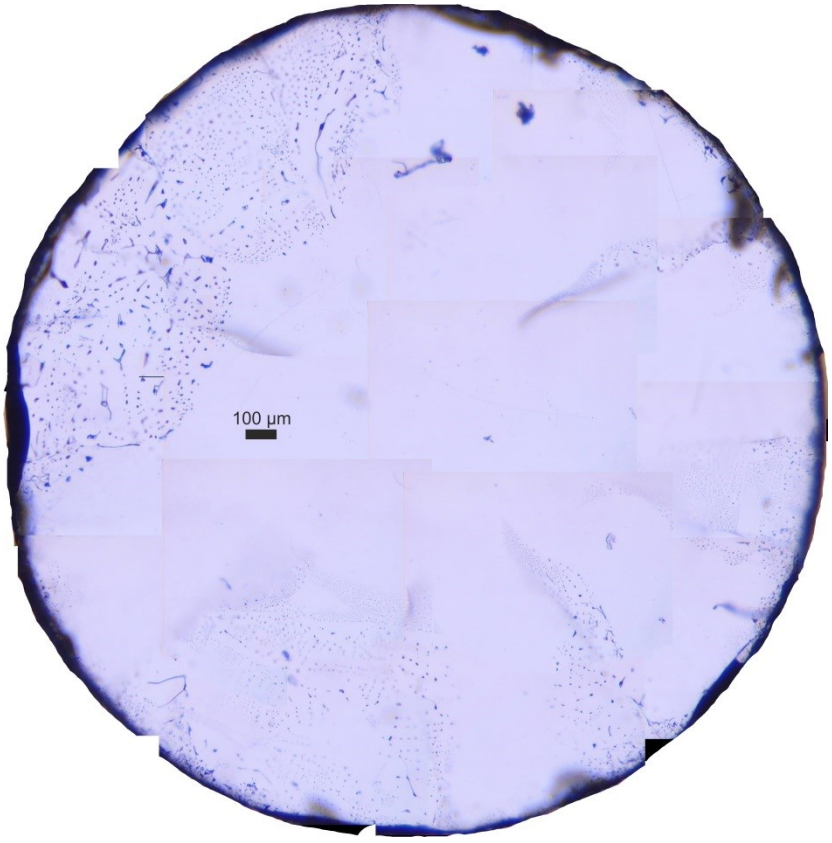

B.b Close-up samples of chapter 4

"*The influence of the α–β phase transition of quartz on fluid inclusions during re-equilibration experiments*"

GMR009a

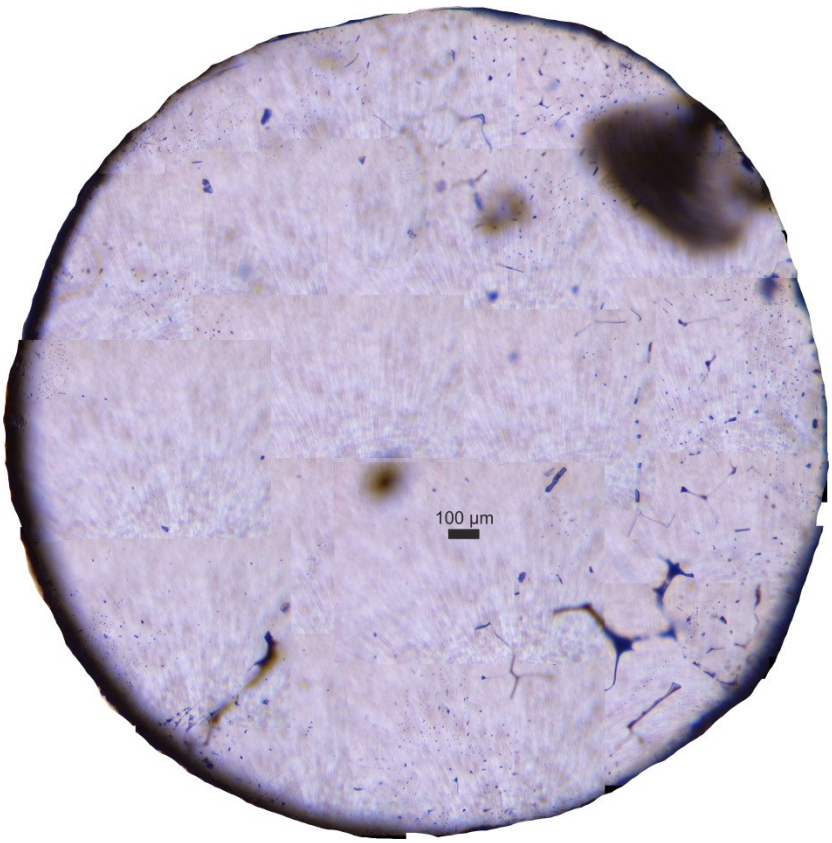

GMR009b

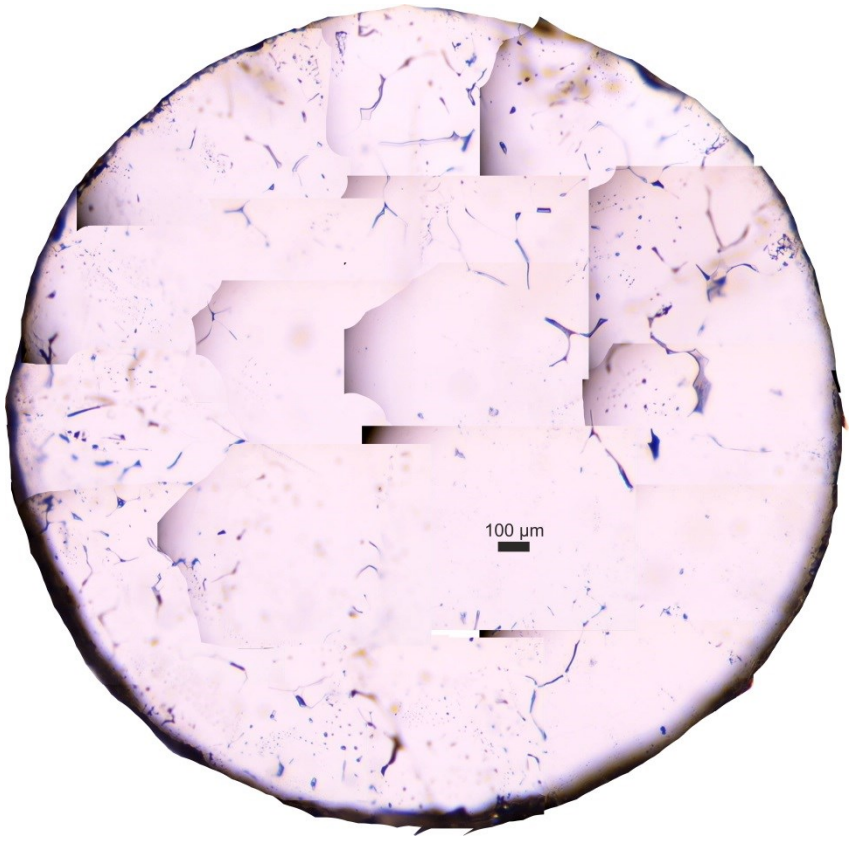

GMR010a

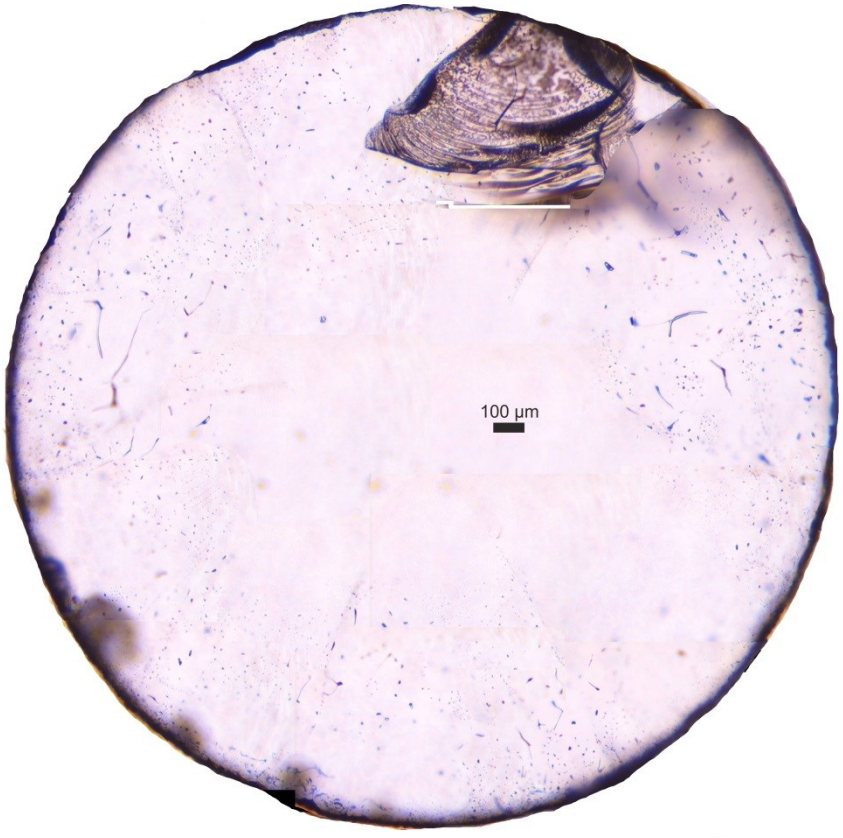

GMR010b

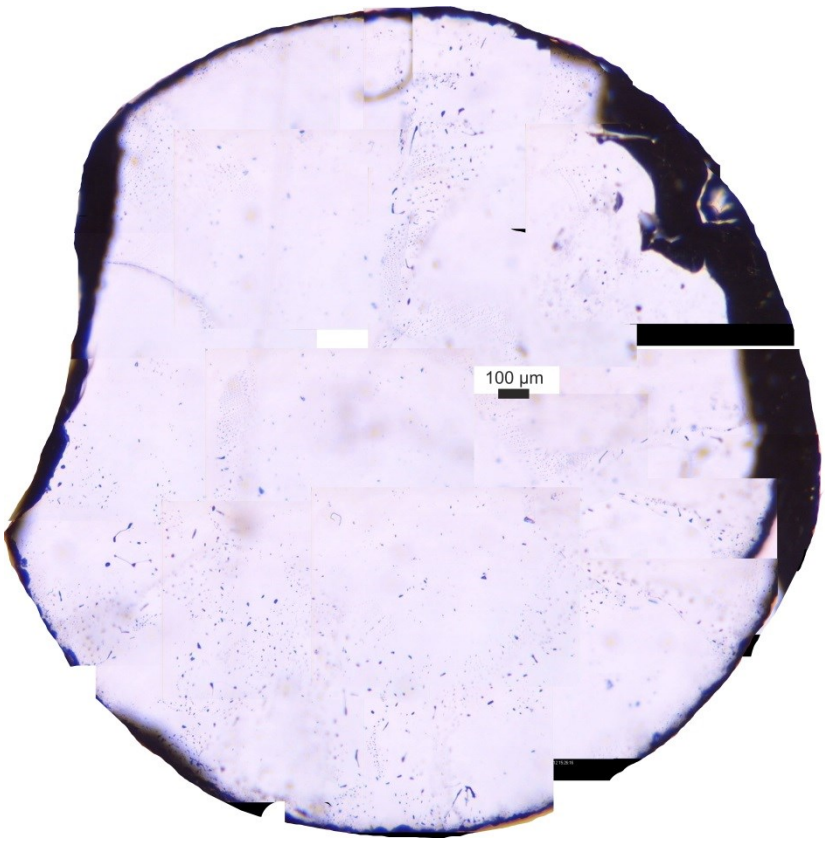

GMR013a

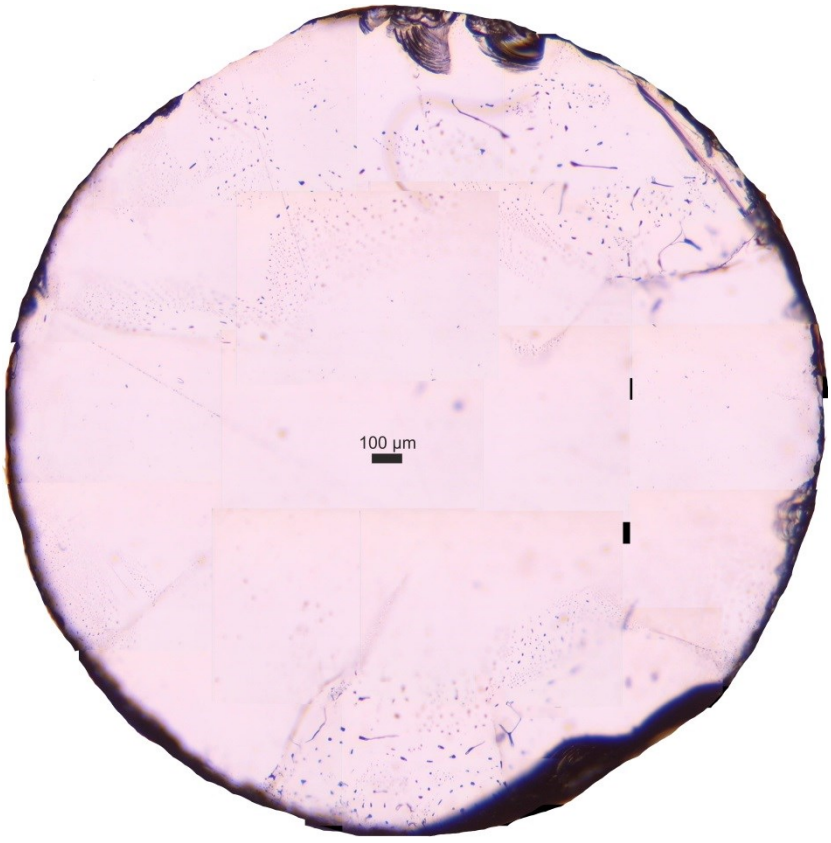

B.c Close-up samples of chapter 5

"Modification in fluid inclusion salinity during re-equilibration experiments at constant experimental P-T"

GMR003c

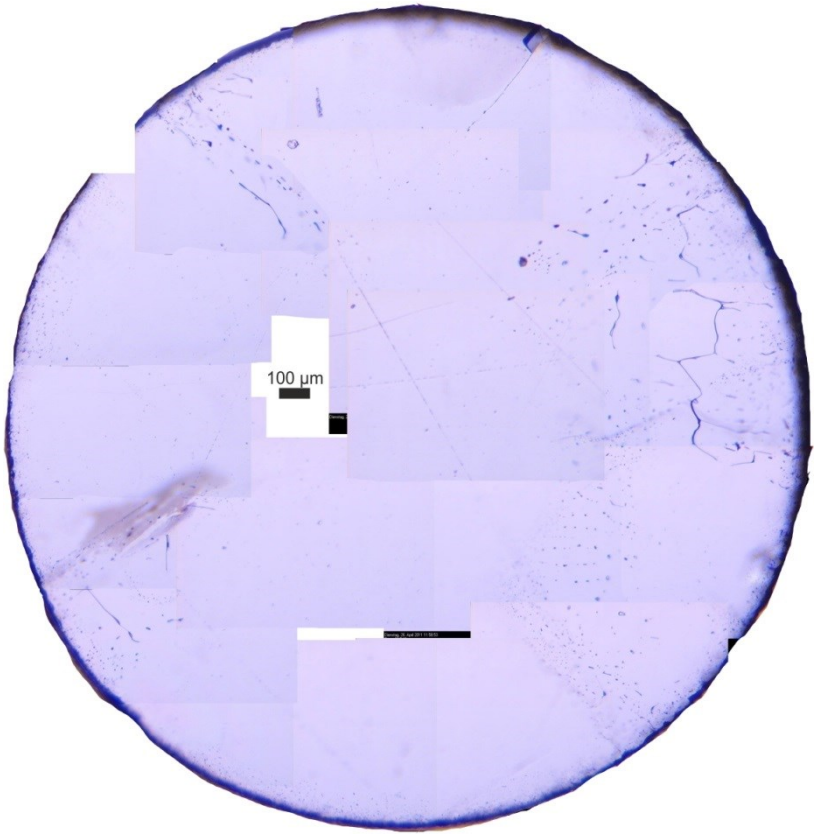

GMR004d

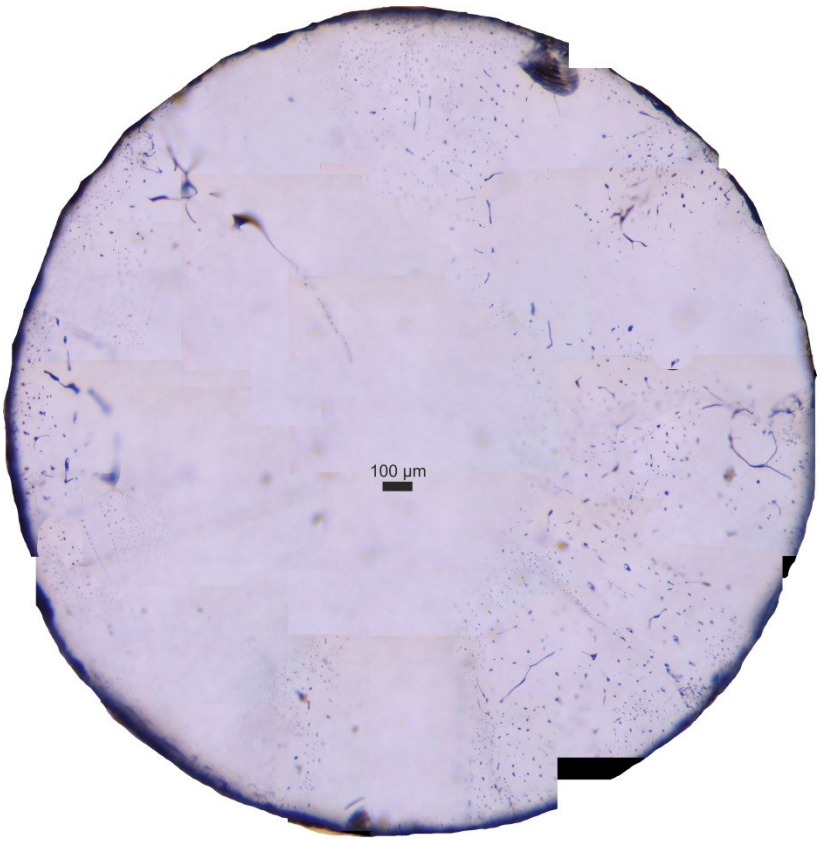

GMR004g

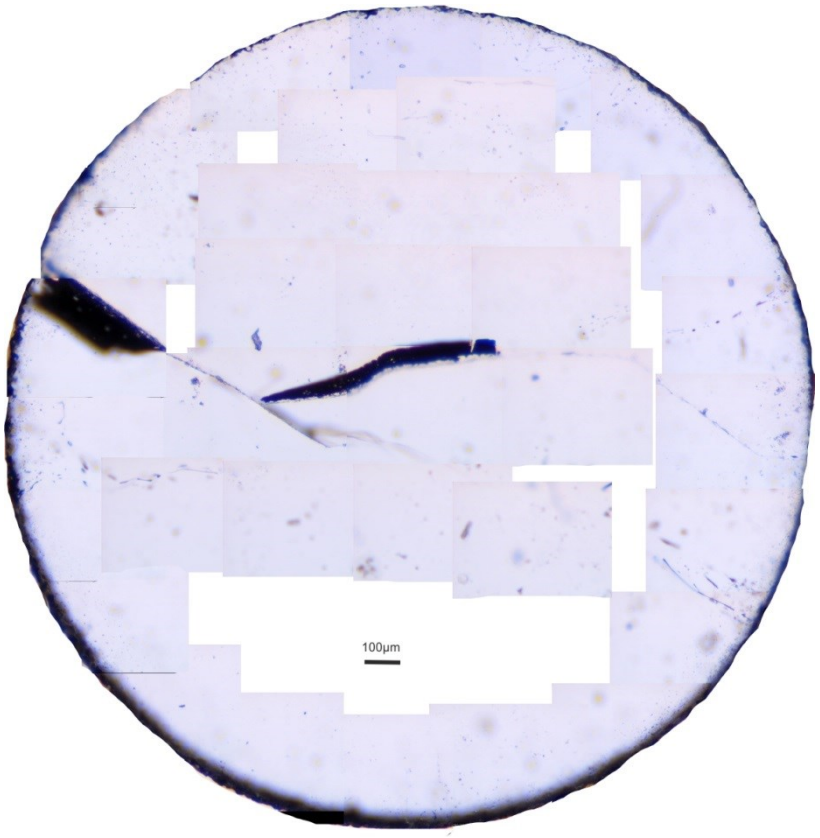

GMR005a

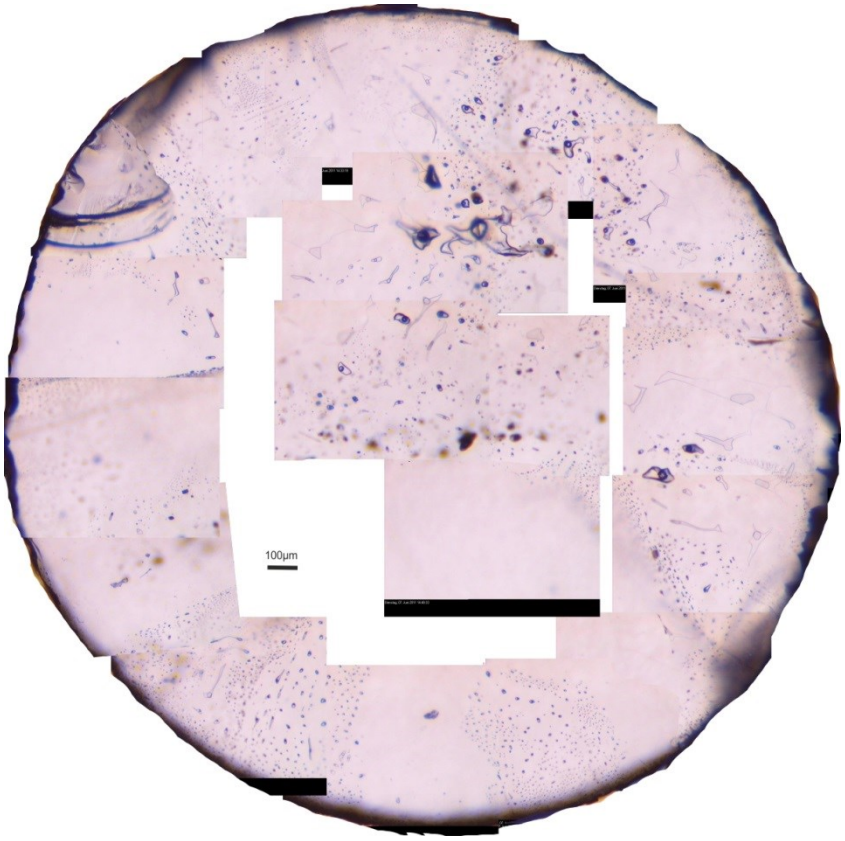

GMR005b

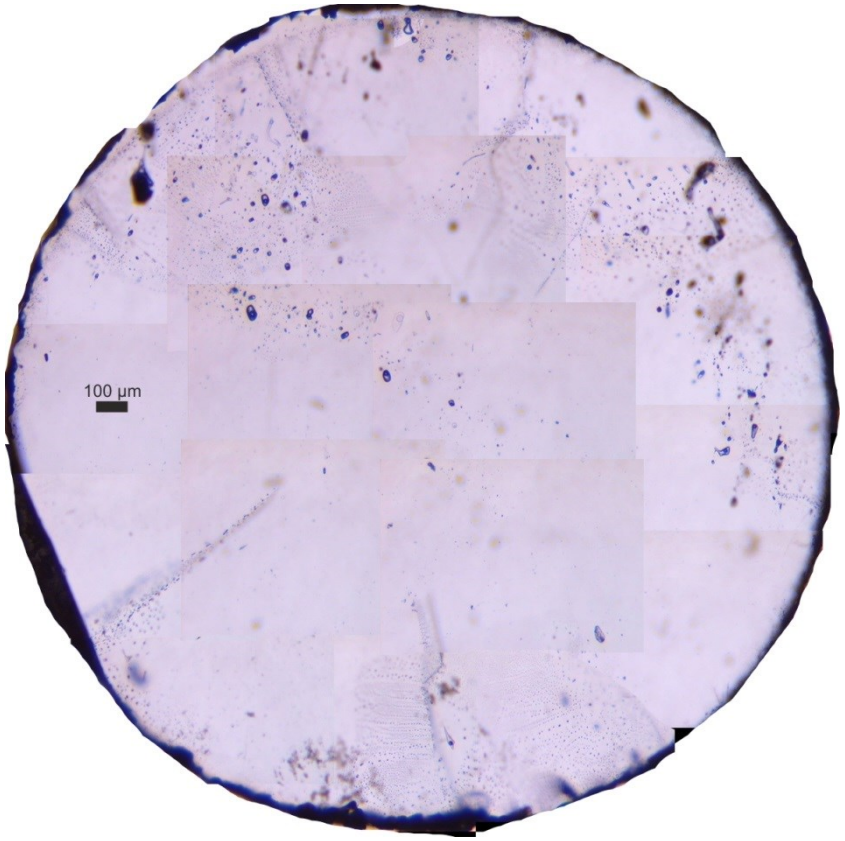

GMR005c

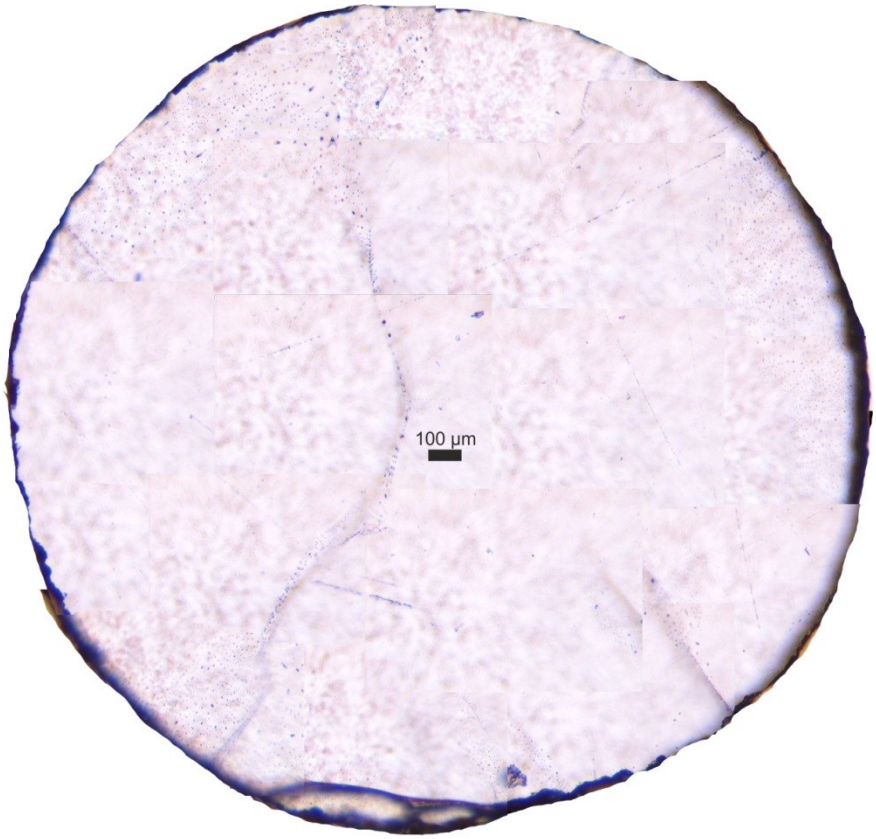

GMR011a

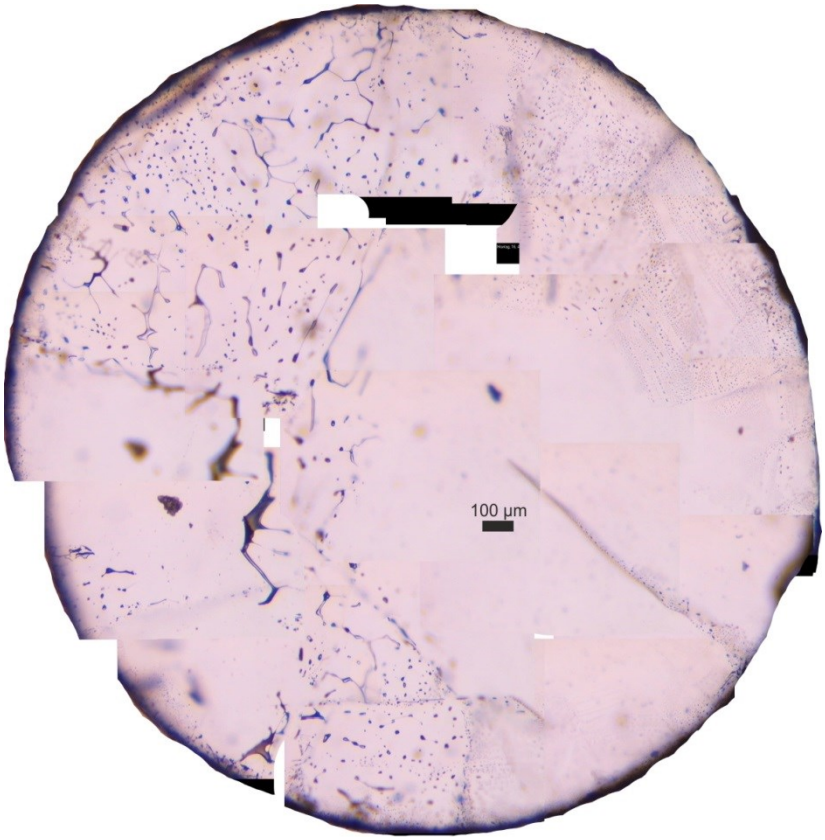

GMR014a

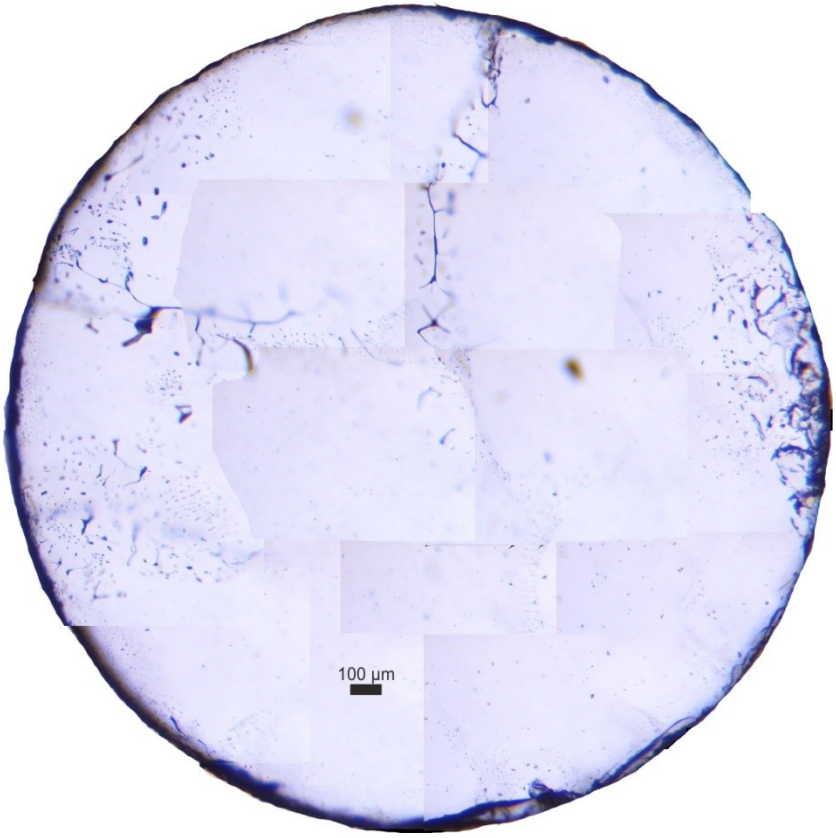

GMR014b

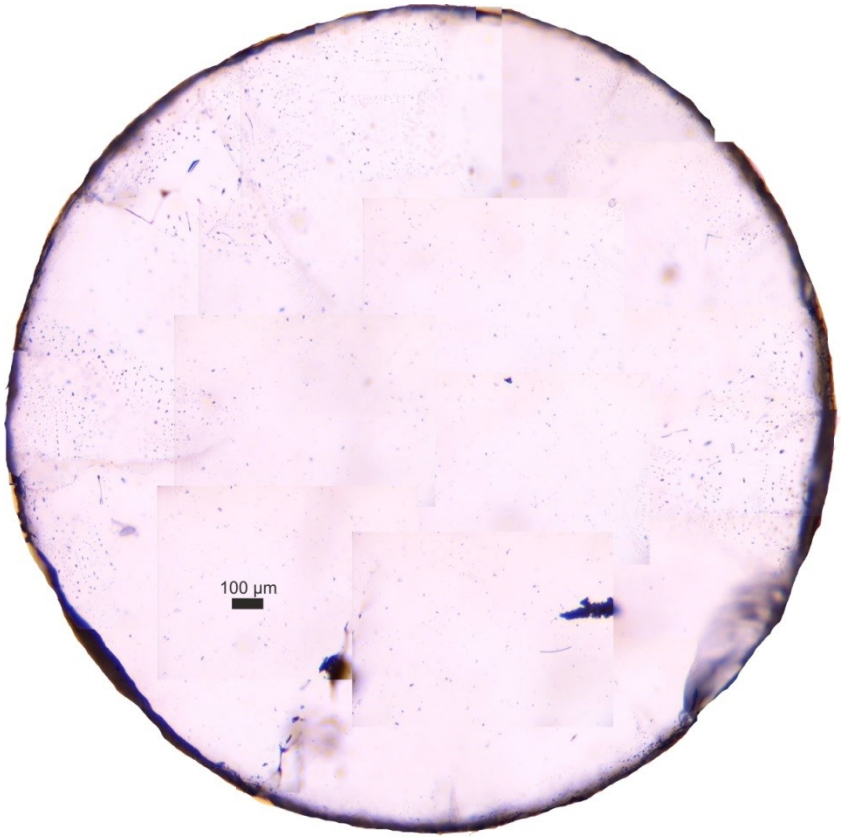

GMR014c

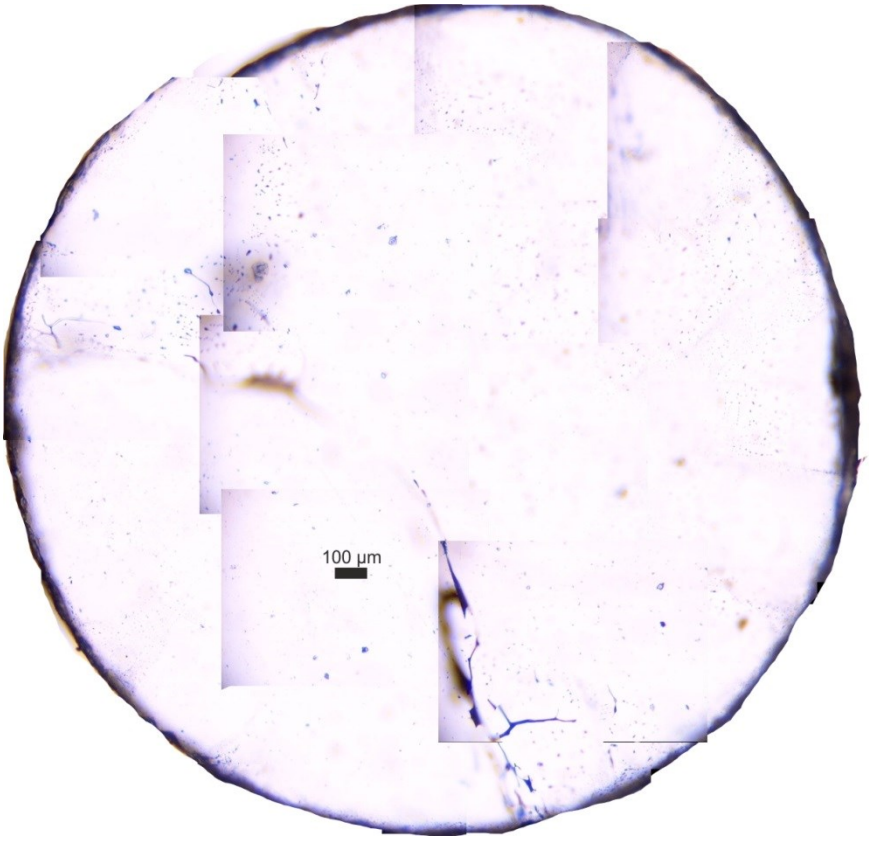

C. Individual fluid inclusion data

Any fluid inclusion data is attached as DVD to this work.